# Alma Mater Studiorum – Università di Bologna

## DOTTORATO DI RICERCA IN

## Scienze Chimiche

Ciclo XXV

**Settore Concorsuale di afferenza: 03/C1–CHIMICA ORGANICA**

**Settore Scientifico disciplinare: CHIM/06–CHIMICA ORGANICA**

# New functionalized ligands for luminescent metal complexes: from design to applications

**Presentata da: Dr. Andrea Baschieri**

**Coordinatore Dottorato:**          **Relatore:**

**Prof. Adriana Bigi**           **Dr. Letizia Sambri**

**Esame finale anno 2013**

# Index

# Abstract

The synthesis of luminescent metal complexes is a very challenging task since they can be regarded as the starting point for a lot of different areas. Luminescent complexes, in fact, can be used for technological, industrial, medical and biological applications. During my PhD I worked with different metals having distinguishing intrinsic properties that make them different from each other and, in particular, more or less suitable for the different possible uses. Iridium complexes show the best photophysical properties: they have high quantum yields, very long lifetimes and possess easily tunable emissions throughout the visible range. On the other hand, Iridium is very expensive and scarcely available. The aim of my work concerning this metal was, therefore, to synthesize ligands able not only to form luminescent complexes, but also able to add functionalities to the final complex, increasing its properties, and therefore its possible practical uses.

Since Re(I) derivatives have been reported to be suitable as probes in biological system, and the use of Re(I) reduces the costs, the synthesized bifunctional ligands containing a pyridine-triazole and a biotin unit were employed to obtain new Re(I) luminescent probes.

Part of my work involved the design and synthesis of new ligands able to form stable complexes with Eu(III) and Ce(III) salts, in order to obtain an emission in the range of visible light: these two metals are quite cheap and relatively non-toxic compared to other heavy metals.

Finally, I plan to synthesize organic derivatives that already possessed an emission thanks to the presence of other many chromophoric groups and can be able to link the Zinc (II), a low cost and especially non-toxic "green" metal. Zinc has not its own emission, but when it sticks to ligands, it increases their photophysical properties.

## 1) The importance of synthesizing luminescent metal complexes

The design and synthesis of luminescent substances is definitely a very current topic of interest for scientific research. In fact many publications can be found in chemical journals, but also in medical, biological and technological reviews, demonstrating how this topic can be considered as a starting point for completely different fields of study.

Today, for example, we witness an impressive expansion of the literature on the luminescence of Ir(III) complexes, as illustrated in Figure 1.
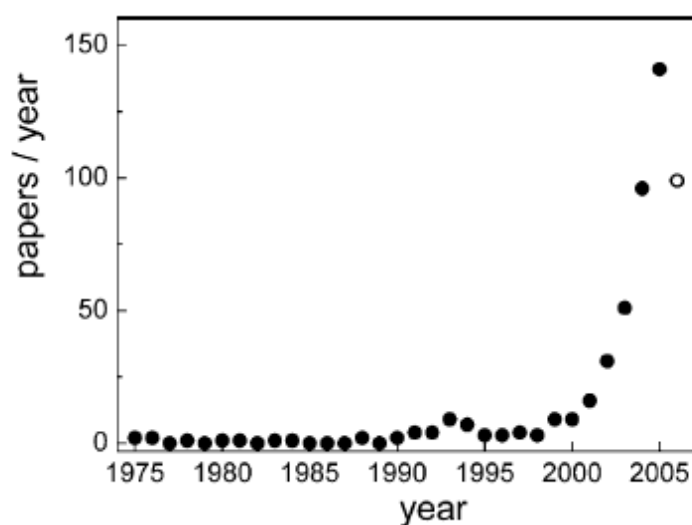


Figure 1: Representative number of papers (*full points*) dealing with the luminescence of iridium(III) complexes in the indicated years; updating is set at August 2006 (*empty point*)

From this diagram, it can be noticed that ca. 90% of the known luminescent Ir(III) complexes, mostly containing cyclometalating ligands, have been reported only since 2000.[1]

Despite the considerable interest, the obtainment of substances for the developing of new materials or devices still presents many problems due to the costs and the poor durability of the finished products. For this reason, it is necessary to continue the research, trying to synthesize organic functionalized molecules, which can be used as ligands for metal cations at low cost and high availability, to form luminescent complexes.

Especially cyclometalated Iridium (III) complexes, but also Rhenium (I), Europium (III), Cerium (III) and Zinc (II) complexes now, can be employed in a lot of different applications. Typically, such complexes are used as sensitizers for outer-sphere electron-transfer reactions,[2,3] photocatalysts,[4] photoreductants,[5] pH sensor,[6,7] biological luminescent probes and assays,[8] medical diagnostics and optical imaging devices,[9,10] but in particular as emissive dopants in multicolor

electroluminescent displays based on organic light emitting devices (OLEDs) and light-emitting electrochemical cells (LECs).

It is now accepted in the electroluminescent displays industry that phosphorescence-based OLEDs offer many advantages over existing display technologies. The most common display technology used for portable applications to flat panel display (FPD) TVs is liquid crystal displays (LCDs). A non-organic LCD display does not emit light; a white fluorescent backlight sitting behind the LCD panel is filtered by switchable polarizers in order to generate the pixel colors and to create the image on the screen. Individual liquid crystals allow light to pass or block it. Since the polarizer filter is employed in LCD, this leads to a loss in efficiency since most of the light is absorbed by the color filters, and creates viewing angle problems due to the polarized emission. On the other hand, OLED displays do not need a backlight since the organic material self-generates light, requiring very low external power and showing, generally, more efficient than LCDs. Additionally, OLEDs do not suffer from viewing angle problems, thus they always display sharp quality images independent of viewing angles. In contrast to conventional inorganic LEDs, OLEDs can result flexible, transparent, and lightweight. The basic structure of an OLED consists of a stack of two or more thin organic layers with a total thickness of about 1000 Å sandwiched between a transparent anode and a metallic cathode (Figure 2). The organic layers consist of a hole transporting layer (HTL), an emissive layer containing a dopant and a host material, and an electron transporting layer (ETL). When an external driving voltage is applied, the introduced positive and negative charges are injected into the organic materials. The positive (holes) and negative (electrons) charges migrate through the device and recombine to form excitons in the emissive layer. The device lights up (produces electroluminescence) as excitons decay radiatively. The emission color depends on the energy of the exciton. Particular structures of the organic layers and the choice of anode and cathode should be considered to highly maximize the recombination process in the emissive layer, thus maximizing the light output from the OLED device.
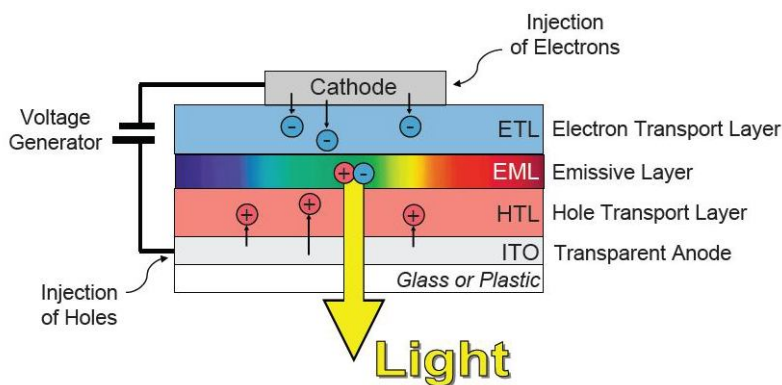


Figure 2: Typical OLED Structure

3

The earliest OLEDs work was reported in 1987 by Tang and Van Slyke from Eastman Kodak labs. They made the first double heterostructure device in which its structure comprised of ITO / diamine HTL / Alq3 / Mg:Ag.[11] A glass substrate was coated with a transparent indium tin oxide (ITO) acting as the anode.

A diamine was used as the hole transporting material and $Alq_3$ (tris(8-hydroxyquinoline) aluminum(III)) served as both an electron transporting layer (ETL) and an emissive layer. Electrons were injected from a Mg:Ag alloy cathode with an additional layer of Ag to protect the Mg from oxidation. In this double layer device, electrons and holes combined at the diamine/$Alq_3$ interface (Figure 3a). This double layer device utilized HTL and ETL to confine excitons and prevent dispersion. The utilization of HTL and ETL could lead to efficient charge carrier injections. The significant problem with this double layer device is that the excitons emitting from a dense and pure matrix typically go through significant self-quenching that leads to poor external quantum efficiency (~1%).[11] In 1989, Tang, Van Slyke and Chen showed that it was possible to add small quantities of a highly fluorescent dye (green Coumarin 540 or red DCM (4-(Dicyanomethylene)-2-methyl-6-(4-dimethylaminostyryl)-4*H*-pyran) fluorescent dyes) to a charge transporting material ($Alq_3$) in the double layer device to easily tune the OLED emission color. By introducing the fluorescent dopant, they were able to improve the device efficiency up to 2.5%.[12] Inside the emissive layer, energy will transfer readily from the host ($Alq_3$) to a dopant with a smaller optical gap resulting in efficient emission from the dopant (Figure 3b). The self-quenching of excitons is also suppressed by lowering the concentration of excitons and the device efficiency is improved. An additional benefit of doping is to control emission colors of OLEDs by doping with different emissive dyes.



Figure 3: (a) Double Layer OLED; (b) Doped-double Layer OLED

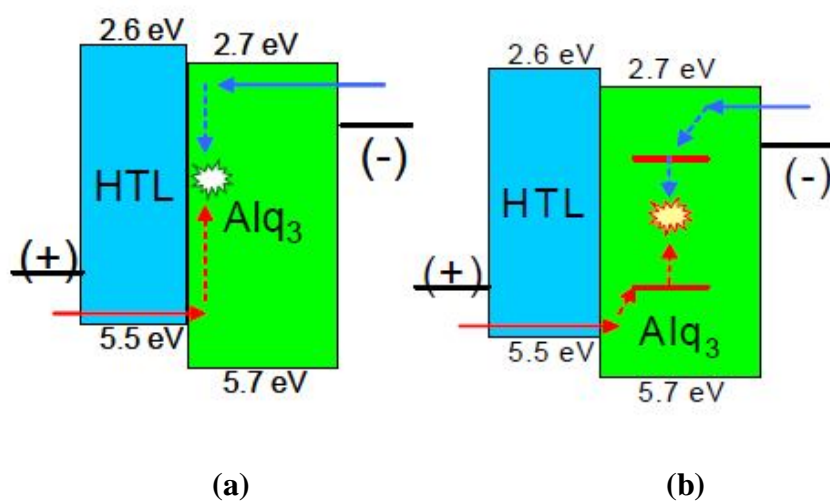Excitons in OLEDs are created in a ratio of about 3:1 (Figure 4), i.e., approximately 75% triplets (spin parallel) and 25% singlets (spin antiparallel).[13] A fluorescence device only utilizes singlet excitons, while the energy of triplet excitons is generally lost to non-radiative decay processes that heat up the device. This inefficient utilization of triplet excitons limits the internal quantum efficiency of fluorescence-based devices to only 25%. Contrary to fluorescence-based devices, OLEDs utilizing phosphorescent materials that emit from triplet excited states are expected to result in higher internal quantum efficiency.
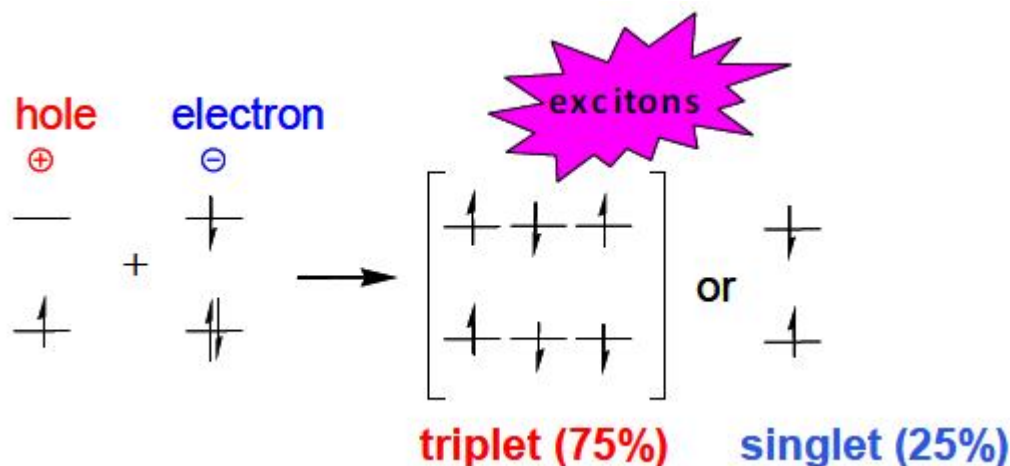


Figure 4: Exciton Formation by Hole-Electron Recombination

OLED displays can be fabricated on different types of substrates ranging from rigid glass to flexible polymers which are usually coated with a transparent conductive anode material, indium tin oxide (ITO). Since most organic molecules have low charge transport mobilities ($<10^{-2}cm^2/Vs$),[14] the films are required to be very thin (~1000 Å) in order to pass enough currents at low operating voltages. Organic films comprised of small molecules are usually grown by vapor deposition (sublimation) onto the substrate under high vacuum conditions ($< 10^{-6}$ torr). On the other hand, high molecular weight polymers, that are not volatile enough for vapor deposition, are typically spin-coated or printed onto the substrate. A low work function metal (e.g. Ca, Al, or Mg) is vapor deposited on top of the organics to serve as the cathode.

To improve the device performance, multi-layered materials are used, each of which serves different functions, i.e. hole carrier, emissive layer, or electron carrier. The most commonly used hole-transporters consist of an organic triarylamine-based compound. A series of metal quinolates are widely utilized as electron transporting materials. The chemical structure of several typical HTL and ETL molecules, i.e. 4,4'-(cyclohexane-1,1-diyl)bis(N,N-di-*p*-tolylaniline) (Cta), *N,N'*-bis-(1-naphthyl)- *N,N'*-diphenylbenzidine (α-NPD), aluminum tris(8 hydroqunilonate) (Alq$_3$), are shown in Figure 5.
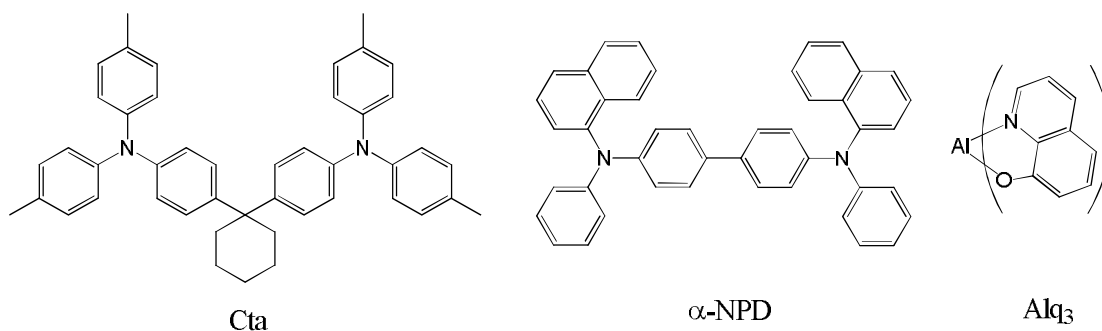
Figure 5: Structures of Typical HTL and ETL Materials Used in OLEDs.

OLEDs and LEECs have attracted also a great deal of attention due to their potential use in lighting. Notably, they are acquiring an increasing market share in ambient illumination thanks to the consolidation of white LED concepts.[15] In fact, the diffusion of artificial lighting is one of the greatest achievements of the past century, in fact for millennia artificial lighting was generated by the open fire. In 1879, taking advantage of the work of many other inventors and after having tested hundreds of different materials as filaments, Thomas Edison patented the incandescent carbon filament lamp, a milestone of modern lighting. Edison's device converted just 0.2% of electricity into light, but it was 20-times more efficient than a candle in converting chemical energy into useful photons.[16,17] In the following decades, electric lighting devices underwent substantial progress in terms of efficiency and all the systems that are still used nowadays were introduced: the tungsten lamp (1906), that dominated residential lighting for one century, the sodium vapor lamp (1930s) and the fluorescent tubes (1940s).[18] The evolutions of these three fundamental designs were introduced in relatively recent times: the halogen lamp, an advanced filament system, entered the market in the 1960s and the compact fluorescence lamp, a sort of hybrid between bulbs and fluorescent tubes, appeared in the 1980s. The tremendous progress made during the 20th century in improving the quality and availability of artificial lighting was accomplished through the use of two main technologies: incandescent- and discharge-based lamps.[19] There is a variety of both type of lamps, but these two traditional lighting concepts have been exploited near to their limit; thus, new lighting approaches have emerged in the last two decades.[20] The emerging concept for illumination is solid-state lighting (SSL),[21] in which selected semiconductor materials are stimulated to produce visible light under the action of an electrical field (electroluminescence). Through this approach, the primary product of these lighting devices is the photon itself, unlike traditional sources where visible light is essentially a byproduct of other processes, such as heating or discharging. As a result, SSL (OLEDs or LEECs) creates visible light with reduced heat generation or parasitic energy dissipation, while its solid-state nature provides for greater resistance, increasing significantly the lifespan of appliances.

6

## 2) Different metals for different properties

### 2.1 - Iridium (III)

Iridium(III) is a $5d^6$ metal center and its d orbitals are split by the interaction with the octahedral ligand field into three stabilized $t_{2g}$ ($d_{xy}$, $d_{xz}$, $d_{yz}$) and two destabilized $e_g$ orbitals ($d_z^2$, $d_{x^2-y^2}$), (Figure 6a). In general the energy difference between these two levels ($\Delta_o$) depends on:

1) the oxidation state of the metal center: the higher the oxidation state, the higher the $\Delta_o$ splitting;

2) the size of the d orbitals: $\Delta_o$ is smallest for 3d metals and progressively increases with 4d and 5d metals;

3) the field strength exerted by the ligands, following the so-called spectrochemical series.

Ir(III) exhibits a high $\Delta_o$ splitting because of the presence of a highly charged ion belonging to the third row of the d-block of the periodic table. As a result, the electronic configuration of the metal center is always in a low-spin state ($t_{2g}$ 6, $e_g$ 0, Figure 6a) and the ligand-field stabilization energy is maximized, which means that Ir(III) complexes are generally stable and rather inert toward substitution. Accordingly, the configuration of the metal orbitals is closed-shell ($A_1g$) and, since the ligand orbitals are fully occupied, the ground-state of the complexes is a singlet ($S_0$). Other transition-metal ions have the same $d^6$ low-spin configuration of Ir (III) (e.g., Os (II), Ru (II) and in the presence of particular ligands, even Fe (II)), however their complexes do not exhibit such remarkable photophysical properties (e.g., emission color tunability, high photoluminescence quantum yields (PLQYs), good photostability, etc.) because the scenario in the excited states is very different (Figure 6b). The reasons are as follow:

a) Fe (II), $3d^6$ configuration: the $\Delta_o$ splitting is very small, hence the lowest-lying excited state is $^1$MC in nature (i.e., centered on eg metal orbitals) and, therefore, not emissive.[22]

b) Ru (II), $4d^6$ configuration: the $\Delta_o$ splitting is increased and the lowest (emissive) excited state is a metal-to-ligand charge transfer triplet ($^3$MLCT), relatively close to $^3$MC states that can be thermally populated and open a competitive radiation less deactivation pathway to either the ground state or to degradation products; accordingly, the PLQY of Ru (II) complexes increase substantially with decreasing temperature.[23]

c) Os (II), $5d^6$ configuration: the $\Delta_o$ splitting is considerable and the $^3$MC states are usually too high to affect emission properties, but the emissive $^3$MLCT excited state has lower energy compared to

Ru (II) analogues (emission bands typically peaking in the red/infrared edge of the spectrum) and this favors radiationless pathways thanks to the "energy gap law";[24] accordingly, PLQYs of these complexes are typically low, often below 1–2%.[25]
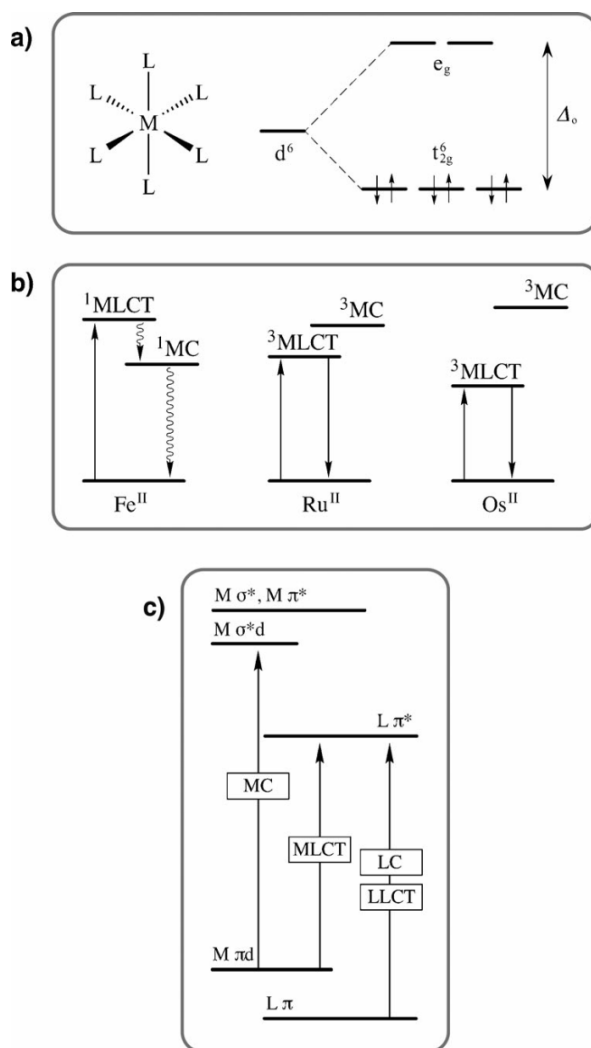


Figure 6: a) Low-spin d6 orbital configuration in octahedral field. b) Qualitative electronic excited states description for Fe(II), Ru(II), and Os(II) metal complexes. c) Electronic energy-level diagram for a generic Ir-complex. MC is metal-centered, LC is ligand-centered, LLCT and MLCT are ligand-to-ligand and metal-to-ligand charge transfer, respectively.

The emission colors from Ir (III) complexes are strongly dependent on the choice of the cyclometalating ligand, with room temperature lifetimes on the order of μs, high quantum efficiencies and good stability. The emission color can be readily tuned from blue to red by judicious modification of the cyclometalating ligands and/or ancillary ligands. In general, multi-color display applications require efficient and stable blue, green and red OLEDs. OLEDs have

been manufactured with $(C^\wedge N)_2Ir(L^\wedge L)$ phosphor dopants, giving efficient green, yellow or red emission (Figure 7).[26]
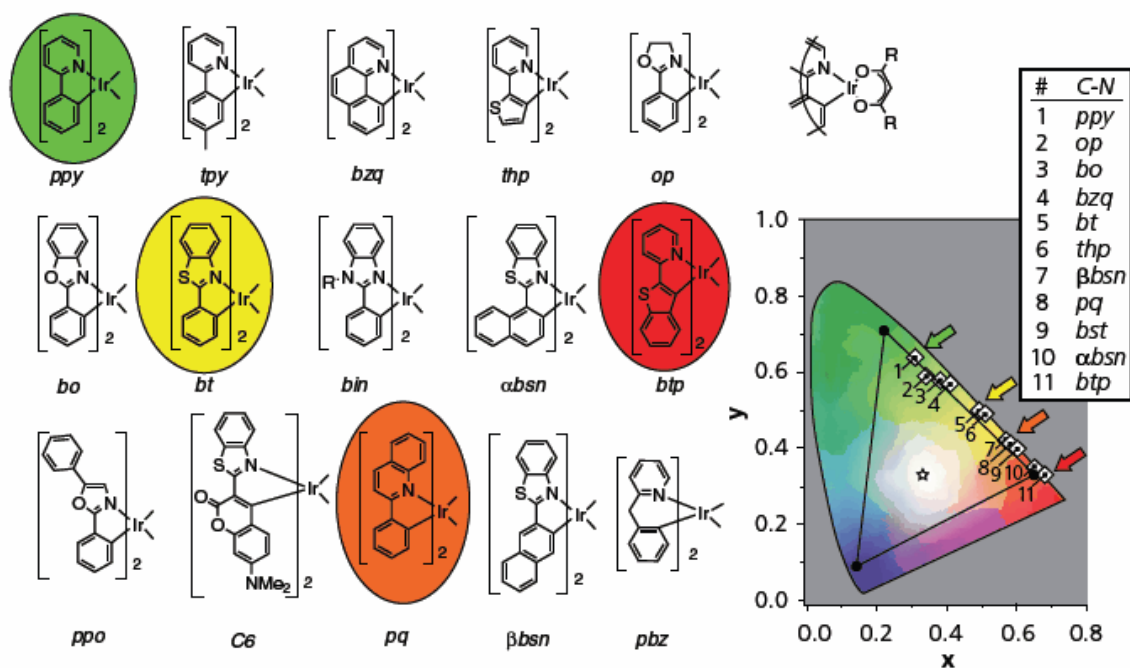


Figure 7: Green to Red Emission Ir Phosphors (from http://www.sigmaaldrich.com/technical-documents/articles/material-matters/achieving-high-efficiency.html)

It is interesting to note that red and green iridium complexes have been well developed to be used in OLEDs, while blue iridium complexes are still less common.

Most Iridium complexes are synthesized in two steps according to the strategy depicted in Figure 8. Commercially available $IrCl_3 \cdot nH_2O$ reacts with a slight excess of the desired cyclometalating ligand $(C^\wedge N)$, the most popular of which are substituted 2-phenylpyridines (Hppy). The reaction is usually carried out in 2-ethoxyethanol heating overnight at around 120° C under argon atmosphere.[27] The product of this reaction is the cyclometalated Ir(III) μ-dichloro bridged dimer $[\{(C^\wedge N)_2Ir(\mu\text{-}Cl)\}_2]$. In Iridium dimer complexes, the Ir_C/Ir_C' bonds are stereochemically *cis* to each other, whereas the Ir_N/Ir_N' are mutually in *trans* position.[28] Tris-cyclometalated iridium(III) complexes are minor byproducts that can be easily separated from the main dichloro-bridged dimer.[29] The $[\{(C^\wedge N)_2Ir(\mu\text{-}Cl)\}_2]$ dimers undergo facile reactions with a variety of monodentate and bidentate neutral imine type chelating ligands (Figure 8) to yield a plethora of different cationic mononuclear complexes in high yields[30] as chloride salts. Subsequently, these can undergo an ion exchange reactions with less-coordinative and less-reactive anions, for example ($PF_6^-$ or $BF_4^-$, to improve the performance of the complex under the electric field in operating devices. When the direct addition

9

of the neutral ligands to the dimer affords low yields, an alternative synthetic route can be utilized, carrying out removal of chlorides by treating the μ-dichloro-bridged dimer with silver triflate or other silver based chloride-abstracting agents.[31] The chloride-free intermediate, for example, [(C^N)$_2$Ir(H$_2$O)$_2$][CF$_3$SO$_3$], can then be treated with the desired neutral ligand under mild reaction conditions.[32] It is even possible to avoid this two-step procedure by directly treating the [{(C^N)$_2$Ir(μ-Cl)}$_2$] dimer with a stoichiometric amount of neutral ligands in the presence of Ag$_2$O, to promote the removal of chloride during the reaction.[33]
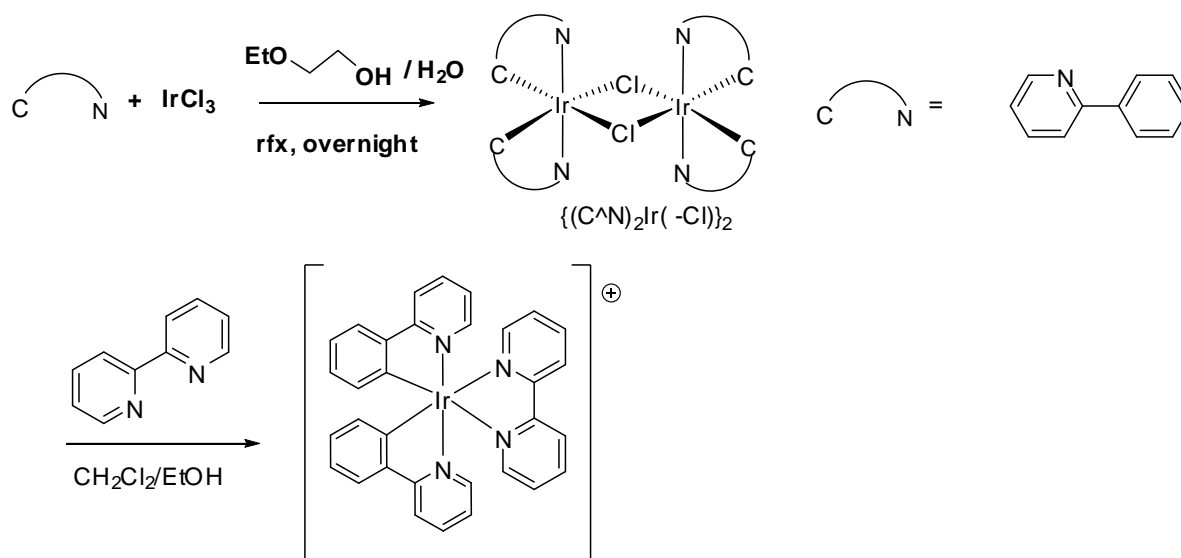


Figure 8: Typical two-step synthesis of a heteroleptic bis-cyclometalated iridium(III) complex.

## 2.2 - Rhenium (I)

The photochemistry of Rhenium complexes occupies a prominent position in the photochemistry of transition metal complexes. Along with early preparative studies on photosubstitution of carbonyl species like Re(CO)$_5$X, the preparation of the remarkably stable yellow complex *fac*-Re(CO)$_3$(phen)Cl (phen= 1,10-phenanthroline) foreshadowed the discovery of the a large class of related luminescent materials by Wrighton and co-workers in the 1970s.[34] As pointed out by Vogler and Kunkley, the current photochemistry of Rhenium complexes is rich, spanning eight oxidation states from formal Re(0) (for example, Re$_2$(CO)$_{10}$) to formal Re(VII) (for example MeReO$_3$).[35] Complexes of Re(I) containing polypyridine or diimine donors, usually with three carbon monoxide co-ligands, continue to be an intense area of interest. The most popular Re(I) family of complexes studied for their luminescent properties is the *fac*-[Re(N^N)(CO)$_3$-(L)]$^{n+}$,[36,37] where N^N represents a neutral conjugated diimine ligand such as 2,2'-bipyridine (bipy) or 1,10-phenanthroline (phen), L is an ancillary ligand, and n = 0 or 1 depending on the respective anionic or neutral charge of the

ligand L. Some of these complexes exhibit exceptional luminescence properties with quantum yield ($\Phi$) values up to 0.6 and extended excited state lifetimes ($\tau$) ranging from the nano to microsecond scale. Manipulation of the photophysical properties is achieved by changing the relative energy of the $\pi^*$ orbitals of the diimine system with the introduction of electron withdrawing (EWGs) or donating groups (EDGs) and/or by varying the crystal field strength of the ancillary ligand L.[38] Generally, cationic *fac*-[Re(N^N)(CO)$_3$(L)]$^{n+}$ complexes, for example, when L is a pyridine-type ligand, possess superior photoluminescence properties compared to their analogous neutral ones where L = Cl$^-$, Br$^-$. These improved properties have been rationalized in terms of a reduced non-radiative decay constant, $k_{nr}$, due to the larger gap between the highest occupied molecular orbital (HOMO) and the lowest unoccupied molecular orbital (LUMO), in agreement with the energy gap law.[39]

Figure 9 illustrates two models used to explain the photochemical properties of rhenium carbonyl complexes. The MLCT absorption band often lies at lower energy on the shoulder of the $\pi \rightarrow \pi^*$ diimine ligand centered transition (LC); hence, both the $^1$MLCT and $^1$LC$^*$ levels are often populated simultaneously. Further, the $^3$MLCT and $^3$LC$^*$ vary in energy relative to one another. Consequently, emission spectra are often found to occur in the 500 nm region with strong vibronic character consistent with a large $^3$LC$^*$ contribution; in other cases the spectra occur near 600 nm and are structureless and assignable to a $^3$MLCT state. Because the emission envelope of the coordinated diimine ligand is red-shifted from that of the free ligand, a combination $^3$LC, $^3$MLCT state is often employed to account for the emission behavior. Emission spectra are also temperature dependent. At 77 K in a frozen matrix, the $^3$MLCT state in some cases is found to rise above the $^3$LC state resulting in ligand centered emission in some systems.[40] For the "parent complexes", [Re(bpy)(CO)$_3$Cl] and [Re(bpy)(CO)$_3$(py)]$^+$, the highest occupied molecular orbital contained 50% or greater Re$_d$ character along with ~20% contributions each from CO and Cl for [Re(bpy)(CO)$_3$Cl] and ~20% contributions from CO for [Re(bpy)(CO)$_3$(py)]$^+$. The lowest unoccupied molecular orbitals consisted of 80% or greater diimine ligand $\pi^*$ character in both cases. Thus the lowest energy optical transition was assigned as a metal-ligand-to-ligand charge transfer transition (MLLCT).[41]
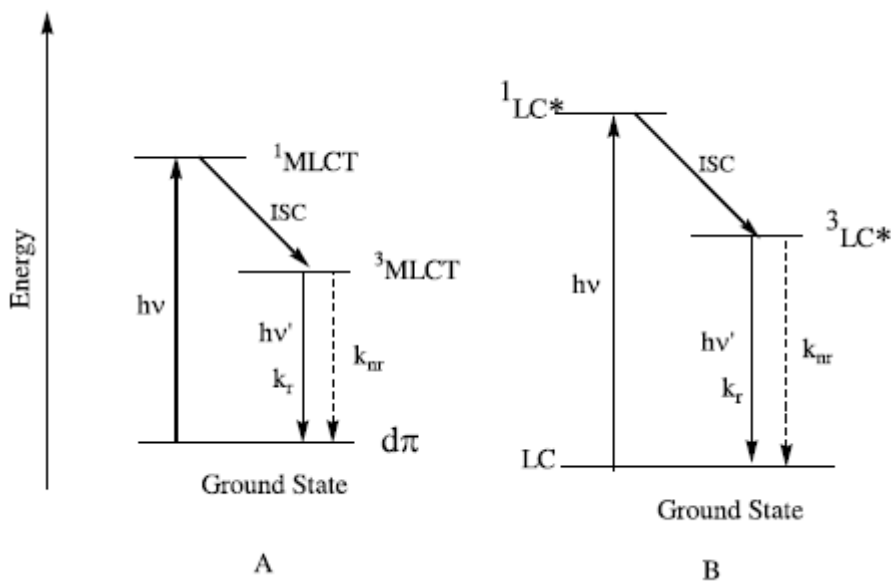
Figure 9: Jablonski Diagrams for [Re(diimine)(CO)$_3$L] Complexes: **A** MLCT Model; **B** Ligand-Centered Model

Re(I) complexes have been employed for various applications, for instance carbonyl derivatives were used as probes in biological systems. [Re(diimine)(CO)$_3$L$a,b,c$]$^+$ complexes, where L$a,b,c$ are shown in Figure 10; diimine = phen, 3,4,7,8-(CH$_3$)4-phen, 2,9-(CH$_3$)$_2$-4,7-Ph$_2$phen and dipyrido[3,2-f:2,3-h]quinoxaline, contain the ligand L with the coordinating pyridine linked to biotin. Biotin binds to the protein avidin and upon binding enhanced the emission of the rhenium chromophore; hence, the complex served as a recorder for the presence of avidin.[42]
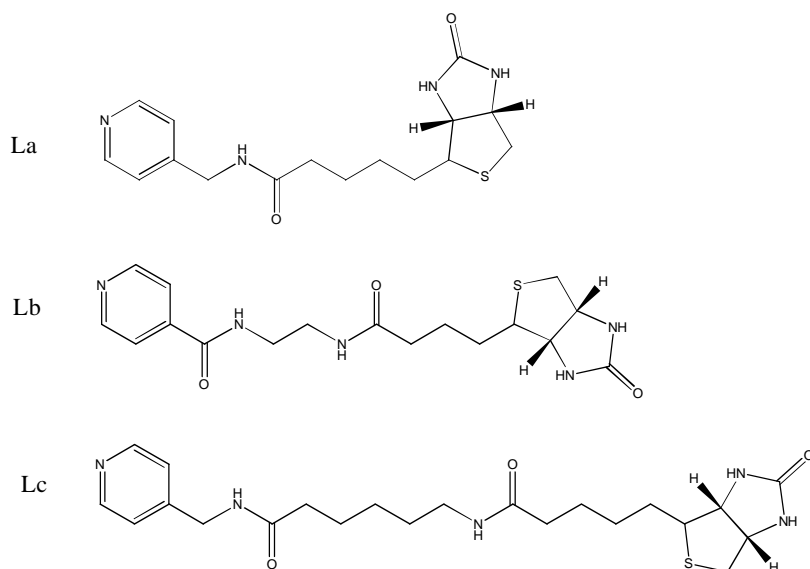


Figure 10: Pyridine ligands

Although not necessarily involving photoactive complexes, a variety of approaches have been used to design radiopharmaceuticals for imaging central nervous system receptors. Ultimately, such

studies are an important extension of photochemical applications of Re (I) complexes since the design of radiopharmaceuticals that luminescence (for detection) and are therapeutic (by radiation) is a topic of current interest.[43] Re (I) complexes are usually studied prior to the preparation of Tc (VII) derivatives since their chemistries are so similar, although the use of Re isotopes for therapy is also possible.

Rhenium complexes have been used as a pH sensor, as the emitting layer in organic light emitting diodes (OLEDs) and exploiting their luminescence sensing, was also used for anion recognition.[44]

## *2.3 - Europium (III) and Cerium (III)*

Complexes of rare earth metals with organic ligands present an astounding class of emissive materials for OLEDs due to peculiarities of their luminescence properties.[45] As defined by IUPAC, rare earth metals are a collection of seventeen chemical elements in the periodic table, namely scandium, yttrium, and the fifteen lanthanides.[46] Most of the studies on these electroluminescent complexes have been limited to lanthanide compounds thanks to their unique ability to emit narrow line-like emission bands in the visible and near-infrared spectral regions. Their most stable oxidation state is +3, particularly in water, with a $[Xe]4f\,n$ configuration. These properties of $Ln^{3+}$ ions are permitted by the existence of 4f electrons which are efficiently shielded from external influences by the overlaying $5s^2$ and $5p^6$ orbitals. It is well known that the ligands in the first and second coordination sphere perturb the electronic configurations of the lanthanide ions only to a limited extent. The f–f transitions are parity and, sometimes, spin forbidden and consist mainly of weak magnetic dipole and induced electric dipole parts. The intensities of the first type are practically not influenced by the coordinating surroundings of the ion, whereas those of the second one are quite sensitive to it.[47] Therefore, selection of organic ligands for luminescent lanthanide complexes is particularly important, considering that they can coordinate to a variety of ligands with different coordination numbers, most typically eight to ten. In most cases this role is played by O-O or O-N chelating groups with extended conjugated systems. In such compounds the luminescence of lanthanide ions is explained commonly by the ligand-to-metal energy transfer from the lowest triplet level of the ligands to a resonance level of the lanthanide ion.[48] The simplified diagram in Figure 11 shows the energy migration paths in rare earth complexes. The metallo-complex may undergo a radiative transition from the singlet state $S_1$ to the ground state $S_0$ (molecular fluorescence). The excited $S_1$ state can be non-radiatively deactivated to the triplet $T_1$ and then radiatively to the ground state $S_0$ (molecular phosphorescence). The complex may undergo non-radiative transitions from the singlet or triplet states to an excited state of the metal ion (in the

case of lanthanide). Additionally, recent theoretical computations indicate that the ligand-to-metal energy transfers also include the ligand-to-metal charge transfer (LMCT).[49] Due to the competition of radiative and non-radiative transitions, it is possible to observe some combination of ligand- and metal-centered emissions.
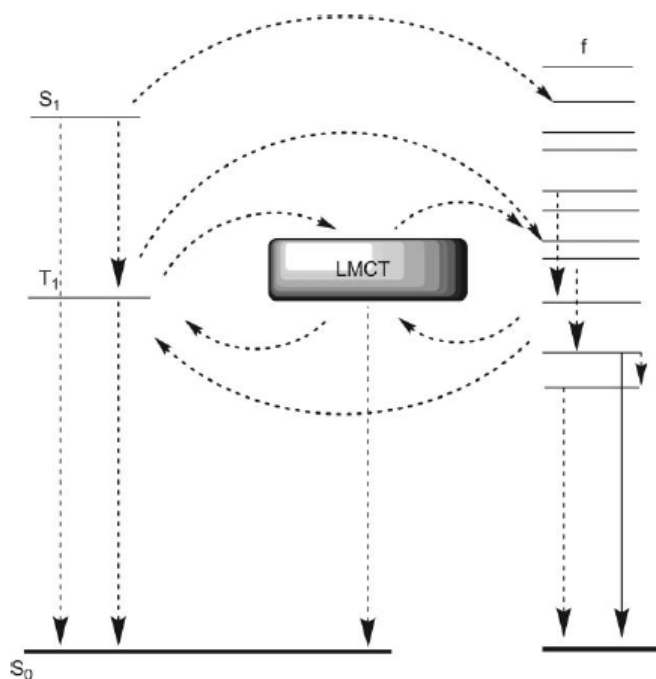


Figure 11: Simplified diagram of energy migration paths.

In general, for rare earth compounds three main types of electronic transitions are considered. The first one is the metal-centered f–f transitions of the lanthanide ions. The block of these metals can be divided in two parts: fluorescent (*e.g.* Pr(III), Nd(III), Ho(III), Er(III) andYb(III) emitting in the NIR region), and phosphorescent ones (*e.g.* orange Sm(III), red Eu(III), ultraviolet Gd(III), green Tb(III), yellow Dy(III) and blue Tm(III)). The second one, also involving metal-centered f–d transitions, interests the promotion of a 4f electron into the 5d subshell, meaning all transitions become spin-allowed. Generally, they occur at energies which are much higher than those of f–f transitions. Their energy depends largely upon the metal environment because the 5d orbitals are external and interact directly with the ligand orbitals.[50] In addition, it has been pointed out (for $Ce^{3+}$ complexes) that the metal-centered f–d transition can be viewed also as a metal-to-ligand charge transfer (MLCT) transition.[51] Finally, ligand-centered or charge-transfer transitions represent the third type of electronic conversions. As a general rule, LMCT states are considered for the complexes of lanthanide ions, having high electron affinity, with organic ligands, which have low oxidation potentials. These transitions are allowed and as the p* ligand orbital is mainly delocalized over the acceptor ligand, the charge-transfer states may cause minimum structural distortion and

facilitate the energy transfer efficiency from ligands to the metal ion. An intermixture of various transitions in the complexes with complicated molecular structures is common and can play a crucial role for good luminescence efficiency.

The relative ordering of these transitions may be changed in several ways: by the selection of the metal, by the choice and modification of the ligand, or by changing the geometry of the complex. Generally speaking, to achieve an efficient emission, a rare earth ion needs a carefully tailored environment consisting of organic ligands that simultaneously provide a rigid and protective coordination shell for minimizing non-radiative deactivation and ensuring effective population to the metal ion excited states through the energy transfer.

As explained above, the lanthanide f–f transitions (electric dipole transitions) are "Laporte-forbidden", therefore, the generation of fluorescence from the lanthanide ion can be difficult. Direct excitation of the lanthanide ion can be achieved, but this only becomes practical with the use of lasers or at high ion concentrations. However, such inherent disadvantages can be overcome by using sensitization techniques[52] (Figure 12). These involve the use of indirect excitation of the lanthanide ion with a sensitizing chromophore (often termed as an antenna), commonly an aromatic system,[53] usually through an intramolecular energy transfer process.[54] The antenna needs to be in close proximity to the lanthanide ion, therefore, generally, a ligand containing an antenna directly coordinates the lanthanide ion.
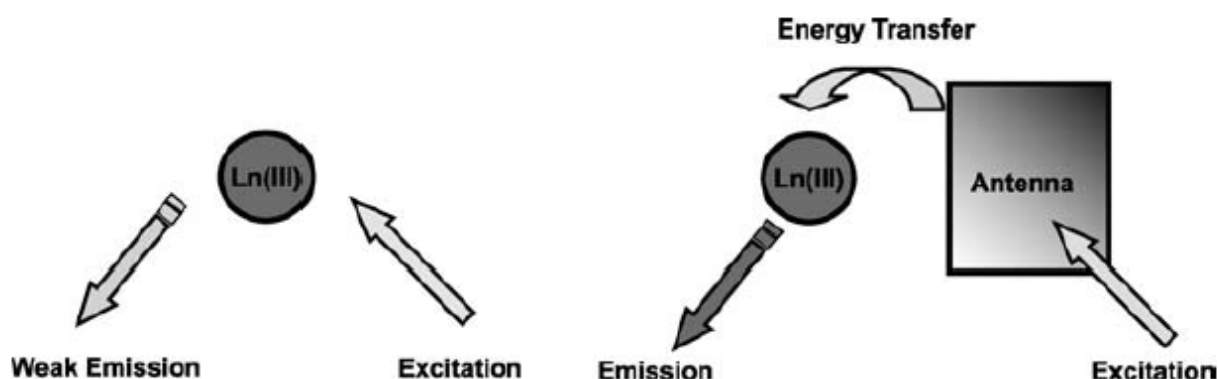


Figure 12: Sensitisation techniques

The presence of coordinated O–H, N–H and C–H oscillators (also in the solvent), associated with unsaturated complexes, has significant implications because non-radiative quenching of the lanthanide excited states can occur through vibrational harmonics of these oscillators.

The hard Lewis acidity of the lanthanide ions results into a specific preference towards ligands incorporating atoms that can act as hard Lewis bases or can be easily polarized. Therefore, combinations of amines and carboxylic groups are commonly used in lanthanide complexation.[55] In

15

order to fully coordinate a lanthanide ion, either a high-level polydentate ligand such as a cryptate (Figure 13a) or a number of smaller ligands (such as 1,3-diketones, Figure 13b) working in cooperation are required. Both (a) and (b) are two of the simplest coordination complexes possible for lanthanide ions. In both cases there are no antennae present. However, the number of bound solvent molecules is decreased considerably from nine (for lanthanide ions in solution) to one or two for the cryptate and three for the 1,3-diketone complexes.



(a)                                    (b)
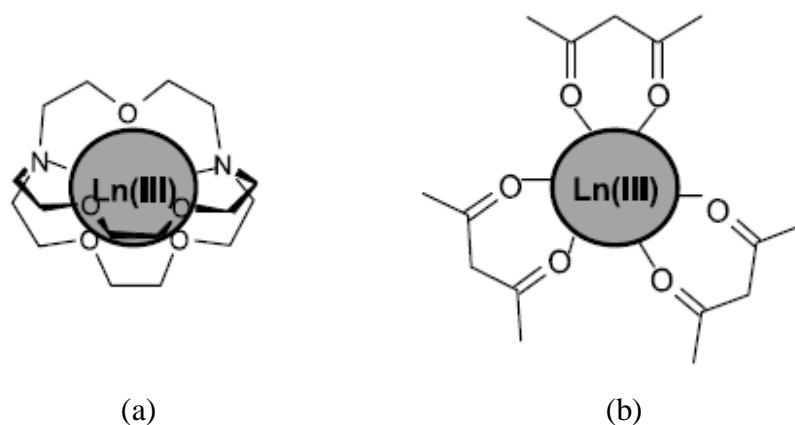
Figure 13: Lanthanide complexes

There are many examples of "podand-type" ligands[56] and the bypyridyl (bpy)-based podand ligand has been used to form lanthanide complexes. These can be considered as ligands with integrated antenna as shown in Figure 14.
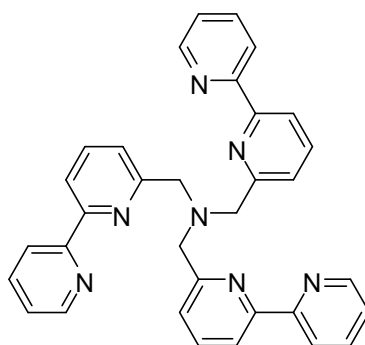


Figure 14. An example of a "podand-type" ligand

Considering the energy level schemes, it can be assumed that there are only three trivalent lanthanides ($Ce^{3+}$, $Pr^{3+}$, $Nd^{3+}$) for which allowed f–d emission can be observed. This three metals exhibit a broad emission band in the UV-vis region, but really only $Ce^{3+}$ is characterized by strong f–d transitions. This indicates that the overlap between the 4f$n$-1 core and the delocalized 5d electron decreases with $n$. Generally, the emission of $Ce^{3+}$ ion occurs in the UV and/or in the blue spectral region and can be red-shifted depending on the ligand environment.[57] However, in some

cases the organic ligands in cerium complexes quench the luminescence of metal ion, and this is why the design of efficient electroluminescent cerium complexes is a very complicated task and examples of such compounds are limited.

Europium complexes have attracted considerable attention as red emitting materials, due to the strong metal-centered luminescence of $Eu^{3+}$. This emission is explained by electronic transitions from the lowest excited state, $5D_0$, to the ground state manifold $7FJ$ ($J = 6–0$) level. The most intense emission line corresponding to $5D_0 \rightarrow 7F_2$ is observed at 614 nm.

A large variety of europium complexes have been synthesized during the last decade with the aim of exploiting their electroluminescent properties. It is well known that the simple homoleptic $\beta$-diketonate europium complexes show a highly efficient photoluminescence, but due to the poor carrier transport ability they do not satisfy the requirements for OLED materials. To improve these properties, two strategies have been developed: (i) introduction of charge transport substituents in the ligands and (ii) introduction of ancillary ligands enhancing an emission of a metal atom.

In recent years a few examples of mixed f–d metal complex have been developed. One of the driving forces for such work has been that the excited states of NIR-emitting ions such as Yb(III), Eb(III), and Nd(III) in particular, can be formed by excitation in the visible region.[58] As many transition metal complexes often have strong MLCT absorption bands in the visible region, then these are ideal as antennae for the population of these ions. This has been elegantly shown by many researchers.[59] This is of particular interest as it opens up new potentials for sensing of biological systems in the NIR. Moreover, the photophysics of transition metal complexes is well established and explored, and many varieties of ligands are available that can be used to construct mixed f–d metal complex (Figure 15).
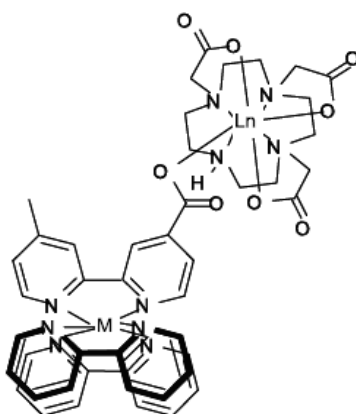


Figure 15: Examples of mixed metal complexes

In an analogues manner, other examples of such mixed complex have been developed.[60,61] For instance, De Cola et al.[61] developed a the system consisting in a heterotrimetallic complex, in which the excitation of the Eu(III) occurs via energy transfer from a Ir(III)-based metal-based antenna.

Interestingly, the emission of almost-white light can be observed if there is only partial energy transfer fromthe excited Ir(III)-based chromophore. If this occurs, the Eu(III) red emission combined with the residual blue emission from the iridium complex gives rise to a global white light emission (Figure 16).
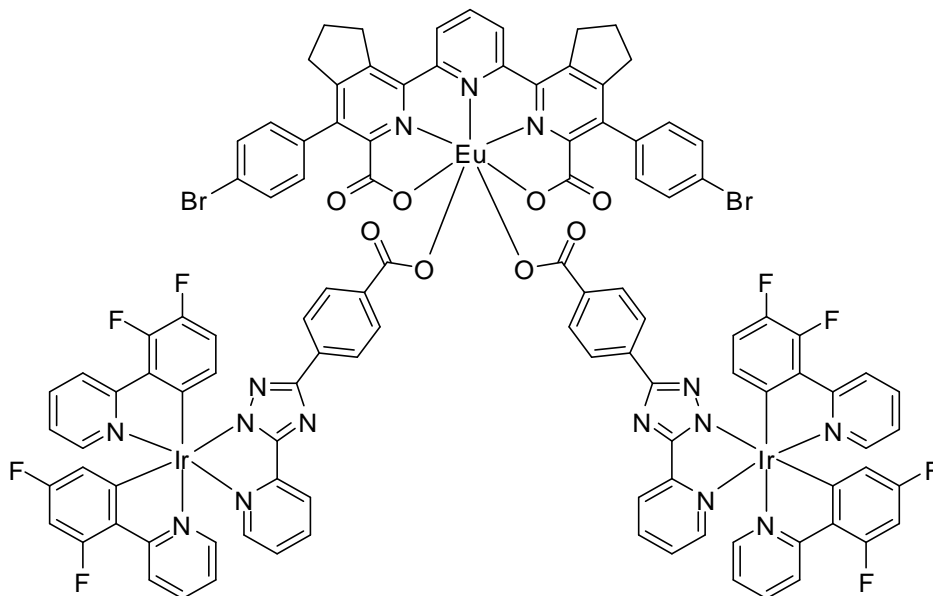


Figure 16: White light emitting mixed complex

## 2.4 - Zinc (II)

No other metal has as many functions in living organisms as zinc.[62] In one of the early reviews on its biochemistry Vallee[63] noted that it occurs in all six groups of the IUBMB (International Union of Biochemistry and Molecular Biology) enzyme classification. The number of enzymes known to contain zinc in the active center now exceeds 1000.[64] In mid 2007 the Brookhaven protein data bank lists some 40 000 structures of proteins, out of which almost 5000 contain zinc, and it has been found that 3% of the human genome contain the code for zinc finger proteins.[65] All this despite the fact that the zinc ion neither possesses color, magnetism or redox properties, nor provides stability or inertness to its complexes: all these characteristic have made zinc considered the "boring element" in teaching and research for decades. In the majority of cases the role of zinc ions in proteins is structural, comparable to that of hydrogen bonds.

The uniqueness of zinc is well-hidden. Unlike iron, present in the blood or in the meat, we do not see it. Unlike cobalt, nickel, copper or cadmium, we can hardly poison ourselves with its compounds. It is only appropriate in this scenario that one has a hard time finding zinc in the textbooks. Thinking about this, one can concluded that when there are no characteristic features leading the way to the unique properties of zinc in biology, their absence may be the clue. Namely,

the non-properties of zinc are the secret of its success. Whether zinc with its filled d shell is a transition metal or not may be a semantic question, but of course its properties resulting from the filled d shell are essential. A rather trivial consequence of the electronic configuration of zinc and hence its chemical properties is its bioavailability. Definitely the redox inertness and the hard-soft properties of zinc play an important role. The intermediate nature of zinc in this respect, not really hard and not really soft, certainly makes it suitable to be bound to and to act in all available donor environments in living organisms.

These non-properties make zinc what it is: available, mobile and versatile.

Recently, there has been growing interest in the photochemistry of luminescent Zn(II) coordination complexes in the form on monomeric, multinuclear, and polymeric species.[66] The zinc(II) ion can be used to assemble different units and build up long rod-like linear structures which can be considered coordination polymers.[67] Zinc complexes with nitrogen ligands display interesting optical properties for LED devices and sensors,[68] but also for application in imaging techniques[69] and as fluorescent sensors in biological systems.[70]

As colourless $d^{10}$ metal ion, Zn(II) can assume coordination geometries from tetrahedral through trigonal-bipyramidal and square-pyramidal to octahedral, hence suitable for the construction of luminescent coordination complexes. In fact, some of the monomeric or multinuclear complexes are electroluminescent materials and used in organic light-emitting diodes (OLEDs).

A μ4-oxo-bridged tetranuclear Zn(II) complex, $Zn_4O(prp)_6$, prp=1$H$-pyrrolo[2,3-b]pyridine,[71] was suggested to be one of the white electroluminescent materials which may be used in OLEDs. In particular, research on Zn (II) complexes as emitting as well as electron transport materials has recently improved advanced.[72] The electron transport layer plays an important role in transporting electrons and blocking holes, thus preventing holes from moving into the electrode without recombining with electrons.[73]

Moreover Zn(II) ion is highly promising with respect to cost and toxicity, therefore a variety of systems with high photoluminescence (PL) quantum yields and electroluminescence performance has already been synthesized.[74] Zn(II) has received attention because of its ability to enhance the emission of the ligands and tune some of the properties[67] (Figure 17). Due to the $d^{10}$ electron configuration of Zn(II) ions, metal-to-ligand charge-transfer (MLCT) processes do not occur in such systems.[75] Only Intraligand Charge Transfer (ILCT) is observed.
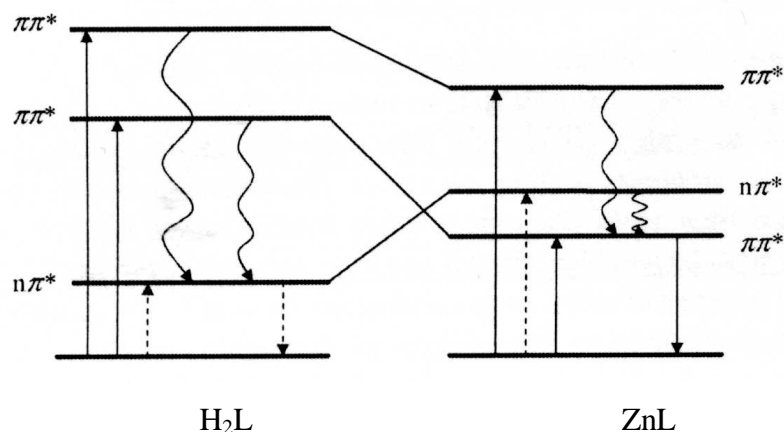
Figure 17: Qualitative states diagram of $H_2L$ and $ZnL$ compounds. Solid line: allowed radiative transitions; dotted line: forbidden (or weak) transitions; curves: non radiative decays.

After the ligand coordinates with Zn(II) ion, as a result of perturbation of the lowest unoccupied molecular orbital (LUMO), the absorption maximum at the longest wavelength is shifted bathochromically, compared to the free ligands. Since MLCT has to be excluded for Zn(II) because of its $d^{10}$ electron configuration, this shift can be explained by ILCT processes.[76] After complexation of the ligand with Zn(II), the emission is usually red-shifted and strongly increases in intensity.[77] Several reports on the structure, photoluminescence and theoretical studies of Zn(II) coordination complexes have been published recently, exploring the relationship between the structure and the photoluminescence properties. These large shifts suggest an enhancement of the $\pi$-conjugation due to the bidentate complexation of the ligand to the $d^{10}$ spectroscopically inactive $Zn^{2+}$ ion, giving rise to a decrease in the $\pi^*$-$\pi$ energy gap of the ligand molecular orbitals responsible for the transitions.[78] The bidentate coordination imposes a planar conformation in the ligands by restricting the rotation about the C bonds.

# 3) Luminescence and luminescent materials

## 3.1- Luminescence

The emission of light is a physical phenomenon which occurs in response to an external stress, which may be in the form of thermal, electrical or chemical energy. This phenomenon is called, in general, luminescence, and, depending on the nature of the external stimulus, it assumes different designations, as reported in Table 1:

| Name | Stimulus |
|---|---|
| Bioluminescence | Enzymatic reaction |
| Chemiluminescence | Chemical Reaction |
| Electrochemiluminescence | Chemical reaction electrochemically induced |
| Electroluminescence | Electricity |
| Photoluminescence | Photons |
| Radioluminescence | Ionizing |
| Sonoluminescence | Sound Waves |
| Thermoluminescence | High temperature |
| Triboluminescence | Mechanical efforts |

Table 1. Types of luminescence according to the excitation source.

The most well-known phenomenon is the photoluminescence and, in this case, the substance able to emit light after absorbing the luminous radiation is called fluorophore.

According to the Boltzmann distribution, at room temperature the population of higher electronic levels is negligible compared to the one of the lowest energy level, the ground state. For this reason, it is assumed that almost all of the molecules are in the lower electronic state, with orbitals occupied by pairs of electrons with paired spins (antiparallel), in order to have total spin equal to 0 and multiplicity equal to 1 (singlet ground state $S_0$). When subjected to excitation, most of the molecules are promoted from the $S_0$ state to an $S_n$ electronic excited state. Regardless of the type of energy provided, the excited state is not stable, therefore exited molecules will return to the ground state through radiative or non-radiative decay mechanisms. The non-radiative decay mechanisms take place without the emission of photons and consist mainly of the following processes:

- *vibrational relaxation*: the excited molecule transfers vibrational energy through collisions with the surrounding molecules of solvent (time $\approx 10^{-12}$ s); this mechanism is favored at high temperatures;
- *internal conversion*: transitions between two electronic states of the same multiplicity (time $\approx 10^{-13}$ s);
- *conversion between systems (intersystem crossing)*: transition between two electronic states of different multiplicity, for example from singlet to triplet (time $\approx 10^{-8}$ s).

The radiative decays occur as emission of photons, and are named in the following ways:
- *fluorescence*: transition from the lowest excited singlet state $S_1$ to the ground state $S_0$ (time $\approx 10^{-9}$ s);
- *phosphorescence*: transition from the triplet lowest excited state $T_1$ to the singlet ground state $S_0$ (time $\approx 10^{-6}$ s);
- *radiation of resonance*: emission with a frequency equal to that absorbed. Occurs only for low pressure gas (time $\approx 10^{-8}$ s).

Observing the specific lifetime of the processes listed above, it can be noted that the non-radiative mechanisms are always competing with the radiative ones, so that the latter may not be displayed at all. This can be due to several factors such as, for example, the great flexibility of the molecular structure, the high temperature, which favors the collisions, or the presence of a solvent able to absorb the energy of the excited molecule.[79] Accordingly, the fluorescence or phosphorescence phenomena are rarely observed, and most of the substances does not present these phenomena at all. The Jabloski diagram is the best way to summarize the above listed mechanisms[80] (Figure 18).

Generally, a molecule excited to a $S_n$ state decays to the excited state $S_1$ (the lowest of the excited states) through internal conversion.[81] Therefore, the fluorescence can be observed only for the decay from $S_1$ to $S_0$,[82] but remaining in competition with the internal conversion.
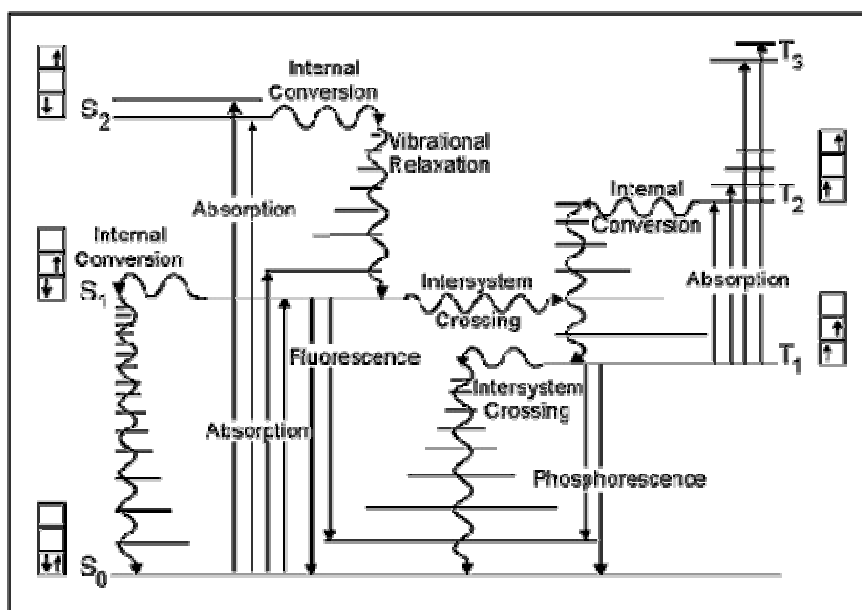
Figure 18. The Jablonski diagram.

The phosphorescence emission occurs only when the intersystem crossing is efficient enough to compete with other mechanisms, allowing the triplet states to become populated, because a transition with a change of spin would not be permitted by the selection rules. Furthermore, on the basis of the maximum multiplicity principle, the triplet states have lower energies of the corresponding singlet states, therefore the phosphorescence emission is observed at longer wavelengths than fluorescence.

A further mechanism that can lead to the deactivation of an excited state is the quenching, which can be:

- *collisional quenching*: a bimolecular process that occurs when a fluorophore and a substance, said *quencher*, able to receive the excess energy possessed by the excited molecule, hit each other.;
- *static quenching*: occurs when a non-fluorescent fluorophore-quencher complex is formed;
- *self-quenching*: a phenomenon which occurs when molecules of the same fluorophore act as a quencher, or in the presence of substances that absorb at the wavelength of emission of the fluorophore.

In particular, the substance that can more easily cause the phenomenon of collisional quenching is molecular oxygen,[83] which has a triplet ground state at lower energy than the singlet state.

The ability of a given substance to emit is quantified with a magnitude, called quantum yield, which is calculated as the ratio of the energy emitted by radiation and the total absorbed energy:

$$\Phi = \frac{k_R}{k_R + k_{NR} + k_Q[Q]}$$

where $k_R$, $k_{NR}$ and $k_Q$ are the rate constants of radiative, non-radiative and quenching processes, respectively. It is evident that to maximize the fluorescence, the speed of the other processes that lead to deactivation of the excited state, i.e. the concentration of quencher, should be reduced as much as possible.

Another parameter which is evaluated in photophysical studies is the lifetime, also called decay time ($\tau$), which is the average time that the molecule spends in the excited state before decaying in a radiative way.

$$\tau = \frac{1}{k_R + k_{NR} + k_Q[Q]}$$

This parameter is essential for the evaluation of the possible applications of different luminescent compounds. The fluorescence and the phosphorescence are distinguished by their lifetime: the first has an average lifetime of the order of nanoseconds, while for the second the lifetimes are usually of the order of microseconds.

### 3.2 - Luminescent materials

Over recent years, materials with luminescent properties have attracted increasing interest thanks to their applications in science and technology. They are mainly used in devices such as light emitting OLEDs (Organic Light-Emitting Diodes) and LEECs (Light-emitting Electrochemical Cells), which is the next-generation technology used in computers, televisions and cell phones flat displays.[84,85]

In these devices, the electroluminescent layer usually consists of a semiconductor film of an organic compound able to emit light as a result of an electrical stimulus. This phenomenon is made possible by the presence of emitters (cationic or neutral), incorporated in the organic matrix.

In this context, it has been observed a significant increase of interest in the synthesis of transition metal complexes (Ir(III), Re(I), Ru(II), Pt(II) and Os(II)) with organic ligands;[86] the reason for such expansion can be attributed to their unique luminescent properties together with high photochemical and thermal stability and a potential internal quantum efficiency of 100%. These complexes are able to exploit the fluorescence emission from singlet excited states as well as the phosphorescence from triplet states, generated by a high spin-orbit coupling, typical of the elements belonging to the second and third transition series, which allows an efficient intersystem crossing.

In particular, Ir(III) complexes exhibit high electroluminescence,[87] electrochemical reversibility and synthetic versatility; in addition they are also characterized by an internal quantum efficiency higher than that shown by the other transition metals complexes,[88,89] which makes them ideal candidates for devices.

24

The luminescent Ir(III) complexes present an octahedral symmetry and can be divided into two categories:

• homoleptic: contains three identical cyclometallated ligands

• heteroleptic: contains two cyclometallated ligands and one ancillary ligand.

Despite the neutral complexes are the object of intense study by the scientific community, since they are the most common dopants used in OLEDs, recently electrically charged derivatives are receiving increasing attention for their applications in LEECs.[90,91,92]

A further reason since the iridium complexes are considered excellent candidates for forming bright materials resides in the possibility of easily tune the wavelength of the emitted radiation, by appropriately varying the ligands.[93,94,95] Indeed, it is possible to obtain stable and efficient emitters in the ranges of the three primary colors,[96] blue (450-470 nm), green (500-550 nm) and red (650-700 nm) (Figure 19), obtaining thus devices that emit throughout the visible spectrum.
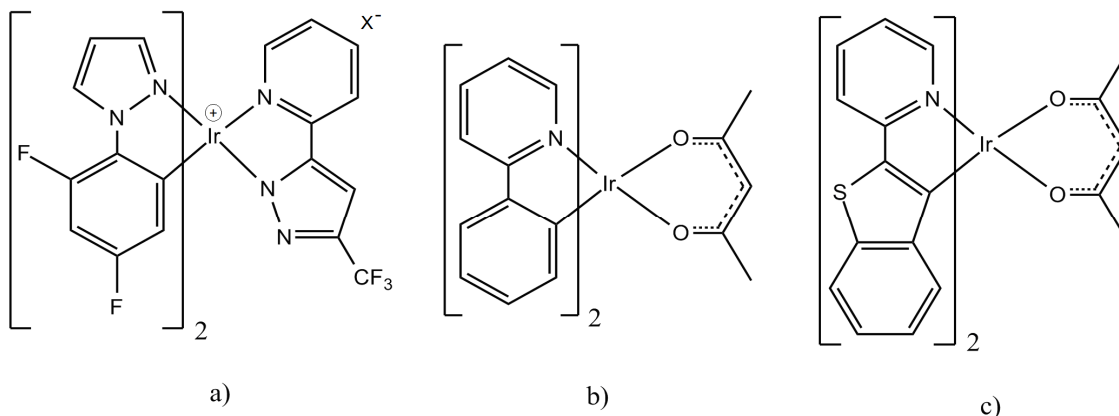


Figure 19: Blu (a), green (b) and red (c) emitting iridium complexes.

## 4) Purpose of the work

As illustrated in the previous sections, the synthesis of luminescent metal complexes is a very challenging task since they can be regarded as the starting point for a lot of different areas. Luminescent complexes, in fact, can be used for technological, industrial, medical and biological applications. They consist of two main parts: the central core of the complex, a metal atom, and organic ligands of various nature bonded to it.

During my PhD I worked with different metals having distinguishing intrinsic properties that make them different from each other and, in particular, more or less suitable for the different possible uses, considering the key strength of each metal.

For example, Iridium complexes show the best photophysical properties: generally, they have high quantum yields, very long lifetimes and possess easily tunable emissions throughout the visible range. On the other hand, Iridium is very expensive (IrCl$_3$· x H$_2$O, 99.9%, 258.5 €/g, Sigma-Aldrich, 2013) and scarcely available, and therefore its use for industrial purposes is not practicable. The aim of my work concerning this metal was, therefore, to synthesize ligands able not only to form luminescent complexes, but also able to add something to the final complex, increasing its properties, and therefore its possible practical uses. In detail, I synthesized new bifunctional ligands good to complex Iridium(III), but that at the same time, containing a functional group (FG) able to perform an additional purpose, i.e. to bio-conjugate particular proteins or suitable to co-polymerize, forming luminescent polymers (Figure20).
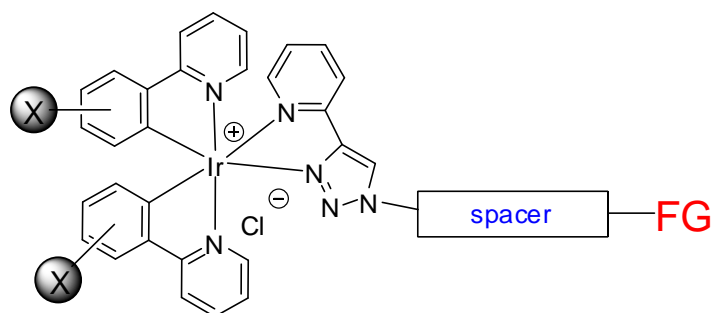


Figure 20: Functionalized Iridium complexes.

In addition, exploiting the iridium properties, new complexes emitting in the blue spectral region, color still difficult to be achieved by reported iridium complexes, were synthesized.

Since Re(I) derivatives have been reported to be suitable as probes in biological system, even if the photophysical properties of its complexes are less impressive than those of Iridium ones, and the use of Re(I) reduces the costs (ReCO$_5$Br, 98%, 115 euro/g Strem Chemicals), the synthesized

bifunctional ligands containing a pyridine-triazole and a biotin unit were employed to obtain new Re(I) complexes able to recognize a specific protein (Figure21).
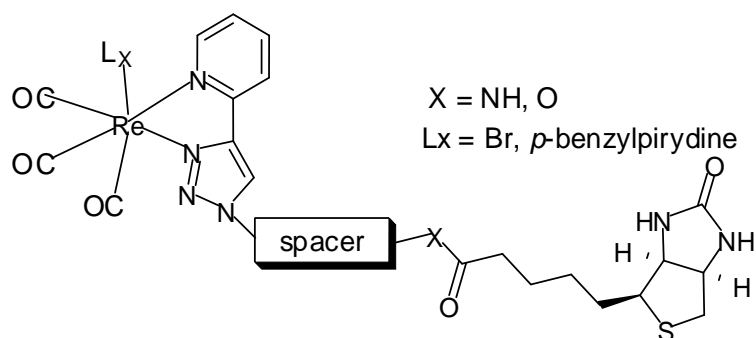


Figure 21: Biotinylated Rhenium complexes

Europium and Cerium belong to the family of lanthanides, and they show their own characteristic emissions when linked to specific ligands. Eu(III) and Ce(III) salts I used are quite cheap (average cost of about 20/25 euro/g) and relatively non-toxic compared to other heavy metals. The aim of my work was to design and synthesize new ligands able to form stable complexes with these two metals, in order to obtain an emission in the range of visible light. Furthermore, owing to the high coordination number displayed by lanthanides, these ligands had to be sufficiently chelating to protect the central metal atom by external agents such as moisture or solvents, which can turn off the final complex emission.

Finally, my work focused on the synthesis of ligands able to link Zinc. Zinc is a low cost ($Zn(ClO_4)_2 \cdot 6H_2O$, 39.4 euro/100g Sigma-Aldrich) and especially non-toxic "green" metal. Zinc has not its own emission, but when it sticks to ligands, it increases their photophysical properties, forming luminescent complexes, that can be used for many purposes.

Therefore I plan to synthesize organic derivatives able to link the Zinc atom through a terpyridine unit, which already possessed an emission thanks to the presence of other many chromophoric groups, such as carbazole (Figure 22).
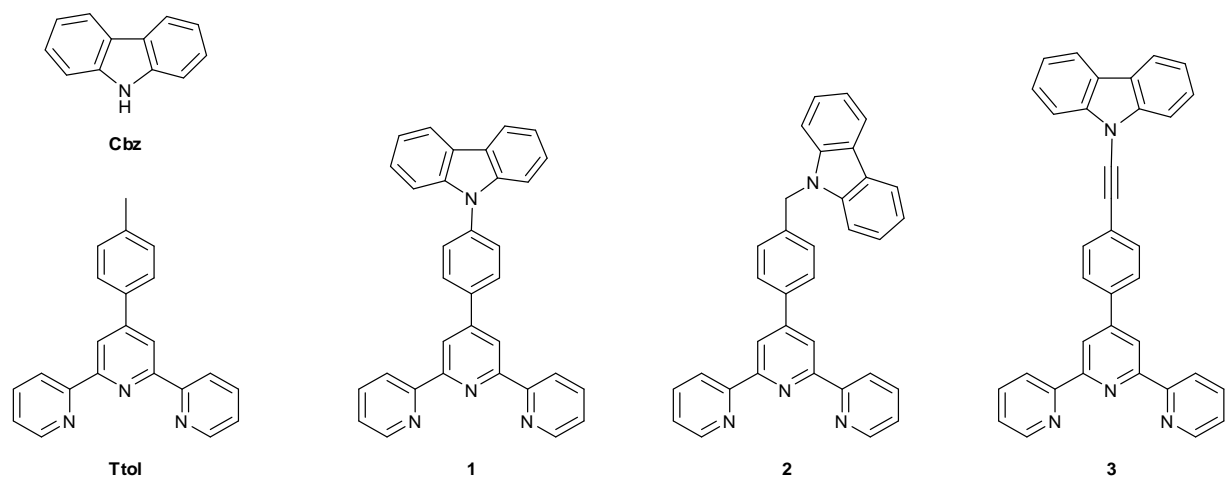
Figure 22: Carbazole-terpyridine derivatives.

# 5) Bibliography

[1] L. Flamigni, A. Barbieri, C. Sabatini, B. Ventura, F. Barigaletti, *Top Curr Chem* **2007**, *281*, 143.

[2] T.J. Meyer, *Acc. Chem. Res.* **1978**, *11*, 94.

[3] B. Schmid, F.O. Garces, R.J. Watts, *Inorg. Chem.* **1994**, *32*, 9.

[4] (a) K.A. Belmore, R.A. Vanderpool, J.C. Tsai, M.A. Khan, K.M. Nicholas, *J. Am.Chem.Soc.* **1988**, *110*, 2004. (b) N.D. Silavwe, A.S. Goldman, R. Ritter, D.R. Tyler, *Inorg. Chem.* **1989**, *28*, 1231.

[5] K.A. King, P.J. Spellane, R.J. Watts, *J. Am. Chem. Soc.* **1985**, *107*, 1431.

[6] VW-W. Yam, C.C. Ko, L.X. Wu, KM.C. Wong, K.K. Cheung, *Organometallics* **2000**, *19*, 1820.

[7] V. Amendola, D. Bacchilega, I. Costa, L. Gianelli, M. Montalti, P. Pallavicini, A. Perotti, L. Prodi, N. Zaccheroni, *J Photochem Photobiol A: Chem* **2003**, *159*, 249.

[8] G. Stochel, A. Wanat, E. Kuli´s, Z, Stasicka, *Coord Chem Rev* **1998**, *171*, 203.

[9] E. Toth, L. Burai, A.E. Merback, *Coord Chem Rev* **2001**, *216*, 363.

[10] S. Petoud, S.M. Cohen, J.C.G. Bünzli, K.N. Raymond, *J Am Chem Soc* **2003**, *125*, 13324.

[11] C. W. Tang, S. A. Van Slyke, *Appl. Phys. Lett.* **1987**, *51*, 913.

[12] C. W. Tang, S. A. Van Slyke, C. H. Chen, *J. Appl. Phys.* **1989**, *65*, 3610.

[13] M. A. Baldo, D. F. O'Brien, M. E. Thompson, S. R. Forrest, *Physical Review B*, **1999**, *60*, 14422.

[14] (a) C. W. Tang, *Inf. Disp.* **1996**, *10*, 16. (b) S. Sibley, M. E. Thompson, P. E. Burrows, S. R. Forrest, *"Optoelectronic Properties of Inorganic Complexes"*, Roundhill, D. M., Fakler, J. Eds.; Plenum Press: New York. (c) P. E. Burrows, G.Gu, V. Bulovic, S. R. Forrest, M. E. Thompson, *IEEE Trans. Electron. Dev.* **1997**, *44*, 1188.

[15] T. Justel, *Luminescence* (Eds.: C. Ronda), Wiley-VCH, Weinheim, **2008**, 179 – 190.

[16] V. Smil, *Creating the Twentieth Century: Technical Innovations of 1867 – 1914 and Their Lasting Impact*, Oxford University Press, Oxford, **2005**.

[17] R. D. Costa, E. Orti, H. J. Bolink, F. Monti, G. Accorsi, N. Armaroli, *Angew. Chem. Int. Ed.* **2012**, *51*, 8178 – 8211.

[18] J. Brox, *Brilliant: The Evolution of Artificial Light*, Houghton Mifflin Harcourt, New York, **2010**.

[19] International Energy Agency, Light's Labour's Lost-Policies for Energy-Efficient Lighting, http://www.iea.org/, 2006.

[20] G. Zissis, S. Kitsinelis, *J. Phys. D* **2009**, *42*, 173001.

[21] C. J. Humphreys, *MRS Bull.* **2008**, *33*, 459 – 470.

[22] A. Juris, V. Balzani, F. Barigelletti, S. Campagna, P. Belser, A. Von Zelewsky, Coord. *Chem. Rev.* **1988**, *84*, 85 – 277.

[23] V. Balzani, G. Bergamini, S. Campagna, F. Puntoriero, *Top. Curr. Chem.* **2007**, *280*, 1 – 36.

[24] R. Englman, J. Jortner, *Mol. Phys.* **1970**, *18*, 145 – 164.

[25] E. M. Kober, J. V. Caspar, B. P. Sullivan, T. J. Meyer, *Inorg. Chem.* **1988**, *27*, 4587 – 4598.

[26] S. Lamansky, P. Djurovich, D. Murphy, F. Abdel-Razzaq, H.-E. Lee, C. Adachi, P. E. Burrows, S. R. Forrest, M. E. Thompson, *J. Am. Chem. Soc.* **2001**, *123*, 4304-4312.

[27] M. Nonoyama, *Bull. Chem. Soc. Jpn.* **1974**, *47*, 767 – 768.

[28] L. Flamigni, A. Barbieri, C. Sabatini, B. Ventura, F. Barigelletti, *Top. Curr. Chem.* **2007**, *281*, 143 – 203.

[29] K. A. King, P. J. Spellane, R. J. Watts, *J. Am. Chem. Soc.* **1985**, *107*, 1431 – 1432.

[30] L. He, J. Qiao, L. Duan, G. F. Dong, D. Q. Zhang, L. D. Wang, Y. Qiu, *Adv. Funct. Mater.* **2009**, *19*, 2950 – 2960.

[31] B. Schmid, F. O. Garces, R. J. Watts, *Inorg. Chem.* **1994**, *33*, 9–14.

[32] J. Li, P. I. Djurovich, B. D. Alleyne, I. Tsyba, N. N. Ho, R. Bau, M. E. Thompson, *Polyhedron* **2004**, *23*, 419 – 428.

[33] C. H. Yang, J. Beltran, V. Lemaur, J. Cornil, D. Hartmann, W. Sarfert, R. Frohlich, C. Bizzarri, L. De Cola, *Inorg. Chem.* **2010**, *49*, 9891 – 9901.

[34] G.L. Geoffroy, M.S. Wrighton, *Organometallic Photochemistry* Academic Press, New York, **1979**.

[35] H. Kunkley, A. Vogler, *Coord Chem Rev* **2000**, *200–202*, 991.

[36] R. A. Kirgan, B. P. Sullivan, D. P. Rillema, *Top. Curr. Chem.* **2007**, *281*, 45.

[37] A. Coleman, C. Brennan, J. G. Vos, M. T. Pryce, *Coord. Chem. Rev.* **2008**, *252*, 2585.

[38] J. M. Villegas, S. R. Stoyanov, W. Huang, D. P. Rillema, *Inorg. Chem.* **2005**, *44*, 2297.

[39] J. V. Caspar, T. J. J. Meyer, *Phys. Chem.* **1983**, *87*, 952.

[40] I.E. Pomestchenko, D.E. Poluansky, F.N. Castellano, *Inorg Chem* **2005**, *44*, 3412.

[41] S.R. Stoyanov, J.M. Villegas, A.J. Cruz, L.L. Lockyear, J.H. Reibenspies, D.P. Rillema, *J Chem Theory Comput* **2005**, *1*, 95.

[42] K.K-W. Lo, W-K. Hui, C.K. Chung, K.H.K. Tsang, T.K.M. Lee, C.K. Li, J.S.Y. Lau, D.C.M. Ng *Coord Chem Rev* **2006**, *250*, 1724.

[43] A.S. Del Negro, Z. Wang, C.J. Seliskar, W.R. Heineman, B.P. Sullivan, S.E. Hightower, T.L. Hubler, S.A. Bryan, *J. Am. Chem. Soc.* **2005**, *127*, 14978.

[44] P.D. Beer, V. Timoshenko, M. Maestri, P. Passaniti, V. Balzani, *Chem Commun* **1999**, 1755.

[45] J. Kido, Y. Okamoto, *Chem. Rev.*, 2002, **102**, 2357.

[46] *Nomenclature of InorganicChemistry: IUPACRecommendations 2005*, ed. N. G. Connelly and T. Damhus, RSC Publishing, Cambridge, **2005**.

[47] G. H. Dieke, *Spectra and Energy Levels of Rare-Earth Ions in Crystals*, Interscience, New York, **1968**; *Physics and Chemistry of luminescent materials*, ed. C. R. Ronda, L. E. Shea and A. M. Srivastava, Electrochem. Soc., **2000**; *Handbook on the Physics and Chemistry of Rare Earths Vol.37*, ed. K. Gschneidner Jr., J.-C. Bunzli and V. Pecharsky, North-Holland, **2007**.

[48] G. A. Crosby, R. E.Whan, R. M. Alire, *J. Chem. Phys.*, 1961, **34**, 743.

[49] W. M. Faustino, O. LM. Malta, G. F de Sa, *J. Chem. Phys.*, 2005, **122**, 054109.

[50] J.-C. G. Bunzli, *Acc. Chem. Res.*, 2006, **39**, 53.

[51] G. Blasse, *Prog. Solid State Chem.*, 1988, **18**, 79.

[52] Parker D, Williams JAG, *J Chem Soc Perkin Trans 2*, **1996**, 1581.

[53] S. Petoud, G. Muller, E.G. Moore, J. Xu, J. Sokolnicki, P.J. Riehl, U.N. Le, S.M. Cohen, K.N. Raymond, *J Am Chem Soc* **2007**, *129*, 77.

[54] D. Parker, *Coord Chem Rev* **2000**, *205*, 109.

[55] S. Petoud, S.M. Cohen, J-C.G. Bünzli, K.N. Raymond, *J Am Chem Soc* **2003**, *125*, 13324.

[56] V. Balzani, E. Berghmans, J.M. Lehn, N. Sabbatini, R .Terode, R. Ziessel, *Helv Chim Acta* **1990**, *73*, 2083.

[57] A. Vogler, H. Kunkely, *Inorg. Chim. Acta*, 2006, **359**, 4130.

[58] D. Imbert, M. Cantuel, J-C.G. Bünzli, C. Bernardinelli, C. Piguet, *J Am Chem Soc* **2003**, *125*, 15698.

[59] S.I. Klink, H.F. Keizer, C.J.M van Veggel, *Angew Chem Int Ed* **2000**, *39*, 4319.

[60] S. Faulkner, B.P. Burton-Pye, *Chem Commun* **2005**, 259.

[61] P. Coppo, M. Duati, V.N. Kozhevnikov, J.W. Hofstraat, L. De Cola, *Angew Chem Int Ed* **2005**, *44*, 1806.

[62] H. Vahrenkamp, *Dalton Trans.* **2007**, 4751-4759.

[63] B. L. Vallee, *Zinc Enzymes*, ed. T. G. Spiro,Wiley, New York, **1983**, 1–24.

[64] D. S. Auld, *Encylopedia of Inorganic Chemistry*, ed. R. B. King, Wiley, New York, 2nd edn, **2007**, *vol. IX*, 5885–5927.

[65] A.Klug, *J. Mol. Biol.*, **1999**, *293*, 215.

[66] S. L. Zheng, X. M. Chen, *Aust. J. Chem* **2004**, *57*, 703-712.

[67] A. D'Aléo, E. Cecchetto, L. De Cola, R. M. Williams, *Sensors* **2009**, *9*, 3604-3626.

[68] E. Kimura, T. Koike, *Chem. Soc. Re*V. **1998**, *27*, 179-184.

[69] (a) S. I. Pascu, P. A. Waghorn, T. D. Conry, H. M. Betts, J. R. Dilworth, G. C. Churchill, T. Pokrovska, M. Christlieb, F. I. Aigbirhio, J. E. Warren, *Dalton Trans.* **2007**, 4988–4997. (b) A. B. Descalzo, H.-J .Xu, Z.-L. Xue, K. Hoffmann, Z. Shen, M. G. Weller, X.-Z. You, K. Rurack, *Org. Lett.* **2008**, *10*, 1581–1584.

[70] (a) V. Buereau, *Inorg. Chem. Commun.* **2004**, *7*, 829–833. (b) Z.Wu, Q. Chen, G. Yang, C. Xiao, J. Liu, S. Yang, J. S. Ma, *Sens. Actuators, B* **2004**, *99*, 511–515.

[71] C. F. Lee, K. F. Khin, S. M. Peng, C. M. Che, *J. Chem Soc., Dalton Trans.* **1993**, 467.

[72] N. Du, Q. Mei, M. Lu, *Synth Metals* **2005**, *149*, 193.

[73] J. Kido, C. Ohtaki, K. Hongawa, K. Okuyama, K. Nagai, *Jpn. J. Appl. Phys.* **1993**, *32*, 917.

[74] A. Winter, C. Friebe, M. Chiper, U. S. Schubert, M. Presselt, B. Dietzek, M. Schmitt, J. Popp, *Chem. Phys. Chem* **2009**, *10*, 787 – 798.

[75] P.-T. Chou, Y. Chi, Chem. *Eur. J.* **2007**, *13*, 380–395.

[76] X. Y. Wang, A. Del Guerzo, R. H. Schmehl, *Chem. Commun.* **2002**, 2344–2345.

[77] Z. Popovic´, M. Busby, S. Huber, G. Calzaferri, L. De Cola, *Angew. Chem. Int. Ed.* **2007**, *46*, 8898 –8902.

[78] Q. Su, W. Gao, Q.-L. Wu, L. Ye, G.-H. Li, Y. Mu, *Eur. J. Inorg. Chem.* **2007**, 4268–4175.

[79] A. Safarzadeh-Amiri, M. Thompson, U. J. Krull, *J. Photochem. Photobiol A: Chem* **1989**, *47*, 299.

[80] P. Elumalai, P. Atkins, J. de Paula *Atkins' Physical Chemistry*, Oxford University Press: Oxford (**2002**).

[81] J. R. Lakowicz *Principles of Fluorescence Spectroscopy*, KA/PP: New York (**1999**).

[82] R. C. Evans, P. Douglas, C. J. Winscom *Coord. Chem. Rev.* **2006**, *250*, 2093.

[83] H. Kautsky *Trans. Faraday Soc.* **1939**, *35*, 216.

[84] C. W. Tang, S. A. VanSlyke, *Appl. Phys. Lett.* **1987**, *51*, 913.

[85] J. H. Burroughes, D. D. Bradley, A. R. Brown, R. N. Marks, K. Mackay, R. H. Friend, P. L. Burns, A. B. Holmes, *Nature* **1990**, *347*, 539.

[86] a) M. A. Baldo, D. F. O'Brien, Y. You, A. Shoustikov, S. Sibley, M. E. Thompson, S. R. Forrest, *Nature* **1998**, *395*, 151. b) C. W. Tang, S. A. VanSlyke, C. H. Chen, *J. Appl. Phys.* **1989**, *65*, 3610. c) J. S. Wilson, A. S. Dhoot, A. J. A. B. Seeley, M. S. Khan, A. Köhler, R. H. Friend, *Nature* **2001**, *413*, 828. d) I. Avilov, P. Minoofar, J. Cornil, L. De Cola, *J. Am. Chem. Soc.* **2007**, *129*, 8247-8258. e) H.-C. Su, F.-C. Fang, T.-Y. Hwu, H.-H. Hsieh, H.-F. Chen, G.-H. Lee, S.-M. Peng, K.-T. Wong, C.-C. Wu. *Adv. Funct. Mater.* **2007**, *17*, 1019–1027.

[87] J. I. Kim, I.-S. Shin, H. Kim, J.-K. Lee. *J. Am. Chem. Soc.* ***2005***, *127*, 1614-1615.

[88] M. A. Baldo, D. F. O'Brien, M. E. Thompson, S. R. Forrest *Phys. Rev. B* **1999**, *60*, 14422-14428.

[89] C. Adachi, M. A. Baldo, M. E. Thompson, S. R. Forrest *J. Appl.Phys.* **2001**, *90*, 5048-5051.

[90] D. Tordera, M. Delgado, E. Ortí, H. J. Bolink, J. Frey, M.. K. Nazeeruddin, E. Baranoff. *Chem. Mater.* **2012**, *24*, 1896−1903.

[91] L. He, L. Duan, J. Qiao, R. Wang, P. Wei, L. Wang, Y. Qiu. *Adv. Funct. Mater.* **2008**, *18*, 2123–2131.

[92] 18.   J. D. Slinker, A. A. Gorodetsky, M. S. Lowry, J. Wang, S. Parker, R. Rohl, S. Bernhard, G. G. Malliaras, *J. Am. Chem. Soc.* **2004**, *126*, 2763-2767.

[93] M. S. Lowry, S. Bernhard, *Chem. Eur. J.* **2006**, *12*, 7970 – 7977.

[94] P. Chou, Y. Chi *Chem. Eur. J.* **2007**, *13*, 380.

[95] A. B. Tamayo, S. Garon, T. Sajoto, P. I. Djurovich, I. M. Tsyba, R. Bau, M. E. Thompson, *Inorg. Chem.* **2005**, *84*, 85.

[96] H.-C. Su, H.-F. Chen, F.-C. Fang, C.-C. Liu, C.-C. Wu, K.-T. Wong, Y.-H. Liu, S.-M. Peng. *J. Am. Chem. Soc.* **2008**, *130*, 3413-3419.

# 6) Bifunctional ligands

## 6.1 - Luminescent Ir(III) methacrylic copolymers

In order to be employed in luminescent devices, the low molecular weight organometallic compounds are usually dispersed in a conductive polymer matrix, necessary to transfer the energy generated by an external electric field to the fluorophore, which, after photoinduced excitation, emits phosphorescent light. However, one of the limitations that can affect the performance of the devices is the high tendency of fluorophores to aggregate or to migrate toward the surface of the emissive layer, difficultly maintaining homogeneous dispersions, required to avoid quenching phenomena.

To overcome these problems, some examples of fluorophores covalently bonded to a polymer chain, and not simply dispersed, are reported in literature.[1-5] Many efforts have been made in order to obtain homogeneous, stable and easily processable material in which the fluorophore is also protected from oxygen and moisture. Among copolymers containing iridium complexes in the side chain, polyethylene oxide (PEO) and polystyrene (PS) functionalized with $Ir(ppy)_2(tpy)$ and $Ir(ppy\text{-}CHO)_2(tpy)$ (where ppy = 2-phenylpiridine, tpy = terpyridine, ppy-CHO = 4-(2-pyridyl) benzaldehyde) are reported.[1] These materials, prepared by spin-coating, emit yellow light; in addition the AFM analysis showed that these thin films are homogeneous and free from defects, such as crystal formation or holes, demonstrating their potentials for electroluminescent devices.

Examples of copolymers of *N*-vinyl carbazole and styrene, functionalized with various iridium (III) complexes,[3-6] are also reported. The photophysical characterization of these products showed an improvement of their performances, if compared to the ones containing the respective "free" complexes.

Part of the research carried out during my PhD lies in this framework. In fact, I plan to obtain a copolymer in which a photoactive iridium complex is covalently linked to a macromolecular chain and to study its luminescence properties in comparison with those of the corresponding low molecular weight emissive compound.

For this purpose, the bifunctionalized ligand 9-(4-(pyridin-2-yl)-1H-1,2,3-triazol-1-yl) undecyl methacrylate (**ptuma**) was synthesized. It is capable, on one hand, to chelate an Ir(III) unit forming a luminescent complex and, on the other hand, to polymerize in the presence of methyl methacrylate (MMA). This ligand was then coordinated to the metal center to obtain the Ir-luminescent monomer **Ir(ppy)₂(ptuma)Cl** which was subsequently copolymerized in the presence of different amounts of MMA, (Figure 3).
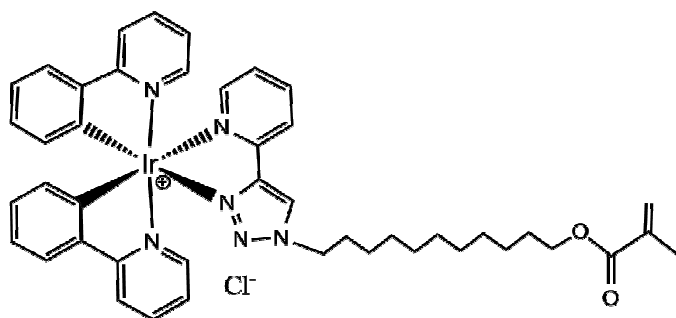
Figure 3: Ir(ppy)₂(ptuma)Cl monomer.

Easily filmable and transparent methacrylic copolymers were then obtained: they are characterized by variable composition and contain an Iridium complex **Poli[Ir(ppy)₂(ptuma)-*co*-MMA]** in the side chain (Figure 4). The presence of the covalent bond between the Ir(III) complex and the main chain ensures a homogenous dispersion of the fluorophores throughout the material, precluding it migration towards the surface and avoiding the formation of aggregates. Furthermore, by varying the amount of fluorophores, it is possible to minimize the quenching phenomenon caused by an eventual proximity of various complexes.
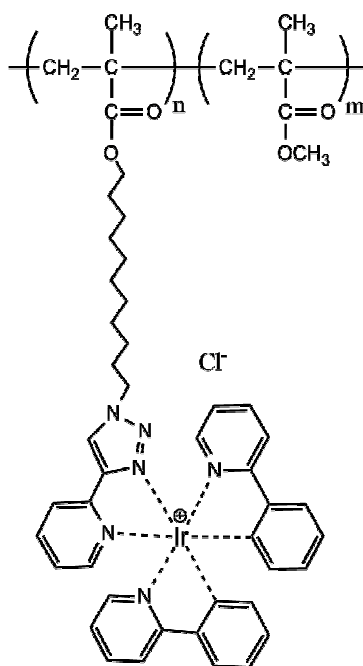


Figure 4: Copolymer Poli[Ir(ppy)₂(ptuma)-*co*-MMA] structure.

### 6.1.1 - Results and discussion

#### *6.1.1.1 -Ligand synthesis*

In detail, ligand **ptuma** was obtained following the synthetic strategy reported in Scheme 1. The azide derived from the reaction of 11-Br-undecanol **1** with NaN₃ underwent to a "click reaction" to form the 1,4-disubstituted 1,2,3-triazole **2** (85% yields from **1**) when treated with 2-alkynylpyridine under CuAAC conditions. The hydroxyl pyridine-triazole **2** was transformed into the methacrylate

ester **ptuma** by reaction with freshly distilled methacryloyl chloride in presence of hydroquinone to prevent possible polymerization side reactions.
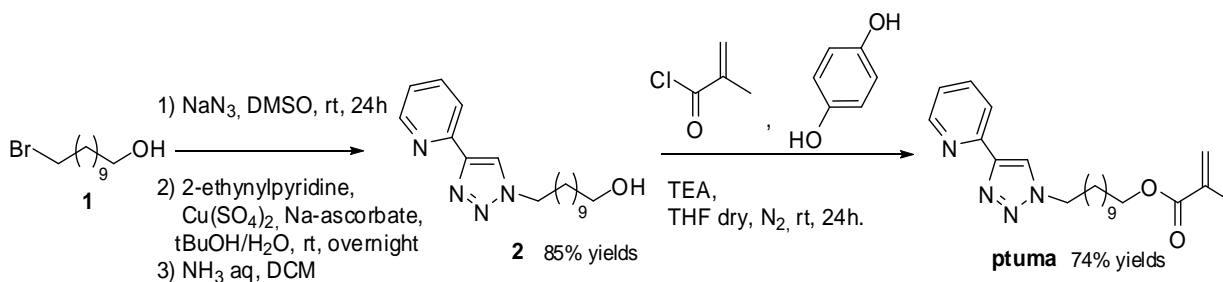


Scheme 1

### 6.1.1.2 – Ir(III)-monomer synthesis and characterization.

The monomer bis-(2-phenylpyridine)-9-(4-(pyridin-2-yl)-1H-1,2,3-triazol-1-yl)undecyl methacrylate-Ir(III), (**Ir(ppy)₂(ptuma)Cl**) was synthesized by reacting the iridium dimer {[(ppy)₂Ir(μ-Cl)]₂},[7, 8] with the ancillary ligand **ptuma** (Scheme 2).
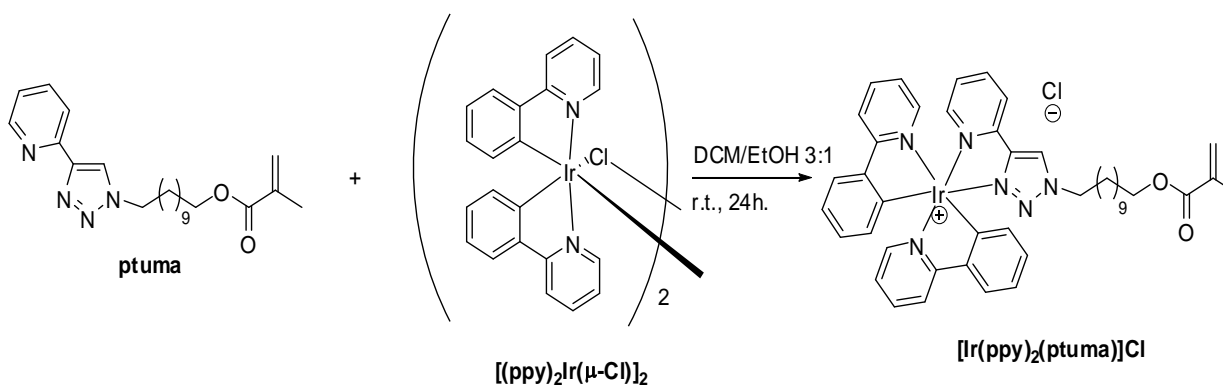


Scheme 2: Ir-monomer synthesis.

### 6.1.1.3 - Synthesis and characterization of polymeric compounds.

The Ir-monomer [**Ir(ppy)₂(ptuma)Cl**] was copolymerized through a radical reaction with methyl methacrylate (MMA) as a co-monomer in different molar ratios, in order to obtain copolymers with variable composition, as reported in Scheme 3. All polymerizations were conducted in a sealed vial at 60 °C, for 72 hours under vacuum, using dry THF as solvent (1 g of monomer in 15 mL of solvent) and 2-2'-azo-bis-isobutyronitrile (AIBN) (2% in weight with respect to the monomer) as a thermal initiator.
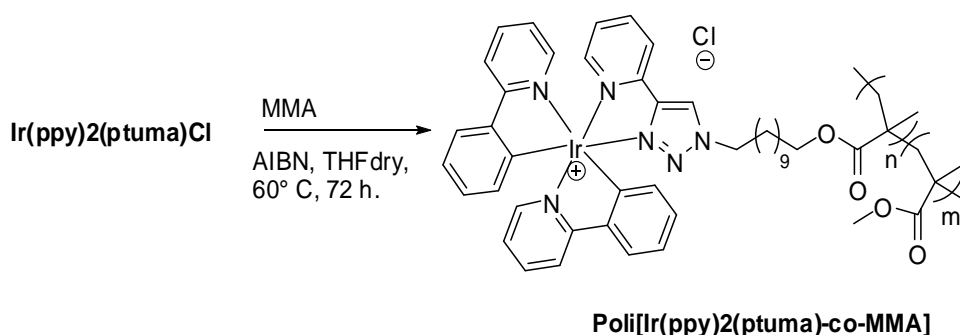
Scheme 3: Copolymers synthesis. Poli[Ir(ppy)$_2$(ptuma)-*co*-MMA]
n=1, m=130, 150, 450, 820, 850, 1100, 2000, 12100.

The obtained copolymers were purified by precipitation, using a methanol/hexane = 3:1 solution to remove the unreacted monomer. In Table 2 the data of the synthesis of several polymers and their average molecular weight determined by gel permeation chromatography (GPC) in THF at 25 ° C, using monodisperse polystyrene samples as standard, are reported

| Feeding reaction (mol) | | Polymer | | | | | |
|---|---|---|---|---|---|---|---|
| Ir(ppy)$_2$(ptuma) | MMA | Ir(ppy)$_2$(ptuma)[a] | MMA[a] | Yield (%)[b] | $\bar{M}_n$ (g/mol)[c] | $\bar{M}_w$/ $\bar{M}_n$[c] | $T_g$ (°C)[d] |
| 1 | 50 | 1 | 130 | 42 | 18800 | 1.7 | 120 |
| 1 | 100 | 1 | 150 | 45 | 20100 | 1.8 | 122 |
| 1 | 200 | 1 | 450 | 40 | 23000 | 1.7 | 123 |
| 1 | 400 | 1 | 820 | 60 | 21300 | 1.7 | 103 |
| 1 | 500 | 1 | 850 | 60 | 37000 | 1.3 | 123 |
| 1 | 1000 | 1 | 1100 | 68 | 22500 | 1.7 | 123 |
| 1 | 2000 | 1 | 2000 | 65 | 32000 | 1.8 | 122 |
| 1 | 10000 | 1 | 12100 | 64 | 38900 | 1.6 | 112 |

Table 2: Copolymers data. [a] Determined by UV-Vis analysis, [b] Calculated as (g of polymer / g of monomer) x 100, [c] Determined by GPC in THF at 25 ° C [d] Glass transition temperature determined by DSC (10 ° C / min) in nitrogen.

The polymerization was confirmed by ^{1}H-NMR spectra, in which the signals enlargement and the disappearance of the vinylic protons at 6.10 and 5:55 ppm can be observed. However, it was not

possible to determine the final composition of the copolymers by $^1$H-NMR analysis, due to the low intensity of the signals of the co-monomer containing the iridium complex.

For this purpose, the absorption spectra of all polymers and the monomer [**Ir(ppy)$_2$(ptuma)Cl**] were recorded. Since the molar absorption coefficient of the complex at 257 nm (the area in which the MMA does not absorb) is known and assuming that it remains unchanged even when the chromophore is attached to a macromolecular chain, it was possible to determine the final composition of the different copolymers (Table 2). From the obtained data, it can be noted that the final composition does not reflect the initial feed: the methacrylic monomer [**Ir(ppy)$_2$(ptuma)Cl**] has, in fact, a low reactivity compared to MMA, probably because of its steric hindrance. Nevertheless, it was possible to obtain copolymers with variable amount of iridium complex.

From the DSC measurements, performed in a temperature range between 25 and 200 ° C, it can be noted that all synthesized polymeric derivatives have only thermal transitions of the second order, typical of glass transitions (Table 2). Endothermic crystalline melting peaks do not appear, in agreement with the substantially amorphous character of these macromolecules in the solid state.

*UV-Vis analysis.*

All the synthesized copolymers and the monomer containing the iridium complex, were characterized by UV-Vis spectroscopy in chloroform solution.

All obtained spectra have two characteristics absorption bands: one in the ultraviolet region, very intense (molar absorption coefficient $4 \cdot 10^4$ L mol$^{-1}$ cm$^{-1}$), centered at about 257 nm and attributable to the $\pi-\pi$ * transitions of ligand aromatic rings.[9, 10] The second one, less intense and enlarged compared to the first, is centered at about 290 nm, and it is due to the metal to ligand charge transfer (MLCT).[9-11]

From the comparison of copolymers and monomer UV-Vis spectra (Figure 5), it is observed that the position of the absorption maxima ($\lambda$ max) does not change.
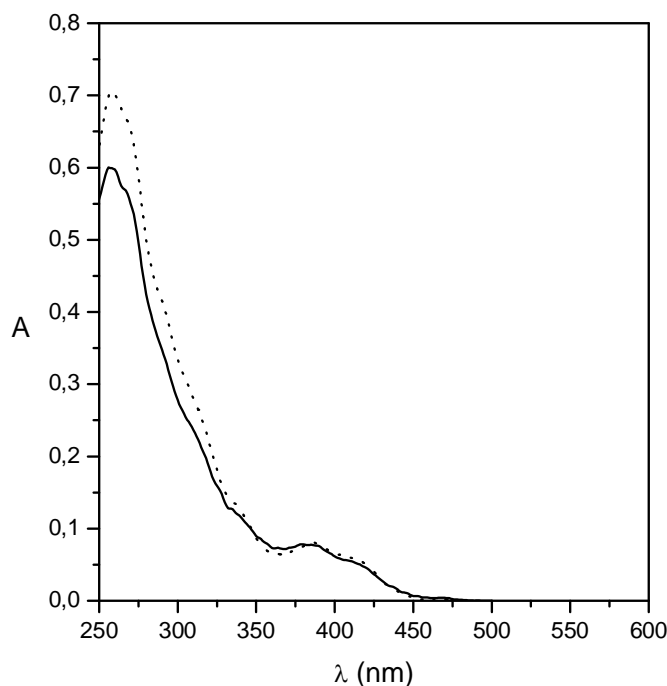
Figure 5: poly[Ir(ppy)$_2$(ptuma)Cl-co-MMA] 1:820 (—) and monomer [Ir(ppy)$_2$(ptuma)Cl] (• • •) UV-vis spectra in chloroform.

This behavior, already reported in literature,[4,5,12] shows that the transition from single isolated unit to the macromolecular system does not involve effects on the energy difference between the ground state and the excited state of the chromophoric system. From the absorption spectra, it was possible to determine the final composition of synthesized copolymers (Table 2), not determinable by $^1$HNMR analysis. Given the molar extinction coefficient of the unit containing the iridium complex as a constant and equal to that of the low molecular weight monomer, it was possible to calculate the relative amount of the two co-monomers in each polymer by absorbance measurements.

*Photophysical properties*

The photophysical properties of the luminescent monomer [Ir(ppy)$_2$(ptuma)] have been studied under the following conditions:

- Solution at 298 K (Sol 298 K);
- Degassed solution at 298 K (Sol deg);
- Frozen solution at 77 K (Sol 77K).

The excitation (Ex) and emission (Em) maxima, the determined lifetimes ($\tau$) and quantum yields ($\Phi$) are reported in Table 3.
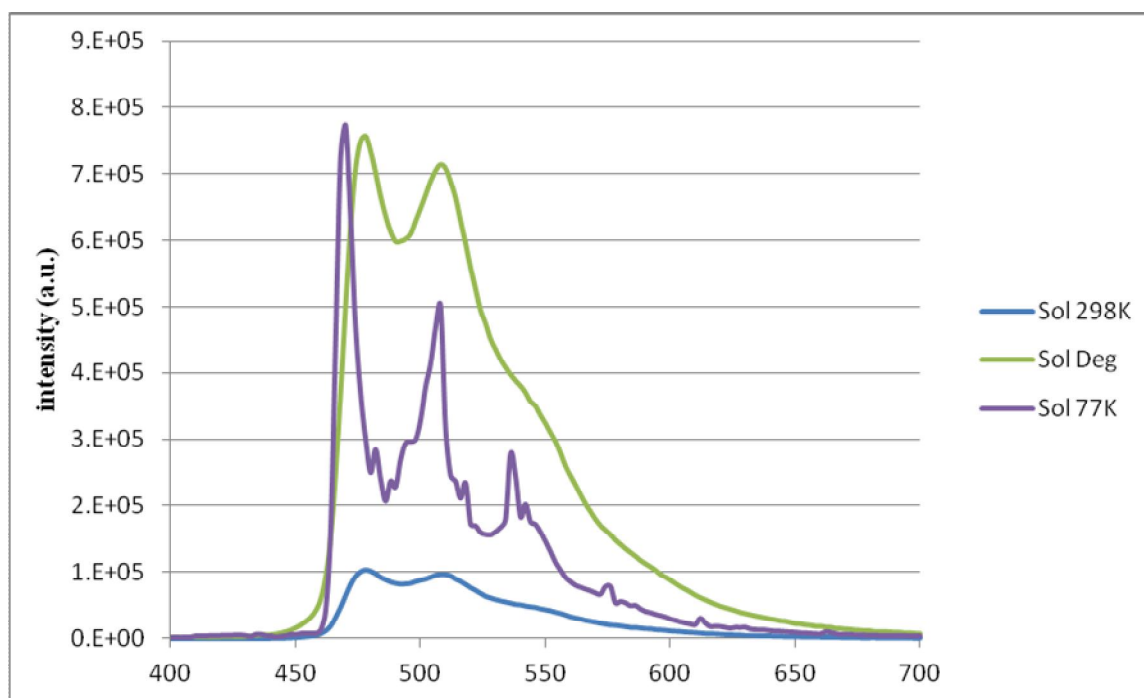
Figure 6: Monomer emission spectra.

As shown in Figure 6, the emission spectrum of the degassed solution is found to have a higher intensity than that of the solution in the presence of oxygen; this is due to the phenomenon of collisional quenching caused by the presence of molecular oxygen dissolved in the solution when it is not degassed. This phenomenon is characteristic of species whose emission originates from a triplet excited state. The spectrum of the frozen system at 77 K shows an increase of the emission intensity due to the decrease of the not competitive radiative processes, and a shift of the emission maximum towards higher energies, in accordance with the nature of MLCT excited state. The data of the monomer, shown in Table 3, also put into evidence as both the lifetimes and the quantum yields improve significantly when the samples is degassed. The lifetime of the frozen solution is even greater.

| Monomer | Ex (λ) | Em (λ) | τ (ns) | Φ |
|---|---|---|---|---|
| Sol. 298K | 266, 382 | 478, 508 | 175 | 6% |
| Sol.Deg. 298K | 266, 382 | 480, 510 | 1646 | 33% |
| Sol 77K | 268, 290, 310 | 470, 506, 536 | 4195 | x |
| solid | 348, 430 | 488, 530 | 91 (34%), 630 (66%) | 0,7 |
| POLI 1:130 | Ex (λ) | Em (λ) | τ (ns) | Φ |
| | 290, 380 | 478, 508 | 2780 | 20,1 |
| POLI 1:150 | Ex (λ) | Em (λ) | τ (ns) | Φ |
| | 290, 380 | 478, 508 | 2800 | 27,1 |
| POLI 1:450 | Ex (λ) | Em (λ) | τ (ns) | Φ |
| | 290, 380 | 478, 508 | 2730 | 35,2 |
| POLI 1:700 | Ex (λ) | Em (λ) | τ (ns) | Φ |
| | 290, 380 | 478, 508 | 2785 | 45,4 |
| POLI 1:820 | Ex (λ) | Em (λ) | τ (ns) | Φ |
| | 290, 380 | 478, 508 | 2915 | 52,3 |
| POLI 1:850 | Ex (λ) | Em (λ) | τ (ns) | Φ |
| | 290, 380 | 478, 508 | 2780 | 49,7 |
| POLI 1:1100 | Ex (λ) | Em (λ) | τ (ns) | Φ |
| | 290, 380 | 478, 508 | 2765 | 54,7 |
| POLI 1:2000 | Ex (λ) | Em (λ) | τ (ns) | Φ |
| | 290, 380 | 478, 508 | 2641 | 60,3 |
| POLI 1:12100 | Ex (λ) | Em (λ) | τ (ns) | Φ |
| | 290, 380 | 478, 508 | 2646 | 59,7 |

Table 3: Photophysical properties.

The emissive properties of the copolymers have been investigated in the solid state, on films of thickness of about 1 μm, obtained by spin-coating. As can be seen from the obtained data (Table 3), the emission maximum [Em (λ)] remain unchanged for all compounds, because the emissive component is only the cyclometallated iridium complex. The lifetimes obtained for all the copolymers, instead, are lower than those of the monomer frozen at 77 K, but higher than those of the monomer in solution. This data are encouraging for a possible application of these materials in devices. The quantum yields exhibited by these films are interesting too. In fact, it can be observed as Φ increases with decreasing the dilution of the iridium complex present in the polymer, reaching an asymptotic value of around 60% for poly [**Ir(ppy)$_2$(ptuma)-co-MMA**] 1:2000 and 1:12100 (Figure 7).
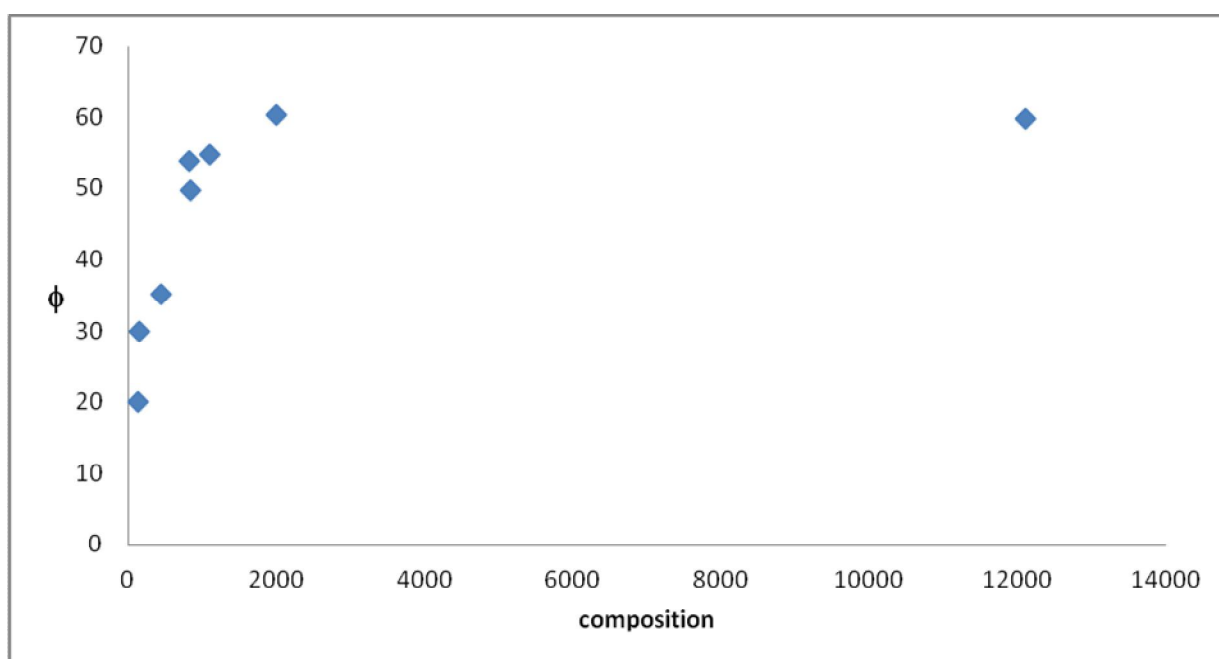


Figure 7: Trend of the quantum yield Φ depending on the amount of MMA in the copolymers.

From these data it can be deduced that the lower concentration, hence the greater dispersion of the iridium complex in polymers, avoids the formation of emissive component aggregates, which would lead to a decrease of the quantum yields and lifetimes, for self-quenching. Given the obtained results, the synthesized materials show promising features to be processed into thin films and used as emissive systems in devices LEECs and / or OLEDs.

### 6.1.2 - Conclusions

In this work the possibility to synthesize polymeric materials containing an organometallic luminescent complex covalently bound to the side chain, in order to improve the performance of the emissive compound has been studied. These new materials being transparent and easily filmable, allow the polymer to increase the photophysical properties of the iridium complex. In fact, it combines the advantage of working in the solid state and in "degassed" environment, to the fact that the iridium complex is located in a diluted matrix which limits any quenching phenomena which should be to lower its emission intensity and consequently lifetimes and quantum yields. The fact that the complex is covalently linked to the polymer chain and not simply mixed with it allows to have homogeneous dispersions and to avoid self-aggregation phenomena (Figure 8).
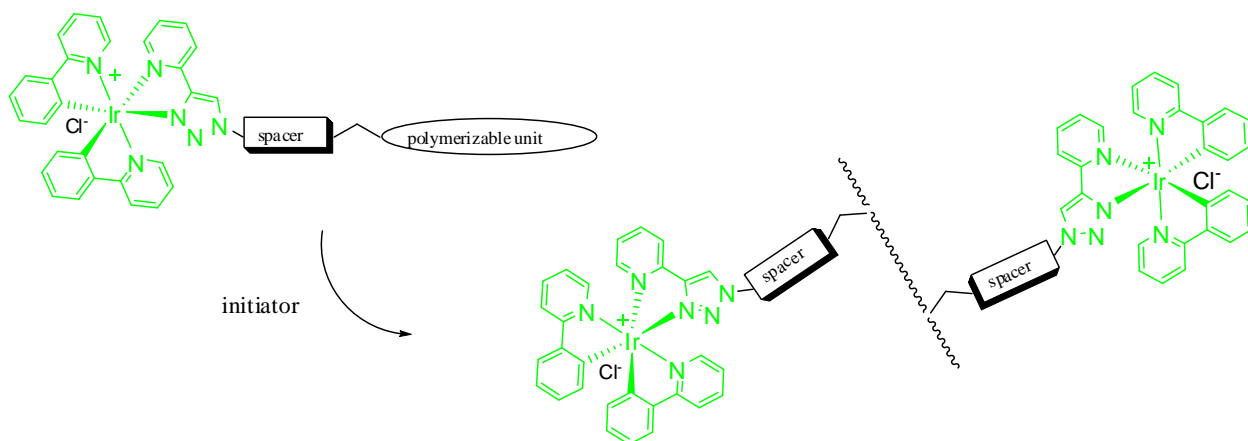


Figure 8: Schematic representation of the polymers.

Specifically, a new cyclometallated iridium complex, bis-(2-fenilpiridina)-9-(4-(pyridin-2-yl)-1*H*-1,2,3-triazol-1-yl)undecylmethacrylate-iridium(III) [**Ir(ppy)₂(ptuma)Cl**], was synthesized and characterized which has been copolymerized in the presence of MMA in different amounts. The final composition of the so obtained new polymeric materials, determined by UV-Vis spectroscopy, showed a lower reactivity of methacrylic monomer containing the iridium complex compared to MMA, probably due to its steric hindrance. Thermal analysis of the copolymers showed their amorphous character in the solid state. The position of the absorption and emission maximum, of the monomer [**Ir(ppy)₂(ptuma)Cl**] and polymeric compounds is unchanged, regardless of the amount of complex present, indicating that the emissive component does not undergo variations after the copolymerization. By the analysis of the lifetimes and quantum yields promising results were obtained, showing a clear improvement in polymeric compounds compared to the luminescent monomer in solution. In addition, the upward trend of the quantum yields with decreasing concentration of the complex, suggests a progressive decrease in the self-quenching effects.

### 6.1.3 - Experimental section

*Solvents and materials*

The methyl methacrylate (MMA) was distilled at reduced pressure (P = 260 mmHg) at 60 ° C under a stream of dry nitrogen before use. The tetrahydrofuran (THF) (Aldrich) was left a few hours onKOH, then distilled on Na-K alloy under an atmosphere of dry nitrogen and subsequently redistilled of Na-K alloy and benzophenone.[13] 2-2'-azobis-isobutyronitrile (AIBN) (Aldrich) was crystallized from absolute ethanol before use. Other commercial reagents and solvents (Aldrich) were used without further purifications.

*Products characterization*

The NMR spectra were obtained at room temperature with a spectrometer Varian MercuryPlus VX 400 (1H, 399.9) using, when possible, to 5-10% solutions in CDCl3. The chemical shifts are expressed in ppm from tetramethylsilane (TMS) as an internal reference. The UV-Vis spectra (250-700 nm) were recorded at 25° C in CHCl3 solutions with a spectrophotometer Perkin Elmer Lambda 19, using quartz cells. The DSC measurements were carried out using a Thermal Analysis DSC Q2000 calorimeter modulated, equipped with a cooling system RCS, adopting a temperature program consisting of three heating from ambient temperature and two coolings with speed 10 ° K / min in nitrogen. The average molecular weights of the polymer samples were determined from solutions of THF using a HPLC Lab Flow 2000, equipped with a Rheodyne injector 7725th, column Phenomenex Phenogel 5μ MXL and a refractive index detector RI Knauer K-2301. The calibration curve was constructed with standard monodisperse polystyrene samples. The emission spectra in the steady state were recorded with a spectrofluorimeter Edinburgh FLS920P equipped with a xenon arc lamp, double excitation monochromators and single issue, a Hamamatsu R928P photomultiplier tube (185-850 nm) with Peltier cooling. The excitation and emission spectra were corrected for intensity of source (lamp and grating) and emission spectral response (detector and grating) by means of the calibration curve supplied with the instrument. The emission lifetimes were determined on the same instrument Edinburgh with the technique Time Correlated Single Photon Counting (TCSPC), using pulsed LEDs (EPLED EPLED 295 or 360, FHWM <800 ps, repetition rate between 10 kHz and 1 MHz) as a source of excitation and the photomultiplier tube as a detector. The quantum yields of emission were determined on dilute solutions, with reference to standard solutions of Ru(bpy)$_3$Cl$_2$ in acetonitrile (*r*)[14]:

$$\Phi = \Phi_r \frac{I}{I_r} \frac{A_r}{A} \frac{n^2}{n_r^2}$$

where *I* is the area of the emission peaks of the complex and the reference sample, *A* is the absorbance and *n* is the refractive index of the solvent.

*Ligand and Ir-monomer synthesis*

**Synthesis of azide 2**: In a 50 ml-two-necked round-bottom flask equipped with a stirring bar, 11-bromo-1-undecanol **1** (0.75 g, 3.0 mmol) and $NaN_3$ (0.39 g, 6.0 mmol) was dissolved in 10 mL of DMSO. The reaction mixture was stirred under at room temperature for 24 h. Then water (15 mL) was added and the aqueous phase was extracted with ethyl acetate (3X 10 ml). The organic layer was dried over $MgSO_4$ and the solvent evaporated to give brown oil (98% yields). The product was used in the next step without further purification.

$^1$H NMR (CDCl3, 300 MHz) δ 3.58 (dt, $J_T$ = 6.5 Hz, $J_D$ = 1.4 Hz, 2H), 3.22 (t, J = 7.0 Hz, 2H), 1.62 - 1.47 (m, 4H), 1.39 - 1.21 (m, 14H).

**Synthesis of ligand 3:** In a 100 ml-two-necked round-bottom flask equipped with a stirring bar, the crude azide **2** (3 mmol) was dissolved in a mixture of tBuOH/$H_2O$=1:1 (20 ml), and 2-ethynyl pyridine **10** (0.45 g, 4.4 mmol), sodium ascorbate (86 mg, 0.4 mmol) and $CuSO_4$ (0.30 g, 1.2 mmol) were added. The reaction was left to stir overnight at room temperature. Then the solvent was removed by vacuum and 35 ml of $CH_2Cl_2$ and 35 ml of aqueous $NH_3$ were added. The mixture was left to stir overnight. The aqueous layer was washed twice with 30 ml of $CH_2Cl_2$, and the organic phase was dried over $MgSO_4$. The solvent was removed and the crude was purified by column chromatography on silica gel (EtOAc/$CH_2Cl_2$ = 6/4, $CH_2Cl_2$/MeOH = 9:1, 85% yields).

$^1$H NMR (CDCl$_3$, 300 MHz) δ 8.57 (dq, $J_D$ = 5.0 Hz, $J_Q$ = 0.9 Hz, 1H), 8.19 (dt, $J_D$ = 8.0 Hz, $J_T$ = 1.13 Hz, 1H), 8.13 (s, 1H), 7.78 (td, $J_T$ = 7.7 Hz, $J_D$ = 1.9 Hz, 1H), 7.23 (ddd, J = 6.1 Hz, J = 4.9 Hz, J = 1.3 Hz, 1H), 4.41 (t, J = 7.3 Hz, 2H), 3.68 - 3.60 (m, 2H), 2.01 - 1.90 (m, 2H), 1.60 - 1.50 (m, 2H), 1.40 - 1.22 (m, 14H). $^{13}$C NMR (CDCl$_3$, 101 MHz) δ 150.6 (C), 149.5 (CH), 148.4 (C), 137.2 (CH), 123.0 (CH), 122.1 (CH), 120.5 (CH), 63.1 ($CH_2$), 50.7 ($CH_2$), 33.0 ($CH_2$), 30.4 ($CH_2$), 29.6 ($CH_2$), 29.50 ($CH_2$), 29.48 ($CH_2$), 29.42 ($CH_2$), 29.08 ($CH_2$), 26.6 ($CH_2$), 25.9 ($CH_2$).

**Synthesis of ptuma:** In a 50 mL three-neck, round bottom flask equipped with a stirring bar, ptuma (0.7 mmol) and 0.2 mL of freshly distilled triethylamine was dissolved in 10 mL of dry THF. The reaction mixture was cooled to 0° C. Methacryloyl chloride (3 equiv.) and hydroquinone (0.02 equiv.) dissolved in 3 mL of dry THF were added dropwise. The reaction mixture was stirred

overnight at r.t. under $N_2$ protection. Then the solvent was removed by vacuum and the crude was dissolved with an aqueous solution $NaHCO_{3(sat)}$ and DCM 1:1. The aqueous phase was extracted with DCM (3 x 10 ml) and the organic layer was dried over $MgSO_4$. Then the solvent was removed by vacuum and the crude was purified by column chromatography on silica gel (DCM/EtOAC = 75:25, 74% yields).

^{1}HNMR (CDCl$_3$): 8.58 (dq, $J_D$ = 4.9 Hz, $J_D$ = 1.0 Hz, 1H), 8.19 (dt, $J_D$ = 7.9 Hz, $J_T$ = 1.2, 1H), 8.13 (s, 1H), 7.78 (td $J_T$ = 7.9 1H, $J_D$ = 1.7 Hz, 1H), 7.23 (m, 1H), 6.09 (sett, $J$ = 0.9 Hz, 1H), 5.54 (quint, $J$ = 1.6 Hz, 1H), 4.42 (t, $J$ = 7.2 Hz, 2H), 4.13 (t, $J$ = 6.69 Hz, 2H), 2.00-1.91 (m, 5H), 1.66 (q, $J$ = 6.73 Hz, 2H), 1.39-1.23 (m, 14H). ^{13}CNMR (CDCl$_3$): 167.5, 150.4, 149.3, 148.3, 136.9, 136.5, 125.1, 122.8, 121.8, 120.2, 64.8, 50.5, 30.2, 29.4, 29.3, 29.2, 29.1, 29.0, 28.6, 26.4, 25.9, 18.3.
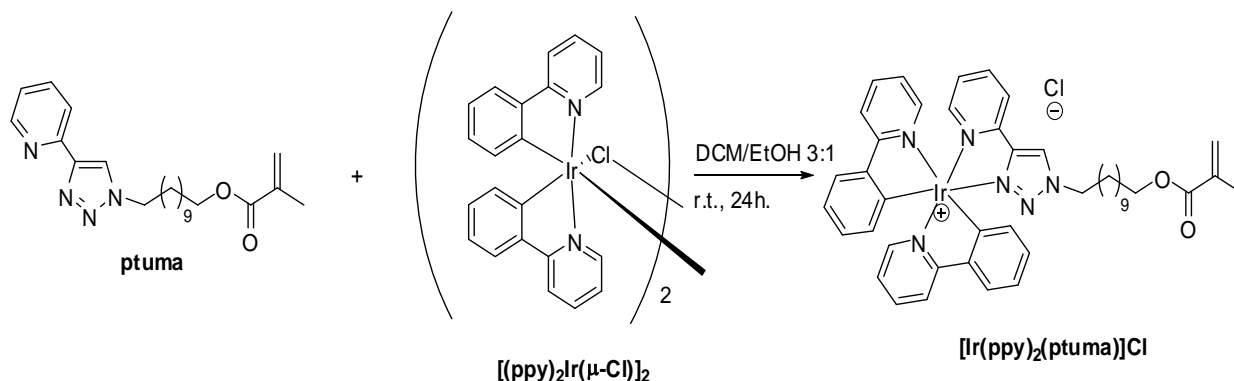


The monomer bis-(2-fenilpiridina)-9-(4-(pyridin-2-yl)-1H-1,2,3-triazol-1-yl)undecyl methacrylate-iridium (III) [MW = 920.54 g / mol] was synthesized by the reaction between the iridium dimer {[(ppy)$_2$Ir(μ-Cl)]$_2$}, the synthesis of which is reported in the literature,[7, 8] and the ancillary ligand 9-(4-(pyridin-2-yl)-1H-1,2,3-triazol-1-yl)undecyl methacrylate (ptuma).

In a 25 ml round-bottom flask equipped with a stirring bar, the ligand **ptuma** (0.039 g, 0.102 mmol) was dissolved in a 3:1 mixture of $CH_2Cl_2$/EtOH (10 mL) and the Iridium dimer (0.058 g, 0.054 mmol) was added. The mixture was left to stir at r.t. 48 h. The solution was evaporated and the resulting residue was dissolved in acetone (0.5 mL) and precipitate with $Et_2O$. The solid was filtered to give pure Ir-monomer (94% yields).

^{1}HNMR (CDCl$_3$, 400 MHz) δ 10.98 (s, 1H), 9.28 (d, $J$ = 8.1 Hz, 1H), 8.01 (t, $J_T$ = 7.88 Hz, $J_D$ = 1.5 Hz, 1H), 7.91 (d, $J_D$ = 8.0 Hz, 2H), 7.80-7.60 (m, 6H), 7.45 (t, 3H), 7.45 (d, $J$ = 5.9 Hz, 1H), 7.20 (t, $J$ = 6.8 Hz,1H), 7.05-6.85 (m, 6H), 6.32 (t, $J_T$ = 6.8 Hz,2H), 6.11-6.09 (m, 1H), 5.55 (q, $J$ = 1.6 Hz, 1H), 4.42 (t, $J$ = 7.6 Hz, 2H), 4.13 (t, $J_D$ = 6.8 Hz, 2H), 2.00-1.90 (m, 5H), 1.66 (q, $J$ = 7.3 Hz, 2H), 1.40-1.15 (m, 14H).

*Copolymers synthesis*
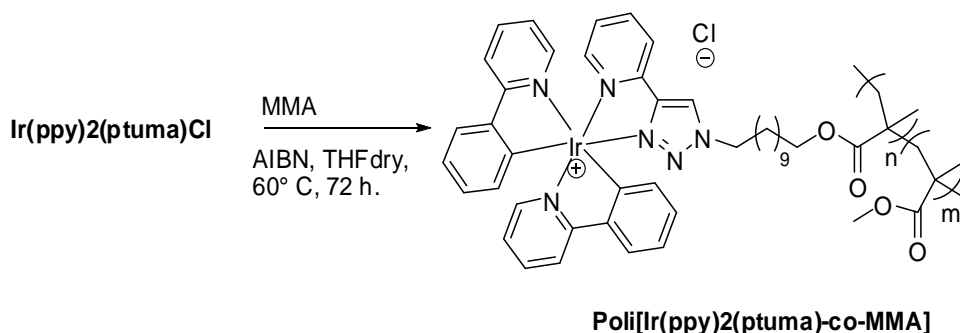


Scheme 2: Copolymers synthesis. Poli[Ir(ppy)$_2$(ptuma)-*co*-MMA]
n=1, m=130, 150, 450, 820, 850, 1100, 2000, 12100

The polymers were synthesized by radical reaction using AIBN (2% by mass in relation to the monomers) as a thermal initiator and anhydrous THF as solvent (1 g of monomer in 15 mL of solvent). All the copolymerization reactions were carried out in a sealed vial for 72 hours under vacuum at 60° C, after performing a series of vacuum-nitrogen cycles in order to deaerate the solutions. The copolymers thus obtained were purified by precipitation in large excess of a solution of methanol / hexane 3:1 and, after being dried at a temperature of 70 ° C under vacuum for several days until a constant weight, were characterized by $^1$HNMR spectroscopy .

As an example is reported the $^1$HNMR spectrum of the copolymer poly [Ir (ppy)$_2$(ptuma)-co-MMA] 1:1100.

$^1$HNMR (CDCl$_3$): 3.79-3.49 (3H, -OCH$_3$), 2.10-1.70 (2H, -CH$_2$- main chain), 1.50-1.20 (-CH$_2$- side chain), 1.11-0.80 (3H, -CH$_3$ main chain) ppm.


*Samples preparation for photoemission measurements*

In order to carry out the analysis of the photophysical properties, the monomer **Ir(ppy)$_2$(ptuma)Cl** was dissolved in dichloromethane: 1 mg of compound dissolved in 10 mL of solvent, and subsequently diluted 1:10. In order to carry out the analysis of the photophysical properties, the monomer [**Ir(ppy)$_2$(ptuma)Cl**] was dissolved in dichloromethane: 1 mg of compound dissolved in 10 mL of solvent, and subsequently diluted 1:10. With regard to the copolymers, were obtained thin films by deposition of a solution in anhydrous THF on a solid support by means of spin-coating. The solutions of the copolymers in THF were placed in an ultrasonic bath for 30 minutes, and filtered using Teflon filters with porosity 0.2 μm, so as to eliminate any residual polymer is not dissolved and dust. As a support, for the preparation of films, were used circular discs of quartz, washed with distilled water and soap. To increase their wettability were kept in an aqueous solution

of NaOH at 30% by weight for 30 minutes in an ultrasonic bath, washed with distilled water and then ethanol and finally dried with hot air flow. 5-6 drops of the solutions prepared were deposited on the supports (at room temperature) for spin-coating, varying speed, acceleration and timing of spinning in order to obtain homogeneous films and without defects. The films thus obtained were kept under high vacuum in a thermostat at 40° C overnight, so as to remove residual solvent.

## *6.1.4 - Bibliography*

1. E. Holder, V. Marin, D. Kozodaev, M. A. R. Meier, B. G. G. Lohmeijer, U. S. Schubert. *Macromol. Chem. Phys.* **2005**, *206*, 989–997.

2. S. Tokito, M. Suzuki, F. Sato *Thin Solid Films* **2003**, *445*, 353–357.

3. X.-Y. Wang, A. Kimyonok, M. Weck. *Chem. Commun*, **2006**, 3933–3935.

4. Y. Koga, K. Matsubara. *Journal of Polymer Science: Part A: Polymer Chemistry* **2009**, *47*, 4358–4365.

5. C. Ulbricht, C. Remzi Becer, A. Winter, U. S. Schubert *Macromol. Rapid Commun.* **2010**, *31*, 827–833.

6. X.-Y. Wang, R. Narayan Prabhu, R. H. Schmehl, M. Weck *Macromolecules* **2006**, *39,* 3140-3146.

7. M. Nonoyama, *Bull. Chem. Soc. Jpn.* **1974**, *47*, 767.

8. S. Lamansky, P. Djurovich, D. Murphy, F. Abdel-Razzaq, R. Kwong, I. Tsyba, M. Bortz, B. Mui, R. Bau, M. E. Thompson, *Inorg. Chem.* **2001**, *40*, 1704-1711.

9. M. S. Lowry, J. I. Goldsmith, J. D. Slinker, R. Rohl, R. A. Pascal, Jr., G. G. Malliaras, S. Bernhard, *Chem. Mater.* **2005**, *17*, 5712.

10. B. Tamayo, S. Garon, T. Sajoto, P. I. Djurovich, I. M. Tsyba, R. Bau, M. E. Thompson, *Inorg. Chem.* **2005**, *44*, 8723.

11. F. Neve, A. Crispini, S. Campagna, S. Serroni, *Inorg. Chem.* **1999**, *38*, 2250.

12. C. Ulbricht, C. R. Becer, A. Winter, D. Veldman, U. S. Schubert, *Macromol. Rapid Commun.* **2008**, *29*, 1919.

13. D. D. Perrin, W. L. F. Amarego, D.R. Perrin, *Purification of Laboratory Chemicals, Pergamon Press*, Oxford, (1966).

14. K. Binnemans, *Chem. Rev.* **2009**, *109*, 4283-4374.

## *6.2 - Biotinylated cyclometallated Ir(III) complexes as luminescent probes for avidin targeting*

### *Biomedical imaging*

Biomedical imaging is a generic process that allows acquiring, in a non-invasively way, an image of a target, inside a living organism. This type of images can be obtained for clinical purposes, to detect, to diagnose or to study a disease, or for scientific purposes allowing studying the anatomy and physiology of the organisms. Biomedical imaging includes several analysis techniques such as radiology, nuclear medicine, endoscopy, thermography and microscopy.

In recent years, thanks to the discovery of new highly selective contrast agents, it was possible to improve the sensitivity and efficiency of non-invasive techniques (Figure1).[1] Such techniques, can be divided according to the type of energy that take advantage of (X-rays, positrons, photons, radio waves) or according to the type of information that can give (anatomical, physiological, cellular and molecular). The macroscopic imaging systems that provide anatomical and physiological information are already widely used in clinical practice, such as computed tomography (CT), magnetic resonance (MR) and ultrasounds. On the other hand, systems furnishing molecular informations are still developing and are rarely used in clinical practice. They include the positron emission tomography (PET), the fluorescence reflectance, and the bioluminescent imaging.
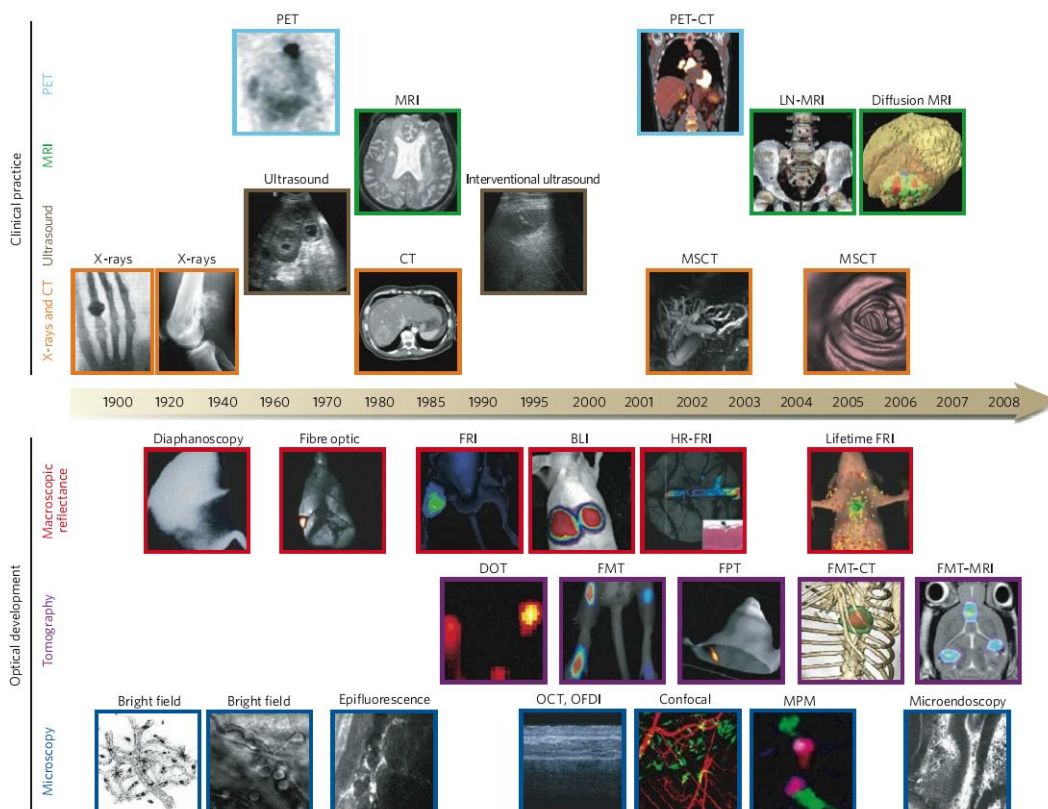


Figure 1: Evolution of biomedical imaging.

The in vivo and in vitro imaging on biological samples, has been carried out for several years, using optical microscopy. Among the available optical imaging techniques, fluorescence microscopy was one of the most powerful, because it allows to observe the luminescence of the sample with a good resolution.[2,3]

The optical imaging techniques rarely take advantage of the intrinsic fluorescence of the biological sample, but usually, employ luminescent organic compounds or luminescent organo-metallic complexes. In these techniques a contrast agent injected near the area of tissue to be monitored absorbs UV or Vis light from an external source, and then releases the energy emitting at a wavelength that is selectively detected.


*Luminescent markers for bio-conjugation*

The importance of luminescent dyes for the qualitative and quantitative determination of analytes is greatly increased and the process of conjugation between a molecular probe and a specific biological receptor consists in the interaction of a suitable functional group present on the fluorophore, with a receptor group present on the target to highlight. Due to the complexity of the systems, to ensure the selectivity is very difficult. Usually this problem is dealt with in three ways:

functionalization of the fluorophores: the fluorophore is functionalized with a group able to react only with the receptor

exploiting the metabolism way, widely used in imaging of cells: the probe is equipped with a molecule that entering in the cell cycles will bring the fluorophore to accumulate in certain organelles rather than in other

key-lock approach: it exploits the particular biological similarities, of some protein with certain organic molecules: the fluorophore bound to the "key" molecule  will be related only to a specific "lock" protein.

It is also essential that the fluorophore able to bind the target will maintain some photophysical properties, after coordination. To minimize possible quenching interactions between the biomolecule and the marker, it is often necessary to outdistance the groups responsible for the emission and thcoordination, through the use of suitable spacers.

The probes labeled with fluorophores are detected by spectroscopic measurements using the absorption and emission wavelengths typical of the fluorophore. The sensitivity obtained with a fluorescent marker is directly related to its molar extinction coefficient ($\varepsilon$) and its fluorescence quantum yield ($\phi$).The organic fluorophores may have ($\varepsilon$) values in the range of $10^5$ L mol$^{-1}$cm$^{-1}$ and ($\phi$) percentages close to 100%. In order to achieve high efficiency, the luminescent probes, should display absorption and emission maxima where the interference with the biological matrix

(auto-fluorescence) is negligible. Furthermore, it is necessary to reduce scattering phenomena due to the presence of macromolecules such as proteins. Scattering and auto-fluorescence, particularly detectable in the visible region, strongly reduce the sensitivity of the method. Therefore a good fluorophore should display the following properties:

- high photochemical stability

- high quantum yield

- tunable emission in the visible region

- high solubility in order to avoid phenomena of self-aggregation

*Organic fluorophores*

The term fluorophore refers to a fluorescent chemical compound that is able to emit light after absorbing photons at a certain wavelength. The most important examples are the derivatives of xanthene (rhodamine and fluorescein). Figure 2
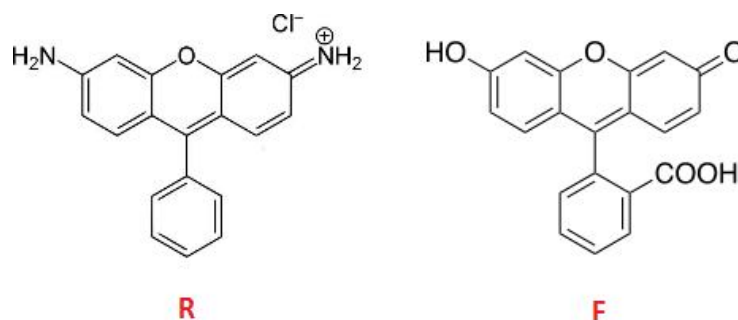


Figure 2: Rhodamine (R), Fluorescein (F).

Despite organic fluorophores are commonly used in biological imaging because of their structural versatility, these molecules have also some limitations: firstly they have very short lifetimes (order of nanoseconds), and secondly they cannot be used for long periods of observation because of their fast photodegradation, caused by their reactivity towards molecular oxygen at the excited states. Each fluorophore can be excited only to a specific wavelength, then the organic fluorophores cannot be used for multi-color imaging. Finally, the fluorescence of organic dyes may overlap the auto-fluorescence of the tissues.

*Organometallic fluorophores*

With respect to transition metals complexes, the most representative examples of organometallic fluorophore are given by coordinatively saturated compounds in which the metal center is coordinated to chelating aromatic ligands. In particular, one of the first reported compound is represented by a polypyridinic Ru(II) complex $[Ru(bpy)_3]^{2+}$ (Figure 3) and its derivatives. Studies

performed on this class of compounds allowed the development of similar derivatives containing other transition metals, such as ciclometallated complex of Ir (III) and tricarbonilic derivatives of Re(I) (Figure 3). In particular, in recent years, the ciclometallated complexes of Ir(III) aroused a growing interest, as they show excellent high quantum yields and lifetimes.
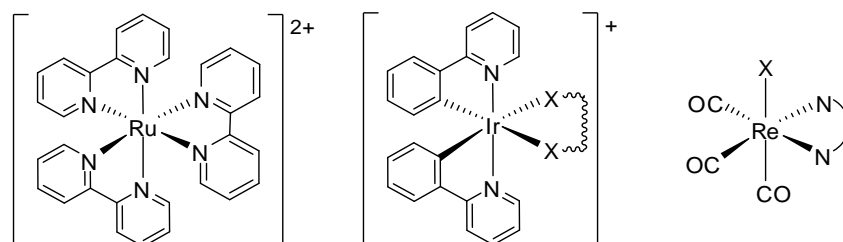


Figure 3: complexes

One of the first considered compounds is represented by the complex $[Ir(ppy)_2(CH_3CN)_2]^+$. It shows a weak emission in aqueous solution, but when it is in the presence of histidine, it increases its emission of 180 times.[4] This was the first example of a new class of organometallic compounds which change its photophysical properties in the presence of a target. From this first example, it was possible to design and synthesize new probes containing luminescent metal complexes.

The employed strategy is to synthesize polyfunctionalized organic molecules, having not only units able to form complexes with suitable metals, but also functional group such as biotin, estradiol and glucose, able to coordinate specific sites to particular proteins, hormones or vitamins. In this way we obtain luminescent organometallic complexes capable of interacting directly with target compounds by changing their fotoemissive properties depending by the presence or the absence of the bio-conjugation.

Among the possible structures that form specific interactions with appropriate receptors, the biotin is very important. This molecule is a vitamin and it is used in many energy cell cycles as a co-factor of ATP-dependent decarboxylase, but its most interesting feature is its ability to form non-covalent interaction with avidin, a specific glycoprotein.[5]

Avidin is a tetrameric or dimeric[6] protein produced in the oviducts of birds, reptiles and amphibians deposited in the whites of their eggs. In chicken egg white, avidin makes up approximately 0.05% of total protein (approximately 1.8 mg per egg). The tetrameric protein contains four identical subunits (homotetramer), each of which can bind to biotin (Vitamin $B_7$, vitamin H) with a high degree of affinity and specificity. The dissociation constant of avidin is measured to be $K_D \approx 10^{-15}$ M, making it one of the strongest known non-covalent bonds.[7]

Owing to the extraordinarily high affinity of biotin to avidin strong binding interactions can be formed and such system has been widely exploited as a powerful tool in a variety of bioanalytical applications. Recently various examples of Iridium (III) polypyridine biotin complexes have been utilized as luminescent probes since, in contrast to biotin-fluorophore conjugates, they show increased emission intensity and lifetimes when bound to avidin. In the reported papers a bipyridine was employed as ancillary ligand in the Ir(III) complexes. All the reported examples have in common a bipyridinic linker to which an amidic pendant of biotin was attached (Figure 4). The presence of avidin show in these complexes an increase in the emission response from 1.5 to 3.3 times compared to the intensity measured in the absence of the target protein, as well as an increased lifetime.[8]
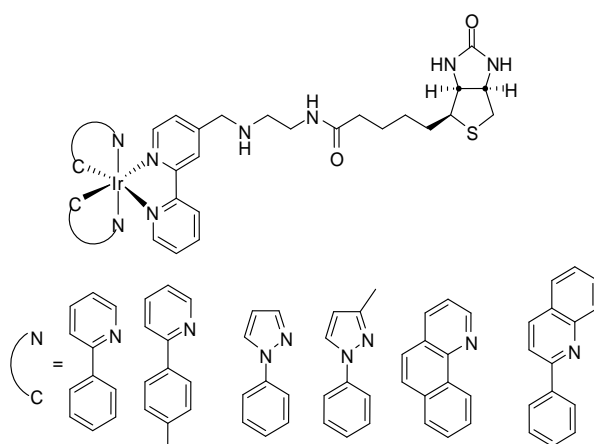


Figure 4: Biotinylated ciclometallated Ir(III) complexes.

However, other nitrogen containing derivatives have been recently employed to obtain highly emissive complexes, such as pyridin-1,2,3-triazoles, easily obtained *via* a click reaction. In recent years, in fact, the CuI-catalyzed azide–alkyne cycloaddition (CuAAC),[9] proved to be a very effective method to afford 1,4-substituted-1,2,3-triazoles (from azides and terminal alkynes) with essentially perfect regioselectivity under mild conditions, becoming an extremely used reaction in several chemical fields.[10]

Taking inspiration from these results I was involved to the design and the synthesis of a new class of bifunctionalized ligands **1**-**3**, (Figure 5), containing both a pyridine-1,2,3-triazole able to coordinate the desired metal and a biotin moiety able to interact with avidin. In addition, the importance of both the linker and the spacer arm between the two parts was investigated by comparing the luminescent properties of the corresponding Ir(III) complexes **4-6**, (Figure 5), alone and in the presence of avidin. In particular, an amide and an ester linker were considered, together with the alkylic and aromatic nature of the spacer arms considering that it has been reported that long spacer-arms can increase the stability of the metal-avidin adducts.
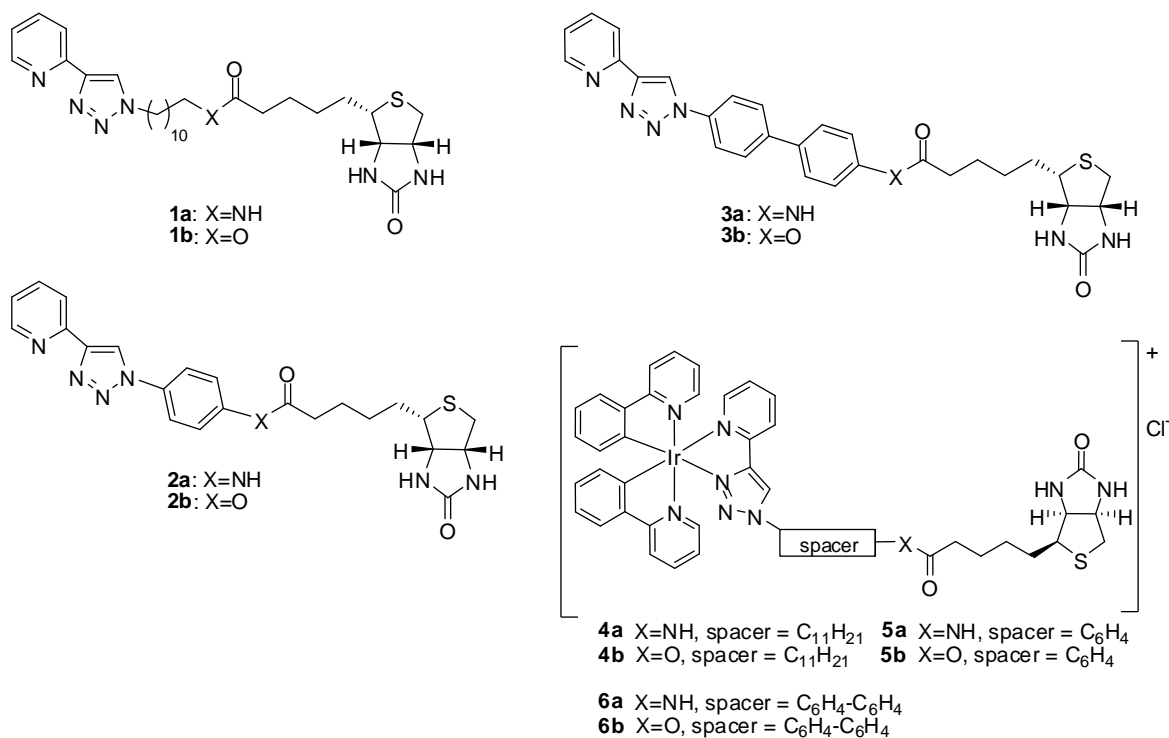
Figure 5: Biotinylated ligands and their Iridium complexes.

## 6.2.1 - Results and Discussion

### 6.2.1.1 - Ligand Design and Synthesis

In detail, ligands **1a-b** were obtained following the synthetic strategy reported in Scheme 1. The azide derived from reaction of 11-Br-undecanol **7** with NaN$_3$ underwent to a "click reaction" to form the 1,4-disubstituted 1,2,3-triazole **8** (85% yields from **7**) when treated with 2-alkynylpyridine under CuAAC conditions. The hydroxyl pyridine-triazole **8** was transformed into the amine **9** by reaction of its corresponding tosylate with NaN$_3$ and subsequent reduction trough a Staudinger reaction. Ligand **1a** was finally obtained by reaction of **9** with biotin-succinimino derivative **11** (92 % yields). On the other hand, the key-intermediate **8** was further employed to give ligand **1b** in 60 % yields by reaction with the biotin acyl chloride **12**.
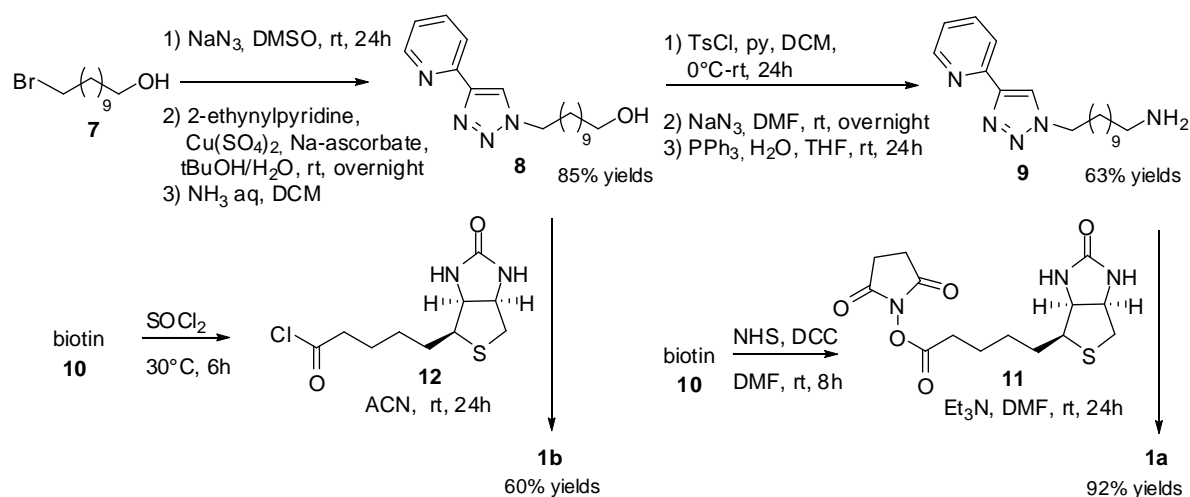
Scheme 1

The synthesis of ligands containing aromatic linkers are reported in Schemes 2 and 3. In particular, ligands **2a** and **2b** were obtained as follows. The aromatic azides from **13** were reacted with 2-ethynylpyridine to give the 2-pyridintriazoles **14a-b** that were then transformed in the corresponding amide **2a** (63% yields) and ester **2b** (55% yields) by reaction with biotin **10** following a previously reported procedure for aromatic substrates (Scheme 2).[11,12]
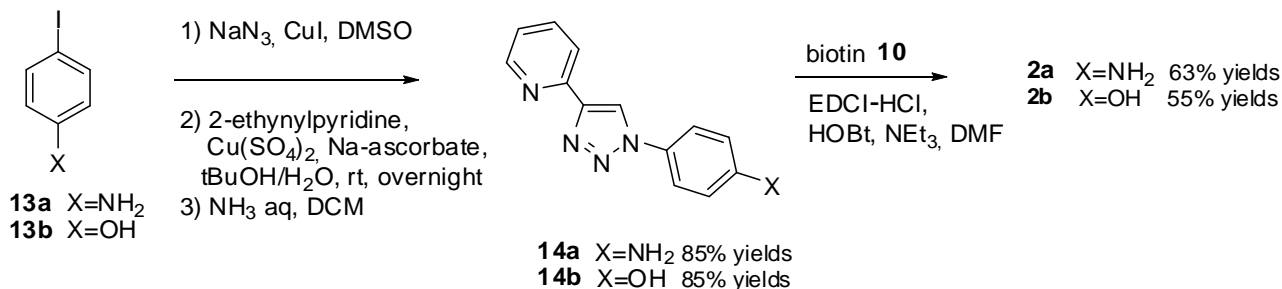


Scheme 2

A similar synthetic approach led to ligands **3a-b** (Scheme 3). The pyridintriazole **16**, obtained by condensation of the appropriate azide from **15** with 2-ethynylpyridine, was submitted to a Suzuki coupling with the desired phenylboronic derivative **17a-b** to give the biphenyl derivatives **18a** (20% yields) and **18b** (35% yields), that were therefore successfully converted into the biotin ligands **3a** (65% yields) and **3b** (55% yields).
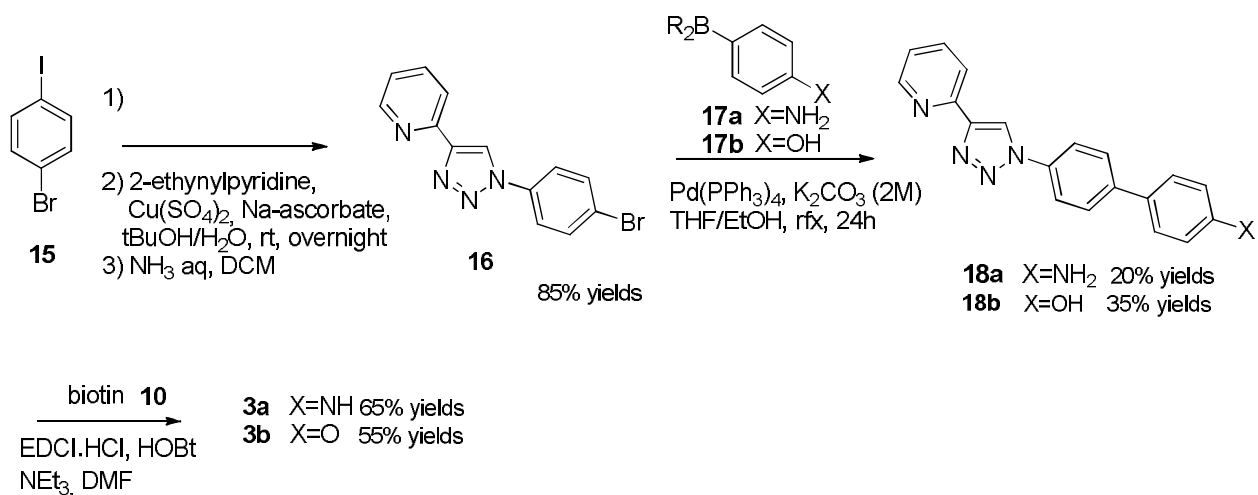
Scheme 3

Therefore the Ir(III)-complexes **4-6** were synthesized through a known procedure by reacting the dimer **19** with the proper ligand,[13] (Scheme 4).
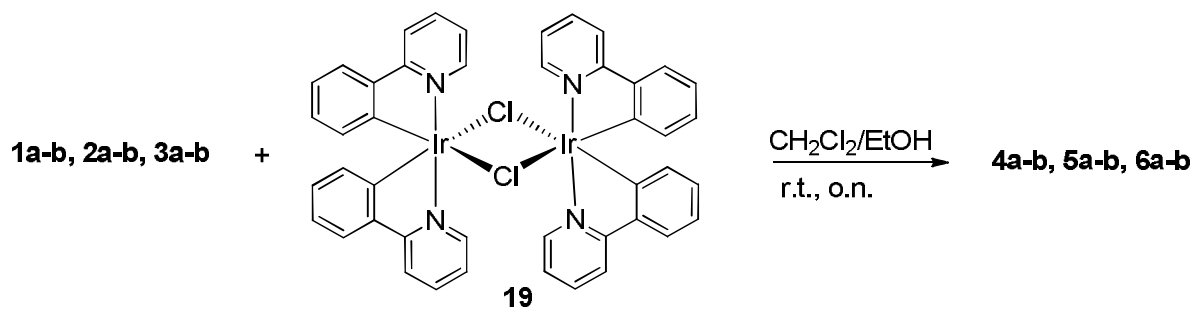


Scheme 4

The absorption and photophysical properties of complexes **4-6** have been studied in DCM and in phosphate buffer solution in order to evaluate the effect of the polarity of the solvent. The collected data are summarized in Table 1.

| Complex (solvent) | $\lambda_{abs}$ (nm): $\varepsilon$ $10^4$(M$^{-1}$ cm$^{-1}$) | $\lambda_{em}$ (nm) | $\lambda_{em}$ (nm) 77 °K | $\tau$ (ns), air | $\tau$ (ns), deair | $\tau$ (ns) 77 °K | $\Phi$ Air | $\Phi$ Deair |
|---|---|---|---|---|---|---|---|---|
| **4a** (DCM) | 255 (4.50), 381 (0.66) | 476, 508 | 474, 506, 545 sh | 144 (90%) 55 (10%) | 419 | 4160 | 0.048 | 0.148 |
| **5a** (DCM) | 269 (4.62), 380 (0.16) | 478, 506, 542 (sh) | 472, 506, 538 | 134 | 508 | 4749 (90%) 1685 (10%) | 0.12 | 0.55 |
| **6a** (DCM) | 270 (6.05), 294 (5.32), 382 (0.69) | 476, 508 | 470, 506, 536, 576 (sh) | 227 | 1185 (88%) 356 (12%) | 5982 (84%) 1714 (16%) | 0.078 | 0.34 |
| **4b** (DCM) | 255 (4.51), 381 (0.55) | 476, 508 | 470, 505, 532 sh | 148 | 1100 | 2130 (20%) 4900 (80%) | 0.064 | 0.60 |
| **5b** (DCM) | 268 (4.67), 383 (0.37) | 476, 508, 544 (sh) | 470, 506, 534 (sh) | 134 | 500 | 3928 | 0.098 | 0.25 |
| **6b** (DCM) | 272 (5.46) 288 (5.10), 382 (0.39) | 476, 506, 544 (sh) | 472, 506, 542 (sh) | 130 | 816 | 4930 (67%) 2854 (33%) | 0.12 | 0.41 |
|  |  |  |  |  |  |  |  |  |
| **4a** (buffer) | 284 (4.05), 374 (3.84) | 478, 504 | / | 569 | / | / | 0.128 | / |
| **5a** (buffer) | 270 (4.05), 285 (3.84), 385 (0.63) | 478, 506 | / | 41 (30%) 305 (70%) | / | / | 0.098 | / |
| **6a** (buffer) | 266 (4.05), 303 (3.84), 406 (0.63) | 478, 506 | / | 473 | / | / | 0.016 | / |
| **4b** (buffer) | 268 (4.05), 376 (3.84) | 478, 508 | / | 622 (60%) 90 (40%) | / | / | 0.07 | / |
| **5b** (buffer) | 255 (2.91), 263 (2.93), 378 (0.27) | 478, 506 | / | 417 | / | / | 0.22 | / |
| **6b** (buffer) | 272 (3.26) 286 (3.15), 387 (0.49) | 478, 504 | / | 393 | / | / | 0.057 | / |

Table 1. Photophysical properties of the obtained complexes.

The absorption spectra of complexes **4-6** in DCM (*ca.* $10^{-4}$ M) show ligand centered (LC) transitions in the UV region ($\lambda<300$ nm), while at lower energy values ($\lambda>300$ nm) the charge transfer transitions (CT) can be found that, in the case of a d$^6$ configuration, are attributed to metal-to-ligand charge transfer (MLCT) processes, (Figure 6). The spectra recorded in a phosphate buffer solution (pH=7.4) show absorption profiles similar to those obtained in the organic solvent. Only

small batho-ipso chromic shifts can be observed. For example in the complex **6a** there is an emission maxima shift to lower energy from λ=270, 294, 382 nm to λ=266, 303, 406 nm.
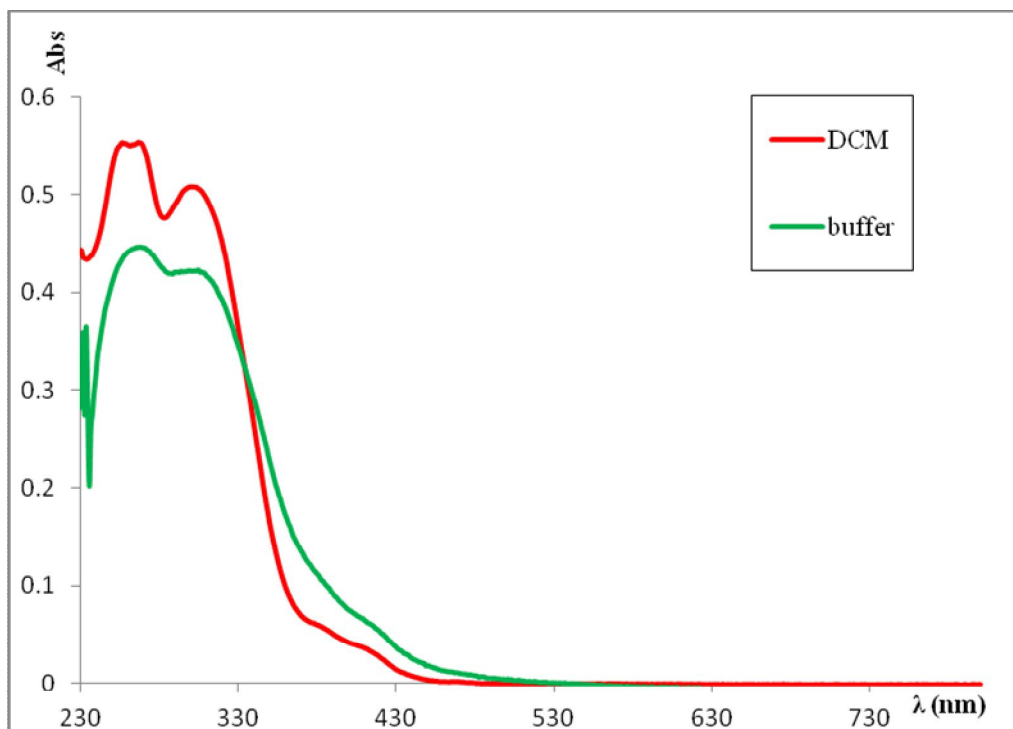


Figure 6: Complex **6a** absorption spectra.

In DCM dilute solution ($<10^{-5}$ M), all the complexes exhibit high luminescence. Using an excitation wavelength of about 380 nm, the complexes show an intense emission at about 475 nm, in the green region. The emission spectra appear structured, showing two intensity maxima (476, 508 nm), due to an emissive excited state with two transitions (LC and MLCT). If the solution is frozen at 77K, it is possible to observe that the contribution to the emission from MLCT transitions is affected by a blue shift, while the contribution to the emission from LC transitions remains unchanged (470, 506, 536, 576 nm), (Figure 7).
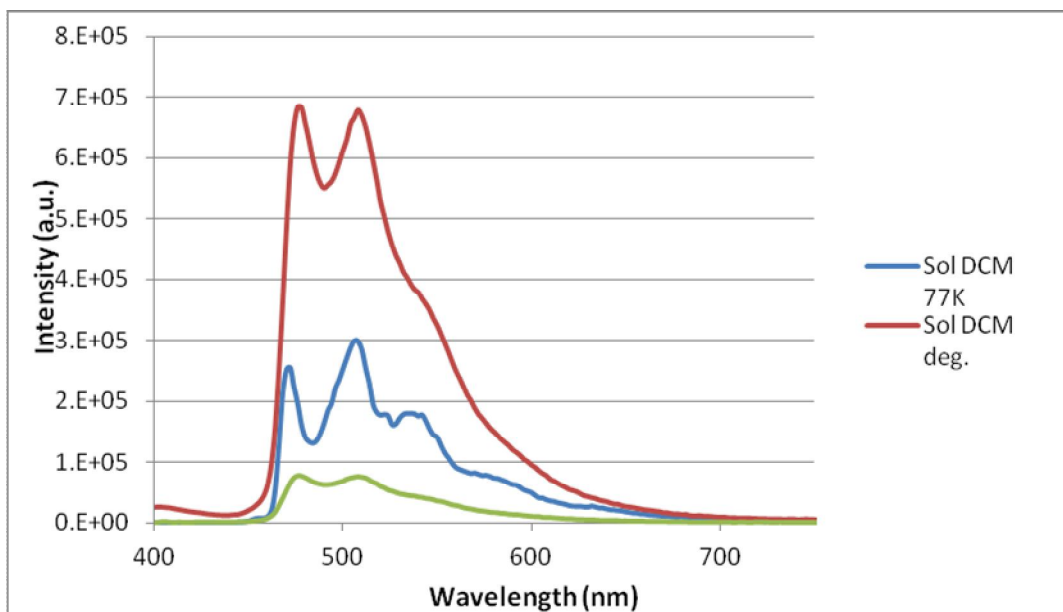
Figure 7: Complex **6a** emission spectra.

The emission quantum yields of the six complexes range from 5% to 15% in oxygenated solutions, while they resulted increased in deaerated solutions (15% to 65%), confirming the phosphorescent nature of the emissions. Also the lifetimes confirm the phosphorescence emission, being in the order of microseconds. In the aqueous environment the profile of the emission does not change, compared to the sample in organic solvent (Figure 8) and this is very important in order to use our complexes as biotinylated probes for avidin detection.
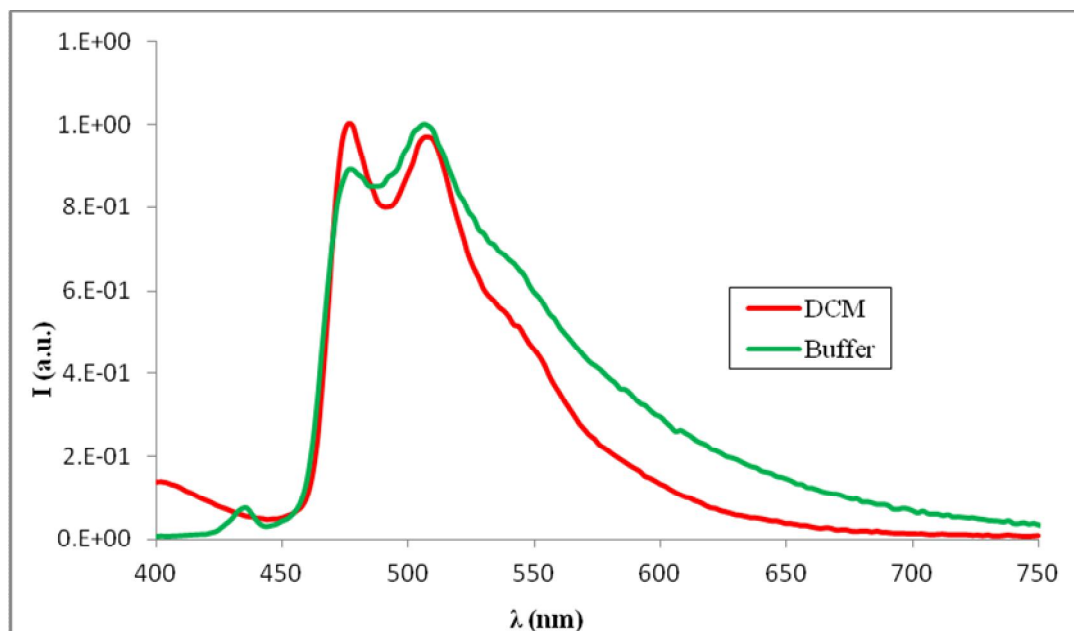


Figura 8: Emission spectra of complex **6a**

### 6.2.1.2 - Avidin-complexes interactions: Emission Titrations[14]

The avidin-binding properties of the biotin complexes **4**-**6** have been investigated by emission titrations of avidin using the complexes as the titrants. Avidin (3.8 μM) was dissolved in a phosphate buffer solution (pH=7.4) and titrations were carried out by adding aliquots of 5 μL of complex solution.

The titration results have been compared with two control experiments in which avidin was absent, and avidin was pre-saturated with excess of unmodified biotin. The titration curves of complexes **4a-b**, **5a-b** and **6a-b** are shown in Figure 9.









60
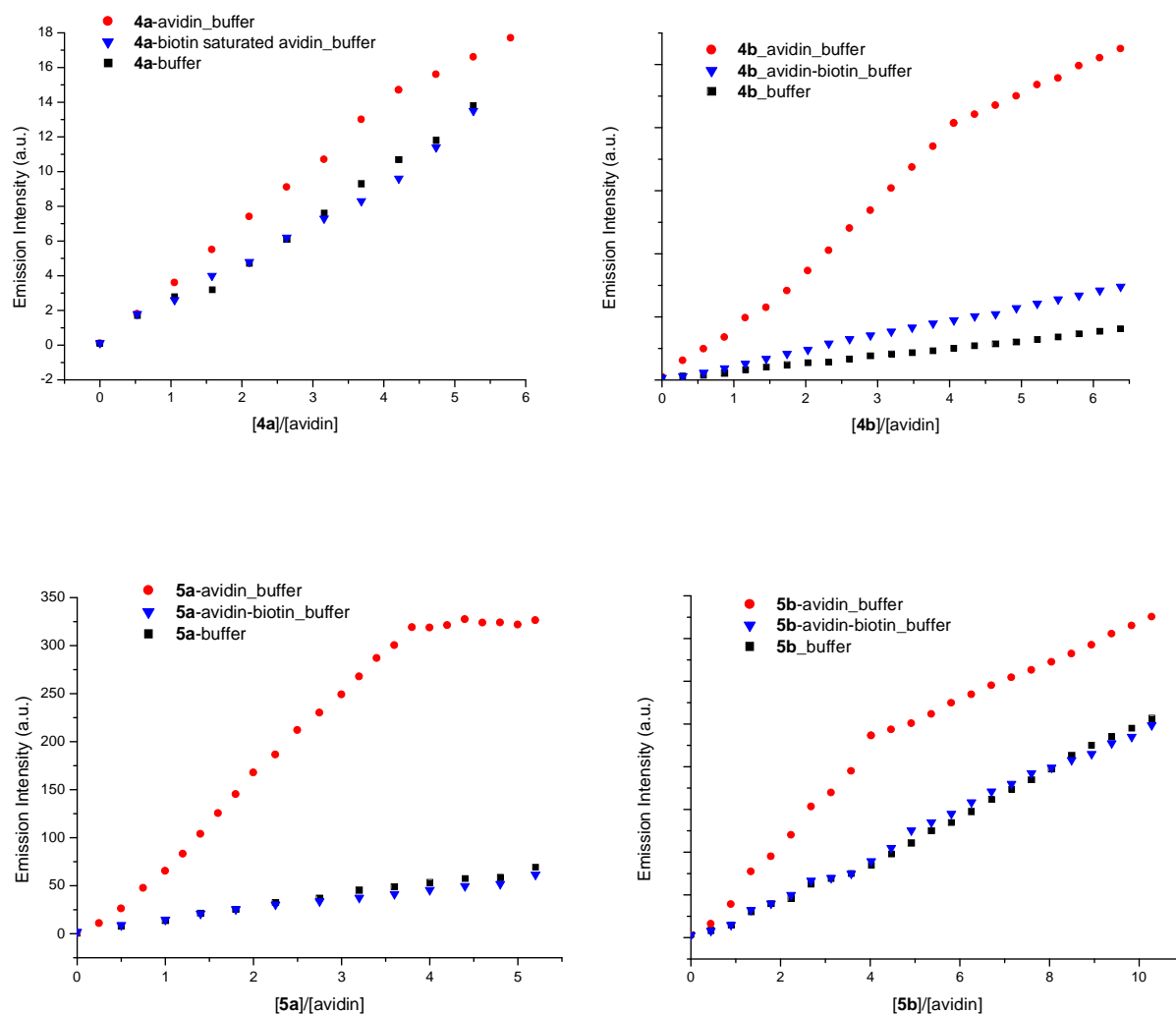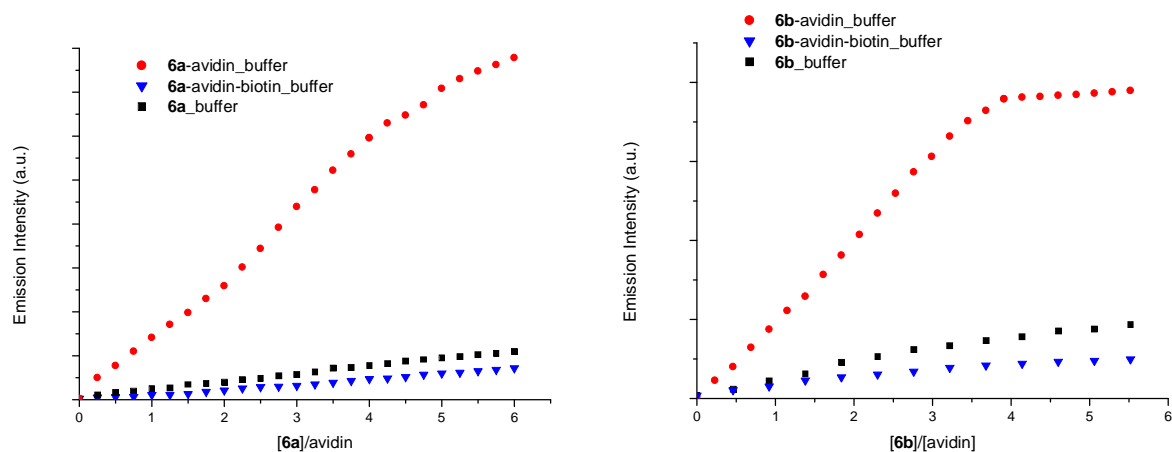
Figure 9: Titration curves

The graphs shows on the X axis the complex/avidin ratio, while on the Y axis the increase of the emission maximum intensity. As shown in Figure 9 in the titration of free avidin, the emission intensity of the complexes increases compared to emission intensity of the complexes in the control experiments. This behaviour is due to the coordination of the biotin with the protein. Bio-conjugation, in fact, may limit the molecular motions of the whole complex, favouring the radiative decays. In the free avidin titration curve after the addition of a certain amount of titrant a point of inflection can be noted. After that point the trend of emission intensity changes and the line slope becomes similar to that found in control experiments. The change of curve slope represents the moment in which the biotinylated complex has saturated all available coordination sites of avidin: in correspondence of this "equivalent point", the concentration of the complex is about four times the concentration of avidin. The further added complex will be not involved in the coordination and therefore the trend of the line looks like the one of the control experiments.

### 6.2.1.3 - HABA assay

The HABA assay is the best way to quantitatively determine the stoichiometry of the interaction avidin-biotinylated complex. HABA (2-(4-Hydroxyphenylazo)benzoic acid) is a colorant that when it is coordinated to the avidin shows an absorption maximum at 500 nm. The affinity HABA-avidin ($K_D = 6*10^{-6}$M) is less strong than the affinity avidin-biotin ($K_D = 10^{-15}$M), therefore when increasing amounts of **4-6** complexes solutions are added to a HABA-saturated avidin solution, the biotinylated complexes remove HABA in the coordinating sites of avidin. A consequent decrease in absorbance at 500 nm, due to the decrease of the amount of the HABA coordinating to avidin is then observed.

Two different assays were performed: in the first one unmodified biotin was added to the HABA saturated-avidin solution, in the second one the complex **4a** was used as titrant.

As shown in the Figure 10, when the concentration biotin/avidin is approximately in a 4:1 ratio (after about 10 additions), the maximum absorption decreases stops. Regarding the complex, more additions are required. This is due to its poor solubility of the complex in the titration medium, so that its concentration is not exactly determinable. Further experiments will be necessary to clarify these inconsistencies.
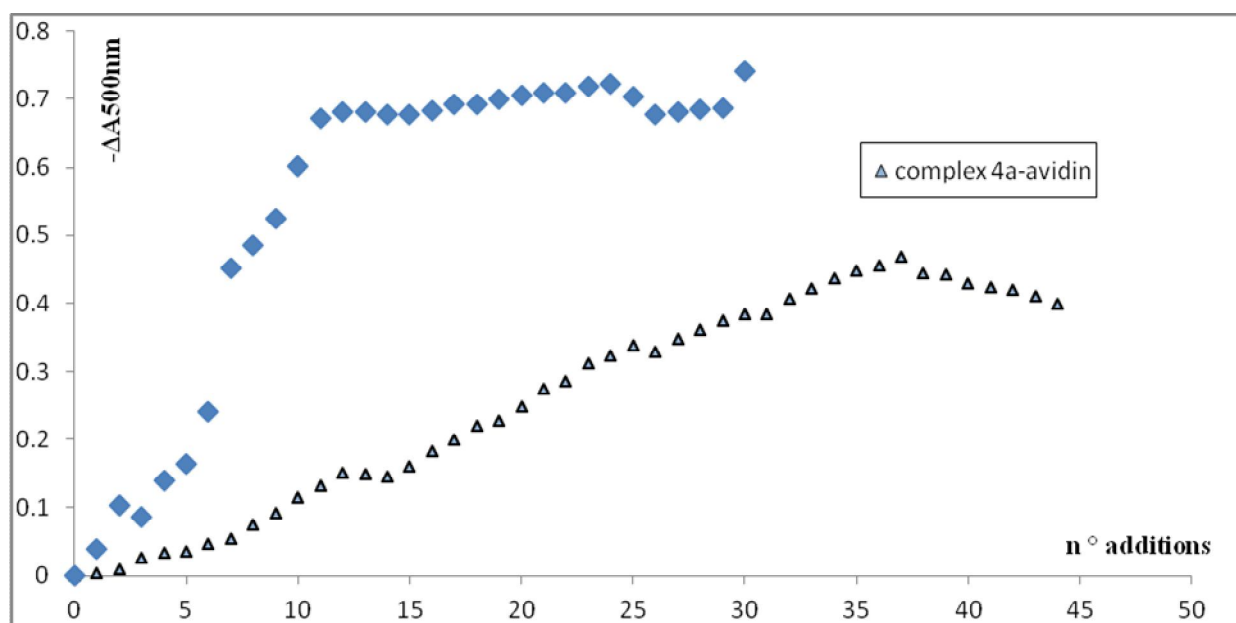


Figure 10: complex Ir (III)-biotin aliquots (5µl), are added to a mixture avidin (7.6µM) and HABA (0.3mM) in a buffer solution of $Na_2SO_4$, pH 7.4 (1 ml) per minute. The absorption spectra of the solution are recorded and subsequently is reported in a graph the value $-\Delta Abs_{500nm}$ (y) and the number of additions (x).[15]

### 6.2.2 -Conclusions

In this work a synthetic method to bifunctional biotinylated ligands containing a pyridine triazole moiety able to form new iridium luminescent complexes was developed. These iridium complexes may be used as luminescent probes thanks to the presence of a Biotin unit on the ligand able to selectively combine avidin, a protein characteristic of egg. the absorption and emission photophysical properties in organic solvent and in aqueous solution buffered to pH 7 .4 have been studied. Subsequently, we studied the interactions biotinylated complex-biological target, by performing the titration of samples containing avidin dissolved in phosphate buffer at pH 7.4, and

using as a titrant, the biotinylated complexes of Ir (III). Finally, we studied the stoichiometry of the interaction avidin - biotinylated complexes via HABA assays. Based on the obtained results, it can be concluded that the complexes possess good photoemissive property that vary in the presence of avidin. This is due to the fact that it establishes a strong interaction between the avidin and the Biotin moiety of Ir (III) complex.

### 6.2.3 - Experimental Section

The solvents and chemicals were used as received from sellers, unless otherwise mentioned. NMR spectra were recorded by using a Varian Mercury 400 MHz or a Varian Inova 600 MHz spectrometer with tetramethylsilane as the internal standard. Elemental analyses were performed on a ThermoQuest Flash 1112 series EA instrument. ESI-MS analysis were performed by direct injection of acetonitrile solutions of the compounds using a WATERS ZQ 4000 mass spectrometer. The IR spectra were recorded with a FT-IR spectrometer Perkin Elmer Spectrum 2000. UV/Vis absorption spectra were measured on a Varian Cary 4 double-beam UV-Vis spectrometer and baseline corrected. Steady-state emission spectra were recorded on an Edinburgh FLS920P spectrofluorimeter equipped with a 450 W Xenon arc lamp, double excitation and single emission monochromators and a peltier cooled Hamamatsu R928P photomultiplier tube (185–850 nm). Emission and excitation spectra were corrected for source intensity (lamp and grating) and emission spectral response (detector and grating) by calibration curve supplied with the instrument. Emission lifetimes were determined on the same Edinburgh instrument with the Time Correlated Single Photon Counting (TCSPC) technique using pulsed picosecond LEDs (EPLED 295 or EPLED 360, FHWM <800 ps, repetition rates between 10 kHz and 1 MHz) as the excitation source and the above-mentioned R928P PMT as detector. The goodness of fit was assessed by minimizing the reduced $\chi^2$ function andvisual inspection of the weighted residuals. The emission quantum yields were determined according to the optically dilute solutions method in ACN solutions with reference to $Ru(bpy)_3Cl_2$ as the standard (r) according to Equation (1),[31] where $I$ refers to the area of the emission peaks of the complex and the reference, A to their absorptions and n is the refractive index of the corresponding solvents.

$$\Phi = \Phi_r \frac{\text{wavelength (nm)}}{I_r} \frac{}{A} \frac{}{n_r^2}$$

**Synthesis of Ligands**

**Ligand 1a**

**Synthesis of azide**: In a 50 ml-two-necked round-bottom flask equipped with a stirring bar, 11-bromo-1-undecanol **7** (0.75 g, 3.0 mmol) and $NaN_3$ (0.39 g, 6.0 mmol) was dissolved in 10 mL of DMSO. The reaction mixture was stirred under at room temperature for 24 h. Then water (15 mL) was added and the aqueous phase was extracted with ethyl acetate (3X 10 ml). The organic layer was dried over $MgSO_4$ and the solvent evaporated to give a brown oil (98% yields). The product was used in the next step without further purification.

$^1$H NMR ($CDCl_3$, 300 MHz) $\delta$: 3.58 (dt, 2H, $J_{HH}$= 6.5, $J_{HH}$= 1.4), 3.22 (t, 2H, $J_{HH}$=7.0), 1.62 - 1.47 (m, 4H), 1.39 - 1.21 (m, 14H).

**Synthesis of ligand 8:** In a 100 ml-two-necked round-bottom flask equipped with a stirring bar, the crude azide (3 mmol) was dissolved in a mixture of tBuOH/$H_2O$=1:1 (20 ml), and 2-ethynyl pyridine (0.45 g, 4.4 mmol), sodium ascorbate (86 mg, 0.4 mmol) and $CuSO_4$ (0.30 g, 1.2 mmol) were added. The reaction was left to stir overnight at room temperature. Then the solvent was removed by vacuum and 35 ml of $CH_2Cl_2$ and 35 ml of aqueous $NH_3$ were added. The mixture was left to stir overnight. The aqueous layer was washed twice with 30 ml of $CH_2Cl_2$, and the organic phase was dried over $MgSO_4$. The solvent was removed and the crude was purified by column chromatography on silica gel (EtOAc/$CH_2Cl_2$ = 6/4, $CH_2Cl_2$/MeOH = 9:1, 85% yields).

$^1$H NMR ($CDCl_3$, 300 MHz) $\delta$: 8.57 (ddd, 1H, $J_{HH}$= 4.9, $J_{HH}$= 1.0, $J_{HH}$= 1.7), 8.19 (dt, 1H, $J_{HH}$= 8.0, $J_{HH}$= 1.0), 8.13 (s, 1H), 7.78 (dt, 1H, $J_{HH}$= 7.7, $J_{HH}$= 1.7), 7.23 (ddd, 1H, $J_{HH}$= 7.4, $J_{HH}$=4.9, $J_{HH}$=1.3), 4.42 (t, 2H, $J_{HH}$= 7.1), 3.63 (t, 2H, $J_{HH}$= 6.6), 2.1 (bs, 1H), 1.90-2.00 (m, 2H), 1.50-1.60 (m, 2H), 1.20-1.40 (m, 14H). $^{13}$C NMR ($CDCl_3$, 101 MHz) $\delta$: 150.6 (C), 149.5 (CH), 148.4 (C), 137.2 (CH), 123.0 (CH), 122.1 (CH), 120.5 (CH), 63.1 ($CH_2$), 50.7 ($CH_2$), 33.0 ($CH_2$), 30.4 ($CH_2$), 29.6 ($CH_2$), 29.50 ($CH_2$), 29.48 ($CH_2$), 29.4 ($CH_2$), 29.1 ($CH_2$), 26.6 ($CH_2$), 25.9 ($CH_2$).

**Synthesis of tosylate ligand:** To a solution of ligand **8** (0.40 g, 1.27 mmol) in dry DCM (15 mL) pyridine (150μL, 1.90 mmol) was added at 0°C under nitrogen atmosphere. TsCl (0.72 g, 3.8 mmol) was added to the solution over 5 min at the same temperature. After 1 h the ice bath was removed and the mixture was stirred at room temperature for 48 h. Then the reaction was quenched with $H_2O$ and extracted three times with $Et_2O$. The combined organic layers were dried over anhydrous $MgSO_4$ and evaporated. The residual product was purified by column chromatography on silica gel (DCM/EtOAc 1:1) to give **tosylate ligand** in 84% yields.

^{1}H NMR (CDCl$_3$, 300 MHz) $\delta$:8.57 (ddd, 1H, $J_{HH}$=4.9, $J_{HH}$=1.8, $J_{HH}$=1.0), 8.19 (dt, 1H, $J_{HH}$=8.0, $J_{HH}$= 1.0), 8.13 (s, 1H), 7.82 - 7.75 (m, 3H), 7.36-7.30 (m, 2H), 7.23 (ddd, 1H, $J_{HH}$=7.5, $J_{HH}$=4.9, $J_{HH}$=1.2 Hz), 4.42 (t, 2H, $J_{HH}$=7.2), 4.00 (t, 2H, $J_{HH}$=6.5), 2.43 (s, 3H), 2.00-1.90 (m, 2H), 1.67-1.56 (m, 2H), 1.40-1.15 (m, 14H).

**Synthesis of azido ligand**: In a 50 ml-two-necked round-bottom flask equipped with a stirring bar, ligand **tosylate ligand** (0.50 g, 1.07 mmol) and NaN$_3$ (0.21 g, 3.19 mmol) was dissolved in 15 mL of DMF. The reaction mixture was stirred at room temperature for 24 h. The solvent was removed by vacuum. Then water (20 mL) and EtOAc (20 mL) were added and the aqueous phase was extracted with ethyl acetate (3X 10 ml). The organic layer was dried over MgSO$_4$ and the solvent evaporated to give **azido ligand** (98% yields). The product was used in the next step without further purification.

^{1}H NMR (CDCl$_3$, 300 MHz) $\delta$: 8.58 (ddd, 1H, $J_{HH}$=4.8, $J_{HH}$=1.7, $J_{HH}$=1.0), 8.19 (td, 1H, $J_{HH}$=7.9, $J_{HH}$=1.1), 8.13 (s, 1H), 7.78 (dt, 1H, $J_{HH}$=7.9, $J_{HH}$=1.8), 7.23 (ddd, 1H, $J_{HH}$=7.5, $J_{HH}$=4.9, $J_{HH}$=1.2), 4.42 (t, 2H, $J_{HH}$=7.2), 3.25 (t, 2H, $J_{HH}$=7.0), 2.00−1.90 (m, 2H), 1.65–1.50 (m, 2H), 1.40–1.20 (m, 14H). ^{13}C NMR (CDCl$_3$, 101 MHz) $\delta$: 150.6 (C), 149.6 (CH), 148.5 (CH), 137.1 (CH), 123.0 (CH), 122.0 (CH), 120.4 (CH), 51.6 (CH$_2$), 50.7 (CH$_2$), 30.4 (CH$_2$), 29.6 (CH$_2$), 29.52 (CH$_2$), 29.47 (CH$_2$), 29.3 (CH$_2$), 29.1 (CH$_2$), 29.0 (CH$_2$), 26.9 (CH$_2$), 26.6 (CH$_2$).

**Synthesis of ligand 9**: In a 50 ml-two-necked round-bottom flask equipped with a stirring bar, **azido ligand** (0.36 g, 1.05 mmol) and triphenylphosphine (0.3 g, 1.26 mmol) was dissolved in 10 mL of THF. Then H$_2$O (50 μL, 2.7 mmol) was added to the solution. The reaction mixture was stirred at room temperature for 48 h. Then the solvent was removed by vacuum and the crude was purified by column chromatography on silica gel (DCM/EtOAc 4:6, DCM/MeOH 8:2) to give **9** in 75% yields.

^{1}H NMR (CDCl$_3$, 300 MHz) $\delta$:8.58 (ddd, 1H, $J_{HH}$=4.8, $J_{HH}$=1.7, $J_{HH}$=1.0), 8.16 (td, 1H, $J_{HH}$=7.9, $J_{HH}$=1.0), 8.13 (s, 1H), 7.78 (dt, 1H, $J_{HH}$=7.7, $J_{HH}$=1.9), 7.23 (ddd, 1H, $J_{HH}$=7.5, $J_{HH}$=4.9, $J_{HH}$=1.1), 4.42 (t, 2H, $J_{HH}$=7.2), 2.66 (bt, 2H, $J_{HH}$=7.0), 2.00–1.86 (m, 4H), 1.50–1.20 (m, 16H). ^{13}CNMR (CDCl$_3$, 101 MHz) $\delta$: 150.6 (C), 149.6 (CH), 148.5 (C), 137.1 (CH), 123.0 (CH), 122.0 (CH), 120.4 (CH), 50.7 (CH$_2$), 42.3 (CH$_2$), 33.6 (CH$_2$), 30.4 (CH$_2$), 29.7 (CH$_2$), 29.6 (2CH$_2$), 29.2 (CH$_2$), 27.0 (CH$_2$), 26.6 (CH$_2$).

**Synthesis of 11**: Biotin **10** (0.20 g, 0.82 mmol), NHS (0.19 g, 1.64 mmol) and (DCC) (0.33 g, 1.64 mmol) were dissolved in 10 mL of anhydrous DMF. The reaction mixture was stirred at room

temperature for 8 h. Then the solvent was removed by vacuum and the crude was washed with MeOH to give pure **11** in 87% yields.

^{1}H NMR (DMSO d6, 400 MHz) $\delta$: 6.4 (bs, 1H), 6.3 (bs, 1H), 4.35–4.25 (m, 1H), 4.16 - 4.10 (m, 1H), 3.15 –3.05 (m, 1H), 2.85–2.75 (m, 5H), 2.65 (t, 2H, $J_{HH}$=7.5), 2.56 (d, 1H, $J_{HH}$=12.4), 1.70–1.55 (m, 3H), 1.55–1.30 (m, 3H). ^{13}CNMR (DMSO d6, 101 MHz) $\delta$:170.9 (C), 169.6 (C), 163.3 (C), 61.7 (CH), 59.8 (CH), 55.9 (CH), 40.4 (CH$_2$), 30.7 (CH$_2$), 28.5 (CH$_2$), 28.2 (CH$_2$), 26.1 (2CH$_2$), 25.0 (CH$_2$). ESI - MS: 364 [M$^+$ + Na].

**Synthesis of ligand 1a**: Ligand **9** (0.21 g, 0.61 mmol) and **11** (0.25 g, 0.79 mmol) were dissolved in 10 mL of anhydrous DMF. Et$_3$N (250 μL, 1.83 mmol) was added to the solution and the reaction mixture was stirred at room temperature for 24 h. Then the solvent was removed by vacuum and the crude was washed with Et$_2$O (3 x 15 ml). The solid was dissolved in CH$_2$Cl$_2$ (0.5 mL) and then precipitated with Et$_2$O to give **1a** in 92% yields.

^{1}H NMR (DMSO d6, 300 MHz) δ 8.60 (s, 1H), 8.58 (dq, J$_D$ = 4.8 Hz, J$_Q$ = 0.9 Hz, 1H), 8.01 (dt, J$_D$ = 7.9 Hz, J$_T$ = 1.1 Hz, 1H), 7.87 (td, J$_T$ = 7.6 Hz, J$_D$ = 1.8 Hz, 1H), 7.69 (bt, J = 5.5 Hz, 1H), 7.32 (ddd, J = 7.6 Hz, J = 4.8 Hz, J = 1.2 Hz, 1H), 6,39 (bs, 1H), 6.33 (bs, 1H), 4.40 (t, J = 6.9 Hz, 2H), 4.28 (dd, J = 7.7 Hz, J = 5.3 Hz, 1H), 4.14 - 4.07 (m, 1H), 3.11 - 3.03 (m, 1H), 3.02 - 2.92 (m, 2H), 2.80 (dd, J =12.2 Hz, J = 5.1 Hz, 1H), 2.56 (d, J = 12.1 Hz, 1H), 2.02 (t, J = 7.3 Hz, 2H), 1.91 - 1.79 (m, 2H), 1.66 - 1.12 (m, 23H). ^{13}C NMR (CDCl$_3$, 101 MHz) δ 173.1 (C), 163.4 (C), 150.6 (C), 149.6 (CH), 148.5 (C), 137.9 (CH), 124.0 (CH), 123.7 (CH), 120.3 (CH), 61.9 (CH), 60.3 (CH), 56.6 (CH), 50.3 (CH$_2$), 41.3 (CH$_2$), 39.7 (CH$_2$), 36.7 (CH$_2$), 30.5 (CH$_2$), 29.9 (CH$_2$), 29.8 (CH$_2$), 29.6 (CH$_2$), 29.5 (CH$_2$), 29.47 (CH$_2$), 29.4 (CH$_2$), 29.1 (CH$_2$), 28.3 (CH$_2$), 27.1 (CH$_2$), 26.6 (CH$_2$), 24.7 (CH$_2$) . ESI - MS: 542 [M$^+$], 564 [M$^+$ + Na].

## Ligand 1b

**Synthesis of ligand 1b**: Biotin **10** (0.19 g, 0.76 mmol) was dissolved in SOCl$_2$ (6 ml). The reaction mixture was stirred at room temperature for 2 h under nitrogen atmosphere. Then the solvent was removed by vacuum and the crude was dissolved in anhydrous ACN (10 mL). To the solution **8** (0.12 g, 0.38 mmol) was added dissolved in other anhydrous ACN (5 mL). This new reaction mixture was stirred at room temperature for 24 h under nitrogen atmosphere. Then the solvent was removed by vacuum and the crude was dissolved with an aqueous solution NaHCO$_{3(sat)}$ and EtOAc 1:1. The aqueous phase was extracted with ethyl acetate (3 x 10 ml) and DCM (2 x 10 ml). The organic layer was dried over MgSO$_4$ and the solvent evaporated. The solid was dissolved in CHCl$_3$ (0.5 mL) and precipitate with Esane to give **1b** in 60% yields.

$^1$H NMR (CDCl$_3$, 400 MHz) δ 8.58 (d, J = 4.2 Hz, 1H), 8.22 - 8.13 (m, 2H), 7.78 (t, J = 7.6 Hz, 1H), 7.26 - 7.20 (m, 1H), 5.25 (bs, 1H), 5.09 (bs, 1H), 4.54 - 4.48 (m, 1H), 4.41 (t, J = 7.1 Hz, 2H), 4.34 - 4.29 (m, 1H), 4.05 (t, J = 6.7 Hz, 2H), 3.19 - 3.12 (m, 1H), 2.91 (dd, J = 12.9 Hz, J = 5.0 Hz, 1H), 2.73 (d, J = 12.9 Hz, 1H), 2.31 (t, J = 7.4 Hz, 2H), 2.00 -1.90 (m, 2H), 1.77 - 1.14 (m, 24H). $^{13}$C NMR (CDCl$_3$, 101 MHz) δ 173.6 (C), 163.1 (C), 150.4 (C), 149.3 (C), 148.2 (CH), 137.0 (CH), 122.8 (CH), 121.9 (CH), 120.3 (CH), 64.5 (CH$_2$), 61.9 (CH), 60.1 (CH), 55.3 (CH), 50.5 (CH$_2$), 40.5 (CH$_2$), 33.9 (CH$_2$), 30.2 (CH$_2$), 29.4 (CH$_2$), 29.35 (CH$_2$), 29.3 (CH$_2$), 29.2 (CH$_2$), 29.0 (CH$_2$), 28.6 (CH$_2$), 28.31 (CH$_2$), 28.26 (CH$_2$), 26.4 (CH$_2$), 25.9 (CH$_2$), 24.8 (CH$_2$). ESI - MS: 543 [M$^+$],565 [M$^+$ + Na].

**Ligand 2a**

**Synthesis of azide**  (following the procedure described in : J. Andersen, U. Madsen, F. Björkling, X. Liang *Synlett*, **2005**, 2209): In a 100 ml-two-necked round-bottom flask equipped with a stirring bar, 4-iodoaniline **13a** (3.51 g, 15 mmol) was dissolved in 30 mL of a DMSO–H$_2$O (5:1) mixture, and NaN$_3$ (1.95 g, 30 mmol) and sodium ascorbate (0.16 g, 0.75 mmol) were added. After bubbling N$_2$ in the solution for 15 min, CuI (0.29 g, 1.5 mmol) and N,N'-dimethylethylendiamine (250 μl, 2.25 mmol) were added and the reaction mixture was stirred under N$_2$ at room temperature. After 4 hours the iodide was completely consumed (TLC check), then water (10ml) was added and the aqueous phase was extracted with ethyl acetate (3X 10 ml). The organic layer was dried over MgSO$_4$ and the solvent evaporated. The $^1$H NMR analysis of the crude product was consistent with literature data (**Wei Zhu and Dawei Ma *Chem. Commun.*, 2004**, 888 – 889) and the product was used in the next step without further purification.

**Synthesis of ligand 14a** (following the procedure described in : *Organometallics*, **2008**, 27, 5430): In a 25 ml-two-necked round-bottom flask equipped with a stirring bar, the crude azide (15 mmol) was dissolved in a mixture of tBuOH:H$_2$O=1:1 (38 ml), and 2-ethynyl pyridine (1.9 equiv.), sodium ascorbate (0.3 equiv) and CuSO$_4$ (0.05equiv.) were added. The reaction was left to stir overnight at room temperature. Then the solvent was removed by vacuum and 150 ml of CH$_2$Cl$_2$ and 150 ml of aqueous NH$_3$ were added. The mixture was left to stir overnight. The aqueous layer was washed twice with 100 ml of CH$_2$Cl$_2$, and the organic phase was dried over MgSO$_4$. The solvent was removed and the crude was purified by column chromatography on silica gel (CH$_2$Cl$_2$/MeOH=97/3, 45% yields).

$^1$H NMR (CDCl$_3$, 300 MHz) δ 8.60 (d, $J_{HH}$=4.10 Hz, 1H), 8.46 (s, 1H), 8.23 (d, $J_{HH}$ =7.95 Hz), 1H), 7.78 (triplo doppietto, $J_{HH}$ =7.74 Hz, 1H),  7.51 (d, $J_{HH}$ =8.63, 2H), 7.27-7.20 (m, 1H), 6.76 (d, $J_{HH}$ =8.73 Hz, 2H), 4.04 (bs, 2H). $^{13}$C NMR (CDCl$_3$, 75 MHz) δ 150.22 (C), 149.47 (CH), 148.53 (C),

147.44 (C), 136.95 (CH), 128.39 (C), 122.94 (CH), 122.11 (CH), 120.34 (CH), 120.08 (CH), 115.27 (CH).

**Synthesis of ligand 2a** (following the procedure described in : *Angewandte,* 46 (34), (**2007**) 6469-64-72): In a 50 ml-two-necked round-bottom flask equipped with a stirring bar, Biotin **10** (0.90 mmol), EDCI*HCl (1.1 mmol),  HOBt (1.1 mmol) and Et$_3$N (1.44 mmol) were dissolved in anhydrous DMF (6 mL) under a nitrogen atmosphere. After 10 min **14a** (0.5 mmol) was added and the reaction was left to stir 72 h at room temperature. Then the solvent was removed by vacuum and the crude was purified by column chromatography on alumina gel (DCM/MeOH = 94:6, 65% yields).

$^1$H NMR (DMSO-d6, 300 MHz) δ 8.60 (d, 1H, J$_{HH}$=4.31 Hz),  8.46 (s, 1H),  8.23 (d, 1H, J$_{HH}$=7.80 Hz),  7.78 (t, 1H, J$_{HH}$=7.80 Hz),  7.51 (d, 2H, J$_{HH}$=8.77 Hz),  7.24 (t, 1H, J$_{HH}$=5.84 Hz), 6.75 (d, 2H, J$_{HH}$=8.50),  4.08 (s, 2H). $^{13}$C NMR (DMSO-d6, 101 MHz) δ 172.01 (C), 163.19 (C), 150.10 (CH), 150.03 (C),  148.51 (C), 140.24 (C), 137.76 (CH), 131.92 (C), 123.73 (CH), 121.43 (CH), 121.79 (CH), 120.21 (CH), 120.74 (CH), 61.51 (CH), 59.67 (CH), 55.84 (CH), 40.31 (CH$_2$), 36.70 (CH$_2$), 28.68 (CH$_2$), 28.55 (CH$_2$), 25.50 (CH$_2$).


**Ligand 3a**

**Synthesis of azide** (following the procedure described in : J. Andersen, U. Madsen, F. Björkling, X. Liang *Synlett*, **2005**, 2209): In a 100 ml-two-necked round-bottom flask equipped with a stirring bar, 1-bromo-4-iodobenzene **15** (3.51 g, 15 mmol) was dissolved in 30 mL of a DMSO–H$_2$O (5:1) mixture, and NaN$_3$ (1.95 g, 30 mmol) and sodium ascorbate (0.16 g, 0.75 mmol) were added. After bubbling N$_2$ in the solution for 15 min, CuI (0.29 g, 1.5 mmol) and N,N'-dimethylethylendiamine (250 μl, 2.25 mmol) were added and the reaction mixture was stirred under N$_2$ at room temperature. After 4 hours the iodide was completely consumed (TLC check), then water (10ml) was added and the aqueous phase was extracted with ethyl acetate (3X 10 ml). The organic layer was dried over MgSO$_4$ and the solvent evaporated. The $^1$H NMR analysis of the crude product was consistent with literature data (**Wei Zhu and Dawei Ma *Chem. Commun.*, 2004**, 888 – 889) and the product was used in the next step without further purification.

**Synthesis of ligand 16** (following the procedure described in : N. K. Barral, A. D. Moorhouse, J. E. Moses, *Org. Lett*., (**2007**), *9*, 1809-1811): In a 25 ml-two-necked round-bottom flask equipped with a stirring bar, the crude azide (2.0 mmol) was dissolved in ACN (8 mL), and 2-ethynyl pyridine (1.9 equiv.), sodium ascorbate (0.3 equiv) and CuSO$_4$ (0.05equiv. in 2 mL of H$_2$O) were added. The

reaction was left to stir overnight at room temperature. Then the solvent was removed by vacuum and 150 ml of EtOAc and 150 ml of aqueous $NH_3$ were added. The mixture was left to stir overnight. The aqueous layer was washed twice with 100 ml of EtOAc, and the organic phase was dried over $MgSO_4$. The solvent was removed and the crude was purified by column chromatography on silica gel ($CH_2Cl_2$/ EtOAc =80/20, 45% yields).

$^1$H NMR (CDCl$_3$, 300 MHz) δ 8.62 (dq, 1H, $J_{HH}$=4.8, $J_{HH}$=1.0), δ 8.52 (bs, 1H), 8.25 (dt, 1H, $J_{HH}$=1.1, $J_{HH}$=7.9), 7.82 (td, 1H, $J_{HH}$=7.9, $J_{HH}$=1.9), 7.75-7.65 (m, 4H), 7.28 (ddd, 1H, $J_{HH}$=1.3, $J_{HH}$=4.9, $J_{HH}$=7.6). $^{13}$C NMR (CDCl$_3$, 101 MHz) δ 149.9 (C), 149.8 (CH), 149.4 (C), 137.2 (CH), 136.1 (C), 133.2 (CH), 122.7 (C), 122.0 (CH), 120.7 (CH), 119. 9 (CH).

**Synthesis of ligand 18** (following the procedure described in: *Chem. Commun.*, **2004**, 1774): In a 25 ml-two-necked round-bottom flask equipped with a stirring bar, ligand **16** (0.602 g, 2.0 mmol) and 4-aminophenylboronic acid pinacol ester **17a** (0.55 g, 2.5 mmol) were dissolved in THF (6 mL). Then was edded EtOH (250 μl) and an aqueous solution of $K_2CO_3$ 2M (2 mL). After bubbling $N_2$ in the solution for 15 min, Pd(PPh$_3$)$_4$ (2.0 mmol) was added and the reaction mixture was stirred under $N_2$ at room temperature. After 48 hours saturated aqueous solution of $NH_4Cl$ and $Na_2CO_3$ were added subsequently to the reaction mixture that was then extracted with DCM. The combined organic layers were dried over $MgSO_4$. After filtration and removal of the solvent, the residue was purified by column chromatography on silica gel (DCM/EtOAc 80:20, 20% yields).

$^1$H NMR (CDCl$_3$, 300 MHz) δ: 8.64 (s, 1H), 8.61 (s, 1H), 8.29 (d, 1H, $J_{HH}$=7.9 Hz), 7.84 (m 3H), 7.70 (d, 2H, $J_{HH}$ =7.5 Hz), 7.46 (d, 2H, $J_{HH}$ =7.5 Hz), 7.30 (s, 1H), δ 6.80 (d, 2H, $J_{HH}$ =7.5 Hz).

**Synthesis of ligand 3a** (following the procedure described in : *Angewandte,* 46 (34), (2007) 6469-64-72): In a 50 ml-two-necked round-bottom flask equipped with a stirring bar, Biotin **10** (0.90 mmol), EDCI*HCl (1.1 mmol),  HOBt (1.1 mmol) and Et$_3$N (1.44 mmol) were dissolved in anhydrous DMF (6 mL) under a nitrogen atmosphere. After 10 min **18** (0.5 mmol) was added and the reaction was left to stir 24 h at room temperature. Then MeOH was edded to the solution and the precipitate was filtered to give pure **3a** (65% yields).

$^1$H NMR (DMSO, 300 MHz) δ 10.05 (s, 1H), 9.38 (s, 1H), 8.68 (d, 1H, $J_{HH}$ =4.2 Hz), 8.13 (m, 3H), 7.96 (td, 1H, $J_{HH}$ =1.8 Hz), 7.89 (d, 2H, $J_{HH}$ =8.8 Hz), 7.65 (s, 4H),  7.42 (ddd, 1H, $J_{HH}$=0.7 Hz, $J_{HH}$=4.9 Hz, $J_{HH}$=7.6 Hz),  6.45 (s, 1H),  6.38 (s, 1H), 4.32 (m, 1H),  4.15 (m, 1H), 2.35 (t, 2H, $J_{HH}$ =7.34 Hz), 1.57-1.40 (m, 9H).

**Ligand 2b**

**Synthesis of azide** (following the procedure described in : J. Andersen, U. Madsen, F. Björkling, X. Liang *Synlett*, **2005**, 2209): In a 10 ml-two-necked round-bottom flask equipped with a stirring bar, 4-iodophenol **13b** (0.660 g, 3 mmol) was dissolved in 6 mL of a DMSO–$H_2O$ (5:1) mixture, and $NaN_3$ (0.390g, 6 mmol) and sodium ascorbate (0.030 g, 0.15 mmol) were added. After bubbling $N_2$ in the solution for 15 min, CuI (0.057 g, 0.3 mmol) and N,N'-dimethylethylendiamine (48 μl, 0.45 mmol) were added and the reaction mixture was stirred under $N_2$ at room temperature. After 4 hours the iodide was completely consumed (TLC check), then water (10ml) was added and the aqueous phase was extracted with ethyl acetate (3X 10 ml). The organic layer was dried over $MgSO_4$ an the solvent evaporated. The ^{1}H NMR analysis of the crude product was consistent with literature data (**Wei Zhu and Dawei Ma *Chem. Commun.*, 2004**, 888 – 889) and the product was used in the next step without further purification.

**Synthesis of ligand 14b:** In a 25 ml-two-necked round-bottom flask equipped with a stirring bar, the crude azide (3 mmol) was dissolved in a mixture of tBuOH:$H_2O$=1:1 (15 ml) , and 2-ethynyl pyridine (1.1 equiv.), sodium ascorbate (0.3 equiv) and $CuSO_4$ (0.05equiv.) were added. The reaction was left to stir overnight at room temperature. Then the solvent was removed by vacuum and 20 ml of $CH_2Cl_2$ and 20 ml of aqueous $NH_3$ were added. The mixture was left to stir overnight. The aqueous layer was washed twice with 10 ml of $CH_2Cl_2$, and the organic phase was dried over $MgSO_4$. The solvent was removed and the crude was purified by column chromatography on silica gel ($CH_2Cl_2$/MeOH=95/5, 80% yields).

^{1}H NMR (300 MHz, $CDCl_3$): $\delta$ 6.95-7.05 (m, 2H), 7.30 (m, 1H), 7.65-7.75 (m, 2H), 7.85 (dt, 1H, *J*=7.8, *J*=1.7), 8.27 (bd, 1H, *J*=8.7), 8.51 (s, 1H), 8.62 (bd, 1H, *J*=5.3). ^{13}C NMR (150 MHz, $CD_3OD$): $\delta$ 117.2 (CH), 121.7 (CH), 122.2 (CH), 123.5 (CH), 124.7 (CH), 130.5 (C), 138.9 (CH), 149.5 (C), 150.5 (CH), 150.9 (C), 159.8 (C). HRMS (m/z) [+], ($C_{13}H_{10}N_4O$)+H *calcd* 239.0933, *found* 239.0927.

**Synthesis of ligand 2b** (following the procedure described in: Org. Biomolec. Chem. 6, (**2008**), 1625-1634): In a 50 ml-two-necked round-bottom flask equipped with a stirring bar, Biotin **10** (0.15 mmol), ligand **14b** and HOBt (0.30 mmol) were added under $N_2$. After 10 min anhydrous DMF (3 mL) was added. After bubbling $N_2$ in the solution for 15 min, $Et_3N$ (0.60 mmol) and EDCI*HCl (0.38 mmol) were added and the reaction mixture was stirred under $N_2$ at room temperature for 24 h. Then further EDCI*HCl (1.5 equiv) was added and the reaction mixture was stirred under $N_2$ at

room temperature overnight. Then the solvent was removed by vacuum and the crude was washed with MeOH to give **2b** in 55% yields.

^{1}H NMR (DMSO, 400 MHz) δ 9.33 (s, 1H), 8.67 (d, $J_{HH}$ =4.28 Hz, 1H), 8.16 (d, $J_{HH}$ =8.15 Hz, 1H), 8.08 (d, $J_{HH}$ =8.88 Hz, 2H), 7.96 (td, $J_{HH}$ =1.74 Hz, 1H), 7.44-7.37 (m, 3H), δ 6.47 (s, 1H), 6.38 (s, 1H), 4.36-4.30 (m, 1H), 4.20-1.40 (m, 1H), 3.20-3.12 (m, 1H), 2.85 (dd, $J_{HH}$ =5.24 Hz), 1H), 2.67-2.61 (m, 2H), 2.59 (s, 1H), 1.76-1.40 (m, 6H). ^{13}C NMR (DMSO d6, 101 MHz) δ 172.13 (C), 163.17 (C), 150.86 (C), 150.14 (CH), 149.93 (C), 148.68 (C), 137.80 (CH), 134.55 (C), 123.82 (CH), 123.76 (CH), 121.98 (CH), 121.92 (CH), 120.26 (CH), 61.48 (CH), 59.67 (CH), 55.76 (CH), 40.33 ($CH_2$), 33.74 ($CH_2$), 28.46 ($CH_2$), 28.37 ($CH_2$), 24.78 ($CH_2$).

**Ligand 3b**

**Synthesis of ligand 18b** (following the procedure described in: *Chem. Commun.*, **2004**, 1774): In a 25 ml-two-necked round-bottom flask equipped with a stirring bar, ligand **16** (0.15 g, 0.498 mmol) and 4-Hydroxyphenylboronic acid **17b** (0.137 g, 0.996 mmol) were dissolved in THF (5 mL). Then was added EtOH (250 µl) and an aqueous solution of $K_2CO_3$ 2M (0.6 mL). After bubbling $N_2$ in the solution for 15 min, Pd(PPh$_3$)$_4$ (2.0 mmol) was added and the reaction mixture was stirred under $N_2$ at 75°C. After 24 hours saturated aqueous solution of $NH_4Cl$ and $Na_2CO_3$ were added subsequently to the reaction mixture that was then extracted with DCM. The combined organic layers were dried over $MgSO_4$. After filtration and removal of the solvent, the residue was purified by column chromatography on silica gel (DCM/EtOAc 85:15, 35% yields).

^{1}H NMR (CDCl$_3$, 300 MHz) δ 8.64 (m, 2H), 8.28 (d, 1H, $J_{HH}$ = 8.23 Hz), 7.85 (m, 3H), 7.71 (d, 2H, $J_{HH}$=8.62 Hz), 7.53 (d,2H, $J_{HH}$=8.62 Hz), 7.96 (d, 2H, $J_{HH}$ =8.70 Hz), 5.82 (bs, 1H).
^{13}C NMR (CD$_3$OD-ACN-d3, 101 MHz) δ: 142.7 (C), 138.5 (C), 133.35 (C), 133.3 (CH), 132.8 (C), 132.7 (CH), 132.6 (CH), 131.9 (C), 130.6 (C), 129.7 (CH), 129.6 (CH), 128.9 (CH), 128.3 (CH), 121.7 (CH), 116.5

**Synthesis of ligand 3b** (following the procedure described in: Org. Biomolec. Chem. **2008,** 6, 1625-1634): In a 50 ml-two-necked round-bottom flask equipped with a stirring bar, Biotin (0.154 mmol), EDCI*HCl (0.385 mmol), HOBt (0.308 mmol) and Et$_3$N ( 0.616 mmol) were dissolved in anhydrous DMF (6 mL) under a nitrogen atmosphere. After 10 min **18b** (0.103 mmol) was added and the reaction was left to stir 24 h at room temperature. Then further EDCI*HCl (1.5 equiv) was added and the reaction mixture was stirred under $N_2$ at room temperature overnight. Then the solvent was removed by vacuum and the crude was washed with MeOH to give **L$_4$** in 55% yields.

$^1$H NMR (DMSO, 400 MHz) δ 9.40 (s, 1H), 8.68 (d, $J_{HH}$ =3.98 Hz, 1H), 8.14 (d, 3H, $J_{HH}$ =8.41 Hz), 7.99-7.91 (m, 3H), 7.82 (d, $J_{HH}$ =8.70 Hz, 2H), 7.42 (t, $J_{HH}$ = 6.30 Hz, 1H), 7.26 (d, J $J_{HH}$ =8.62 Hz, 2H), 6.48 (s, 1H), δ 6.38 (s, 1H), 4.35-4.30 (m,1H), 4.20-4.14 (m, 1H), 3.20-3.12 (m, 1H), 2.85 (dd, $J_{HH}$ =5.07 Hz, 1H), 2.65-2.57 (m, 3H), 1.85-1.40 (m, 6H). $^{13}$C NMR (DMSO d6, 101 MHz) δ 172.2 (C), 163.2 (C), 150.9 (C), 150.1 (CH), 150.0 (C), 148.7 (C), 140.1 (C), 137.8 (CH), 136.78 (C), 136.25 (C), 128.46 (CH), 128.35 (CH), 128.83 (CH), 122.90 (CH), 121.68 (CH), 121.06 (CH), 120.29 (CH), 40.34 (CH$_2$), 33.80 (CH$_2$), 28.47 (CH$_2$), 28.40 (CH$_2$), 24.85 (CH$_2$).

**Synthesis of Dimer**
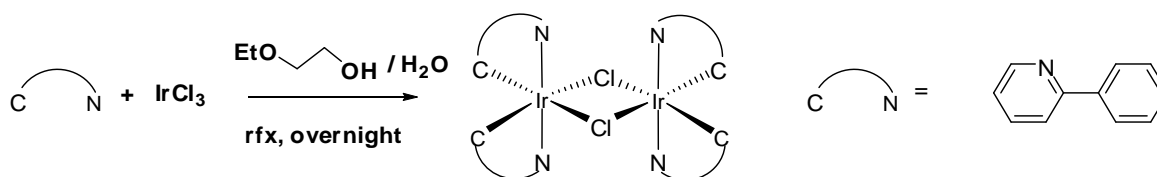


a) M. Nonoyama, *Bull. Chem. Soc. Jpn.* **1974**, *47*, 767.; b) S. Lamansky, P. Djurovich, D. Murphy, F. Abdel-Razzaq, R. Kwong, I. Tsyba, M. Bortz, B. Mui, R. Bau, M. E. Thompson, *Inorg. Chem.* **2001**, *40,* 1704-1711.

**Synthesis of Complexes**

**Synthesis of complex 4a.** In a 50 ml round-bottom flask equipped with a stirring bar, the ligand **1a** (0.050 g, 2 equiv) was dissolved in a 3:1 mixture of CH$_2$Cl$_2$/EtOH (15 mL) and the Iridium dimer **19** (0.054 g, 0.05 mmol) was added. The mixture was left to stir at r.t. 24 h. The solvent was removed and the crude was dissolved in DCM (1 mL) and precipitate with Et$_2$O to give **4a** in 60% yields.

$^1$H NMR (CDCl$_3$, 400 MHz) δ 10.68 (s, 1H), 9.11 (d, J = 8.0 Hz, 1H), 8.04 (td, J$_T$ = 7.7 Hz, J$_D$ = 1.5 Hz, 1H), 7.90 (d, J = 8.4 Hz, 2H), 7.80 -7.70 (m, 3H), 7.69 -7.62 (m, 3H), 7.47 (d, J = 5.7 Hz, 1H), 7.23 - 7.18 (m, 1H), 7.06 - 6.83 (m, 6H), 6.49 (bt, J = 5.3 Hz, 1H), 6.31 (t, J = 7.6 Hz, 2H), 5.78 (bs, 1H), 5.17 (bs, 1H), 4.53 - 4.39 (m, 3H), 4.36 - 4.30 (m, 1H), 3.28 - 3.11 (m, 3H), 2.90 (dd, J = 12.8 Hz, J = 4.9 Hz, 1H), 2.75 (d, J = 12.6 Hz, 1H), 2.31 -2.21 (m, 2H) 2.00 - 1.06 (m, 24H). ESI -MS: 1042 [M$^+$].

**Synthesis of complex 4b.** In a 10 ml round-bottom flask equipped with a stirring bar, the ligand **1b** (0.018 g, 2 equiv) was dissolved in a 3:1 mixture of CH$_2$Cl$_2$/EtOH (4 mL) and the Iridium dimer **19** (0.018 g, 0.017 mmol) was added. The mixture was left to stir at r.t. 24 h. The solvent was removed and the crude was dissolved in DCM (0.5 mL) and precipitate with Et$_2$O to give **4b** in 80% yields.

$^1$H NMR (CDCl$_3$, 400 MHz) δ 10.65 (s, 1H), 9.14 (d, J = 7.6 Hz, 1H), 8.02 (t, J$_T$ = 7.0 Hz, 1H), 7.89 (d, J$_D$ = 8.0 Hz, 2H), 7.79 -7.60 (m, 6H), 7.46 (d, J$_D$ = 5.5 Hz, 1H), 7.19 (t, J$_T$ = 6.4 Hz, 1H), 7.06 - 6.72 (m, 6H), 6.30 (t, J = 7.5 Hz, 2H), 5.53 (bs, 1H), 5.34 (bs, 1H), 4.54 - 4.36 (m, 3H), 4.33 - 4.26 (m, 1H), 4.05 (t, J$_T$ = 6.7 Hz, 2H), 3.18 - 3.09 (m, 1H), 2.88 (dd, J$_D$ = 12.6 Hz, J$_D$ = 4.7 Hz, 1H), 2.77 (d, J = 12.7 Hz, 1H), 2.31 (t, J = 7.1 Hz, 2H), 1.97 - 1.86 (m, 2H), 1.78 - 1.53 (m, 3H), 1.50 - 1.37 (m, 3H), 1.36 - 1.06 (m, 16H).

**Synthesis of complex 5a.** In a 10 ml round-bottom flask equipped with a stirring bar, the ligand **2a** (0.014 g, 2 equiv) was dissolved in a 3:1 mixture of CH$_2$Cl$_2$/EtOH (5 mL) and the Iridium dimer **19** (0.015 g, 0.014 mmol) was added. The mixture was left to stir at r.t. 48 h. The solvent was removed and the crude was purified by column chromatography on silica gel (CH$_2$Cl$_2$/ MeOH = 90/10, 70% yields).

$^1$H NMR (DMSO-d6, 400 MHz) δ 10.40 (s, 1H), 10.01 (s, 1H), 8.46 (d, 1H, $J_{HH}$ =7.78 Hz), 8.28-8.20 (m, 3H), 7.96-7.86 (m, 4H), 7.86-7.80 (m, 3H), 7.72 (d, 3H, $J_{HH}$ =6.97 Hz), 7.66 (d, 1H, $J_{HH}$ =5.30), 7.56 (t, 1H, $J_{HH}$=6.33 Hz), 6.17 (d, 2H, $J_{HH}$ =4.33 Hz), 7.00 (t, 1H, $J_{HH}$ =7.50 Hz), 6.90 (q, 2H, $J_{HH}$ 7.50 Hz), 6.79 (t, 1H, $J_{HH}$ =7.50 Hz), 6.41 (s, 1H), 6.35 (s, 1H), 6.20-6.12 (m, 2H), 4.31-4.23 (m, 1H),4.12-4.08 (m, 1H), 3.10 (m, 1H), 2.80 (dd, 1H, $J_{HH}$ =4.70 Hz), 2.56 (d, 1H, $J_{HH}$ =12.40 Hz), δ 2.34 (d, 2H, $J_{HH}$ =6.47 Hz), 1.60-1.05 (m, 6H). $^{13}$C NMR (DMSO-d6, 150 MHz) δ 172.21 (C), 167.68 (C), 166.94 (C), 163.18 (C), 152.80 (C), 150.40 (CH), 150.03 (CH), 149.93 (C), 149.45 (CH), 149.38 (C), 149.14 (C), 146.81 (C), 144.49 (C), 144.52 (C), 141.37 (C), 140.62 (CH), 139.28 (CH), 139.18 (CH), 131.90 (CH), 131.28 (CH), 131.02 (CH), 130.65 (CH), 129.90 (CH), 127.59 (CH), 125.66 (CH), 125.44 (CH), 124.98 (CH),124.43 (CH), 124.20 (CH), 123.37 (CH), 122.91 (CH$_2$), 122.92 (CH), 122.08 (CH), 120.32 (CH), 120.15 (CH), 61.50 (CH), 59.66 (CH), 55.81 (CH), 36.63 (CH$_2$), 36.33 (CH$_2$), 28.66 (CH$_2$), 28.53 (CH$_2$), 25.38 (CH$_2$).
ESI - MS: 964 (M$^+$, 100)

**Synthesis of complex 5b.** In a 50 ml round-bottom flask equipped with a stirring bar, the ligand **2b** (0.05 g, 2 equiv) was dissolved in a 3:1 mixture of CH$_2$Cl$_2$/EtOH (10 mL) and the Iridium dimer **19** (0.04 g, 0.037 mmol) was added. The mixture was left to stir at r.t. 48 h. The solvent was removed and MeOH was added. Then the solid was filtered off and washed with MeOH (2 mL). The solution was evaporated and the resulting residue was dissolved in MeOH (0.5 mL) and precipitate with Et$_2$O. The solid was filtered to give pure complex **5b** (50% yields).

$^1$H NMR (CD$_3$OD, 400 MHz) δ 9.62 (s, 1H), 8.28 (d, 1H, $J_{HH}$ =8.2 Hz), 8.05 (m, 3H), 7.80-7.95 (m, 9H), 7.68 (d, 1H, $J_{HH}$ =7.6 Hz), 7.55 (m, 5H), 7.35-7.40 (m, 1H),7.05-6.92 (m, 3H), 6.88 (dt, 2H, $J_{HH}$ =1 Hz, $J_{HH}$ =7.6 Hz), 6.73 (t, 1H, $J_{HH}$ =7.59 Hz),6.15 (dd, 2H, $J_{HH}$ =3.00 Hz), 4.45-4.55 (m,

2H), 3.40-3.50 (m, 1H), 2.90-3.10 (m, 2H), 2.35 (t, 2H, $J_{HH}$ =7.34 Hz), 1.90-1.40 (m, 6H). $^{13}$C NMR (DMSO d6, 150 MHz) δ 171.83 (C), 167.69 (C), 166.96 (C), 161.67 (C), 150.38 (CH), 149.97 (C), 149.49 (CH), 149.32 (C), 149.26 (C), 146.74 (C), 144.51 (C), 144.46 (C), 141.70 (C), 140.66 (CH), 140.07 (C), 139.30 (CH), 139.20 (CH), 135.01 (CH?), 133.07 (CH?), 131.90 (CH), 131.31 (CH), 130.66 (CH), 129.92 (CH), 127.96 (CH), 127.68 (CH), 127.51 (CH), 125.70 (CH), 125.46 (CH), 124.99 (CH), 124.44 (CH), 124.22 (CH), 123.38 (CH), 122.92 (CH), 122.33 (CH), 121.71 (CH), 120.33 (CH), 119.91 (CH), 70.36 (CH), 59.02 (CH$_2$), 56.27 (CH), 53.22 (CH), 36.57 (CH$_2$), 27.09 (CH$_2$), 25.56 (CH$_2$), 25.41 (CH$_2$).

ESI - MS: 1040 (M$^+$).

**Synthesis of complex 6a.** In a 10 ml round-bottom flask equipped with a stirring bar, the ligand **3a** (0.014 g, 2 equiv) was dissolved in a 3:1 mixture of CH$_2$Cl$_2$/EtOH (4 mL) and the Iridium dimer **19** (0.016 g, 0.015 mmol) was added. The mixture was left to stir at r.t. 48 h. The solvent was removed and the resulting residue was dissolved in MeOH (0.5 mL) and precipitate with Et$_2$O. The solid was filtered to give pure complex **6a** (60% yields).

$^1$H NMR (CDCl$_3$, 400 MHz) δ 11.6 (s, 1H), 9.33 (d, 1H, $J_{HH}$ =7.68 Hz),8.10 (d, 2H, $J_{HH}$ =8.56 Hz), 7.99 (t, 1H, $J_{HH}$ =7.70 Hz), 7.84 (d, 2H, $J_{HH}$ =8.23 Hz), 7.70 (d, 4H, $J_{HH}$=5.76 Hz), 7.60 (m, 2H), 7.43 (d, 1H, $J_{HH}$ =5.69 Hz), 7.25 (m, 3H), 7.00-6.75 (m, 6H), 6.33 (dt, 2H, $J_{HH}$ =7.4 Hz, $J_{HH}$=5.7 Hz), 4.45 (m, 1H), 4.25 (m, 1H), 3.10 (m, 1H), 2.82 (dd, 1H, $J_{HH}$ =3.97 Hz), 2.67 (d, 1H, $J_{HH}$ =13.03 Hz), 2.45 (t, 2H, $J_{HH}$ =7.41 Hz), 1.70 (m, 4H), 1.43 (t, 2H, $J_{HH}$ =7.66 Hz). $^{13}$C NMR (CDCl$_3$, 101 MHz) δ 170.70 (C), 167.39 (C), 166.51 (C), 162.57 (C), 150.37 (C), 148.91 (C), 148.86 (C), 148.53 (C) , 148.51 (CH), 148.47 (CH), 148.45 (CH), 147.35 (CH), 145.23 (C), 142.71 (C), 142.64 (C), 138.97 (CH), 137.02 (CH), 136.98 (CH), 132.44 (C), 130.93 (CH), 130.70 (CH), 129.68 (CH), 129.01 (CH), 128.72 (CH), 125.83 (CH), 125.15 (CH), 124.29 (CH), 123.67 (CH), 123.31 (CH), 122.33 (CH), 122.23 8CH), 121.84 (CH), 121.67 (CH), 121.21 (CH), 120.61 (CH), 118.55 (CH), 118.43 (CH), 60.93 (CH), 59.15 (CH), 54.42 (CH), 39.57 (CH$_2$), 32.80 (CH$_2$), 27.30 (CH$_2$), 23.63 (CH$_2$). ESI - MS: 965 (M$^+$).

**Synthesis of complex 6b.** In a 10 ml round-bottom flask equipped with a stirring bar, the ligand **3b** (0.016 g, 2 equiv) was dissolved in a 3:1 mixture of CH$_2$Cl$_2$/EtOH (4 mL) and the Iridium dimer **19** (0.016 g, 0.015 mmol) was added. The mixture was left to stir at r.t. 48 h. The solvent was removed and the crude was purified by column chromatography on silica gel (CH$_2$Cl$_2$/ MeOH = 90/10, 30% yields).

$^1$H NMR (CDCl$_3$, 400 MHz) δ 11.79 (s, 1H), 9.38 (d, 1H), 8.16 (d, $J_{HH}$ =8.51 Hz, 2H), 8.06 (t, $J_{HH}$ =7.53 Hz, 1H), 7.92 (dd, $J_{HH}$ =3.66 Hz, 2H), 7.81-7.73 (m, 4H), 7.70-7.64 (m, 4H), 7.57-7.51 (m, 3H), 7.27 (s, 1H), 7.15 (d, $J_{HH}$ =8.59 Hz, 2H), 7.07-6.95 (m, 4H), 6.95-6.85 (m, 2H), 6.34 (dd, $J_{HH}$ =2.20 Hz, 2H), 5.75 (s, 1H), 5.18 (s, 1H),4.55-4.45 (m, 1H), 4.35-4.30 (m, 1H), 3.22-3.16 (m, 1H), 2.92 (dd, $J_{HH}$ =4.95 Hz, 1H), 2.75 (d, $J_{HH}$ =12.67 Hz, 1.90-1.40 (m, 6H).

$^{13}$C NMR (CDCl$_3$, 101 MHz) δ 171.06 (C), 167.45 (C), 166.57 (C), 162.26 (C), 149.62 (C), 149.04 (C),148.94 (C), 148.50 (C), 148.47 (CH), 148.42 (CH), 147.38 (CH), 145.32 (C), 142.71 (C), 142.64 (C), 140.59 (C), 147.38 (CH), 145.32 (C), 142.71 (C), 142.64 (C), 140.59 (C), 138.96 (CH), 136.97 (CH), 136.92 (CH), 136.12 (C), 134.28 (C), 130.95 (CH), 130.70 (CH), 129.70 (CH), 129.03 (CH), 127.37 (CH), 127.13 (CH), 125.90 (CH), 125.05 (CH), 125.41 (CH), 123.67 (CH), 123.30 (CH), 122,29 (CH), 121.81 (CH), 121.67 (CH), 121.20 (CH), 121.14 (CH), 119.74 (CH), 118.52 (CH), 118.41 (CH), 60.92 (CH), 59.12 (CH), 54.33 (CH), 39.55 (CH$_2$), 32.97 (CH$_2$), 29.68 (CH$_2$), 27.34 (CH$_2$), 23.72 (CH$_2$).

ESI - MS: 1041 (M$^+$)

### 6.2.4 - Bibliography

1. P. Sharma, S. Brown, G. Walter, S. Santra, and B. Moudgil, *Nanoparticles for bioimaging, Advances in Colloid and Interface Science*, 123, **2006**,471-485.

2. R. Weissleder & M. J. Pittet, "Imaging in the era of molecular oncology", *Nature*, 452, 7187, **2008**, 580-589.

3. Petty, Howard R, "Fluorescence microscopy: established and emerging methods, experimental strategies, and applications in immunology", *Microscopy research and technique*, 70, 8, **2007**, 687 709.

4. D.-L. Ma, W.-L. Wong, W.-H. Chung, F.-Y. Chan, P.-K. So, T.-S. Lai, Z.-Y. Zhou, Y.-C. Leung, K.-Y. Wong, *Angew., Chem. Int. Ed.*, 47, **2008**, 3735.

5. N. M. Green, *Methods Enzymol.*, 184, **1990**, 51-67.

6. K.P. Nurminen, S.H. Helppolainen, J.A.E. Määttä, K.K. Halling, J.P. Slotte, T. Huhtala, T. Liimatainen,; S. Ylä-Herttuala, *Biochemical Journal* **2007**, *405*, 397–405.

7. N.M. Green, *The Biochemical Journal* **1963**, *89*, 585.

8. K.K.-W. Lo, J.S.-W. Chan, L.-H. Lui, C.-K. Chung, *Organometallics*, 23, **2004**, 3108.

9. a) V. V. Rostovtsev, L. G. Green, V. V. Fokin, K. B. Sharpless, *Angew. Chem., Int. Ed.*, **2002**, *41*, 2596; b) R. Huisgen, in *1,3-Dipolar cycloaddition chemistry*, ed. A. Padwa, Wiley, New York, 1984, vol. 1, p. 1.

10.    a) S. Rana, J. W. Cho, *Nanoscale*, **2010**, *2*, 2550-2556. b) G. Franc, A. K. Kakkar, *Chem. Soc. Rev.* **2010**, *39*, 1536–1544; c) C. Wangler, R. Schirrmacher, P. Bartenstein, B. Wangler, *Curr. Med. Chem.,* **2010**, *17*, 1092-1116; d) D. Astruc, L. Liang, A. Rapakousiou, J. Ruiz, *Acc. Chem. Res.*, **2012**, *45*, 630–640; e) H. C. Kolb, K. B. Sharpless, *Drug Discovery Today* **2003**, *8*, 1128; f) P. Wu, V. V. Fokin, *Aldrichimica Acta* **2007**, *40*, 7; g) C. W. Tornøe, C. Christensen, M. Meldal, *J. Org. Chem.* **2002**, *67*, 3057; h) M. Meldal, C. W. Tornøe, *Chem.Rev.* **2008**, *108*, 2952.

11.    A.Alaoui, F. Schmidt, M. Amessou, M.Sarr, D. Decaudin, J. Florent, L. Johannes, *Angew. Chem Int. Ed*, 46, **2007**, 6469-6472.

12.    S. G. Davies , D. A. B. Mortimer, A. W. Mulvaney, A. J. Russell, H. Skarphedinsson, A. D. Smith, R. J. Vickers, *Org. Biomol. Chem.*, 6, **2008**, 1625-1634.

13.    a) M. Nonoyama, *Bull. Chem. Soc. Jpn.* **1974**, *47*, 767. b) S. Lamansky, P. Djurovich, D. Murphy, F. Abdel-Razzaq, R. Kwong, I. Tsyba, M. Bortz, B. Mui, R. Bau, M. E. Thompson, *Inorg. Chem.* **2001**, *40*, 1704-1711.

14.    Y. Z. Kenneth, K.-W. L. Kenneth, *Inorg. Chem.* **2009**, *48*, 6011–6025

15.    K.K.-W. Lo, J.S.-W. Chan, L.-H. Lui, C.-K. Chung, *Organometallics*, 23, **2004**, 3108.

## 6.3 - Biotinylated cyclometallated Re(I) complexes as luminescent probes for avidin targeting

As previously mentioned, during recent years, the development of new luminescent probes containing transition metals complexes for biological imaging has received high attention. These probes are constituted by a emissive unit which consists precisely in a luminescent metal complex, and an other fragment able to identify a specific biological target. In this work some of the previously described binders containing a chelating unit separated from biotin by an amide bridge were used to synthesize tricarbonilic derivatives of Rhenium (I). The obtained luminescent complexes, thanks to their good emission properties, allowed us to work with a metal certainly cheaper than Iridium and certainly suitable for biological investigations.[1]

The design and the synthesis of a new class of bifunctionalized ligands $L_1$-$L_3$, (Figure 1), containing both a pyridine-1,2,3-triazole and a biotin unit have been reported in the previous chapter.

In this project we choose the ligands containing an amide bond to investigate luminescent properties of the corresponding Re(I) complexes $ReL_1(Br)$, $ReL_2(Br)$, $ReL_3(Br)$, $ReL_1(pir)$ and $ReL_2(pir)$. (Figure 1), and their variation in the presence of the avidin target. In particular, the importance of the nature of the amide linker was evaluated, considering that it has been reported that long spacer-arms can increase the stability of the metal-avidin adducts.
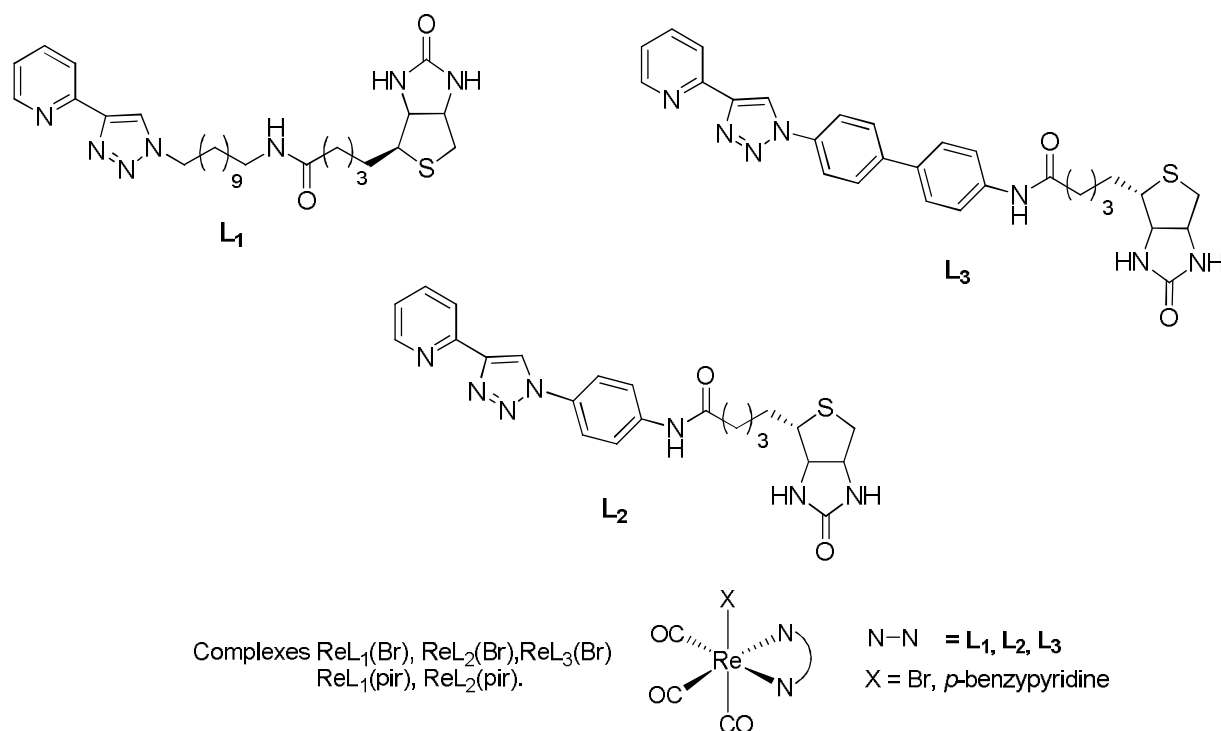


Figure 1

### 6.3.1 - Results and Discussion

#### 6.3.1.1 - Complexes synthesis

After the preparation of the ligands, the next step the synthesis of the corresponding Re (I) neutral complexes. The ligands $L_1$, $L_2$ and $L_3$ were reacted with Re(CO)$_5$Br using respectively toluene, ethanol and a mixture of toluene/ethanol = 1/1, as solvents owing to the different solubility of the starting materials, at reflux under N$_2$ (Scheme 1), to give the complexes ReL$_1$(Br), ReL$_2$(Br) and ReL$_3$(Br).



Scheme 1
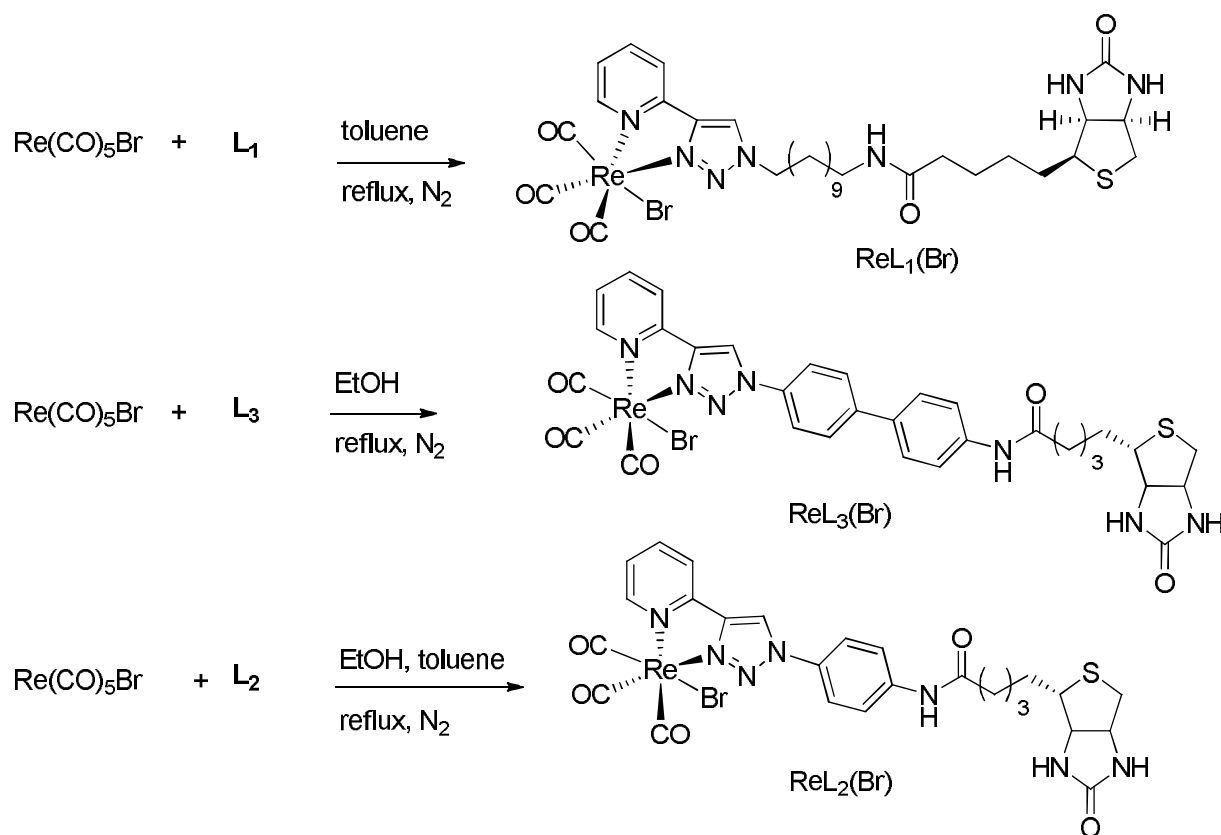
In addition, with the aim of improving the solubility of the complexes in an aqueous environment where interaction with biotin takes place, two cationic complexes were obtained by substituting the bromide on Rhenium with a neutral ligand such as $p$-benzylpyridine in complexes ReL$_1$(Br) and ReL$_2$(Br).

The synthesis was performed in two steps. Firstly, the complex ReL$_1$(Br) was reacted, in a mixture of DCM and methanol at room temperature, with silver triflate to extract the bromide. The precipitated silver bromide was subsequently removed by filtration and the solvent was removed by evaporation. In the second step, the crude product was dissolved in THF and reacted at reflux with $p$-benzilpiridine which linked to the metal center, leading to the complex ReL$_1$(pir) (Scheme 2). An analogous procedure made it possible to synthesize the complexes ReL$_2$(pir) (Scheme 2).
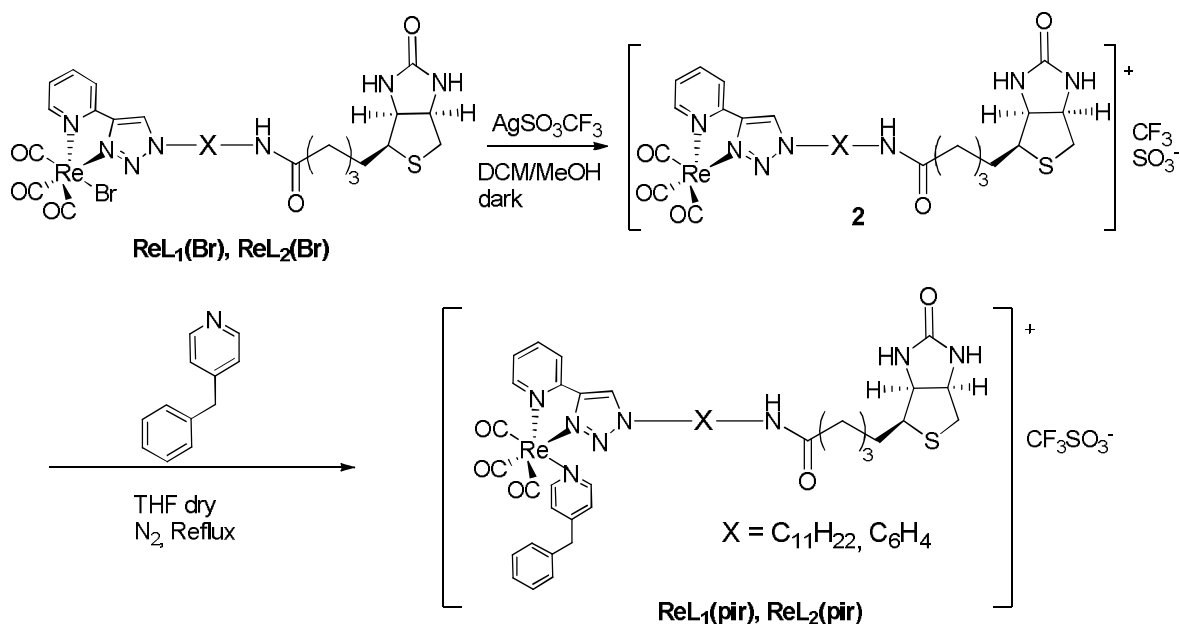
Scheme 2: Complexes ReL$_1$(pir) and ReL$_2$(pir) synthesis.

The obtained complexes were fully characterized by NMR analysis. Interestingly, the IR analysis allowed to achieve two important informations on the ionic character of the new complexes. As example, the IR spectra of ReL$_2$(Br) and ReL$_2$(pir) are reported in Figure 2. Switching from the neutral specie (the brominated derivative) to the cationic one (the pyridine complex) the three carbonyl groups coordinated to the metal centre maintain a facial geometry, as indicated by the typical IR band shape; moreover, the character of the cationic complex is evidenced by the shift of carbonyl (M-CO) stretchings towards higher wave numbers.
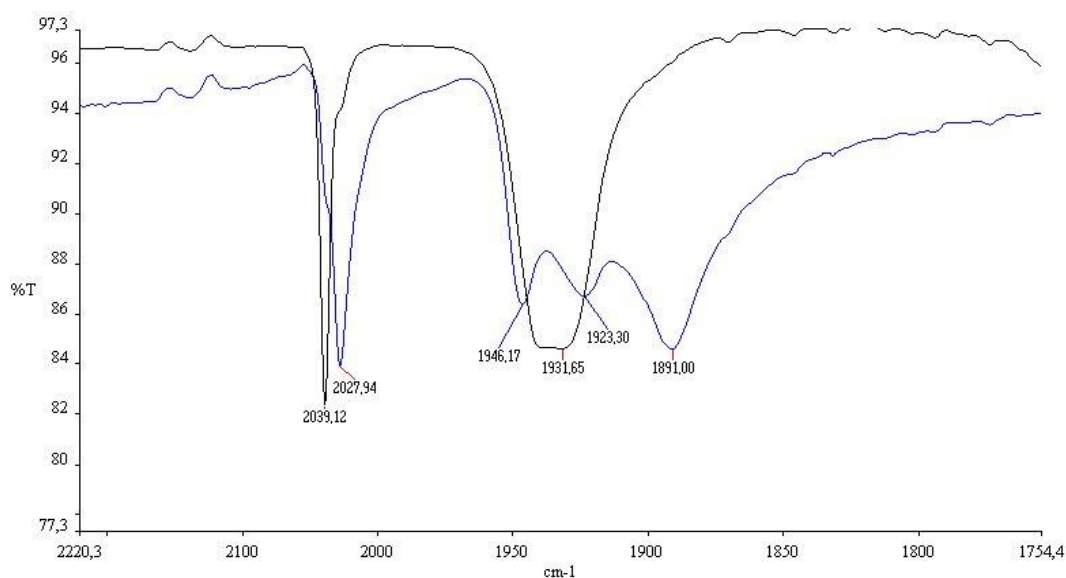


Figure 2: IR spectrum of the neutral complex ReL$_2$(Br) (blue); IR spectrum of the cationic complex ReL$_2$(pir) (black).

### 6.3.1.2 - Photophysical properties

Once the synthesis procedure of the complexes was optimized and completed, we moved to the study of the photophysical properties of these new systems in order to evaluate their potential use as biological probes. The characterization of the absorption and emission properties of the compounds was initially carried out in dichloromethane ($CH_2Cl_2$).

As regards to the absorption spectra, the profiles are consistent with the structure of an octahedral complex, in which the π-π* transitions centered on binders are observed at wavelengths below 300 nm and MLCT transitions in the area between 330 and 450 nm.

The UV-vis absorption spectra of species $ReL_1(Br)$ and $ReL_1(pir)$ (Figure 3) and $ReL_2(Br)$ and $ReL_2(pir)$ (Figure 4), in dichloromethane, are reported below. The absorption spectrum of the complex $ReL_1(Br)$ presents two bands, well evident, with maxima at 240 and 352 nm and a shoulder at 274 nm, as shown in Figure 3.

It is interesting to note that from a neutral to a cationic complex the absorption maximum shifts to lower energies. Such shifts may be attributed to the charge increase of the complex, and are observed in all the complexes.
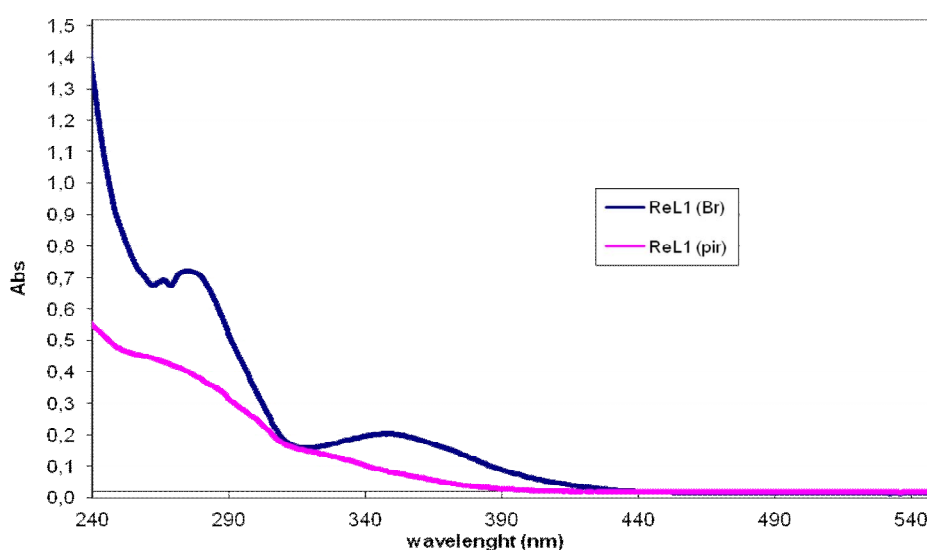


Figure 3
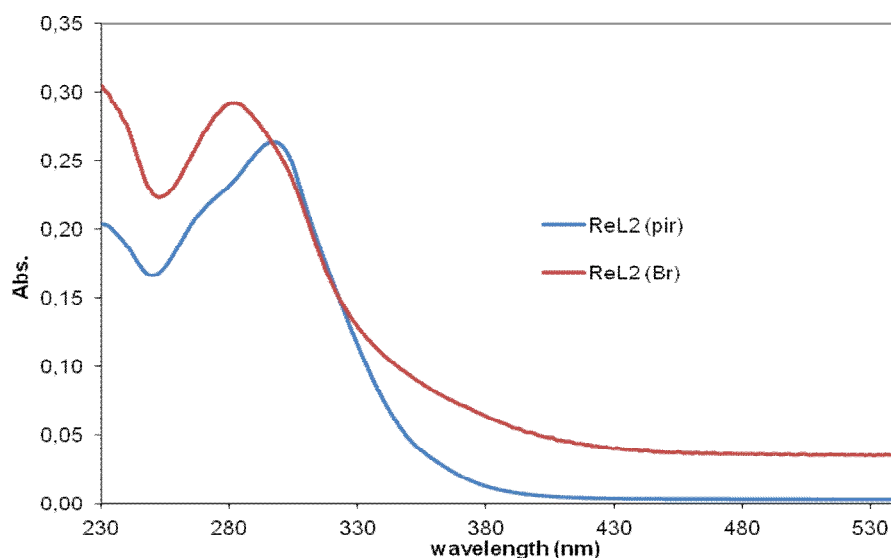
Figure 4

In Figure 5 the excitation and emission spectra of the complex $ReL_2(Br)$, at room temperature in the presence of oxygen are reported. In these species a certain difference between the profile of the excitation and absorption, is frequently observed especially when the emission comes from excited states of MLCT nature.
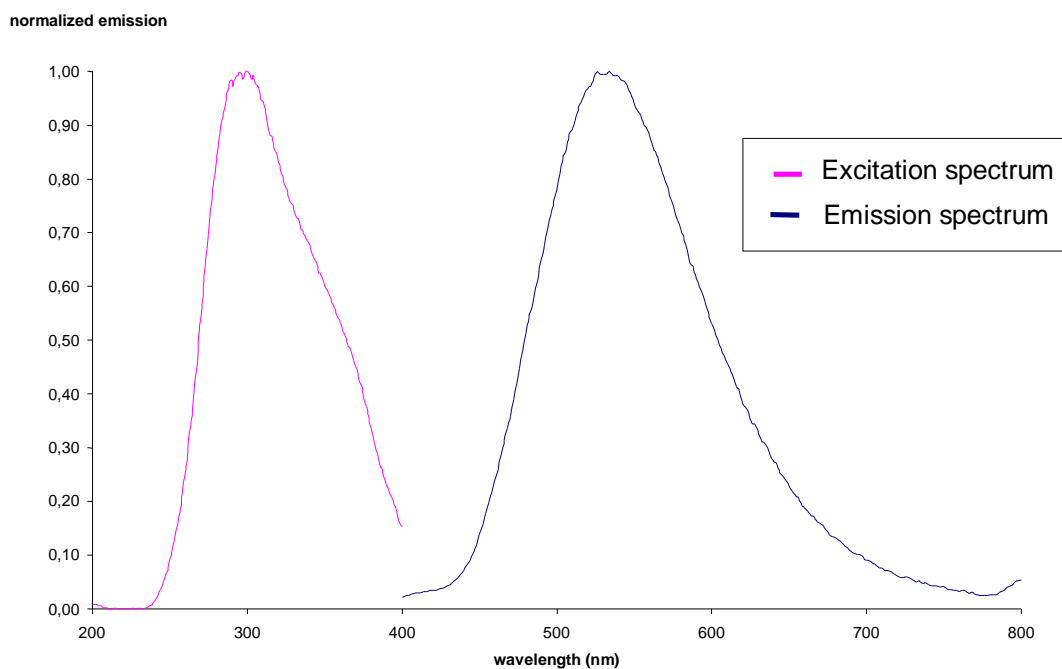


Figure 5

As can be seen from the profiles of the spectra, there is a considerable distance in energy between the excitation (or absorption) spectrum, and the emission spectrum. This is dueto the so called "Stokes shift".

To easily compare the emission properties of the four complexes, their emission spectra are reported together in Figure 6.
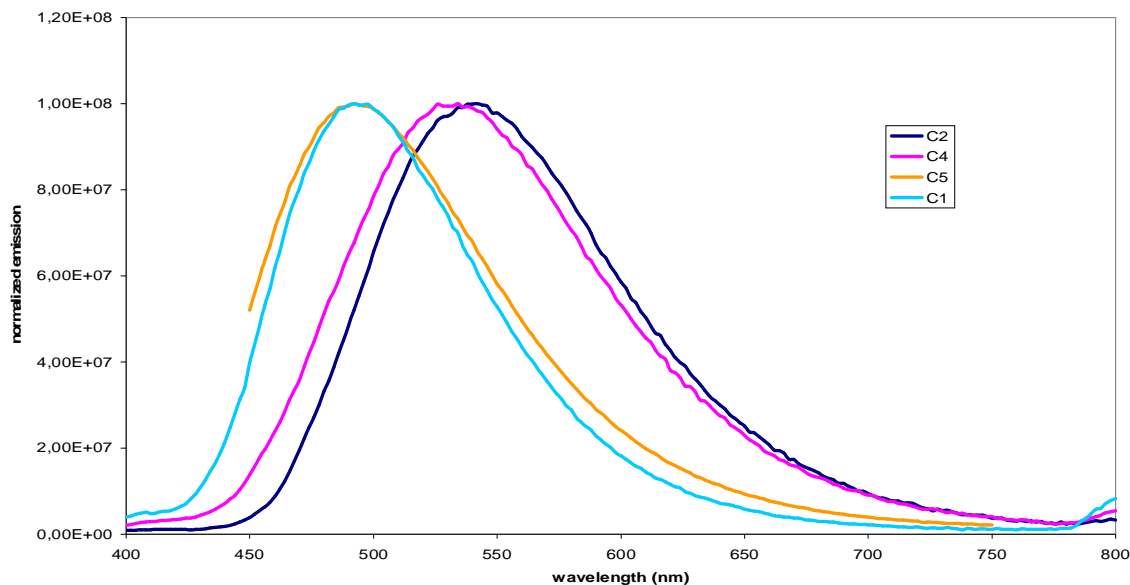


Figure 6: Emission spectra; C2=ReL$_1$(Br), C4=ReL$_2$(Br), C5=ReL$_2$(pir), C1=ReL$_1$(pir)

As underlined from the recorded spectra, all the complexes are luminescent and exhibit their maximum emission in a range of wavelengths from 494 nm to 540 nm. From the Figure 6 it can be noted how, in the cationic complexes, the emission maximum moves to lower wavelengths, respect to the neutral complexes.

Emission spectra were recorded also in the absence of oxygen and at 77 K. the registered maxima are reported in Table 1.

| COMPLEX | λ with O$_2$ (ns) | λ Deaerated sol. (nm) | λ 77K (nm) |
|---|---|---|---|
| ReL$_1$(Br) | 540 [288] | 539 [390] | 486 [340] |
| ReL$_2$(pir) | 494 [293] | 496 [293] | 458 [322] |
| ReL$_2$(Br) | 534 [301] | 542 [301] | 490 [306] |
| ReL$_1$(pir) | 494 [392] | 496 [380] | 470 [360] |

Table 1: Emission maxima, [wavelength of excitation]

As Ir(III) complexes, even the Re(I) complexes are phosphorescent and the emissions derive from a of an excited triplet state. In fact, even if the value of the maximum emission does not vary, from a solution in the presence of oxygen to a degassed, its intensity changes considerably as shown in Figure 7.
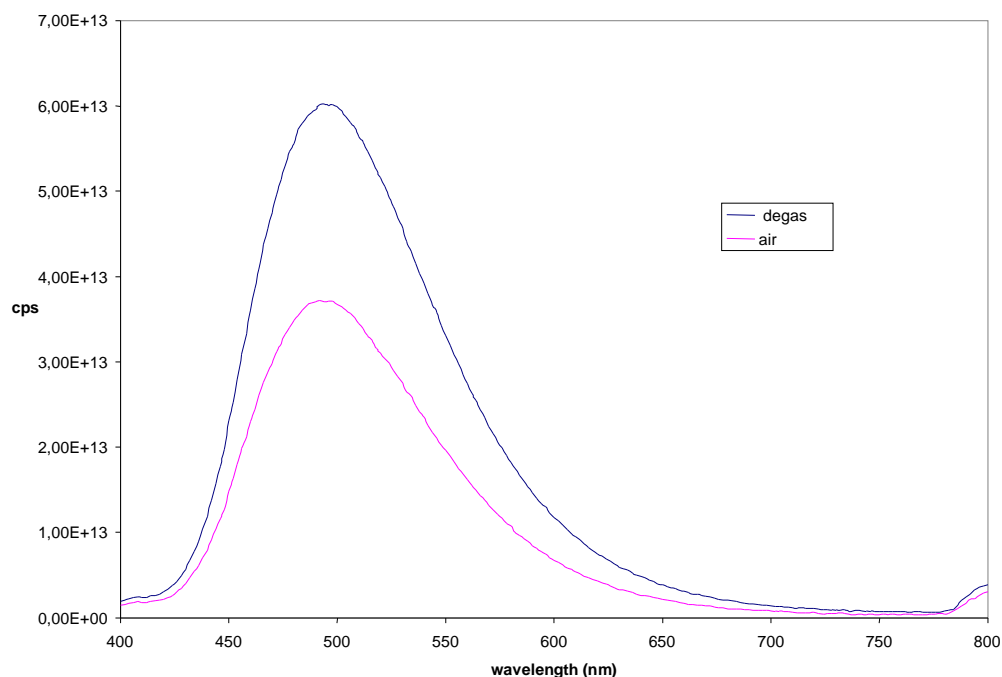
Figure 7: ReL$_1$(pir) emission

The characterization is performed by changing some parameters. These variations are important, as they allow to distinguish the nature of the different excited states from which luminescence derives. In particular, carrying out the analysis at 77 K, the energy dissipation due to phenomena with non-radiative constant, such as vibrations and rotations, is minimized; this implies a luminescence increase, as well as a lengthening of the lifetime. For these Re (I) complexes, a shift of the emission maximum at higher energies has been observed from a spectrum registered at room temperature to a frozen one. Such behavior is typical of such complexes that present MLCT transitions. In these conditions, the emission maxima range from 458 nm to 490 nm (Table 1). In Figure 8 the comparison between the emission spectrum of ReL$_1$(pir) recorded at 77 K and at room temperature is shown, highlighting the shift of the $\lambda_{max}$.
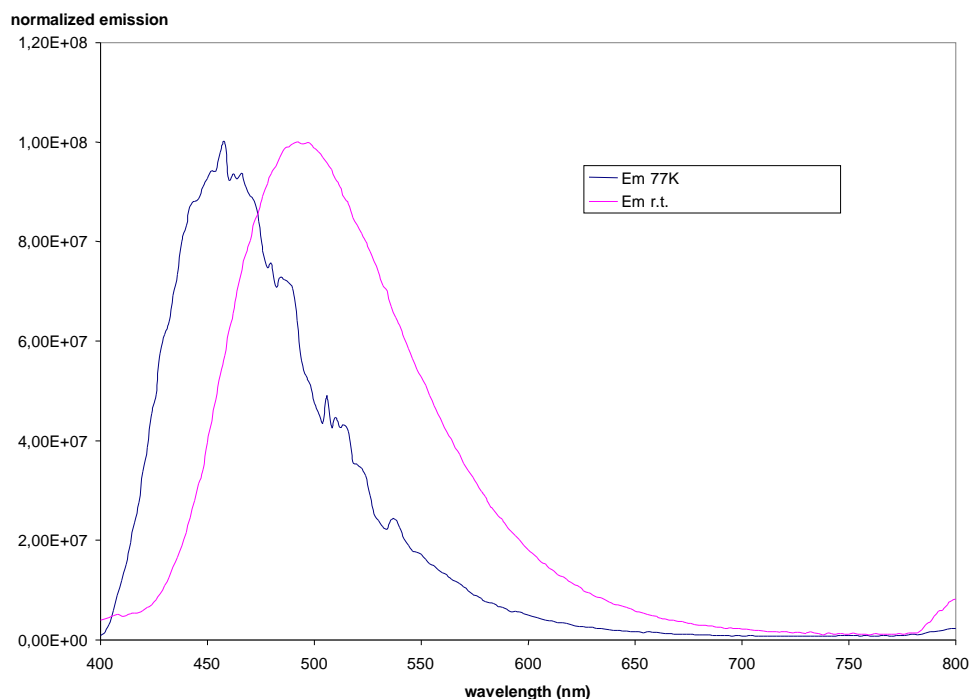
Figure 8: Comparison of emission spectra of the complex $ReL_1(pir)$ recorded at ambient temperature and 77 K.

Finally, the quantum yields and the lifetimes of the obtained complexes were determined in various conditions. The simplest way to determine the quantum yield of a fluorophore is based on a comparison with a standard of known quantum yield.[2] The quantum yield of emission of these reference compounds are almost independent on the wavelength of excitation, so it is possible to use them in all their absorbance range.

The unknown quantum yield is calculated using the following formula:[3]

$$\phi = \frac{n°\text{emitted photons}}{n°\text{absorbed photons}} = \phi_r \frac{I}{I_r} \frac{A_r}{A} \frac{n^2}{n_r^2}$$

where $\Phi$ is the quantum yield of the emission of the sample, $I$ is the area subtended by the spectrum all over the $\lambda$ emission range, $A$ is the absorbance at $\lambda$ excitation and n is the refractive index of the solvent.

In Table 2 the values of quantum yield measured in the presence of oxygen and in degassed solution are reported.

| COMPLEX | Φ with O₂ | Φ Deaerated sol. |
|---|---|---|
| ReL$_1$(Br) | 0,0454 | 0,0318 |
| ReL$_2$(pir) | 0,0834 | 0,146 |
| ReL$_2$(Br) | 0,0308 | 0,184 |
| ReL$_1$(pir) | 0,192 | 0,206 |

Table 2: Complexes quantum yields

Regarding the detection of the lifetimes of luminescence the technique of "time correlated single photon counting" (TCSPC), commonly called "single photon", was used. The lifetimes of the complex, in dichloromethane, measured in three different conditions, in the presence of oxygen, in degassed solution and 77 K are summarized in Table 3.

| COMPLEX | τ with O₂ (ns) | τ Deaerated sol. (ns) | τ 77 K (ns) |
|---|---|---|---|
| ReL$_1$(Br), | 123,5 | 163,9 | 8470,0 |
| ReL$_2$(pir) | 241,6 | 496,3 | 1000,0 (3,3 %)) 6469,2 (96,7 %) |
| ReL$_2$(Br) | 131,6 | 609,4 | 8806,4 |
| ReL$_1$(pir) | 2,3 (11,9 %)) 305,9 (88,1 %) | 2,4 (6,5 %) 584,2 (93,5 %) | 7,4 (58,2 %) 22,8 (41,8 %) |

Table 3: Complexes lifetime

Analyzing the tabulated data, an increase of the lifetimes is observed from a room temperature solution in the presence of oxygen to a degassed solution, demonstrating the nature of the triplet excited state from which the emission originates.


### *6.3.1.3 - Interaction between the biotinylated complexes of Re (I) and avidin*

The study of the photophysical properties of these new complexes of Re (I) showed that they present a number of features good for their use as luminescent probes.

The next step is to determine if the photophysical properties of the biotinylated Re(I)-complexes undergo some variations upon interaction with avidin, in order to be considered a good probe for avidin. To perform such type of study is necessary, above all, to characterize the complexes in an aqueous solvent. Typical experiments of biotin-avidin bio-conjugation are generally conducted in aqueous solutions maintained at pH 7.4 by means of sodium or potassium phosphate buffers. The biotin-avidin interaction was verified by monitoring the variation of the complex

photoluminescence properties, in the presence of avidin. It was therefore necessary, even before placing in contact our complexes with the avidin, to evaluate their fotoemissive properties in aqueous solution, buffered to pH = 7.4. The obtained data are reported in Table 4 and show how the two complexes (ReL$_1$(pir) and ReL$_2$(pir)) are luminescent even in aqueous solution, with the maximum emission at 508 nm, shifted towards red if compared with the data obtained in dichloromethane, ($\lambda_{max}$= 494 nm for both complexes).

| Complex | $\lambda_{max}$ (nm) | $\tau$ (ns) | $\Phi$ |
|---------|---------------------|-------------|--------|
| ReL$_1$(pir) | 508 [293] | 101,19 | 0,00428 |
| ReL$_2$(pir) | 508 [298] | 176,42 | 0,0473 |

Table 4: Emission maxima in aqueous solution, [wavelength of excitation]

Subsequently, in order to verify the interaction of the complexes ReL$_1$(pir) and ReL$_2$(pir) with the avidin some titration experiments were performed. Specifically, according to a protocol reported in the literature,[4] avidin solutions were titrated using complexes of Re(I) in buffer solution of known concentration, and the increase in the emission intensity was measured after each addition.

Figure 9 shows the "multiscan" graph of the titration of avidin with the complex ReL$_1$(pir). Each curve represents the emission spectrum of the solution, after each addition of titrant.
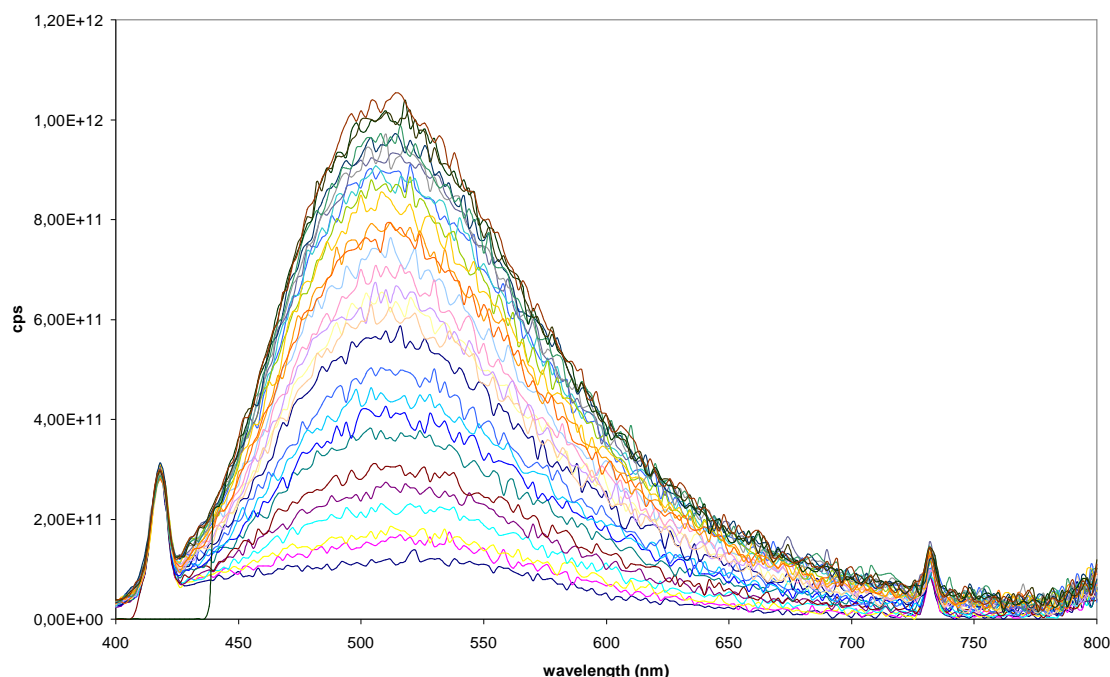


Figure 9: Multiscan titration.

In order to verify that such behavior is actually due to the interaction of the complex with the avidin, it is necessary to carry out two control titrations: one by adding increasing amount of the

complex solution to a buffer solution in the absence of avidin, and a second one in which a buffer solution containing avidin pre-saturated with an excess of free biotin is titrated with the complex solution. The trends of the titration are expressed in a graph in which the increase of the intensity of the emission maximum (Y-axis) is reported as a function of the amount of added complex (X-axis).

The analogous literature examples reported that in such titration graphs the avidin-complex curve and those of control experiments presented different angular coefficients. Furthermore, a change of slope in the titration curves, ie a point of inflection, can be observed in the avidin-complex curve. This point corresponds to the saturation of avidin by the biotin, whether it comes from the biotinylated complex or from free biotin. After this equivalence point, the slope of the avidin-complex curve is generally similar to that of control experiments.

In the titration of our Re(I) complexes, we observed analogous trends. In Figures 10 and 11 the graphs related to the experiments conducted using as the titrant complex $ReL_1(pir)$ and complex $ReL_2(pir)$ are reported.
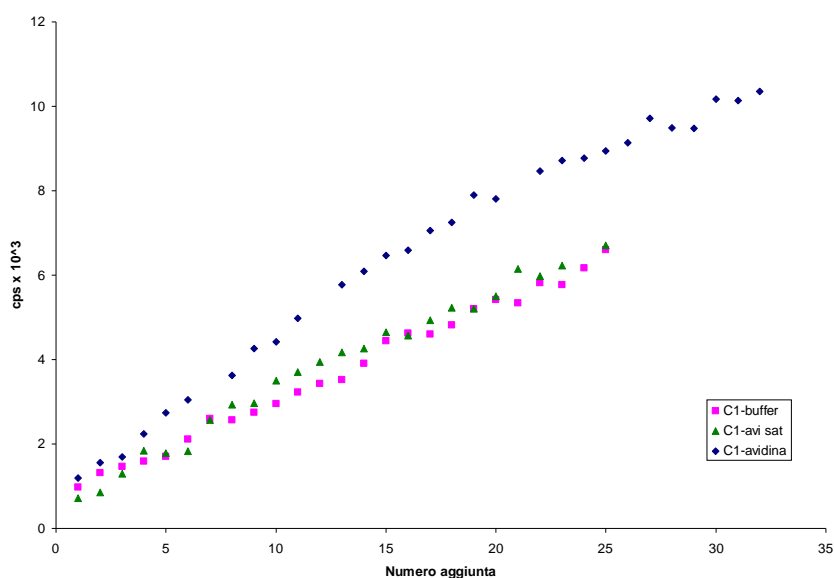


Figure 10: Titration curves of avidin 3.8 uM (blue), a solution of avidin and biotin 3.8 uM $4.75*10^{-5}$ M (green) and a solution of 50 mM phosphate buffer (pink) with a solution in phosphate buffer + 10% DMSO of complex $ReL_1(pir)$. Each addition corresponds to 10 mL of titrant.
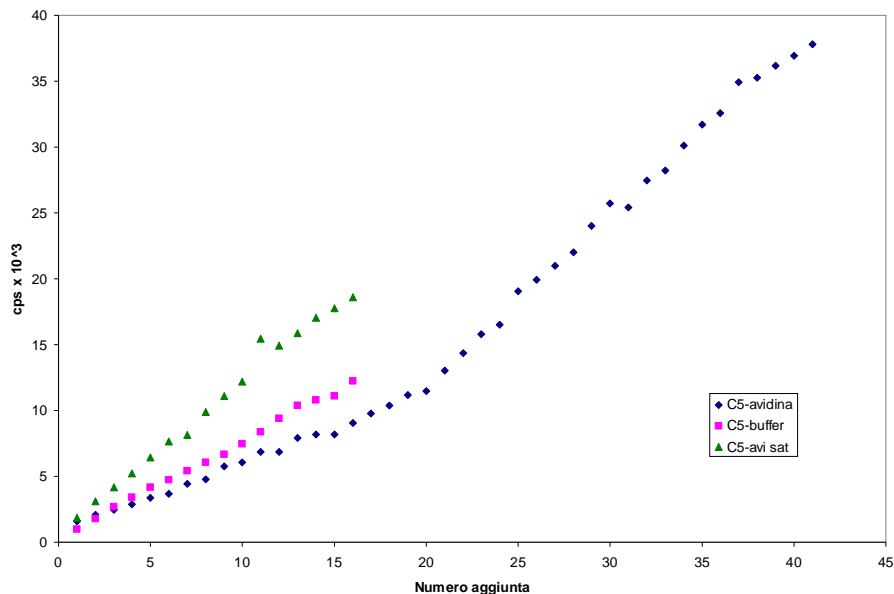
Figure 11: Titration curves of avidin 3.8 uM (blue), a solution of avidin and biotin 3.8 uM 4.75*10$^{-5}$ M (green) and a solution of 50 mM phosphate buffer (pink) with a solution in phosphate buffer + 10% DMSO complex of ReL$_2$(pir). Each addition corresponds to 10 mL of titrant.

For both experiments, the avidin-complex curves display a first linear part up to the flexion point (for both tests detectable about the twentieth addition), after which the curve shows a trend comparable to that of the control titrations. Specifically, the two tests show two different cases of change in emission intensity of the complexes in the presence of avidin, compared to control titrations. In the experiment in Figure 10, in the first section of the curves, there is an increase of angular coefficients compared to those of the control experiments, while, in the section after the inflection, there a slight decrease is registered. An opposite situation occurs in the test in the Figure 11, in which, in the first section, it is possible to observe a decrease in the angular coefficients and, after the inflection, a significant increase of the latter.

Even if the presence of a bioconjugation between the complexes and avidin can be deducted from the reported titrations, with regard to the quantitative analysis of the amount of complex necessary to completely saturate avidin, we run into some problems concerning the low solubility of the complex in an aqueous environment, which has not allowed to obtain solutions of known concentration of titrant.

## 6.3.2 - Conclusions

The study of the photophysical properties of the obtained Re(I) complexes, in dichloromethane, except for the **L₃** species, showed photoemissive processes of phosphorescent nature and therefore distinguishable from autofluorescence of samples, hypothesis corroborated by time-resolved measurements. The cationic complexes ReL₁(pir) and ReL₂(pir), were further characterized in a phosphate buffer at pH = 7.4 +10% DMSO.

From this characterization it was observed as the complexes maintain their phosphorescent photoemittive properties also in this aqueous solvent. This made it possible to analyze the interaction of these two species with a water soluble glycoprotein specific for biotin: avidin.

In the titration of a avidin solution with the complex ReL₁(pir), it is observed how the emission intensity of the latter increases compared to that measured in control experiments. In the second titration, performed with the species ReL₂(pir), an opposite situation is encountered, namely a decrease of emission intensity compared to control titrations. The change in emission intensity is due to the coordination of the complex-biotin to the protein. In the graphs an inflection point is observable after the addition of a certain quantity of complex; after that point the trend of the intensity of emission changes slope and becomes analogous to the behavior found in the control experiments. It can be assumed that the change of slope represents the moment in which the equivalence point is reached, but there was no possibility to perform a quantitative analysis because of the poor solubility of the complexes in aqueous medium, in spite of the use of cationic complexes instead of neutral ones. Future studies, may relate precisely the issue of solubility, in order to be able to prepare solutions of known concentration of titrant.

## 6.3.3 - Experimental section

**Synthesis of Complex ReL₁(Br)**

Re(CO)₅Br (0.117 g, 0.228 mmol) and ligand **L₁** (0.120 g, 0.221 mmol) were dissolved in anhydrous toluene (15 ml) and the solution was left to stir at 130°C under $N_2$ for 24 h. The cooled mixture is filtered and the obtained solid was washed with MeOH (3 x 15 ml), dissolved in the minimum amount of acetone and precipitated with Et₂O. The obtained product **ReL₁(Br)** was isolated by centrifugation (80% yields, mp= 169 -171°C). $^1$H NMR (CD₃OD, 600 MHz) δ 8.97 (d, J = 5.4 Hz, 1H), 8.95 (s, 1H), 8.18 - 8.11 (m, 2H), 7.54 (td, $J_T$ = 8.7 Hz, $J_D$ = 2.6 Hz, 1H), 4.59 (t, J = 7.5 Hz, 2H), 4.48 (dd, J = 7.7 Hz, J = 5.0 Hz, 1H), 4.29 (dd, J = 7.9 Hz, J = 4.5 Hz, 1H), 3.22 - 3.16 (m, 1H), 3.13 ($J_T$ = 7.0 Hz, $J_D$ = 1.7 Hz, 2H), 2.91 (dd, J = 12.8 Hz, J = 5.0 Hz, 1H), 2.69 (d, J = 12.7 Hz, 1H), 2.18 (t, J = 7.6 Hz, 2H), 2.06 - 1.98 (m, 2H), 1.76 - 1.25 (m, 25H). $^{13}$C NMR

(CD$_3$OD, 150 MHz) δ 197.2 (C), 195.7 (C), 188.6 (C), 174.8 (C), 164.9 (C), 153.2 (CH), 149.8 (C), 149.0 (C), 140.1 (CH), 126.0 (CH), 125.0 (CH), 122.5 (CH), 62.3 (CH), 60.5 (CH), 55.9 (CH), 52.2 (CH), 40.0 (CH$_2$), 39.3 (CH$_2$), 35.8 (CH$_2$), 29.8 (CH$_2$), 29.5 (CH$_2$), 29.3 (CH$_2$), 29.2 (CH$_2$), 28.8 (CH$_2$), 28.6 (CH$_2$), 28.4 (CH$_2$), 26.9 (CH$_2$), 26.2 (CH$_2$), 25.9 (CH$_2$). ESI - MS: 892 [M$^+$], 914 [M$^+$ + Na].

**Synthesis of Complex ReL$_2$(Br)**

In a 50 ml-two-necked round-bottom flask equipped with a stirring bar, Re(CO)$_5$Br, (0.23 mmol) and the ligand **L$_2$** (0.19 mmol) was dissolved in a mixture of Tol/EtOH = 1:1 (16 mL) and refluxed for 24 h. The solution was cooled to room temperature and the solvent was removed by vacuum. The crude was washed with Acetone to give product **C$_4$** in 95% yield.

$^1$H-NMR (DMSO): δ = 1.30-1.70 (m, 6H), 2.30-2.40 (m, 2H), 2.60 (d, 1H, J=12.3), 2.84 (dd, 1H, J=12.3, J=4.9), 3.10-3.20 (m, 1H), 4.10-4.20 (m, 1H). 4.30-4.40 (m, 1H), 6.36 (bs, 1H), 6.45 (bs, 1H), 7.65-7.75 (m, 1H), 7.90-8.00 (m, 4H), 8.25-8.40 (m, 2H), 9.03 (d, 1H, J=5.3), 9.90 (bs, 1H), 10.30 (s, 1H).

$^{13}$C-NMR (DMSO): δ = 25.4 (CH$_2$), 28.6 (CH$_2$), 28.7 (CH$_2$), 36.7 (CH$_2$), 40.3 (CH$_2$), 55.8 (CH), 59.7 (CH), 61.5 (CH), 120.3 (CH), 122.1 (CH), 123.1 (CH), 124.4 (CH), 127.1 (CH), 130.6 (C), 141.2 (CH), 141.6 (C), 149.0 (C), 149.4 (C), 153.8 (CH), 163.2 (C), 172.2 (C), 189.3 (C), 193.8 (C), 196.6 (C).

**Synthesis of Complex ReL$_3$(Br)**

In a 50 ml-two-necked round-bottom flask equipped with a stirring bar, Re(CO)$_5$Br, (0.11 mmol) and the ligand **L$_3$** (0.085 mmol) were dissolved in EtOH (10 mL) and refluxed for 24 h. The solution was cooled to room temperature and the solid was filtered to give pure product **C$_3$** in 15% yield.

$^1$H-NMR (DMSO): δ = 1.10-1.80 (m, 6H), 2.30-2.40 (m, 2H), 2.59 (d, 1H, J=12.8), 2.84 (dd, 1H, J=4.9, J=12.8), 3.10-3.20 (m, 1H), 4.10-4.20 (m, 1H), 4.30-4.40 (m, 1H), 6.35 (bs, 1H), 6.45 (bs, 1H), 7.65-7.75 (m, 1H), 7.77 (bs, 4H), 8.01 (d, 2H, J=8.8), 8.09 (d, 2H, J=8.8), 8.30-8.40 (m, 2H), 9.05 (d, 1H, J=5.6), 10.03 (s, 1H), 10.05 (bs. 1H).

$^{13}$C-NMR (DMSO): δ = 25.5 (CH$_2$), 28.6 (CH$_2$), 28.7 (CH$_2$), 36.7 (CH$_2$), 40.3 (CH$_2$), 55.9 (CH), 59.7 (CH), 61.5 (CH), 119.9 (CH), 121.7 (CH), 123.1 (CH), 124.5 (CH), 127.2 (CH), 127.7 (CH), 128.2 (CH), 133.0 (C), 134.6 (C), 140.1 (C), 141.3 (CH), 142.0 (C), 148.9 (C), 149.5 (C), 153.8 (CH), 163.2 (C), 171.8 (C), 183.6 (C), 189.3 (C), 196.6 (C).

**Synthesis of Complex ReL₁(pir)**

In a 50 ml-two-necked round-bottom flask equipped with a stirring bar, the complex **ReL₁(Br)** (0.08 mmol) was dissolved in a mixture of DCM/MeOH = 3:1 (12 mL), and $AgSO_3CF_3$ (1.5 equiv.) was added. The reaction flask was wrapped in aluminium foil and the reaction was left to stir overnight at room temperature. Then the solid was filtered off and washed with DCM (2 mL). The solution was evaporated and the resulting residue was dissolved in anhydrous THF (5 mL), under a nitrogen atmosphere. *p*-Benzyl-pyridine (1 equiv.) was added, and the reaction mixture was stirred at 70° C under a nitrogen atmosphere for 24 h. Then the solvent was removed by vacuum and the crude was purified by column chromatography on alumina gel (DCM/MeOH = 96:4, 35% yields).

$^1$H-NMR ($CDCl_3$): δ = 1.10-1.80 (m, 22H), 1.90-2.05 (m, 2H), 2.14 (t, 2H, J=7.3), 2.65 (d, 1H, J=13.6), 2.83 (dd, 1H, J=5.0, J=13.6), 3.05-3.15 (m, 3H), 3.86 (s, 2H), 4.20-4.30 (m, 1H), 4.40-4.45 (m, 1H), 4.53 (t, 2H, J=7.2), 5.30 (bs, 1H), 5.90 (bs, 1H), 6.20 (bs, 1H), 6.95-7.05 (m, 4H), 7.20-7.30 (m, 3H), 7.48-7.53 (m, 1H), 7.97-8.00 (m, 2H), 8.01-8.15 (m, 1H), 8.38 (d, 1H, J=10.2), 8.95 (d, 1H, J=5.0), 9.33 (d, 1H, J=3.8).

$^{13}$C-NMR ($CDCl_3$): δ = 24.6 ($CH_2$), 24.7 ($CH_2$), 25.1 ($CH_2$), 25.6 ($CH_2$), 25.7 ($CH_2$), 26.9 ($CH_2$), 27.0 ($CH_2$), 27.4 ($CH_2$), 27.5 ($CH_2$), 28.0 ($CH_2$), 28.3 ($CH_2$), 28.6 ($CH_2$), 34.9 ($CH_2$), 38,4 ($CH_2$), 39.6 ($CH_2$), 40.0 ($CH_2$), 51.9 ($CH_2$), 54.5 (CH), 59.1 (CH), 60.8 (CH), 123.6 (CH), 125.9 (CH), 126.4 (CH), 126.5 (CH), 128.1 (CH), 128.2 (CH), 135.4 (C), 140.7 (CH), 140.8 (CH), 148.1 (C), 148.9 (C), 150.3 (CH), 151.2 (CH), 154.2 (C), 162.6 (C), 172.2 (C), 189.5 (C), 192.8 (C), 195.0 (C).


**Synthesis of Complex ReL₂(pir)**

In a 50 ml-two-necked round-bottom flask equipped with a stirring bar, the complex **ReL₁(Br)** (0.17 mmol) was dissolved in a mixture of DCM/Acetone/MeOH = 16:16:1 (16.5 mL), and $AgSO_3CF_3$ (1.5 equiv.) was added. The reaction flask was wrapped in aluminium foil and the reaction was left to stir overnight at room temperature. Then the solid was filtered off and washed with DCM (2 mL). The solution was evaporated and the resulting residue was dissolved in anhydrous THF (15 mL), under a nitrogen atmosphere. *p*-Benzyl-pyridine (5 equiv.) was added, and the reaction mixture was stirred at 70° C under a nitrogen atmosphere for 24 h. Then the solvent was removed by vacuum and the crude was purified by column chromatography on alumina gel (DCM/MeOH = 98:2, DCM/MeOH = 93:7, 35% yields).

$^1$H-NMR ($CD_3OD$): δ = 1.45-1.85 (m, 6H), 2.45 (t, 2H, J=7.3), 2.7 (d, 1H, J=12.6), 2.92 (dd, 1H, J=12.6, J=5.0), 3.19-3.25 (m, 1H), 3.92 (s, 2H), 4.32 (dd, 1H, J=4.6, J=8.2), 4.50 (dd, 1H, J=5.0,

J=8.2), 7.10-7.15 (m, 2H), 7.15-7.25 (m, 6H), 7.75-7.80 (m, 1H), 7.90-8.00 (m, 4H), 8.20-8.25 (m, 1H), 8.26-8.30 (m, 1H), 8.30-8.35 (m, 2H), 9.29 (d, 1H, J=5.9), 9.52 (s, 1H).

$^{13}$C-NMR (CD$_3$OD): δ = 25.2 (CH$_2$), 28.1 (CH$_2$), 28.4 (CH$_2$), 36.3 (CH$_2$), 39.7 (CH$_2$), 40.2 (CH$_2$), 55.6 (CH), 60.2 (CH), 61.9 (CH), 120.4 (CH), 121.5 (CH), 123.1 (CH), 126.6 (CH), 127.4 (CH), 128.5 (CH), 128.8 (CH), 131.0 (C), 137.6 (C), 141.2 (C), 141.4 (CH), 149.1 (C), 149.7 (C), 151.7 (CH), 153.7 (CH), 155.6 (C), 164.7 (C), 173.3 (C), 190.8 (C), 193.8 (C), 195.3 (C).

### 6.3.4 - Bibliography

1.      a) K. K.-W. Lo, W.-K. Hui, D. C.-M. Ng *J. Am. Chem. Soc*. **2002**, 124, 9344-9345. b) M.-W.Louie, H.-W. Liu, M. H.-C. Lam, Y.-W. Lam, K. K.-W. Lo *Chem. Eur. J.* **2011**, *17*, 8304 – 8308

2.      J. N. Demas, G. A. Crosby, *J. Phys. Chem.* (**1971**), *75*, 991–1024.

3.      D. F. Eaton, *Pure Appl. Chem*. (**1988**), *60*, 1107.

4.      K. K.-W. Lo, K. Y. Zhang, S. P.-Y. Li, *Eur. J. Inorg. Chem.*, (**2011**), 3551-3568.

# 7) Tripodal triazole-based ligands

The recent advance of "click chemistry" has boosted the number of molecules available for several leading-edge fields, including medicinal chemistry, biology and material sciences.[1] Among "click" reactions, the Cu(I)-catalyzed azide alkyne cycloaddition (CuAAC)[2] has received extraordinary attention since it is the most effective method to afford 1,4-substituted-1,2,3-triazoles from a wide range of usable substrates, with essentially perfect regioselectivity under mild conditions.[3] In addition, the development of the CuAAC reaction resulted in an renewed interest toward the employment of 1,4-functionalized-1,2,3-triazoles in coordination chemistry because of their potential to act as N-donor ligands.[4] In fact, in recent years, various bi-, tri-, and polydentate 1,2,3-triazole-containing structures have been synthesized and studied as metal ligands.[4a] In particular, polydentate ligands can be exploited to coordinate high coordination number ions such as lanthanides, which possess fascinating and versatile photophysical properties.[5] In fact, in recent years the considerable progresses in lanthanide chemistry have led the applications of lathanides-based compounds in the fields of optical materials,[6] sensors,[7] bioassays[8] and diagnostics.[9] Among lanthanides, Cerium is the most abundant of the rare earth elements, one of the least expensive, it displays low to moderate toxicity and it played an important role in organic synthesis.[10] Furthermore, $Ce^{3+}$ ion exhibits a 5d–4f emission with a large absorption in the UV region and a short luminescence lifetime due to allowed electric dipole transitions.[11] Generally, the emission of $Ce^{3+}$ ion occurs in the UV spectral region but it can be red-shifted depending on the environment.[5,12] Taking advantage from these characteristics, some interesting applications in emitting devices have been carried out, especially by adding $Ce^{3+}$ ions to inorganic crystals.[11, 13] On the other hand, investigations on the luminescence properties of $Ce^{3+}$ ion in organic coordination environments remain rather rare,[14] although studies on the photophysical proprieties of $Ce^{3+}$ in halides, organometallics, and polymer films has been reported.[15]

In this project,[16] we exploited a triple click reaction to synthesize of a new series of symmetrical tertiary amines carrying in each side arm an aryl substituted aromatic triazole moiety and its use as coordinating agent of $Ce^{3+}$ to obtain luminescent complexes.

## 7.1 - Results and Discussion

We employed a recently reported protocol[17] to perform a new triple one-pot "click reaction" to obtain ligands **L1** and **L2**. The procedure involves the *in situ* formation of aryl azides from the reaction of the corresponding amines **1** with *t*-BuONO and TMSN$_3$, and the subsequent addition of tripropargylamine **2**, CuSO$_4$ and a reducing agent to give the tris triazole amines **L1** and **L2** without any intermediate work-up procedure, (Scheme 1). **L1** and **L2** were obtained in good yields (61% and 67% respectively), probably owing also to the autocatalytic activity previous reported for this kind of products.[18]
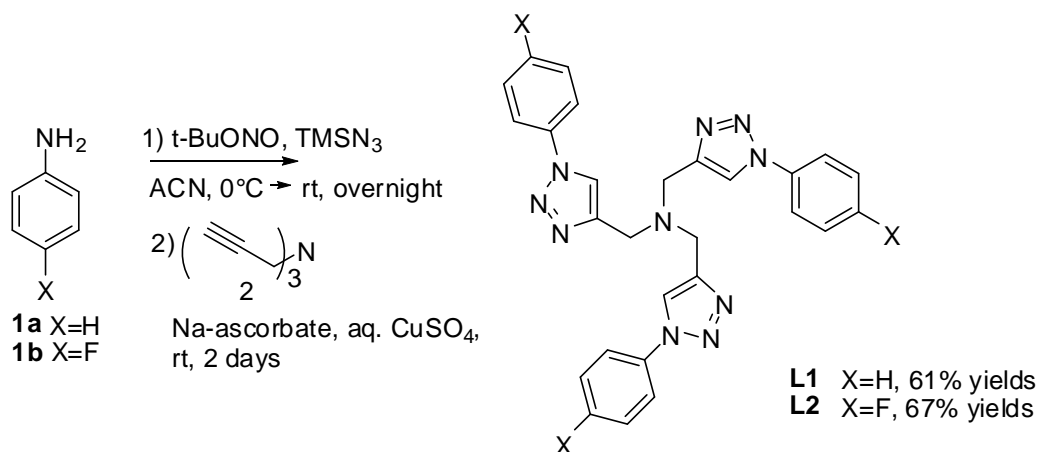


**Scheme 1**. Synthesis of ligands **L1** and **L2**.

The X-ray structure of **L2** as ammonium salt, with nitrate as counteranion, was obtained. The structure is reported in Figure 1 and the corresponding crystallographic parameters in Table 1.
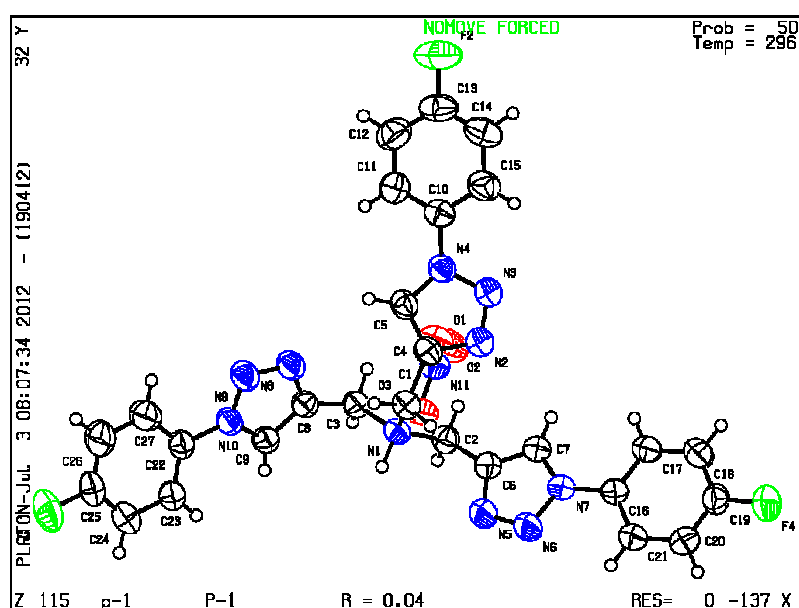


**Figure 1**. Crystal structure of $[L2H]^+NO_3^-$

94

**Table1**. Crystallographic parameters for **L2** and **3b**

| | L2 | 3b |
|---|---|---|
| Empirical formula | $C_{27}H_{22}F_3N_{11}O_3$ | $C_{43}H_{17}CeF_3N_{21}O_9$ |
| Formula weight | 605.56 | 1168.05 |
| Temperature (K) | 298(2) | 298(2) |
| $\lambda$ (Å) | 0.71073 | 0.71073 |
| Crystal system | Triclinic | Hexagonal |
| Space Group | P-1 | $P6_5$ |
| $a$ (Å) | 6.177(2) | 22.287(5) |
| $b$ (Å) | 14.820(5) | 22.287(5) |
| $c$ (Å) | 16.615(6) | 14.581(3) |
| $\alpha$ (°) | 65.935(4) | 90 |
| $\beta$ (°) | 82.870(4) | 90 |
| $\gamma$ (°) | 78.528(4) | 120 |
| $V$ (Å$^3$) | 1359.6(8) | 6272(2) |
| Z | 2 | 6 |
| $D_{calcd}$ | 1.479 | 1.969 |
| $\mu$ (mm$^{-1}$) | 0.116 | 1.166 |
| F(000) | 624 | 3678 |
| Crystal size (mm) | 0.35×0.10×0.10 | 0.30×0.15×0.15 |
| Crystal shape | Sticks | Brick |
| Crystal color | Colorless | Pale yellow |
| $\theta$ range (°) | 1.53 – 26.00 | 1.75 – 24.83 |
| Limiting indices | -7 ≤ h ≤ 7; -18 ≤ k ≤ 18; -20 ≤ l ≤ 20 | -26 ≤ h ≤ 26; -26 ≤ k ≤ 26; -17 ≤ l ≤ 17 |
| Reflections | 12043 | 43891 |
| Reflections (independent) | 5298 (R = 0.0207) | 7184 (R = 0.0448) |
| Completeness to $\theta_{max}$ (%) | 99.1 | 99.0 |
| Max. and min. transmission | 0.9604 - 0.9884 | 0.6925 – 0.8263 |
| Refinemend methods | full-matrix least-squares on $F_o^2$ | |
| Data/restraints/parameters | 5298 / 0 / 400 | 7184/ 5 / 431 |
| Goodness-of-fit on $F^2$ | 1.028 | 1.003 |
| Final R indices [I > 2σ(I)] | $R_1$ = 0.0408; $wR_2$ = 0.1021 | $R_1$ = 0.0397; $wR_2$ = 0.0999 |
| R indices (all data) | $R_1$ = 0.0622; $wR_2$ = 0.1150 | $R_1$ = 0.0537; $wR_2$ = 0.1065 |
| Largest diff peak/hole (e/ Å$^3$) | -0.151 and 0.131 | -0.342 and 0.542 |

The coordination ability of ligands **L1** and **L2** towards $Ce^{3+}$ ion was tested by reaction with various cerium(III) salts having anions with different coordinating characteristics.[19]

The complexes of **L1** and **L2** with $Ce(NO_3)_3$, $Ce(ClO_4)_3$ and $Ce(OTf)_3$ were prepared in acetonitrile (ACN), using cerium salts that were carefully washed with DCM to remove any residual acidity. Slow diffusion of diethyl ether in the reaction mixture induced the precipitation of **3a-b**, **4a-b** and **5a-b** complexes (Figure 2).

As expected, owing to the ability of nitrate ion to strongly coordinate metals because of its bidentate character, the reaction with $Ce(NO_3)_3$ gave heteroleptic complexes **3a** and **3b** in which only one ligand coordinated to the metal (Figure 2). On the contrary, to obtain homoleptic $Ce^{3+}$ complexes containing two coordinating organic fragments, ligands **L1** and **L2** were reacted with cerium salts carrying generally not coordinating counteranions such as $Ce(ClO_4)_3$ and $Ce(OTf)_3$, yielding the desidered complexes **4a-b** and **5a-b** (Figure 2).
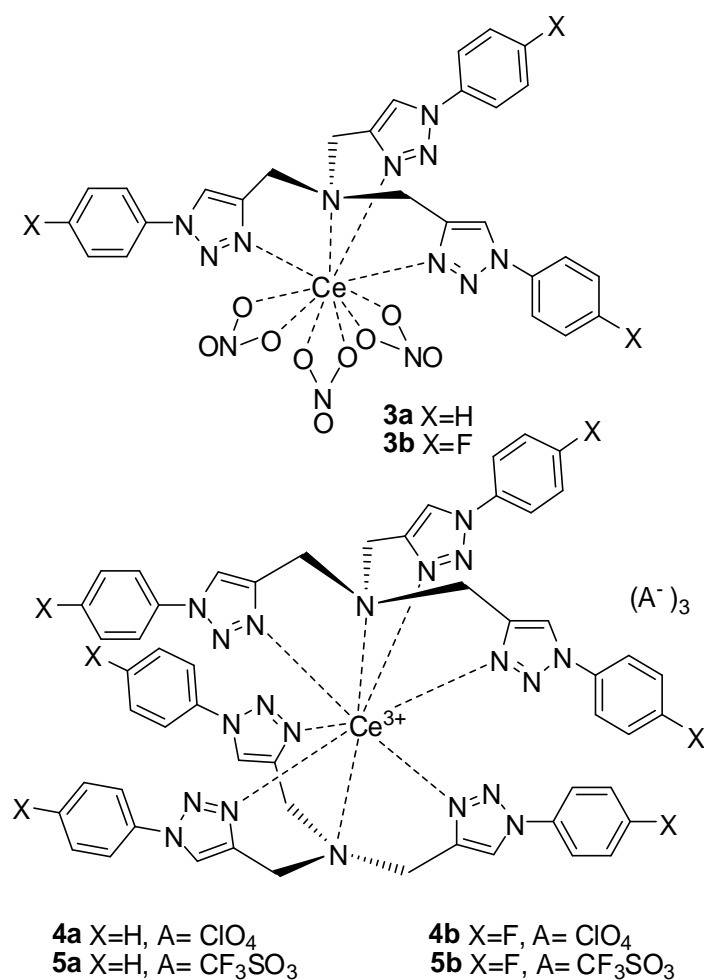


**Figure 2**: Complexes **3a-b**, **4a-b** and **5a-b**

Compound **3b** crystallizes in the hexagonal space group *P6₅*, with six molecules per unit cell (Table 1). Cerium is bound to six oxygen atoms from the three nitrates, as well as to the four nitrogens of the tripodal ligand, thus yielding a ten-coordinated centre. As from Figure 3, the heteroleptic complex has $C_3$ symmetry, and the asymmetric unit correspond to a whole molecule.
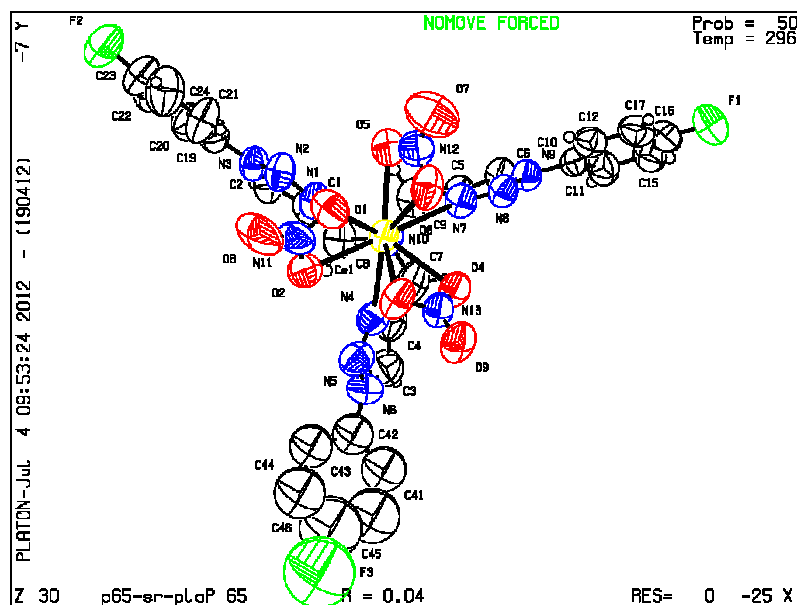


**Figure 3**.Crystal data for complex **3b**

Unfortunately, any attempt to obtain good crystals of compounds **3a**, **4a-b** and **5a-b** failed, thus an experimental structure of these complexes is not available. However, a computational approach could afford to a reasonable structure of the complexes, provided that a reliable theoretical model is found. Given the scarce literature data on computations of organic compounds containing cerium,[20] a preliminary investigation was conducted on the complex **3b** where the theoretical results could be compared with the experimental structure observed in the solid state.

The calculations were performed using the B3LYP functional and the SDD basis set,[21, 22] which has proven to be effective for inorganic compounds such as cerium oxide.[23] Although DFT calculations were performed as single molecule in gas phase, whereas X-rays structure is affected by solid state constraints, the optimized structure of **3b** is very close to the experimental one (Figure 4), showing Ce-N bond distances similar to that experimentally measured (Table 2)
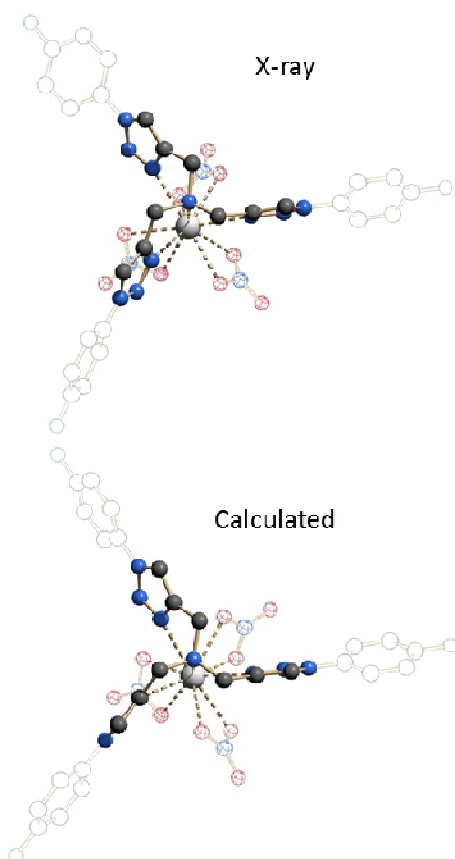
**Figure 4**. X-rays (top) and calculated (bottom) structures of **3b**.

It should be noted that the largest mismatch (about 8% of the experimental value) was observed for the bond between the cerium and the sp$^3$ nitrogen of the ligand, that is quite sensitive to any conformational change. The good match between the calculated and the experimental geometry of the complex indicate that this computational approach should be reliable also for the optimization of the homoleptic complexes **4-5**. The geometry optimization of complex **4b** was performed on the isolated cation ($3^+$) in the doublet state, by the preliminary optimization of the core containing the six triazole rings, and adding the phenyl rings in a subsequent optimization step. The final structure (Figure 5, bottom) shows that the cerium is octa-coordinated, with total symmetry D$_{3d}$, and Ce-N bond distances very similar to those observed for complex **3b** (Table 2).

| Distances | Exp. Dist. in **3b** (Å) | Calcd. for **3b** (Å) | Calcd. for **4b**, **5b** (as $3^+$ cation, Å) |
|---|---|---|---|
| Ce-N(CH$_2$)$_3$ | 2.826 | 3.05 | 2.91 (average) |
| Ce-N(triazole) | 2.69 (average) | 2.66 (average) | 2.56 (average) |

**Table 2**. Experimental and calculated Ce-N distances in complexes **4b**, **5b** and **6b**. Calculations at the B3LYP/SDD level.
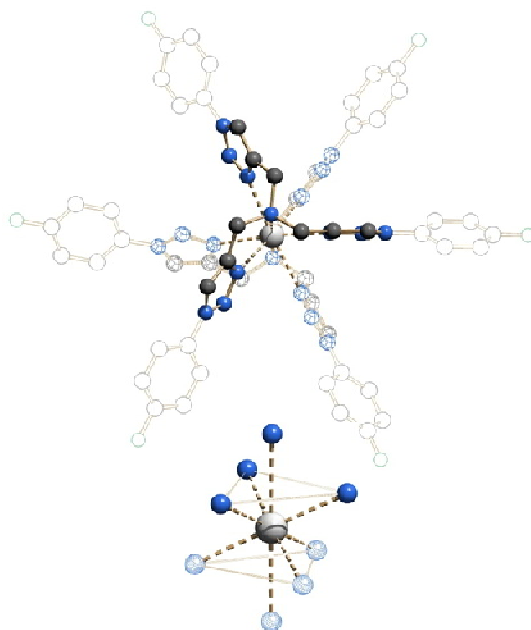
**Figure 5**. Calculated structures of **4b** and **5b**. Top: complete structure; bottom: coordination geometry of $Ce^{3+}$

All the obtained complexes were studied using a variety of techniques. The FT-IR spectra of complexes as solid samples gave a confirmation of their structures. In fact, typical peaks of the nitrate groups[24] appear at *ca* 1500 cm$^{-1}$, 1306 cm$^{-1}$, 1026 cm$^{-1}$ and 816 cm$^{-1}$ and the difference between two strongest absorptions of the nitrate groups is about 200 cm$^{-1}$, confirming that the $NO_3^-$ groups coordinate to the lanthanide ion as bidentate ligands.[24e] Otherwise, **4a-b** and **5a-b** showed characteristic frequencies of free anion, i.e. about 1600, 1110, 1090 and 624 for perchlorates[25] and 1275, 1030, 759, 638 and 517 for triflates.[26]

NMR analysis of the complexes produced very interesting results, giving evidence that both homoleptic and heteroleptic complexes are stable in solution. The $^1$H-NMR spectra revealed the formation of metal-ligand interactions through a massive broadening of most of the signals with respect to the pure ligands, together with large variations in chemical shifts.[27]

$^1$H-NMR spectra recorded in acetonitrile-d$_3$ at 25°C on **4b** and on **5b** showed a broad signal at about -3 ppm. On the contrary, the spectra of **3b** complex did not show the signal at -3 ppm, but a very broad signal centered at about -0.5 ppm. Having assigned all the other signals, in the cases of **4b** and **5b**, the signals at -3.2 ppm must be assigned to the three CH$_2$ bonded to the central nitrogen of the tripodal ligand. The huge upfield shift can be ascribed to the proximity to the paramagnetic $Ce^{3+}$, that acts as an internal shift reagent.[28] On one side the observation of this paramagnetic shift is a proof of the presence of a cerium complex in solution, on the other side it is not a definitive

proof of the existence of the homoleptic complex in solution. For this reason, a NMR sample of **4b** was prepared using about 1.5 eq of ligand with respect to $Ce(ClO_4)_3$. NMR spectra recorded in acetonitrile-$d_3$ showed a signal at -3.0 ppm and a smaller signal at -0.5 ppm (about 50% by integration). On addition of small portions of **L$_2$**, the signal at -0.5 ppm disappeared and the signal of the free ligand (4.1 ppm) eventually appeared when the ligand was in excess (Figure 6 ).[29]
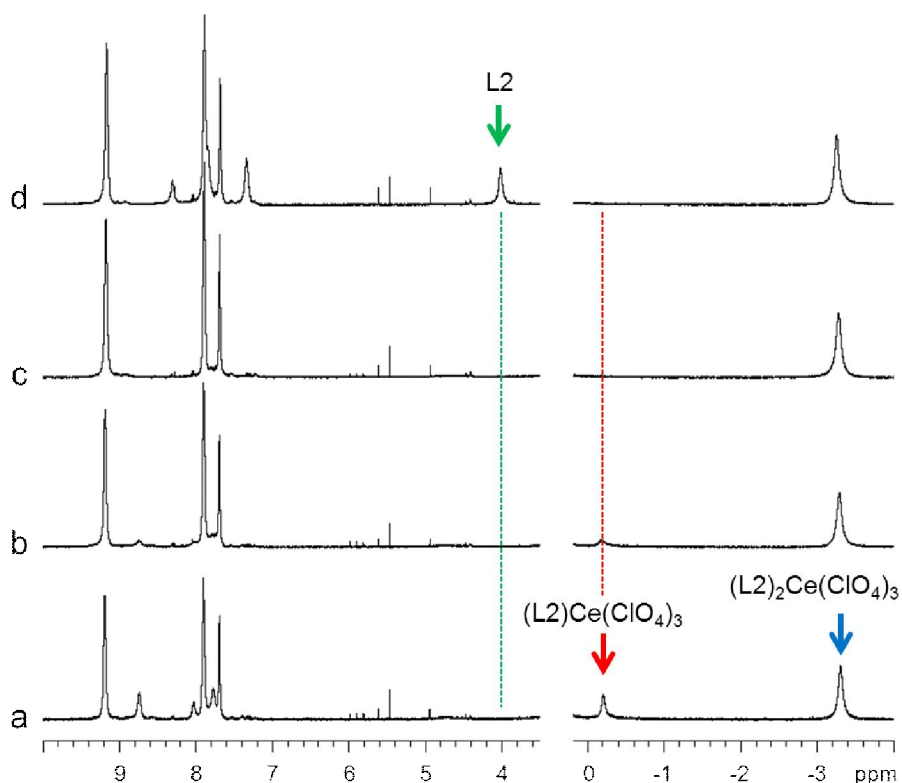


**Figure 6**. ^{1}H NMR spectra of compound **4b**. Spectrum a) corresponds to a sample prepared with 1.5 eq. of ligand. Spectra b-d were recorded after consecutive addition of free ligand, showing the disappearance of the signal at -0.2 ppm and the raising of the signal of the free ligand (green arrow) when the ratio is bigger than 2:1. The signal of the homoleptic complex at -3.35 ppm (blue arrow) grows in integral without any change in chemical shift.

This behavior unequivocally showed that the signal at -3.0 ppm corresponds to the $(L2)_2Ce(ClO_4)_3$ complex **4b**, whereas the signal at -0.5 ppm is due to the $(L2)Ce(ClO_4)_3$ complex. The same behavior was observed in the case of the triflate **5b**.

On the contrary, the spectra acquired on the nitrate complex **3b** prepared using 1.5 eq of **L2** still showed a very broad signal at about -0.5ppm. To ascertain if a dynamic process took place, variable temperature spectra were recorded. On lowering the temperature, the upfield signal sharpens and moves upfield to -3.4 ppm at -20°C, and a second signal appears at 4.0 ppm, the latter being coincident with the chemical shift of the free ligand. This behaviour can be ascribed to the chemical exchange of the ligand between the complexed and the free status, the broad signal observed at

+25°C being the weighted average of the two chemical shift when the exchange is fast in the NMR timescale. The chemical shift of the upfield signal at -20°C is almost coincident with the signals of the perchlorate and triflate compounds (albeit a temperature shift is possible). To understand whether the signal at -3.4 ppm observed at -20°C corresponded to a temperature induced upfield shift of the heteroleptic complex or to the formation of the homoleptic complex, a set of spectra was recorded at 0°C for the three compounds **3b**, **4b** and **5b**. (Figure 7). At this halfway temperature the upfield signal of the perchlorate and triflate compounds moved to about -4 ppm whereas the signal of the nitrate complex was found at -1.9 ppm. The different chemical shift observed for **3b** confirms the exclusive formation of the heteroleptic compound in the case of nitrate anion, as experimentally observed by X-ray.
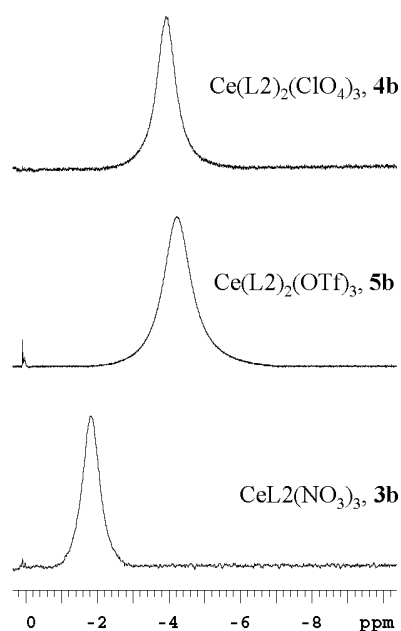


**Figure 7**. $^1$H NMR spectra (600 MHz in CD$_3$CN) recorded at 0°C for the three L2-complexes **3b**, **4b** and **5b.**

The samples can be stored at room temperature at least for 48 hours without noticeable variation of the spectra, thus indicating that all the complexes are stable in acetonitrile solutions. Moreover, dilution NMR analysis was performed (concentration range $5 \times 10^{-3}$-$5 \times 10^{-5}$ M) showing that neither the concentration nor the amount of water in the solvent affected the nature of the species in solution.

The ESI-MS spectra of homoleptic complexes **4a-b** and **5a-b** recorded in acetonitrile showed peaks corresponding to the (**L1**)$_2$Ce$^{3+}$ motifs with 0-3 charge-balancing ions, whereas peaks corresponding to the (**L1**)Ce$^{3+}$ species were not detected, confirming again that the homoleptic motif is favored in solution. A representative example is reported in Figure 8. On the contrary, the

spectra of heteroleptic complexes **3a-b** showed both kind of peaks, probably since rearrangements can occur during the analysis[30] and the different instrumental response depending on the compound charge.
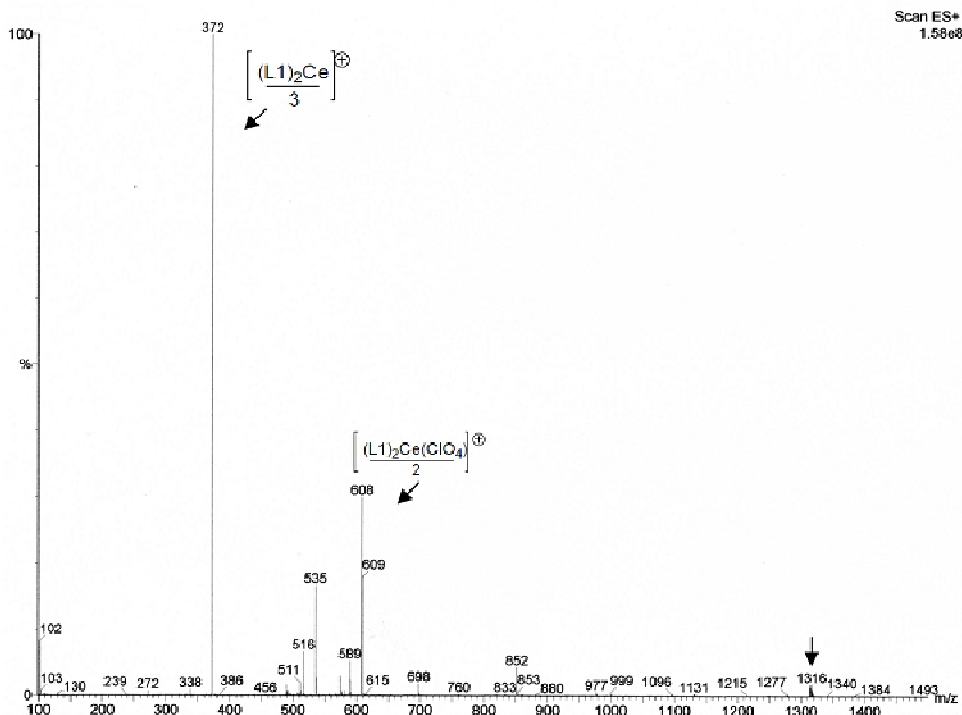


**Figure 8**. Mass spectrum of complex **4a**.

The photophysical properties of the new complexes are summarised in Table 3. The absorption spectra of the **L1**-$Ce^{3+}$-complexes in ACN solution, together with those of the starting $Ce^{3+}$ salts and of the free ligand **L1**, all of which were measured from samples at the same concentration ($5.0 \times 10^{-5}$ M), are reported in Figure 9.
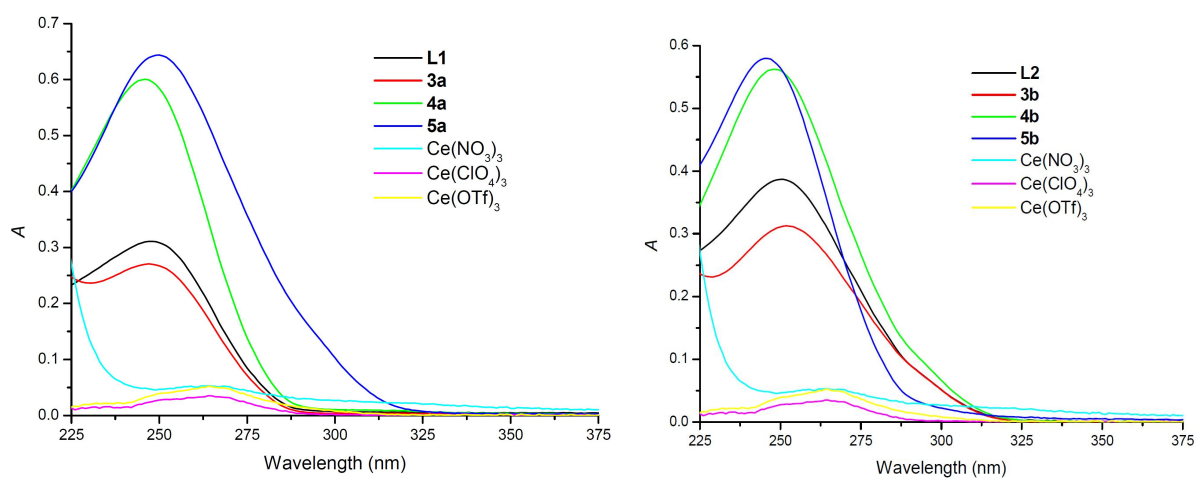


**Figure 9**. Absorption spectra of $1 \times 10^{-5}$M ACN solutions of **L1**, **3a**, **4a** and **5a** (left), **L2**, **3b**, **4b** and **5b** (right), and $5 \times 10^{-5}$M ACN solution of $Ce^{3+}$ salts.

In particular, the spectrum of each **L1**-Ce$^{3+}$ complex does not macroscopically differ from that of the free ligand **L1**, as all of the absorption profiles display ligand centered (LC) π–π* transitions centered at ca. 250 nm. However, the formation of the various homoleptic [Ce(**L1**)$_2$]$^{3+}$ species, namely **4a** and **5a**, is witnessed by fact that the intensity of this band almost doubles those relative to the heteroleptic complex **3a** and the free ligand **L1,** respectively (Figure 5). As expected, totally different absorption profiles were displayed by all of the Ce(III) saline precursors (Figure 9). The spectra of these latter species, in fact, consist of very weak transitions in the wavelength range comprised between 250 and 270 nm.

A substantially analogous behaviour was displayed by the ligand **L2** and the whole series of the corresponding Ce$^{3+}$-**L2** complexes (Figure 9).

| Compound | Absorption $\lambda_{max}$(nm): $10^4\varepsilon$ ($M^{-1}$ $cm^{-1}$) | Emission λ (nm) | τ (ns) | Φ |
|---|---|---|---|---|
| **L1** | 247 (3.1) | 454 | 4 | <0.1% |
| **L2** | 250 (3.8) | 386, 408, 430 | 4 | <0.1% |
| **3a** (L1Ce(NO$_3$)$_3$) | 247 (2.7) | 456 | 10 | 1.0% |
| **4a** ((L1)$_2$Ce(ClO$_4$)$_3$) | 246 (6.0) | 486 | 21 | 1.5% |
| **5a** ((L1)$_2$Ce(OTf)$_3$) | 250 (6.4) | 476 | 22 | 1.0% |
| **3b** (L2Ce(NO$_3$)$_3$) | 252 (3.1) | 416 | 10 | 0.5% |
| **4b** ((L2)$_2$Ce(ClO$_4$)$_3$) | 248 (5.6) | 418 | 22 | 1.0% |
| **5b** ((L2)$_2$Ce(OTf)$_3$) | 245 (5.8) | 406 | 27 | 0.5% |

**Table 3**. Photophysical data of ligands and Ce(III)-complexes in ACN solutions (5.0x10$^{-5}$M).

All the compounds that are reported here, including the "free" ligands **L1** and **L2**, are luminescent at room temperature in acetonitrile solutions (water content less than 1%). The spectra were recorded at various concentrations (from $10^{-3}$ to $10^{-5}$ M) and no appreciable differences were observed. At a glance, the emission spectra of the **L1** containing Ce$^{3+}$ complexes do not differ appreciably from that of the ligand **L1** that was obtained in the same conditions. However, the different nature of the excited states from which emissions originates in the Ce$^{3+}$-**L1** complexes is suggested by the analysis of their excitation spectra. As depicted in Figure 10, the excitation spectra of the various Ce$^{3+}$-**L1** species display two different contributions at ca. 275 and 335 nm, respectively, while a single maximum centred at ca. 275 nm is observed in the excitation spectrum of the free ligand **L1**.

The emission profile of the heteroleptic complex **3a** resemble the one of **L1**, with a maximum around 456 nm, whereas a red shift to 486 and 476 nm was observed for the homoleptics **4a** and **5a** respectively.

**Figure 10**. Normalized excitation and emission spectra of ligands **L1** and the corresponding cerium (III) complexes, **3a**, **4a** and **5a** in ACN at r.t..

Relative to the triazole-based fluorinated **L2** and to the corresponding $Ce^{3+}$ complexes, the analysis of the fluorescence spectra enlighten some differences with respect to the previous cases (Figure 11). Indeed, upon excitation at 300 nm, the free ligand **L2** displays a vibronically structured emission spectrum with maxima centered at 386 and 430 nm, respectively. This emission profile turns to broad and structureless as the $Ce^{3+}$-**L2** complexes are formed, also giving rise, in most cases, to substantially different excitation spectra. It is also worth noting that, at opposite with what observed for the **L1**-$Ce^{3+}$ type complexes, no particularly evident difference was detected from the comparison of the steady-state emission spectrum of the heteroleptic compound **3b** with respect to those of the homoleptics **4b** and **5b**.
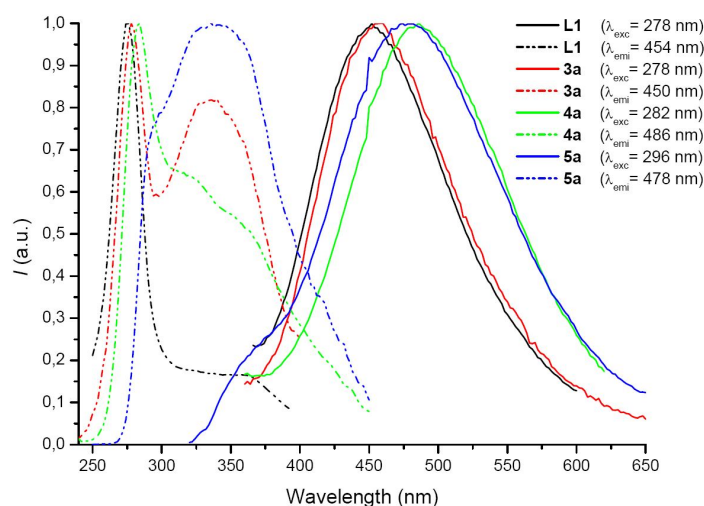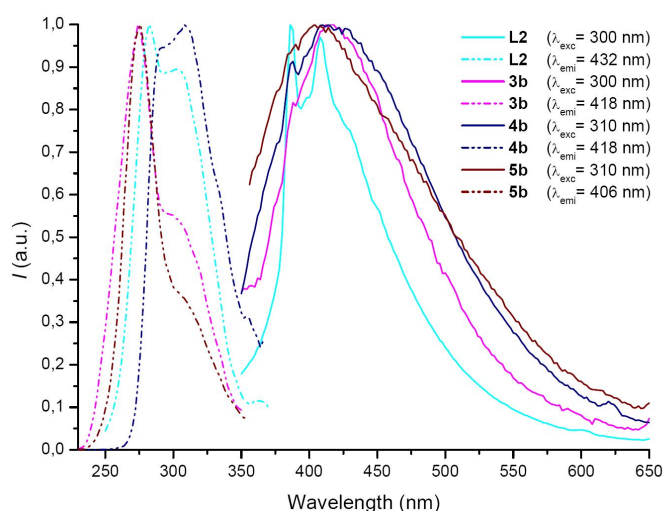


**Figure 11**. Normalized excitation and emission spectra of ligands **L2** and the corresponding cerium (III) complexes, **3b**, **4b** and **5b** in ACN at r.t..

The measured lifetime decays ($\tau$) of the new complexes, which are comprised between 10 and 27 ns, are comparable with those previously reported for Cerium (III) derivatives[7d, 9] and one order of magnitude higher than those displayed by the free ligands, suggesting the $Ce^{3+}$ ion as responsible of the emissions. The emission quantum yields ($\Phi$) values that were determined from diluted ($5x10^{-5}$ M) acetonitrile solutions of all the new $Ce^{3+}$ complexes vary from 0.5% to 1.5% and are significantly lower than those relative to a series of similar $(L)_2Ce^{3+}$ species.[14] This discrepancy could be attributed to a partially fulfilling "Ce(III)-encapsulating attitude" displayed by the ligands employed in this work.

## 7.2 - Conclusions

Two new tripodal aromatic triazole-based ligands **L1** and **L2** have been synthesized and exploited to obtain blue-emitting $Ce^{3+}$ complexes. Depending on the counteranion , different structures of heteroleptic and homoleptic compounds were obtained. These complexes were studied using a variety of techniques, which revealed the important role that the counteranion plays in the characteristics of such systems. Studies are in progress in our laboratories to evaluate the effect of different triazole substituents on the formation and on the nature of Cerium (III) and other Lanthanide (III) complexes.

## 7.3 - Experimental Section

The solvents and chemicals were used as received from sellers, unless otherwise mentioned.

NMR spectra were recorded by using a Varian Mercury 400 MHz or a Varian Inova 600 MHz spectrometer with tetramethylsilane as the internal standard.

Elemental analyses were performed on a ThermoQuest Flash 1112 series EA instrument.

ESI-MS analysis were performed by direct injection of acetonitrile solutions of the compounds using a WATERS ZQ 4000 mass spectrometer.

The IR spectra were recorded with a FT-IR spectrometer Perkin Elmer Spectrum 2000.

UV/Vis absorption spectra were measured on a Varian Cary 4 double-beam UV-Vis spectrometer and baseline corrected. Steady-state emission spectra were recorded on an Edinburgh FLS920P spectrofluorimeter equipped with a 450 W Xenon arc lamp, double excitation and single emission monochromators and a peltier cooled Hamamatsu R928P photomultiplier tube (185–850 nm). Emission and excitation spectra were corrected for source intensity (lamp and grating) and emission spectral response (detector and grating) by calibration curve supplied with the instrument. Emission lifetimes were determined on the same Edinburgh instrument with the Time Correlated Single Photon Counting (TCSPC) technique  using pulsed picosecond LEDs (EPLED 295 or EPLED 360, FHWM <800 ps, repetition rates between 10 kHz and 1 MHz) as the excitation source and the

above-mentioned R928P PMT as detector. The goodness of fit was assessed by minimizing the reduced $\chi^2$ function andvisual inspection of the weighted residuals. The emission quantum yields were determined according to the optically dilute solutions method in ACN solutions with reference to Ru(bpy)$_3$Cl$_2$ as the standard (r) according to Equation (1),[31] where $I$ refers to the area of the emission peaks of the complex and the reference, A to their absorptions and n is the refractive index of the corresponding solvents.

$$\Phi = \Phi_r \, \frac{I}{I_r} \, \frac{A_r}{A} \, \frac{n^2}{n_r^2}$$

**Ligands synthesis**: Ligands **L1** and **L2** were obtained following synthetic scheme according to a previous reported one-pot 'click reaction'.[17]

**General procedure.** In a 50 mL round-bottom flask, the desired aniline **1** (1.67 g, 15.0 mmol) was dissolved in CH$_3$CN (30 mL) and cooled to 0 °C

in an ice bath. To this stirred mixture, $t$BuONO (2.32 g, 2.68 mL, 22.5 mmol) was added dropwise, followed by TMSN$_3$ (2.07 g, 2.37 mL, 18.0 mmol). The resulting solution was stirred and left to reach room temperature during the night. Then, tripropargylamine **2** (0.39 g, 420 μL, 3.0 mmol), CuSO$_4$·5H$_2$O (190 mg, 0.75 mmol) in 4.4 mL of H$_2$O and sodium ascorbate (0.97 g, 4.5 mmol) were then added and the reaction was left to stir at room temperature for 2 days. Most of the solvent was evaporated and the crude was dissolved in 30 ml of a 1/1 mixture of CH$_2$Cl$_2$/aq NH$_3$. After 3 h stirring, the layers were separated and the water was further extracted with ethyl acetate. The collected organic phases were dried over MgSO$_4$, the solvent evaporated and the crude product was purified by flash chromatography over neutral Al$_2$O$_3$.

**Tris ((1-phenyl-1$H$-1, 2, 3-triazol-4-yl)methyl)amine (L1):** Pale yellow solid, 0.89 g, 61 % yields; mp= 148.8-149.6 °C; $^1$H NMR (CDCl$_3$) $\delta$ 3.99 (s, 6H), 7.40-7.48 (m, 3H), 7.50-7.67 (m, 6H), 7.75-7.81 (m, 6H), 8.27 (s, 3H); $^{13}$C NMR (CDCl$_3$) $\delta$ 47.0 (CH$_2$), 120.5 (CH), 122.0 (CH), 128.7 (CH), 129.7 (CH), 137.1 (C), 144.6 (C). IR (KBr, cm$^{-1}$): 3131, 3057, 2842, 1600, 1504, 1335, 1235, 1221, 1168, 1048, 989, 906, 825, 756, 687, 520. C$_{27}$H$_{24}$N$_{10}$ (488.22): calcd. C 66.38, H 4.95, N 28.67; found C 66.75, H 5.16, N 28.89. ESI-MS: 489 [M+1]$^+$

**Tris ((1-(4-fluorophenyl)-1$H$-1, 2, 3-triazol-4-yl) methyl)amine (L2)**: Pale yellow solid, 1.09 g, 67 % yields; mp= 179.5-180.3 °C; $^1$H NMR (CDCl$_3$) $\delta$ 3.96 (s, 6H), 7.15-7.30 (m, 6H), 7.54-7.56 (m, 6H), 8.22 (s, 3H); $^{19}$F NMR (CDCl$_3$) $\delta$ -112.5 (3F); $^{13}$C NMR (CDCl$_3$) $\delta$ 47.3 (CH$_2$), 116.7 (CH, $J_{CF}$=23.3), 122.2 (CH), 122.4 (CH, $J_{CF}$=8.7), 133.3 (C, $J_{CF}$=3.5), 144.7 (C), 162.2 (C, $J_{CF}$=249.2). IR (KBr, cm$^{-1}$): 3129, 3092, 2929, 2833, 1602, 1517, 1447, 1332, 1233, 1155, 1048,

835, 610, 521. $C_{27}H_{21}F_3N_{10}$ (542.19): calcd. C 59.77, H 3.90, N 25.82; found C 59.43, H 3.55, N 26.03. ESI-MS: 543 [M+1]$^+$

**Complexes synthesis**: After optimization of ligand/Ce(III) salt ratio, all the complexes were prepared in a similar way, as follow. The Ce(III) salts were suspended in $CH_2Cl_2$, and the mixtures were left to stir for 2 h at r.t. The solvent was filtered off and the solids were dried *in vacuum*. Then, an acetonitrile solution of the appropriate Ce(III) salt (0.05 mmol in 2 ml) was added to a solution of the ligand (0.1 mmol) in 4 ml of acetonitrile. The resulting mixture was stirred for 1 h at room temperature, and then left in diethyl ether vapours. After several days, a precipitate or crystals were formed, that were collected, dried in air and submitted to analysis.

**(L1)Ce(NO$_3$)$_3$ 3a**: From Ce(NO$_3$)$_3$·6H$_2$O. 33.0 mg, 81 % yields. IR (KBr, cm$^{-1}$): 3136, 2915, 2848, 1594, 1502, 1465 ($\nu_{NO3}$), 1384, 1306 ($\nu_{NO3}$), 1233, 1188, 1067, 1026 ($\nu_{NO3}$), 993, 816 ($\nu_{NO3}$), 761, 687. $^1$H NMR (CDCl$_3$) $\delta$ -0.58 (bs, 6H), 7.4 (bs, 3H), 7.65 (bs, 3H), 7.72 (bs, 6H), 8.07 (bs, 6H); $C_{27}H_{24}CeN_{13}O_9$ (814.09): calcd. C 39.81, H 2.97, N 22.35; found C 40.01, H 3.10, N 22.90. ESI-MS: 752 [(L1)Ce(NO$_3$)$_2$]$^+$.

**(L1)$_2$Ce(ClO$_4$)$_3$ 4a**: From Ce(ClO$_4$)$_3$·xH$_2$O. 55.2 mg, 78 % yields. IR (KBr, cm$^{-1}$): 3120, 3057, 2842, 1637, 1598($\nu_{ClO4}$), 1501, 1466, 1384, 1235, 1196, 1115 ($\nu_{ClO4}$), 1111($\nu_{ClO4}$), 1089 ($\nu_{ClO4}$), 986, 759, 689, 624 ($\nu_{ClO4}$), 521. $^1$H NMR (CDCl$_3$) $\delta$ -3.20 (bs, 6H), 7.57 (bs, 3H), 7.92 (bs, 3H), 9.00 (bs, 6H); $C_{54}H_{48}CeCl_3N_{20}O_{12}$ (1413.19): calcd. C 45.82, H 3.42, N 19.79; found C 45.98, H 3.87, N 20.01. ESI-MS: 1316 [(L1)$_2$Ce(ClO$_4$)$_2$]$^+$, 608 [(L1)$_2$Ce(ClO$_4$)/2]$^+$, 372 [(L1)$_2$Ce/3]$^+$.

**(L1)$_2$Ce(SO$_3$CF$_3$)$_3$ 5a**: From Ce(SO$_3$CF$_3$)$_3$. 57.8 mg, 74 % yields. IR (KBr, cm$^{-1}$): 3146, 3016, 2927, 2855, 1598, 1504, 1468, 1275 ($\nu_{SO3}$), 1245, 1168 ($\nu_{SO3}$), 1030 ($\nu_{SO3}$), 991, 911, 832, 759 ($\nu_{SO3}$), 690, 638 ($\nu_{SO3}$), 517 ($\nu_{SO3}$). $^1$H NMR (CDCl$_3$) $\delta$ -3.27 (bs, 6H), 7.54 (bs, 3H), 7.91 (bs, 3H), 7.99 (bs, 6H), 8.99 (bs, 6H); $C_{57}H_{48}CeF_9N_{20}O_9S_3$ (1563.20): C 43.76, H 3.09, N 17.91; found C 43.92, H 3.19, N 18.03. ESI-MS: 633 [(L1)$_2$Ce(SO$_3$CF$_3$)/2]$^+$, 372 [(L1)$_2$Ce/3]$^+$.

**(L2)Ce(NO$_3$)$_3$ 3b**: From Ce(NO$_3$)$_3$·6H$_2$O. 36.0 mg, 83 % yields. IR (KBr, cm$^{-1}$): 3431, 3143, 2957, 1627, 1513, 1465 ($\nu_{NO3}$), 1288, 1262, 1229, 1152, 1099, 1070, 1023 ($\nu_{NO3}$), 803 ($\nu_{NO3}$), 735, 617. $^1$H NMR (CDCl$_3$) $\delta$ -0.50 (bs, 6H), 7.48 (bs, 9H), 8.11 (bs, 6H); $C_{27}H_{21}CeF_3N_{13}O_9$ (868.06): calcd. C 37.33, H 2.44, N 20.96; found C 37.95, H 2.87, N 21.10. ESI-MS: 806 [(L2)Ce(NO$_3$)$_2$]$^+$, 372 [(L1)Ce(NO$_3$)/2]$^+$.

**(L2)$_2$Ce(ClO$_4$)$_3$ 4b**: From Ce(ClO$_4$)$_3$·xH$_2$O. 60.9 mg, 80 % yields. IR (KBr, cm$^{-1}$): 3084, 2950, 1604 ($\nu_{ClO4}$), 1517, 1384, 1233, 1122, 1117 ($\nu_{ClO4}$), 1104 ($\nu_{ClO4}$), 1086 ($\nu_{ClO4}$),, 1045, 839, 625 ($\nu_{ClO4}$), 525. $^1$H NMR (CDCl$_3$) $\delta$ -3.30 (bs, 6H), 7.69 (bs, 3H), 7.90 (bs, 6H), 9.19 (bs, 6H);

$C_{54}H_{42}CeCl_3F_6N_{20}O_{12}$ (1521.13): found C 42.57, H 2.78, N 18.39; found C 42.83, H 3.08, N 18.63. ESI-MS: 1422 $[(L2)_2Ce(ClO_4)_2]^+$, 662 $[(L2)_2Ce(ClO_4)/2]^+$, 408 $[(L2)_2Ce/3]^+$.

**(L2)$_2$Ce(SO$_3$CF$_3$)$_3$ 5b**: From Ce(SO$_3$CF$_3$)$_3$. 57.8 mg, 69 % yields. IR (KBr, cm$^{-1}$): 3426, 3144, 1653, 1609, 1517, 1450, 1270 ($\nu_{SO3}$), 1237, 1163 ($\nu_{SO3}$), 1100, 1067, 1030 ($\nu_{SO3}$), 840, 637 ($\nu_{SO3}$), 517 ($\nu_{SO3}$). $^1$H NMR (CDCl$_3$) $\delta$ -3.14 (bs, 6H), 7.59 (bs, 3H), 7.81 (bs, 6H), 9.03 (s, 6H); $C_{57}H_{42}CeF_{15}N_{20}O_9S_3$ (1671.14): C 40.94, H, 2.53, N 16.75; found C 41.20, H 2.96, N 17.02. ESI-MS: 1672 $[(L2)_2Ce(SO_3CF_3)_3 +1]^+$, 1522 $[(L2)_2Ce(SO_3CF_3)_2]^+$, 687 $[(L2)_2Ce(SO_3CF_3)/2]^+$.

**Calculations details:**

Calculations on **3b** and on the 3+ cation of **4b** and **5b** were performed by the Gaussian 09 rev A.02 series of programs using the unrestricted B3LYP functional and the SDD basis set applied to all the atoms. Due to the difficulties experienced with standard convergence criteria, all the calculations employed the quadratically convergent SCF procedure together with a loose convergence criteria ("scf=(QC,conver=6)" keyword). However, to check the optimized structures, harmonic vibrational frequencies were calculated at the same level of theory. As revealed by the frequency analysis, imaginary frequencies were absent and the visual inspection of the lowest energy normal mode showed a conformational motion of one ligand versus the second one.

## 7.4 - Bibliography

[1]    a) C. W. Tornøe, M. Meldal, in *Peptides: the wave of the future*, M. Lebl, R. A. Houghten, ed.; Kluwer Academic Publishers, Dordrecht, **2001**, pp. 263; b) H. C. Kolb, M. G. Finn, K. B. Sharpless, *Angew. Chem., Int. Ed.*, **2001**, *40*, 2004-2021.

[2]    a) V. V. Rostovtsev, L. G. Green, V. V. Fokin, K. B. Sharpless, *Angew. Chem., Int. Ed.*, **2002**, *41*, 2596; b) R. Huisgen, in *1,3-Dipolar cycloaddition chemistry*, ed. A. Padwa, Wiley, New York, 1984, vol. 1, p. 1.

[3]    a) S. Rana, J. W. Cho, *Nanoscale*, **2010**, *2*, 2550-2556. b) G. Franc, A. K. Kakkar, *Chem. Soc. Rev.* **2010**, *39*, 1536–1544; c) C. Wangler, R. Schirrmacher, P. Bartenstein, B. Wangler, *Curr. Med. Chem.,* **2010**, *17*, 1092-1116; d) D. Astruc, L. Liang, A. Rapakousiou, J. Ruiz, *Acc. Chem. Res.*, **2012**, *45*, 630–640; e) H. C. Kolb, K. B. Sharpless, *Drug Discovery Today* **2003**, *8*, 1128; f) P. Wu, V. V. Fokin, *Aldrichimica Acta* **2007**, *40*, 7; g) C. W. Tornøe, C. Christensen, M. Meldal, *J. Org. Chem.* **2002**, *67*, 3057; h) M. Meldal, C. W. Tornøe, *Chem.Rev.* **2008**, *108*, 2952.

[4]    a) B. Happ, D. Escudero, M. D. Hager, C. Friebe, A. Winter, H. Görls, E. Altuntaş, L. González, U. S. Schubert, *J. Org. Chem.* **2010**, *75*, 4025–4038; b) Z. E. A. Chamas, X. Guo, J.-L. Canet, A. Gautier, D. Boyer, R. Mahiou, *Dalton Trans.* **2010**, *39*, 7091–7097.

[5]     a) P. Hänninen, H. Härmä, *Lanthanide Luminescence: Photophysical, Analytical and Biological Aspects* Ed. Springer Verlag Heidelberg Berlin 2011; b) S. V. Eliseeva, J.-C. G. Bünzli, *Chem. Soc. Rev.* **2010**, *39*, 189–227; c) M. A. Katkova, M. N. Bochkarev *Dalton Trans.* **2010**, *39,* 6599–6612; d) A. Vogler, H. Kunkely, *Inorg. Chim. Acta* **2006**, *359*, 4130–4138.

[6]     a) G. Bergamini, E. Marchi, P. Ceroni, *Coord. Chem. Rev.* **2011**, *255*, 2458–2468; b) S. Dang, J.-H. Zhangb, Z.-M. Sun, *J. Mater. Chem.* **2012**, *22*, 8868-; c) J. Kido, Y. Okamoto, *Chem. Rev.* **2002**, *102*, 2357–2368; d) T. Oyamada, Y. Kawamura, T. Koyama, H. Sasabe, C. Adachi, *Adv. Mater.* **2004**, *16*, 1082–1086; e) M. K. Lam, K. L. Kwok, S. C. Tse, S. K. So, J. B. Yuan, L. M. Leung, M. L. Gong, *Opt. Mater.* **2006**, *28*, 709–713.

[7]     a) C. Lincheneau, F. Stomeo, S. Comby, T. Gunnlaugsson, *Aus. J. Chem.* **2011**, *64*, 1315-1326; b) T. Terai, H. Ito, K. Kikuchi, T. Nagano *Chem. Eur. J.* **2012**, *18*, 7377–7381; c) M. Schäferling *Angew. Chem. Int. Ed.* **2012**, *51*, 3532–3554; d) C. D. S. Brites, P. P. Lima, N. J. O. Silva, Angel Millán, V. S. Amaral, F. Palacio, L. D. Carlos, *New J. Chem.* **2011**, *35*, 1177–1183; e) I. Hemmila, S. V. Laitala, *J. Fluoresc.* **2005**, *15*, 529–542.

[8]     a) E. G. Moore, A. P. S. Samuel, K. N. Raymond, *Acc. Chem. Res.* **2009**, **42**, 542–552; b) S. Shinoda, H. Tsukube *Analyst* **2011**, *136*, 431-435; c) L. Tian, Z. C. Dai, L. Zhang, R. Y. Zhang, Z. Q. Ye, J. Wu, D. Y. Jin, J. L. Yuan, *Nanoscale* **2012**, *4*, 3551-3557; d) Y. Liu, X. Wu, C. He, Y. Jiao, C. Duan, *Chem. Commun.* **2009**, 7554–7556.

[9]     a) J. Zhang, Y. Li, X. Hao, Q. Zhang, K. Yang, L. Li, L. Ma, S. Wang, X. Li, *Mini-Rev. Med. Chem.* **2011**, *11*, 678-694; b) M. Bottrill, L. Kwok, N. J. Long, *Chem. Soc. Rev.* **2006**, *35*, 557–571; c) S. Aime, D. Delli Castelli, S. Geninatti Crich, E. Gianolio, E. Terreno, *Acc. Chem. Res.* **2009**, *42*, 822–831; d) P. Escribano, B. J. López, J. Planelles-Aragó, E. Cordoncillo, B. Viana, C. Sanchez, *J. Mater. Chem.* **2008**, *18*, 23–40.

[10]    a) G. Bartoli, E. Marcantoni, M. Marcolini, L. Sambri, *Chem. Rev.*, **2010**, *110*, 6104–6143; b) V. Sridharan, J. C. Menéndez, *Chem. Rev.*, **2010**, *110*, 3805–3849; c) V. Nair, L. Balagopal, R. Rajan, J. Mathew, *Acc. Chem. Res.*, **2004**, *37*, 21-30; d) G. A. Molander, *Chem. Rev.* **1992**, *92*, 29-68, e) G. Bartoli, E. Marcantoni, L.Sambri, *Synlett* **2003**, 2101-2116.

[11]    C. Tang, Y. Bando, D. Golberg, R. Ma, *Angew. Chem. Int. Ed.* **2005**, *44*, 576–579.

[12]    a) J.-C. G. Bünzli, *Acc. Chem, Res.* **2006**, *39*, 53; b) M. E. Azenha, H. D. Burrows, S. M. Fonseca, M. L. Ramos, J. Rovisco, J. Seixas de Melo, A. J. F. N. Sobral, K. Kogej, *New J. Chem.* **2008**, *32*, 1531-1535; c) T. Yu, W. Su, W. Li, R. Hua, B. Chu, B. Li, *Solid-State Electron.* **2007**, *51*, 894; d) G.-C. Han, Y.-N. Liu, *Luminescence* **2010**, *25*, 389–393.

[13]    a) C. Canevali, M. Mattoni, F. Morazzoni, R. Scotti, M. Casu, A. Musinu, R. Krsmanovic, S. Polizzi, A. Speghini, M. Bettinelli, *J. Am. Chem. Soc.* **2005**, *127*, 14681–14691; b) H. Deng, S.

Yang, S. Xiao, H.-M. Gong, Q.-Q. Wang *J. Am. Chem. Soc.* **2008**, *130*, 2032-2040; c) R. Le Toquin, A. K. Cheetham, *Chem. Phys.s Lett.* **2006**, *423*, 352–356; d) K. Klier, A. C. Miller, L. L. Zhang, M. K. Hatalis, *Chem. Mater.* **2008,** *20,* 1359–1366; e) T.i Li, F. Li, J. Lü, Z. Guo, S. Gao, R. Cao, *Inorg. Chem.* **2008**, *47*, 5612-5615.

[14]    a) X.-L. Zheng, Y. Liu, M. Pan, X.-Q. Lü, J.-Y. Zhang, C.-Y. Zhao, Y.-X. Tong, C.-Y. Su *Angew. Chem. Int. Ed.* **2007**, *46*, 7399, and cited references.

[15]    a) D. F. Aull, H. P. Jenssen, *Phys. Rev. B* **1986**, *34*, 6640–6646; b) S. T. Frey, W. D. Horrocks, Jr*., Inorg. Chem.* **1991**, *30*, 1073–1079; c) P. N. Hazin, C. Lakshminarayan, L. S. Brineq, J. L. Knee, J. W. Bruno, W. E. Streib, K. Foltingt, *Inorg. Chem.* **1988**, *27*, 1393–1400; d) W. Li, T. Mishima, H. Adachi, J. Shiokawa, *Inorg. Chim. Acta* **1987**, *131*, 287–291;e) M- J. Tapia, H. D. Burrows *Langmuir* **2002**, *18*, 1872-1876; f) K. V. Vasudevan, N. A. Smith, B. L. Scott, B. L. Bennett, R. E. Muenchausen, J. C. Gordon *Dalton Trans.* **2012**, *41*, 1924–1927; g) H. Kunkely, A. Vogler, *J. Photochem. Photobiol. A-Chem.* **2002**, *151*, 45–47; i) S. Giuffrida, G. G. Condorelli, L. L. Costanzo, G. Ventimiglia, A. Di Mauro, I. L. Fragalà *J. Photochem. Photobiol. A-Chem.* **2008**, *195*, 215–222.

[16]    A. Baschieri, A. Mazzanti, S. Stagni, L. Sambri, *Eur. J. Inorg. Chem.* **2013**, in press, DOI: 10.1002/ejic.201201361.

[17]    K. Barral, A. D. Moorhouse, J. E. Moses, *Org. Lett.*, **2007**, *9*, 1809-1811.

[18]    a) T. R. Chan, R. Hilgraf, K. B. Sharpless, V. V. Fokin *Org. Lett.,* **2004**, *6*, 2853-2855. b) V. O. Rodionov, V. V. Fokin, M. G. Finn, *Angew. Chem., Int. Ed.* **2005**, *44*, 2210; c) P. S. Donnelly, S. D. Zanatta, S. C. Zammit, J. M. White, S. J. Williams, *Chem. Commun.*, **2008**, 2459–2461.

[19]    a) P. Di Bernardo, A. Melchior, M. Tolazzi, P. L. Zanonato Coord. Chem. Rev. **2012**, 256, 328–351; b) J.-C. G. Bünzli, C. Mabillard, *Inorg. Chem.*, **1986**, *25*, 2750; c) J.-C. G. Bünzli, A. Milicic-Tang, in *Handbook on the Physics and Chemistry of Rare Earths*, eds. K. A. Gschneidner and L. Eyring, Elsevier, Amsterdam, 1995, vol. 21, ch. 145, pp. 306–366.

[20]    a) A. Ikeda-Ohno, S. Tsushima, C. Hennig, T. Yaita, G. Bernhard, *Dalton Trans.* **2012**, *41*, 7190-7192; b) I. Kostovaa, N. Trendafilovab, I. Georgieva, *Spectrosc. Lett.* **2007**, *40*, 65-81.

[21]    X. Y. Cao, M. Dolg, *J. Mol. Struct. (Theochem)*, **2002**, *581*, 139-47.

[22]    SDD basis set as implemented in Gaussian 09 Rev. A.02. M. J. Frisch, G. W. Trucks, H. B. Schlegel, G. E. Scuseria, M. A. Robb, J. R. Cheeseman, G. Scalmani, V. Barone, B. Mennucci, G. A. Petersson, H. Nakatsuji, M. Caricato, X. Li, H. P. Hratchian, A. F. Izmaylov, J. Bloino, G. Zheng, J. L. Sonnenberg, M. Hada, M. Ehara, K. Toyota, R. Fukuda, J. Hasegawa, M. Ishida, T. Nakajima, Y. Honda, O. Kitao, H. Nakai, T. Vreven, J. A. Montgomery, Jr., J. E. Peralta, F. Ogliaro, M. Bearpark, J. J. Heyd, E. Brothers, K. N. Kudin, V. N. Staroverov, R. Kobayashi, J.

Normand, K. Raghavachari, A. Rendell, J. C. Burant, S. S. Iyengar, J. Tomasi, M. Cossi, N. Rega, J. M. Millam, M. Klene, J. E. Knox, J. B. Cross, V. Bakken, C. Adamo, J. Jaramillo, R. Gomperts, R. E. Stratmann, O. Yazyev, A. J. Austin, R. Cammi, C. Pomelli, J. W. Ochterski, R. L. Martin, K. Morokuma, V. G. Zakrzewski, G. A. Voth, P. Salvador, J. J. Dannenberg, S. Dapprich, A. D. Daniels, Ö. Farkas, J. B. Foresman, J. V. Ortiz, J. Cioslowski, and D. J. Fox, Gaussian, Inc., Wallingford CT, 2009.

[23]    J. Kullgren, C.W.M. Castleton, C. Müller, D. Muñoz Ramo, K. Hermansson, *J. Chem. Phys.* **2010**, *132*, 054110.

[24]    a) Z.-Z. Yan, G.-L. Dai, H.-D. Liang, Y.-Q. Lin, *Luminescence* **2011**, *26*, 218-222; b) K. Nakamato, *Infrared and Raman Spectra of Inorganic and Coordination Compounds*, Part B, Applications in Coordination, Organometallic, and Bioinorganic Chemistry, 6th Ed., Wiley, New York, 2009; c) N. F. Curtis, Y. M. Curtis. *Inorg Chem* **1964**, *4*, 804-809; d) M. R. S. Foreman, M. J. Hudson, M. G. B. Drew, C. Hill, C. Madic *Dalton Trans.* **2006**, 1645-1653; e) K. Lei, W. Liu, K. Yu *Monat. Chemie*, **2006**, *137*, 413-417.

[25]    M. Pan, M.-H. Lan, X.-T. Wang, C. Yan, Y. Liu,C.-Y. Su, *Inorg. Chim. Acta* **2010**, *363*, 3757–3764.

[26]    D. H. Johnston, D. F. Shiver *Inorg. Chem.* **1993**, *32*, 1045-1047.

[27]    a) P. Dröse, S. Blaurock, C. G. Hrib, L. Hilfert, F. T. Edelmann, *Z. Anorg. Allg. Chem.* **2011**, *637*, 186–189; b) I. Kostova, V.K. Rastogi, W. Kiefer, A. Kostovski, *Appl. Organometal. Chem.* **2006**, *20*, 483-493; c) J. W. Walton, R. Carr, N. H. Evans, A. M. Funk, A. M. Kenwright, D. Parker, D. S. Yufit, M. Botta, S. De Pinto, K.-L. Wong, *Inorg. Chem.* **2012**, *51*, 8042−8056.

[28]    a) I. Bertini, Y-M. Lee, C. Luchinat, M. Piccioli, L. Poggi, *Chembiochem*, **2001**, *2*, 550-558; b) I. Bertini, M.B.L. Janik, G. Liu, C. Luchinat, A. Rosato, *J. Magn. Reson.* **2001**, *148*, 23-30.

[29]    B. E. Aroussi, N. Dupont, G. Bernardinelli, J. Hamacek, *Inorg. Chem.* **2010**, *49*, 606-615.

[30]    An additional interpretation could be due to the sensitivity of the ESI spectrometer that is much higher in the case of charged species with respect to neutral ones. In this framework the presence of a tiny amount of homoleptic complex would be easily detected.

[31]    K. Binnemans *Chem. Rev.* **2009,** *109,* 4283–4374

# 8) Carbazole-Terpyridine ligands

Carbazole (**Cbz**) and 2,2':6',2"-terpyridine (**Tpy**) are molecular units of outstanding importance in materials, coordination and supramolecular chemistry. Carbazole is a luminescent[1] nitrogen-bridged diphenyl which can be easily functionalized[2,3] with a large variety of substituents or undergo polymerization to afford new materials with tailored chemical and physical properties.[4-6] Polycarbazoles, for instance, are extensively utilized for their electric and optical properties as hole transporters, electron donors or blue emitters in optoelectronic devices.[7,8] On the other hand, 2,2':6',2"-terpyridine, along with a huge number of related derivatives,[9] has been the object of intensive investigations particularly in the area of metallo-supramolecular complexes involving, among others, $Ru^{II}$, $Os^{II}$, $Fe^{II}$, $Pt^{II}$ and $Zn^{II}$ ions.[10-17] Their optical, electrochemical, luminescent, magnetic, catalytic and therapeutic properties make them attractive for applications in the areas of solar energy conversion, optoelectronic devices, sensors and medicinal chemistry, as comprehensively reviewed in recent years.[18-24] Despite the impressive number of papers related to carbazole- and terpyridine-based organic and inorganic photoactive systems, only a limited number of reports deal with molecules, metal complexes or materials in which these two widely exploited subunits are combined.[25-32] In this context, we decided to take advantage of the complementary electron donor (D, **Cbz**) and acceptor (A, **Tpy**) character of these two subunits and prepare D-π-A conjugated systems[33,34] in which carbazole and terpyridine are linked through a phenylene bridge directly attached to the Tpy unit. D-π-A molecules are utilized for different applications in materials science including nonlinear optics and fluorescent probes, just to mention the most frequent.[35,36] One of the key electronic properties of D-π-A is that, compared to the individual subunits, they may exhibit intramolecular charge-transfer (ICT) absorption and/or emission bands, typically solvent-dependent and red-shifted relative to those arising from the local excited (LE) states centred on the separated moieties.[37] Some examples of D-π-A systems involving carbazole as donor have been reported,[37] but the use of the versatile terpyridine moiety as acceptor partner in this context remains rather unexplored.[26] We thought that this combination might open a straightforward route to tuneable organic luminescent materials. Herein, we report[38] on the synthesis, electrochemistry and photophysical properties of **1**,[26] **2** and **3** (Figure 1), in which the bridging units between **Cbz** and **Tpy** are constituted by phenylene, methylene-phenylene and ethynylene-phenylene, respectively. The observed electronic transitions, which in some cases entail double luminescence, have been investigated by means of Density Functional Theory (DFT) and Time Dependent DFT (TD-DFT)[39-41] in an effort to get a deeper insight into the relationship between structure and properties.

Carbazole (**Cbz**) and 4'-p-tolyl-2,2':6',2"-terpyridine (**Ttpy**, Figure 1) have been also studied for comparison purposes.
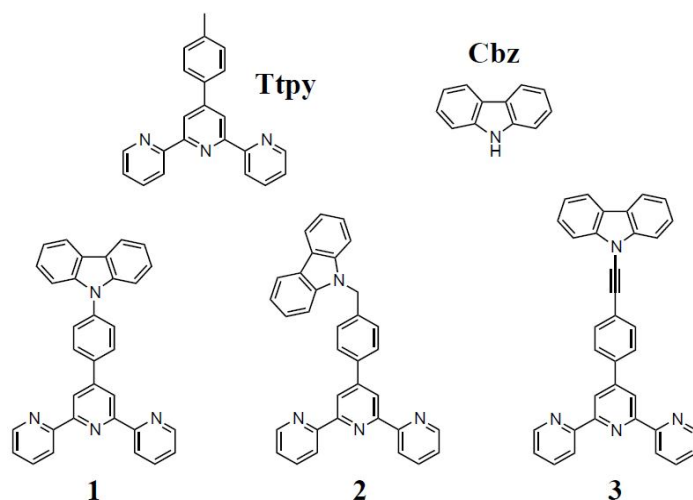


**Figure 1**: Chemical structure of the synthesized compounds **1-3** and of the reference samples **Cbz** and **Ttpy**.

## 8.1 - Results and discussion

### 8.1.1 - Synthesis and characterization

The syntheses of **Ttpy** and 4'-(4-bromophenyl)-2,2':6',2"-terpyridine **4**, used as starting material for the synthesis of **1**, were carried out according to a previously published procedure.[42] Terpyridine derivative **1** was prepared in 40% yield by an Ullmann-type condensation of **4** with carbazole **Cbz** using a modified literature method,[26] as reported in Scheme 1.
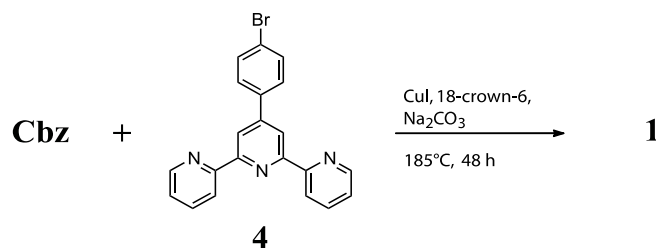


**Scheme 1**: Synthesis of **1**.

Compound **2** was obtained following the synthetic sequence reported in Scheme 2. The N-alkylation product formed by reaction of **Cbz** with the benzylic bromide **5** led to the derivative **6** (60% yield). The cyanide moiety was effectively reduced with DIBAL-H to give the corresponding aldehyde **7** (94% yield), which is the key intermediate to obtain the desired terpyridine. In fact, the

one-step condensation of **7** with 2-acetylpyridine, in the presence of KOH and aqueous ammonia as nitrogen source, led to carbazole-terpyridine **2** in 35% yield under mild reaction conditions.
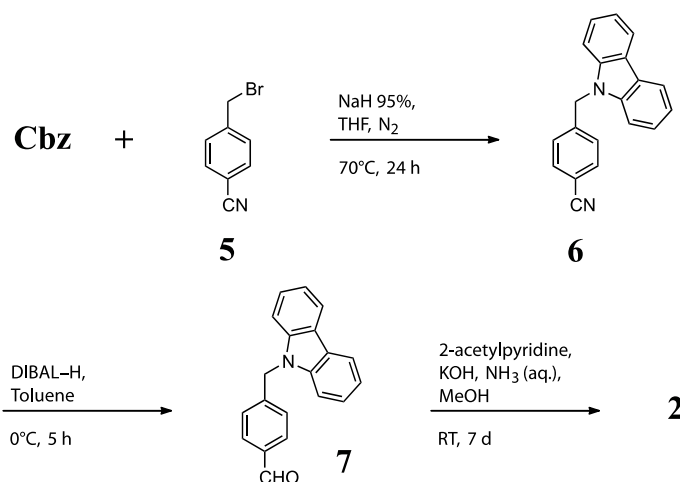


**Scheme 2**: Synthesis of **2**.

Finally, the synthetic strategy to obtain **3** is reported in Scheme 3. Syntheses of α-haloalkynes are usually based on the use of terminal alkynes as starting materials. However, these are often unstable, lowering the final yield. Therefore, the useful intermediate α-bromoalkyne **9** was directly obtained by reacting trimethylsilyl-substituted precursor **8** with NBS (95% yield, Scheme 3) obviating the need of deprotection and, as a consequence, saving one preparation step.[43] The ethynyl-carbazole derivative **10** was obtained in 75% yield via Cu[I]-catalyzed cross-coupling[44] of alkynyl bromide **9** with **Cbz** using a catalytic amount of CuSO$_4$ • 5H$_2$O and 1,10-phenanthroline. The rigid π-conjugated carbazole-terpyridine **3** was prepared in only one step[45] by condensation of the p-substituted benzaldehyde **10** and an excess of 2-acetylpyridine (60% yield).
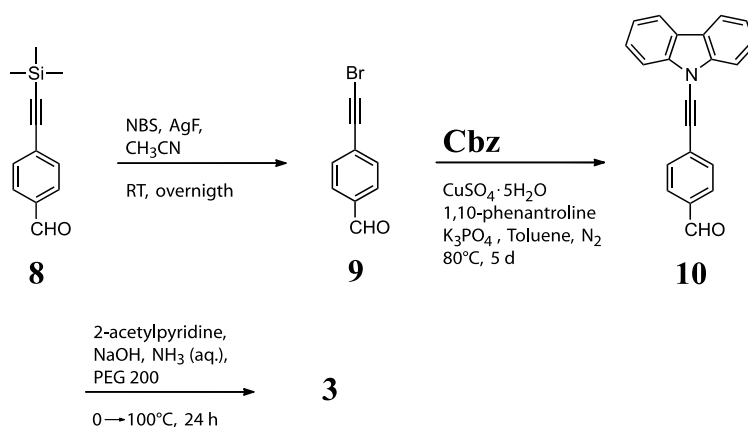


**Scheme 3**: Synthesis of **3**.

### 8.1.2 - Electrochemical properties

The electrochemical behaviour of **1-3** was investigated by cyclic voltammetry (CV) in deaerated DMF *vs.* SCE (Figure 2).
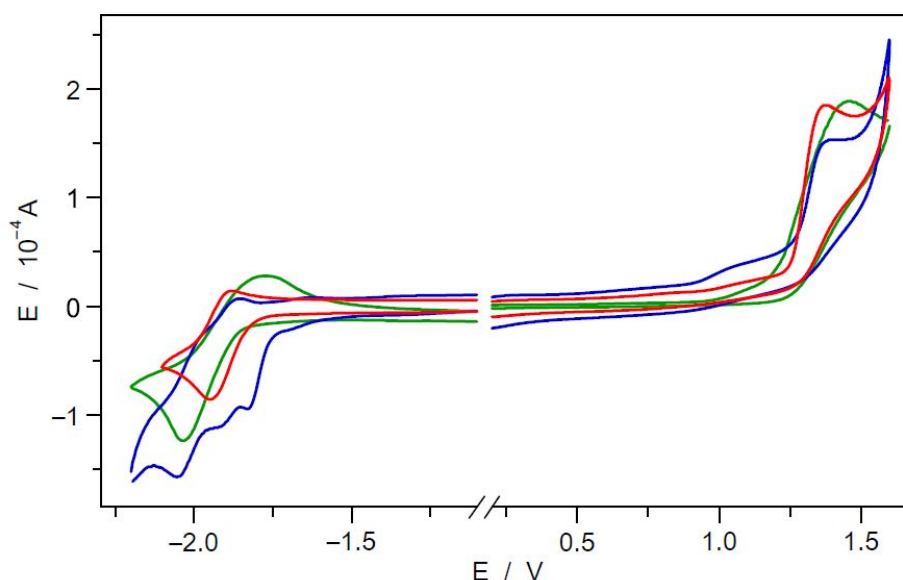


**Figure 2**: Cyclic voltammograms of **1** (red), **2** (green) and **3** (blue) in DMF solution with 0.1 TBAF at 0.05 V s$^{-1}$ (concentration 1÷10 mM).

CVs were also recorded in the same conditions for the reference compounds **Cbz** and **Ttpy**. **Cbz** displayed only an irreversible monoelectronic wave in the anodic side, whereas for **Ttpy** only a reversible process in the cathodic side was observed. Compounds **1** and **2** exhibit a quasi-reversible monoelectronic process at about –1.9 V, which is attributable to the reduction of the terpyridine moiety according to both literature reports[46] and a direct comparison with **Ttpy**. On the other hand, in the case of **3**, two monoelectronic irreversible processes are observed at –1.82 V and –2.06 V, possibly due to electrochemical polymerization of the ethynyl moiety.[47]

| | Cbz | Ttpy | 1 | 2 | 3 |
|---|---|---|---|---|---|
| $E°_{red}$ (V) | --- | –1.96 | –1.92 | –1.91 | –1.82[a] <br> –2.06[a] |
| $E_p^{ox}$ (V) | +1.14 | --- | +1.34 | +1.31 | +1.36 |

**Table 1**: Redox potentials of **Cbz**, **Ttpy** and **1-3** in DMF. [a] The value is the peak potential since the process is irreversible.

In the anodic region the electrochemical processes are centred on the carbazole moiety and are always irreversible, due to coupling reactions between radical cations.[48] The oxidation of pristine carbazole occurs at +1.14 V, a lower potential compared to the related processes of **1-3**. This effect is brought about by the groups directly attached to the carbazole nitrogen, which are known to shift anodically the oxidation potential. From the electrochemical data (Table 1) it is possible to calculate the energy content of charge-separated states for **1-3**, corresponding to the oxidation of carbazole and the reduction of the terpyridine moieties. The energy of these states can be estimated by the following equation:

$$-\Delta H^\circ = E^\circ{}_{red} - E^\circ{}_{ox} - T\Delta S^\circ = E^\circ{}_{red} - E^\circ{}_{ox} - 0.1\ eV$$

where $E^\circ{}_{ox}$ and $E^\circ{}_{red}$ are the standard potentials of the oxidation and reduction waves recorded by cyclic voltammetry.[49,50] This equation can be suitably applied only to electrochemically reversible couples but, in case one process is irreversible, the peak potential can be used instead of $E^\circ$. The resulting values are +3.16 (**1**), +3.12 (**2**) and +3.08 (**3**) eV. These ICT states are at relatively high energy but in principle can be populated upon excitation of the singlet energy levels of the Cbz or the Ttpy moiety, which are located at +3.66 and +3.80 eV (as derived from the 77 K fluorescence spectra of pristine **Cbz** and **Ttpy**).

### 8.1.3 - DFT and TD-DFT calculations

To gain insight into the mechanisms which rule the electronic distribution in the ground and excited states of **1-3,** all the series was investigated by means of DFT and TD-DFT using the hybrid functional PBE0.[51,52] The electron density plots of **1-3** (Figure 3) evidence that the HOMO is always centred on the Cbz moiety; in the case of the conjugated **1** and **3**, HOMO is also extended over the adjacent aryl ring, whereas, in case **2**, the methylene bridge virtually breaks the π-conjugation. On the contrary, the LUMO is always extensively localized on the Ttpy moiety. Accordingly, electrochemical oxidation is centred on Cbz, while the reduction entails Ttpy.

The examination of the natural charges obtained by the NBO population analysis[53,54] evidences that -CH$_2$- is an electron donor and breaks the π-conjugation between the two moieties. Compared to **1**, the extra charge of the anion and cation in **2** are more strongly localized on the Ttpy and Cbz moiety, respectively. On the contrary, ethynylene acts as an effective wire and electrons are extensively delocalized all across **3**. However, the anionic form of this molecule acquires a perpendicular arrangement of the two moieties.
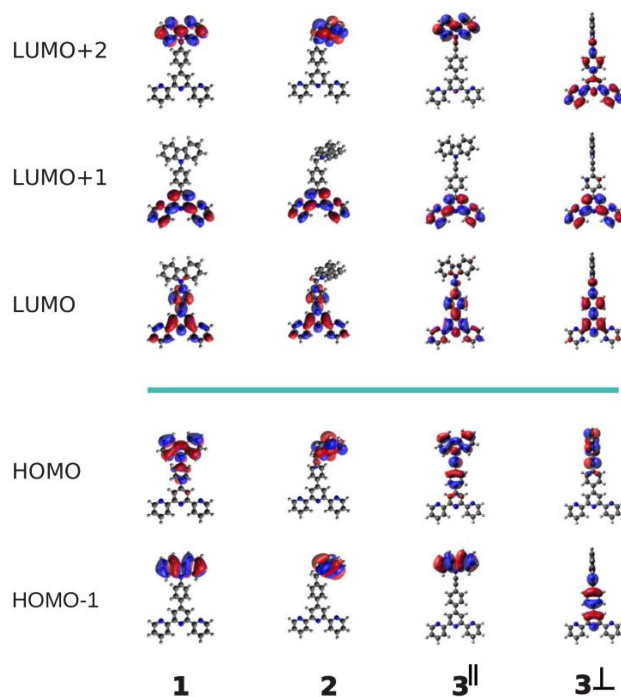
**Figure 3:** Electron density plot of **1-3**.[55]

An estimation of the energy of charge separated states in **1-3** was performed, to be compared with values obtained by cyclic-voltammetry data and considering the average energy required for the formation of the cationic and anionic species through the calculated ionization potentials (IP) and electron affinities (EA). The calculated energies of 3.29 (**1**), 3.34 (**2**), and 3.10 (**3**) eV, are in good agreement with the values estimated by CV data (Table 2), supporting the suitability of the molecular modelling adopted to describe the electronic properties of these compounds in the ground state. To investigate the electronic properties of **1-3**, transitions to singlet excited states were calculated by PCM-TD-PBE0 using the default linear response method (LR).[56] Actually, this method is considered a good compromise between accuracy and computational cost to describe the transitions to excited states of medium/large molecules in solution. Moreover, it was already applied successfully to the analysis of the absorption spectra of several systems in solution, also displaying a partial CT character.[57] The assignments of the absorption spectra of **1-3** above 250 nm are based on 24 vertical excitation energies (VEE) calculated both in toluene (TOL) and acetonitrile (ACN) solutions and are discussed in detail in the next section. The calculated transitions to the excited states are characterized by means of the two main contributions by single excitations referring to the electron density plots of **1-3** shown in Figure 3. The shapes of the frontier orbitals point to low energy ICT transitions characterized by Cbz→Ttpy excitations in all cases. Excitations localized on the two moieties of the ligands contribute to the description of transitions to higher

117

excited states. Notably, the calculated absorption spectra in toluene do not substantially differ from those obtained in polar solvent, in good agreement with what observed experimentally. For comparison, the electronic transitions of **1-3** were also investigated by means of the hybrid long range corrected functional CAM-B3LYP, which is also indicated to characterize CT excitations.[58] Though PCM-TD-CAM-B3LYP overestimates the excitation energies of **1-3** with respect to those calculated by the PBE0 hybrid functional and observed in the absorption spectra,[59,60] it indicates that local excitations (LEs) on the two moieties of **1-3** play a relevant role even for lower-energy excited states. Actually, in the case of **2**, it assigns low-lying states to Cbz→Cbz and Ttpy→Ttpy transitions, in order of increasing energy.

| | **1** | **2** | **3** | **Solvent** |
|---|---|---|---|---|
| $\Delta E^{exp.}$ | 3.16/392 | 3.12/397 | 3.08/402 | DMF |
| $\Delta E^{calc.}$ | 3.29/377 | 3.34/371 | 3.10/400 $\perp$ | DMF |
| $\Delta E^{S0}_{LR}$ | 3.51/353 (0.3581) | 3.77/329 (0.0009) | 3.42/362 (1.2216) $\parallel$ | TOL |
| $\Delta E^{S0}_{LR}$ | 3.52/353 (0.9988) | 3.74/331 (0.0052) | 3.41/363 (1.1687) $\parallel$ | ACN |
| $\Delta E^{S1}_{LR}$ | 3.30/375 (1.2045) | 3.17/391 (0.0357) | 3.03/409 (1.5705) $\parallel$ | TOL |
| $\Delta E^{S1}_{LR}$ | 3.15/393 (1.4105) | 3.16/392 (0.0622) | 2.87/432 (1.7430) $\parallel$ <br> 2.88/430 (0.0000) $\perp$ | ACN |
| $\Delta E^{S1}_{SS}$ | 2.18/568 (0.0945) | --- | 2.45/505 (0.9831) $\parallel$ | ACN |

The Cbz-Ttpy coplanar ($\parallel$) and perpendicular ($\perp$) conformers of **3** are indicated. The oscillator strengths are reported within brackets.

**Table 2**: Separated state energies/wavelengths (eV/nm) estimated by cyclic voltammetry ($\Delta E^{exp.} = -\Delta H^0_{CV}$) and calculated by PCM-PBE0/6-311+G(2d,p) ($\Delta E^{calc.} = IP - EA$). $S_0 \rightarrow S_1$ transition energies/wavelengths calculated by PCM-LR-PBE0/6-311+G(2d,p) at the $S_0$ geometries ($\Delta E^{S0}_{LR}$), PCM-LR-PBE0/6-311+G(d) ($\Delta E^{S1}_{LR}$) and PCM-SS-PBE0/6-311+G(d) at the $S_1$ geometries ($\Delta E^{S1}_{SS}$).

To investigate the emission properties of **1-3** in apolar and polar solvents the structural relaxation of their first excited state was modelled by the PCM-LR-TD-PBE0 method,[57] both in TOL and ACN solutions. The calculated deexcitation energies are reported in Table 2. The relaxation process in the first excited state is always driven by the fact that an extra charge is delocalized on Ttpy after HOMO→LUMO excitation, so that the whole Ttpy moiety planarizes, in agreement with what found experimentally by Siebert et al. for π-conjugated terpyridines.[61] In the case of **3** both the planar and the perpendicular arrangements of Cbz and Ttpy were considered in acetonitrile. It

turned out that in the first excited state these two conformers are close in energy ($\Delta E < 0.11 eV$) while in the ground state, where the π-conjugation between Cbz and the central aryl ring largely stabilizes the energy of the planar conformer, the perpendicular one is not foreseen by the adopted molecular modelling. As previously mentioned, the perpendicular conformation of **3** is favoured when an extra negative charge is localised on Ttpy. The emission from the first excited state of **1-3** in acetonitrile solution was also modelled using the PCM-SS-TD-PBE0/6-311+G* method[62] to investigate the effect of solvent equilibration on the emission in polar solvents. A large red shift is calculated for the $S_1 \rightarrow S_0$ transition when the relaxation of the solvent electronic polarization in the deexcitations process is considered. The calculated transition wavelengths of 568 nm for **1** and 505 nm for **3** are in reasonable agreement with those of the emission data (see below), while they result largely overestimated with respect to the experimental findings in the case of **2** (> 1000 nm). This very odd result suggests that the CT transition calculated by TD-PBE0 does not adequately characterize the first excited state of **2**. It must be pointed out that the appropriate modelling of emission should include the PCM correction for the excited state and the GS at the excited state geometry,[62] but it largely underestimates the deexcitations energies also of **1** and **3**. However, the calculations suggest that the large red shift observed in the emission spectra of these compounds in polar solvents can be attributed to solvent equilibration effects.

### *8.1.4 - Photophysical properties*

UV-Vis absorption, luminescence and excited state lifetime data have been obtained at room temperature (RT) in three solvents of different polarity (*i.e.*, toluene (TOL), dichloromethane (DCM) and acetonitrile (ACN)). In order to allow a comprehensive comparison between spectroscopic and electrochemical data, a complete study was also performed in a solvent in which both types of measurements were carried out, *i.e.* DMF. These data are only partially reported in this paper, since the photophysical properties of all the compounds in DMF are virtually identical to those in ACN. Because of a rather complicated scenario at room temperature, further studies have been carried out at 77 K in butyronitrile glass in order to suppress solvent reorganization effects and/or thermal equilibration of different emitting states.

### *UV-Vis absorption*

In Figure 4 are gathered the room-temperature electronic absorption spectra of **Cbz**, **Ttpy** and **1-3** in ACN and TOL; in the latter solvent, spectra start from 300 nm due to solvent absorption.
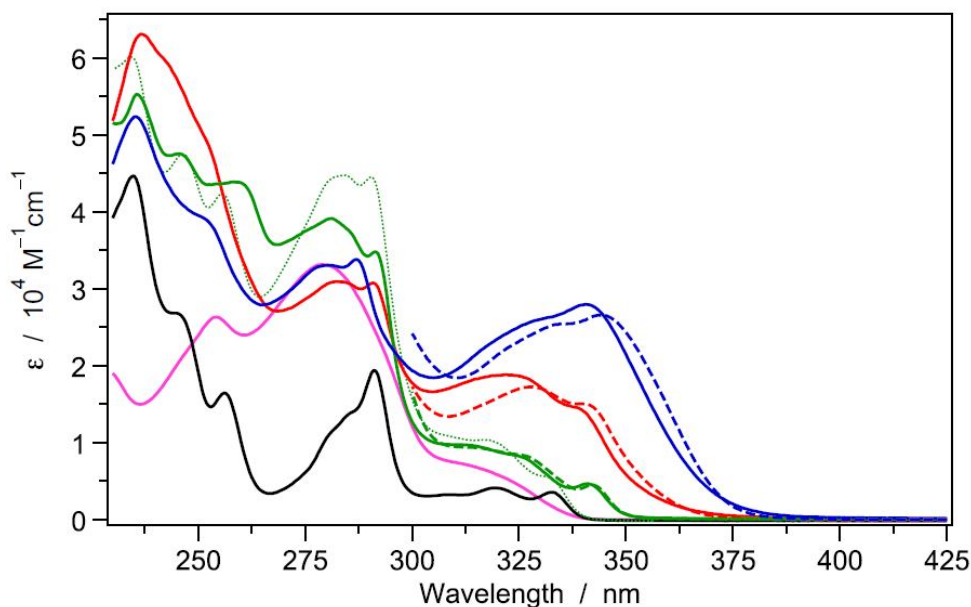
**Figure 4**: Room-temperature absorption spectra of **1** (red), **2** (green) and **3** (blue) in acetonitrile (full) and toluene (dashed). Absorption spectra of reference molecules **Cbz** (black) and **Ttpy** (pink) are also reported. The spectral profiles obtained from the sum of the spectra of **Cbz** and **Ttpy** is also reported for comparison (light-dashed green).

While **Cbz**, **Ttpy** and **2** do not display intense absorption at $\lambda > 300$ nm, the extensively conjugated systems **1** and **3** show strong features ($\varepsilon > 15000$ M$^{-1}$ cm$^{-1}$) originated by the large transition dipole moment along the long molecular axis, which characterizes their $S_0 \rightarrow S_1$ transition (see Supporting Information). All of the compounds exhibit a minor bathchromic shift of the lowest energy absorption features by increasing the polarity of the solvent. This change is more pronounced for the conjugated systems **1** and **3** than for **2**, while absorption spectra of **Cbz** and **Ttpy** are virtually unaffected by the solvent. Moreover, compared to the sum of the spectra of **Cbz** and **Ttpy** (light-dashed green spectrum in Figure 4), bichromophoric systems exhibit a progressively less resolved and red-shifted vibronic structure of the lowest energy band in the following order: **2**, **1**, **3**. These observations suggest the presence of low-energy transitions exhibiting some charge-transfer character in **1** and **3**. This is confirmed by the analysis of the single excitations contributing to the $S_0 \rightarrow S_1$ transitions, which are always largely characterized by HOMO-LUMO transitions with Cbz$\rightarrow$Ttpy character (see Fig. 3), when calculated by the PBE0[51,52] hybrid functional. Though it is known that in the case of CT transitions the kind of functional used can significantly underestimate the excitation energies and oscillator strengths,[63,64] such an effect is not dramatic for **1-3** upon comparison with experimental UV-Vis spectra (Figure 4). In fact, the calculated vertical excitation energies (VEEs) of $S_0 \rightarrow S_1$ in ACN are 3.52 eV (353 nm) for **1**, 3.74 eV (332 nm) for **2**, and 3.41

120

eV (364 nm) for **3**. These theoretical values are very close or virtually coincident with those calculated in TOL (see Table 2). However, as mentioned above, in the case of **2**, TD-CAM-B3LYP gives a different description of the $S_0 \rightarrow S_1$ transition assigning it to Cbz→Cbz. Moreover, contrary to **2**, **1** and **3** have transition dipole moments completely aligned along the long molecular axis with large oscillator strengths, in agreement with the trend shown by the intensities observed in the first band of the absorption spectra. Besides the transition to the first excited state, the lowest energy absorption band of **1-3** entails transitions up to $S_0 \rightarrow S_6$ in the TD-PBE0 scenario. Specifically, in order of increasing energy, two transitions mainly contribute to its intensity, *i.e.* one with predominant HOMO-(LUMO+2) excitation (Cbz→Cbz) that is found to be weak and of comparable intensities in all the three molecules and one calculated at about 305 nm due to (HOMO-2)-LUMO excitation (Tpy→Ttpy). The absorption bands at 240-300 nm are assigned to transitions largely characterized by excitations starting from the four highest occupied MOs and ending onto the four lowest unoccupied MOs, with contributions from other excitations. Particularly, transitions up to $S_0 \rightarrow S_{12}$ are characterized by the (HOMO-2)-(LUMO+1) excitation (Tpy→Tpy) calculated at 281-284 nm and by the (HOMO-1)-(LUMO+2) (Cbz→Cbz) transition at 273-277 nm with significant oscillator strengths. The $S_0 \rightarrow S_{15,16}$ transitions of **1** and **3**, calculated at 260-264 nm with large oscillator strengths, are mainly originated by the (HOMO-3)-LUMO and (HOMO-3)-(LUMO+1) (Ttpy→ Ttpy,Tpy) transitions, while in **2** these excitations characterize the $S_0 \rightarrow S_{11,12}$ transitions at 273-275 nm. It must be pointed out that the comparison among the absorption spectra and the TD-PBE0 calculated ones, which nicely reproduce the observed spectral features of **1-3**, does not evidence any inadequacy of the theoretical method used for the proposed assignments. However, as it was mentioned before, the long range corrected TD-CAM-B3LYP method suggests that the transition energies of LEs should largely contribute to the description of the low excited states, particularly in the case of **2**. Only the following analysis of the emission spectra will resolve the nature of the low excited states of **1-3**.

### *Luminescence at 298 K*

The emission properties of **1-3** and their reference compounds **Cbz** and **Ttpy** were investigated at RT in solvents of different polarity (*i.e.*, toluene, dichloromethane, acetonitrile and dimethylformamide). All photophysical data are summarized in Table 3, while in Figure 5 only the emission spectra in TOL and ACN are reported.
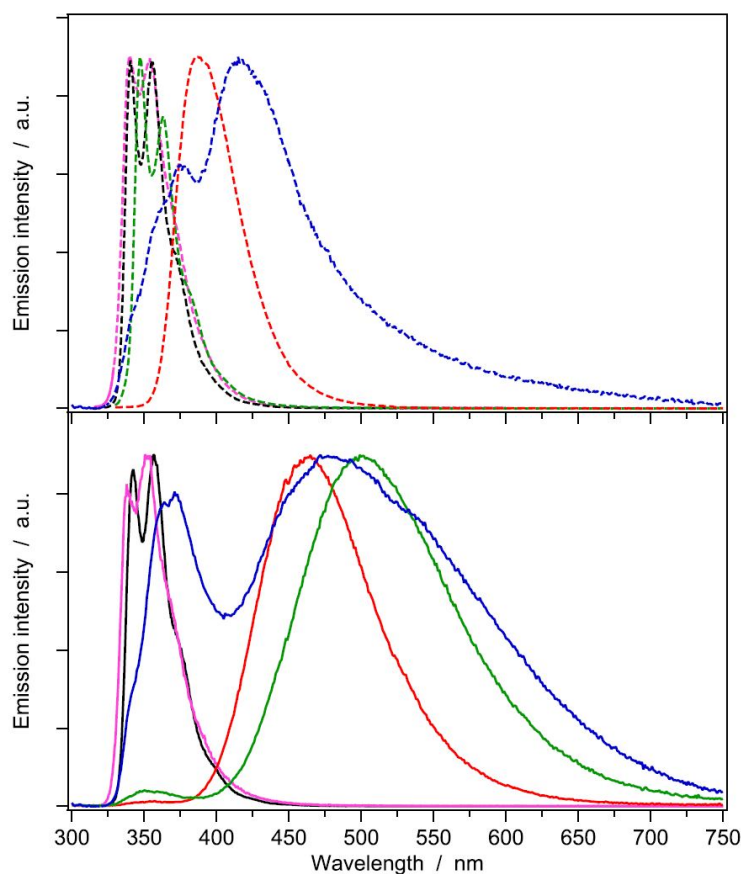
**Figure 5**: Normalized emission spectra of **1** (red), **2** (green) and **3** (blue) in toluene (top, dashed) and acetonitrile (bottom, full) at room temperature. Emission spectra of reference molecules **Cbz** (black) and **Ttpy** (pink) are also reported for comparison; $\lambda_{exc}$ = 310 nm for toluene solutions, $\lambda_{exc}$ = 275 nm for acetonitrile solutions.

| | TOL | | DCM | | ACN | | DMF | |
|---|---|---|---|---|---|---|---|---|
| | $\Phi$ (%) | $\tau$ (ns) | $\Phi$ (%) | $\tau$ (ns) | $\Phi$ (%) | $\tau$ (ns) | $\Phi$ (%) | $\tau$ (ns) |
| **Cbz** | 33.3 | 7.6 | 24.4 | 6.7 | 25.8 | 7.4 | 37.8 | 10.3 |
| **Ttpy** | 18.6 | 2.2 | 13.7 | 1.8 | 11.0 | 1.4 | 10.9 | 1.3 |
| **1** | 62.8 | 2.1 | 65.4 | 4.4 | 47.8 | 5.8 | 55.0 | 6.1 |
| **2** | 15.3 | 4.3 | 6.7 | ** | 5.6 | 10.9 | 11.7 | ** |
| **3** | 2.8 | ** | 1.9 | ** | 1.4 | ** | 0.5 | ** |

** Biexponential decay.

**Table 3**: Room-temperature photophysical data of **1-3** in different solvents, together with reference molecules **Cbz** and **Ttpy**.

In line with the trend of absorption spectra, **Cbz** and **Ttpy** show almost solvent-independent luminescence profiles, with minor red-shifts in the most polar medium (< 2 nm); fluorescence spectra clearly indicate that the lowest singlet states of **Cbz** and **Ttpy** are virtually isoenergetic at room temperature. By contrast, **1-3** exhibit substantial spectral variations of the emission bands as a

function of solvent, much more pronounced compared to the absorption spectra.[31] At higher polarity, fluorescence bands loose the vibronic structure and are red-shifted, suggesting a charge-transfer character. Such a result is not surprising on the basis of theoretical findings which evidence the presence of charge transfer transitions (Cbz→Ttpy). Most notably, the emission colours of **1**, **2**, **3** in ACN are, respectively, blue, yellow and white. Excited-state exciplex interactions are ruled out because emission profiles do not change up to a concentration of $10^{-3}$ M. The most straightforward case is **2**, where the Cbz and Ttpy moieties are decoupled by the presence of a methylene bridge. In this case two well-defined behaviours can be detected: (1) in low polarity media (*e.g.*, TOL), a very structured band at 347 nm is observed; (2) as the solvent polarity increases (*e.g.*, ACN), a new broader and unstructured band arises at longer wavelengths ($\lambda_{max} \approx 500$ nm). Despite the fact that **Cbz** and **Ttpy** singlets are almost isoenergetic, on the basis of 77 K data, we ascribe the localized emission in TOL to the singlet of the carbazole moiety; on the other hand, the broad band observed in ACN is attributed to an ICT excited state, whose energy is stabilized in the polar solvent. Actually, also in acetonitrile, a weak but still discernible emission signal in the region below 400 nm suggests the presence of some residual emission very similar in shape to what observed in apolar toluene (LE <–> ICT equilibrium).[37,65] Passing to the highly conjugated system **1**, a broad and unstructured band is observed in any solvents (Figure 5). Such band is strongly red shifted upon increasing solvent polarity ($\lambda_{max} = 387$ *vs.* 464 nm in toluene and acetonitrile, respectively). The emission behavior observed in acetonitrile can be attributed to the fast reorganization of the polar solvent after excitation, as suggested by PCM-TD-SS-PBE0[62] calculations, further corroborating the CT character of the associated transition. The case of **3** is more complicated since multiple emissions are observable in any solvents: one structured around 370 nm and one or more at lower energies. The structured band does not shift with solvent polarity and is considerable in all solvents; it is assigned to a LE which occurs at the diphenylacetyl unit in the perpendicular conformer. On the other hand the broader feature, which becomes more pronounced and more red-shifted by increasing the polarity of the medium, is attributed to the vibronic structure of the emission from the CT state of the relaxed planar structure, since the oscillator strength of the other conformer is null for such transition. Excitation spectra of **1-3** match the absorption profiles at any emission wavelengths (see SI). This crucial observation suggests that molecules are excited at the same ground state geometry but, upon excitation, two or even more excited states can be made available.[37] Among the various combinations molecule/solvent, the sharpest case of dual emission appears to be **2** in ACN where the weak higher energy emission is attributed to a local excited state (LE) of **Cbz**, whereas the predominant broader band is assigned to an ICT state accessible in the polar medium. For **3** the situation is much more complex, with emission bands attributable to LE

and CT states, which occur as a consequence of the peculiar nature of the alkyne bridge which allows more excited state conformations.

Luminescence decays are monoexponential for **1** and **2** when detected at the emission maxima with lifetimes of the order of a few nanoseconds, suggesting singlet character of the related excited state. For **3**, emission decays are multiexponential, with the longer component having increasing amplitude on the low-energy side of the spectrum, indicating an increasing weight of the lowest energy charge-transfer component attributed to the planar conformer.

### *77 K fluorescence*

In order to corroborate the contribution of charge-transfer transitions to the fluorescence bands of **1-3**, emission spectra were recorded also at 77 K in a solvent that provides transparent glasses preventing detection of scattered light (*i.e.*, butyronitrile, Fig. 6).



**Figure 6**: Normalized fluorescence spectra of **1** (red), **2** (green) and **3** (blue) in butyronitrile glass at 77 K, together with the ones of reference molecules **Cbz** (black) and **Ttpy** (pink). Phosphorescence is purposely removed from the spectrum; $\lambda_{exc}$ = 280 nm.

Under these conditions, solvent reorganization effects are substantially decreased and thermal equilibration between closely-spaced states is virtually suppressed. As a consequence, ICT levels are expected to be drastically increased in energy, limiting spectral tuning as a function of solvent polarity. Indeed, all spectra display only one emission band, typically similar to the one detected in the most apolar medium at room temperature, *i.e.* toluene. While the 77 K fluorescence band of **Cbz** is literally superimposed to that at 298 K, in the case of **Ttpy** a blue shift of 6 nm is observed upon

cooling ($\lambda_{max}$ = 334 nm); therefore, at 77 K, **Ttpy** singlet becomes higher in energy if compared to **Cbz**. This different behaviour for the two molecules can be rationalized by considering that the HOMO–LUMO transition of Ttpy entails the promotion of one electron centred on the terpyridine moiety (HOMO) to a more delocalized orbital (LUMO), differently from carbazole where HOMO and LUMO are largely superimposed. On the other hand, **2** displays a strongly vibronically resolved fluorescence band and almost no shift (less than 2 nm) is observed if compared to the room temperature spectrum in TOL. This emission profile resembles that of standard N-alkyl-substituted carbazoles and, as typically found for this kind of molecules,[1] the lowest singlet level is slightly lower in energy compared to pristine **Cbz** (in this case, $\lambda_{max}$ = 345 *vs.* 339 nm). This result shows that, at 77 K, the methylene bridge of **2** is able to isolate the carbazole and terpyridine moieties, preventing significant electronic interactions between them. This is not the case in **1**, where the observed broad band ($\lambda_{max}$ = 380 nm) is attributable to an ICT transition, blue shifted of more than 10 nm relative to 298 K due to the lack of solvation effects. This emission energy value (3.26 eV) is in good agreement with the theoretical one and the estimation of the ICT energy performed by cyclic voltammetry (Table 1). The behaviour of **3** turns out to be more straightforward compared to room temperature. At 77 K, in fact, this molecule exhibits only one wide band at $\lambda_{max}$ = 383 nm, with a vibronic shoulder at 379 nm. The profile of this band is similar to **1** and attributed to the ICT state. Since at 77 K the equilibrium between planar and orthogonal conformers of **3** is suppressed (ratio of 99:1), only the most stable conformer is present in the glass, the conjugated planar one. Such a scenario can explain why, in the case of **3**, only the CT emission band is observed at 77 K, while at least two emissions were observed at room temperature: a LE band at 365 nm attributed to the orthogonal conformer, and a CT band, which is attributable to a planar conformer (415 nm in TOL). At 77 K only the latter can be detected since only the planar conformer occurs in the low temperature regime.

### *77 K phosphorescence*

Triplet phosphorescence spectra of **1-3**, together with those of the reference molecules **Cbz** and **Ttpy** were also recorded (Fig. 7).
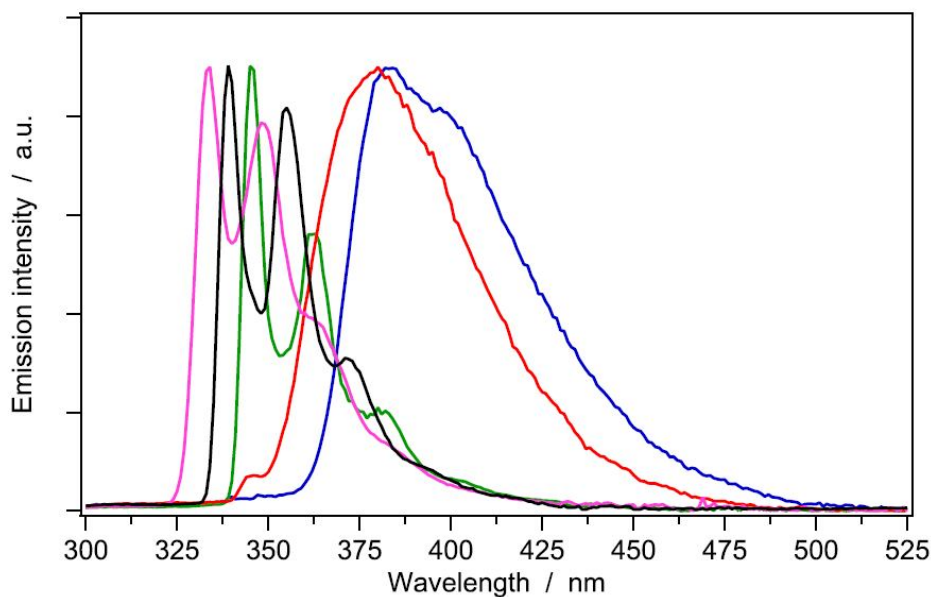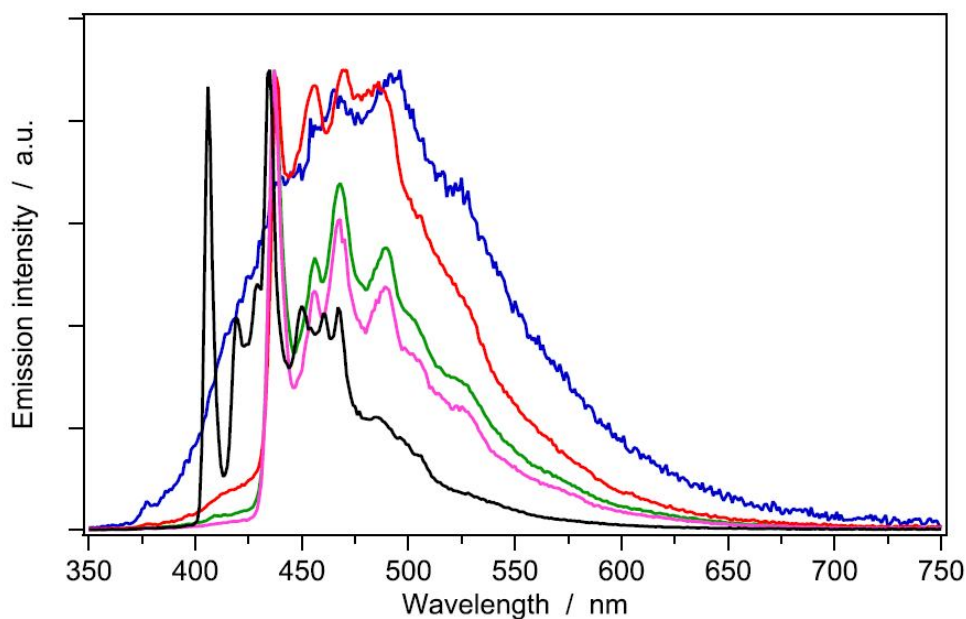
**Figure 7**: Normalized phosphorescence spectra of **1** (red), **2** (green) and **3** (blue) in butyronitrile glass at 77K, together with the ones of reference molecules **Cbz** (black) and **Ttpy** (pink). In order to discard fluorescence, a delay of 100 μs is applied in all the cases; $\lambda_{exc}$ = 310 nm.

The triplet of **Cbz** ($\lambda_{0-0}$ = 406 nm; τ = 7.2 s) is higher-lying than that of **Ttpy** ($\lambda_{0-0}$ = 437 nm; τ = 1.7 s) by about 0.21 eV. Because of this energy gap, the emitting triplet in **1-3** is always centered on the terpyridine moiety (see Figure 7 for comparison) and this is supported by the triplet lifetimes of **1-3** (*i.e.*, 1.4 s, 1.7 s and 1.2 s, respectively) which are quite similar to that of **Ttpy**. This behaviour is particularly evident in the case of **2**, in which the vibronic progressions and the triplet lifetime are virtually identical to those of **Ttpy**. The vibronic features of **Ttpy** are clearly discernible also in the conjugated systems **1** and **3**, but the bands are broader probably due to the establishment of excited state conformeric equilibria even at 77 K on the very long timescale of triplet levels. Broadening is particularly remarkable for **3**, which is a white triplet emitter. The lifetime decay of this compound is not perfectly monoexponential as for all the other compounds.

## 8.2 - Conclusions

Due to their remarkable electronic properties carbazole and 2,2':6',2"-terpyridine are widely utilized building blocks in several fields of research (*e.g.*, supramolecular chemistry) and technology (*e.g.*, optoelectronics), but their combination remains still rather unexplored. We have synthesized three bischromophoric Cbz-Tpy systems **1**,[26] **2** and **3** and systematically investigated their electronic and photophysical properties by means of theoretical, electrochemical and photophysical methods.

The complementary electron donor-acceptor character of **Cbz** and **Ttpy** affords bichromophoric systems with highly tuneable luminescence properties all across the Vis spectral region (Fig. 5b). In the case of **3** the presence of multiple emissions can afford white photoluminescence under specific conditions of solvent and temperature (Figs. 5b and 7).

Comparison of the emission spectra at room temperature and 77 K and in solvents of different polarity, in combination with DFT and TD-DFT methods, provides deeper insight into the nature of the lowest electronic excited states of **1**-**3**, particularly localized *vs.* charge transfer. For the highly conjugated systems **1** and **3**, characterized by strong ICT transitions, the hybrid functional PBE0 best characterizes electronic levels, whereas the long-range corrections considered by TD-CAM-B3LYP are necessary for an accurate determination of the electronic transitions in the case of the decoupled system **2**. The fact that all the emission bands in acetonitrile show large broadenings and unstructured shapes is attributed to solvent relaxation effects on the ICT state, as indicated by the PCM-TD-SS-PBE0 molecular modelling.

The results presented in this work are a springboard for expanding the family of Cbz-Tpy chromophores and luminophores via chemical functionalization, bridge tuning and metal complexation. We are currently working to implement the use of these systems in optoelectronic devices and sensors.[66]

## 8.3 - Experimental section

### *Materials and methods*

$^1$H, $^{13}$C, NMR spectra were recorded on a Varian AS 300 or on a Mercury 400 spectrometer. Chemical shifts ($\delta$) are reported in ppm relative to residual solvent signals for $^1$H and $^{13}$C NMR ($^1$H NMR: 7.26 ppm for CDCl$_3$; $^{13}$C NMR: 77.0 ppm for CDCl$_3$). $^{13}$C NMR spectra were acquired with $^1$H broadband decoupled mode. Mass spectra were recorded on a micromass LCT spectrometer using electrospray (ES) ionisation techniques. Analytical grade solvents and commercially available reagents were used as received, unless otherwise stated. Chromatographic purifications were performed using 70-230 mesh silica.

### *Synthesis of derivatives*

### 4'-[*p*-(Carbazole-9-yl)phenyl]-2,2':6',2''-terpyridine (1)[26]

The mixture of carbazole (168 mg, 1.0 mmol), 4'-(*p*-bromophenyl)-2,2':6',2''-terpyridine **4** (388 mg, 1.0 mmol), potassium carbonate (207 mg, 1.5 mmol), CuI (10 mg, 0.05 mmol) and 18-crown-6

(7 mg, 0.025 mmol) was heated at 185°C under stirring for 48 h. After the reaction mixture was cooled to ambient temperature, chloroform and water were added. The aqueous phase was discarded, and the organic phase was washed with distilled water (3 x 10 mL), dried over anhydrous MgSO$_4$ and then evaporated. Precipitation of a concentrated solution of the crude product in 1 mL DCM with methanol (25 mL) afforded **1** as a white solid in 40% yield (190 mg). $^1$H NMR (CD$_3$Cl, 300 MHz) $\delta$ 8.86 (s, 2H), 8.76 (qd, , $J$= 4.7 Hz, $J$= 0.8 Hz, 2H), 8.72 (td, $J$= 8.0 Hz, $J$= 0.9 Hz, 2H), 8.20-8.12 (m, 4H), 7.91 (dt, $J$= 7.6 Hz, $J$= 1.8 Hz, 2H), 7.77-7.71 (m, 2H), 7.53-7.29 (m, 8H); $^{13}$C NMR (CD$_3$Cl, 75 MHz) $\delta$ 156.4, 149.6, 149.4, 140.9, 138.7, 137.8, 137.2, 129.1, 127.6, 126.3, 124.2, 123.8, 121.6, 120.6, 120.4, 119.1, 110.1; ESI-MS: 475 [M$^+$ + 1], 497 [M$^+$ + Na].

### 4-[(9H-Carbazol-9-yl)methyl] benzonitrile (6)

Carbazole (418 mg, 2.5 mmol), 4-(bromomethyl)benzonitrile **5** (490 mg, 2.5 mmol) and NaH 95% (90 mg, 3.75 mmol) were dissolved in anhydrous THF (10 mL), and the reaction mixture was stirred at 70° C under a nitrogen atmosphere for 24 h. After the reaction was terminated the solvent was evaporated, distilled water was added, and the resultant solution was extracted with DCM (3 x 15 mL). The collected organic layer was dried over anhydrous MgSO$_4$ and then evaporated. The residue was purified by silica gel column chromatography using a mixture of CH$_2$Cl$_2$/petroleum (4:6) to give product **6** as a white solid in 60% yield (420 mg). $^1$H NMR (CD$_3$Cl, 300 MHz) $\delta$ 8.19 (d, $J$ = 7.8 Hz, 2H), 7.55 (d, $J$ = 8.3 Hz, 2H), 7.48 (m, 2H), 7.36-7.28 (m, 4H), 7.21 (d, $J$ = 8.0 Hz, 2H), 5.55 (s, 2H); $^{13}$C NMR (CD$_3$Cl, 75 MHz) $\delta$ 142.9, 140.6, 132.9, 127.3, 126.4, 123.4, 120.9, 120.0, 118.8, 111.7, 108.8, 46.4; ESI-MS: 305 [M$^+$ + Na].

### 4-[(9H-Carbazol-9-yl)methyl] benzaldehyde (7)

To a solution of 4-((9H-carbazol-9-yl)methyl) benzonitrile **6** (419 mg, 1.48 mmol) in anhydrous toluene (10 mL) DIBAL-H (1.5 M in toluene, 1.5 mL, 2.23 mmol) was added at 0° C. After 5 h the ice-bath was removed and the solution was stirred overnight at room temperature. HCl 1M (25 mL) was added slowly and after 5 h the mixture was extracted with DCM (3 x 15 mL). The combined organic phase was dried on anhydrous MgSO$_4$ and then evaporated to give pure product **7**, as a white solid in 94% yield (398 mg). $^1$H NMR (CD$_3$Cl, 400 MHz) $\delta$ 9.92 (s, 1H), 8.17 (d, $J$ = 7.7 Hz, 2H), 7.76 (d, $J$ = 8.2 Hz, 2H), 7.48-7.43 (m, 2H), 7.43-7.24 (m, 6H), 5.54 (s, 2H); $^{13}$C NMR (CD$_3$Cl, 100 MHz) $\delta$ 191.9, 144.4, 140.7, 136.0, 130.5, 127.2, 126.3, 123.4, 120.8, 119.9, 108.9, 46.6; ESI-MS: 308 [M$^+$ + Na].

**4'-[4-(9H-Carbazol-9-ylmethyl)phenyl]-2,2':6',2''-terpyridine (2)**

2-Acetylpyridine (130 µL, 1.15 mmol) was added to a solution of 4-((9H-carbazol-9-yl)methyl) benzaldehyde **7** (143 mg, 0.5 mmol) in MeOH (3 mL). Finely ground KOH (65 mg, 1.15 mmol) and aqueous $NH_3$ (2 mL, 30%, 1.23 mmol) were then added to the solution that was left to stir at room temperature for 7 days. The precipitated solid was collected by filtration and washed with MeOH (3 x 20 mL) to give pure product **2** as a white solid in 30% yield (73 mg). ^{1}H NMR ($CD_3Cl$, 300 MHz) $\delta$ 8.70 (d, $J$ = 4.6 Hz, 2H), 8.67 (s, 2H), 8.64 (d, $J$= 8.1 Hz, 2H), 8.16 (d, $J$= 7.7 Hz, 2H), 7.86 (dt, $J$= 7.6 Hz, $J$= 1.9 Hz, 2H), 7.80 (d, $J$= 8.3 Hz, 2H), 7.50-7.24 (m, 10H), 5.60 (s, 2H); ^{13}C NMR ($CD_3Cl$, 75 MHz) $\delta$ 156.4, 156.2, 150.0, 149.4, 140.9, 138.3, 138.1, 137.1, 128.0, 127.3, 126.2, 124.1, 123.3, 121.6, 120.7, 119.6, 119.1, 109.1, 46.7; ESI-MS: 489 [$M^+$ + 1], 511 [$M^+$ + Na].

**4-(Bromoethynyl) benzaldehyde (9)**

4-[(Trimethylsilyl)ethynyl] benzaldehyde **8** (1.5 g, 7.4 mmol) and AgF (940 mg, 7.4 mmol) were dissolved in $CH_3CN$ (75 mL). The reaction flask was wrapped in aluminium foil and NBS (1.32 g, 7.4 mmol) was added. The mixture was stirred overnight at room temperature. Then the solid was filtered off and washed with $CH_3CN$ (25 mL). The solution was evaporated and the resulting residue was dissolved in $Et_2O$ and washed with water (3 x 25 mL). The organic part was dried over anhydrous $MgSO_4$ and then evaporated to give product **9** as a white solid in 95% yield (1.47 g). ^{1}H NMR ($CD_3Cl$, 300 MHz) $\delta$ 10.01 (s, 1H), 7.83 (d, $J$= 8.5 Hz, 2H), 7.60 (d, $J$= 8.3 Hz, 2H); ^{13}C NMR ($CD_3Cl$, 75 MHz) $\delta$ 191.5, 136.0, 132.8, 129.7, 129.1, 79.5, 54.9; ESI-MS: 231 [$M^+$ + Na].

**4-[(9H-Carbazol-9-yl)ethynyl] benzaldehyde (10)**

To a solution of 4-(bromoethynyl)benzaldehyde **9** (90 mg, 0.44 mmol)in 5 mL of anhydrous toluene carbazole (67 mg, 0.4 mmol), $K_3PO_4$ (170 mg, 0.8 mmol), $CuSO_4$-$5H_2O$ (20 mg, 0.08mmol) and 1,10-phenanthroline (30 mg, 0.16 mmol) were added. The reaction mixture was purged with nitrogen and heated at 80° C for 5 days. The progress of the reaction was monitored by TLC. Upon completion, the reaction mixture was dried *in vacuo* and the residue was dissolved in water and extracted with DCM (3 x 15 mL). The combined organic phases were dried with anhydrous $MgSO_4$ and then evaporated. The crude residue was purified by silica gel flash chromatography using a mixture of $CH_2Cl_2$/petroleum (4:6) to give product **10** as a pale white solid in 75% yield (89 mg). ^{1}H NMR ($CD_3Cl$, 400 MHz) $\delta$ 10.02 (s, 1H), 8.04 (d, $J$= 7.6 Hz, 2H), 7.89 (d, $J$= 8.4 Hz, 2H), 7.74-7.70 (m, 4H), 7.55 (dt, $J$= 7.4 Hz, $J$= 1.2 Hz, 2H), 7.38 (dt, $J$= 7.5 Hz, $J$= 1.1 Hz, 2H); ^{13}C NMR ($CD_3Cl$, 100 MHz) $\delta$ 191.5 140.4, 135.1, 131.2, 130.0, 129.8, 127.2, 124.1, 122.8, 120.8, 111.6, 83.6, 75.3; ESI-MS: 296 [$M^+$ + 1], 318 [$M^+$ + Na].

## 4'-[4-(9H-Carbazol-9-ylethynyl)phenyl]-2,2':6',2''-terpyridine (3)

2-Acetylpyridine (135 µL, 1.2 mmol) was added to a stirred suspension of crushed NaOH (48 mg, 1.2 mmol) in PEG 200 (1mL) at 0° C. After 10 min 4-[(9H-carbazol-9-yl)ethynyl] benzaldehyde **10** (148 mg, 0.5 mmol) was added and stirring was continued at 0° C for 2 h. Then concentrated aqueous NH$_3$ solution (1.5 mL) was added and the suspension stirred at 100° C for 24 h. The precipitate was isolated by vacuum filtration and washed with water ( 50 mL) and ethanol (10 mL) to give product **3** as a brown solid in 60% yield (150 mg).$^1$H NMR (CD$_3$Cl, 400 MHz) $\delta$ 8.78 (s, 2H), 8.75 (d, *J*= 5.5 Hz, 2H), 8.69 (d, *J*= 8.0 Hz, 2H),8.05 (d, *J*= 8.1 Hz, 2H), 7.97 (d, *J*= 8.5 Hz, 2H), 7.90 (dt, *J*= 7.8 Hz, *J*= 1.7 Hz, 2H), 7.76 (t, *J*= 9.2 Hz, 4H), 7.56 (t, *J* = 7.7 Hz, 2H) 7.40-7.35 (m, 4H); $^{13}$C NMR (CD$_3$Cl, 100 MHz) $\delta$ 156.4, 156.3, 149.6, 149.4, 140.6, 137.9, 137.1, 131.9, 127.6, 127.0, 124.1, 124.0, 123.9, 122.4, 121.6, 120.6, 118.8, 111.6, 80.6, 74.8; ESI-MS: 499 [M$^+$ + 1], 521 [M$^+$ + Na].

### Electrochemistry

Cyclic voltammetry was performed in a three electrode cell equipped with a SCE reference electrode and a platinum plate counter electrode in DMF solution with 0.1 M tetrabutyl-ammonium hexafluorophosphate (TBAF, electroanalysis grade) as supporting electrolyte, and containing the investigated compounds in the 1-10 mM concentration range. Glassy carbon (GC) (d = 3 mm) and platinum rod (d = 2 mm) working electrodes were used, respectively, in cathodic and anodic investigation in order to minimize passivation processes. All experiments were performed in nitrogen atmosphere at room temperature. The iR compensation (positive feedback) was used in all measurements. Electrochemical experiments were carried out with CH Instruments Mod. 660 C potentiostat, controlled by a personal computer via CH Instruments software. The values of the cathodic and anodic peak potentials were recorded for both the electrochemical processes. When the electrochemical behaviour is quasi-reversible the values of formal potentials (see Table 1) were also calculated from the half-sum of the cathodic and anodic peak potential.

### Theoretical calculations

The electronic properties of **1-3** were investigated by means of Density Functional Theory (DFT) and Time-Dependent DFT (TD-DFT)[39-41] implemented in Gaussian 09.[67] Bulk solvent effects were always taken into account in the calculations using the polarizable continuum model (PCM).[68] The parameter free DFT hybrid model PBE0[51,52] was employed to optimize the molecular geometries of the neutral and ionic species in DMF using the 6-311+G* basis set.[69,70] The electron distribution of the examined systems was investigated using the 6-311G(2d,p) basis set by means of the natural

bond population analysis (NBO version 3.1).[53,54] The ionization potentials (IPs) and electron affinities (EAs) were calculated by the so-called ΔSCF method using the 6-311+G(2d, p) basis set. The transitions to the singlet excited states of **1-3** in TOL and ACN were calculated by TD-PBE0/6-311+G(2d,p) at the GS geometry using the default linear response method (LR).[56,71] $S_1 \rightarrow S_0$ emission energies were calculated by the LR-TD-PBE0/6-311+G* method[57] after optimization of the $S_1$ state geometry, which started from the planar conformation in the case of **1** and **3**. For the latter, also the perpendicular arrangement of the **Cbz** and **Ttpy** moieties was considered. The first excited state was also modelled via the state-specific (SS) method[56,62,71] in acetonitrile. This method accounts also for solvent relaxation in the de-excitation process and calculates the energy by making the electrostatic potential generated by the excited state density self-consistent with the solvent reaction field. The non-equilibrium time regime, in which only the solvent electronic polarization is in equilibrium with the excited state electron density, was considered. Transitions to the singlet states of **1-3** were also calculated by the long range corrected hybrid functional CAM-B3LYP[58] at the PBE0 calculated geometries.

**Photophysics**

The luminescence measurements were conducted in fluorescence cuvettes of 1 cm path length. Absorption spectra were recorded with a Perkin-Elmer λ950 spectrophotometer. The uncorrected emission spectra were recorded with an Edinburgh Instruments FLS920 spectrometer with a Peltier-cooled Hamamatsu R928 photomultiplier tube (185–850 nm). An Edinburgh Instruments Xe900 450 W xenon arc lamp was the source of excitation light. The corrected emission spectra were calculated by applying a calibration curve supplied with the instrument. Luminescence quantum yields (Φ) in solution were calculated by the method of Demas and Crosby[72] from the corrected spectra on a wavelength scale (nm) using an air-equilibrated solution of quinine sulfate in 1 N $H_2SO_4$ (Φ = 0.546)[73] as reference. Room-temperature emission lifetimes were determined with the time correlated single photon counting technique using an IBH spectrometer equipped with a NanoLed excitation source at 331 nm; the detector was a red-sensitive (up to 850 nm) Horiba Jobin Yvon TBX Picosecond Photon Detection Module. The 77 K luminescence lifetimes were acquired using the same Edinburgh FLS920 spectrometer equipped with a μF 920H flash lamp as excitation source. The fitting of the experimental data to single or multiple-exponential decays was carried out with the software provided by the instrument manufacturer. To record the 77 K luminescence spectra, the samples were put in quartz tubes (2 mm inner diameter) and inserted in a special quartz Dewar flask filled up with liquid nitrogen.

## 8.4 - Bibliography

1. S. M. Bonesi and R. Erra-Balsells, *J. Lumin.*, 2001, **93**, 51-74.

2. A. R. Katritzky, G. W. Rewcastle and L. M. V. Demiguel, *J. Org. Chem.*, 1988, **53**, 794-799.

3. S. E. Creutz, K. J. Lotito, G. C. Fu and J. C. Peters, *Science*, 2012, **338**, 647-651.

4. J. V. Grazulevicius, P. Strohriegl, J. Pielichowski and K. Pielichowski, *Prog. Polym. Sci.*, 2003, **28**, 1297-1353.

5. N. Dubey and M. Leclerc, *J. Polym. Sci. Pol. Phys.*, 2011, **49**, 467-475.

6. S. R. Cowan, N. Banerji, W. L. Leong and A. J. Heeger, *Adv. Funct. Mater.*, 2012, **22**, 1116-1128.

7. J. L. Li and A. C. Grimsdale, *Chem. Soc. Rev.*, 2010, **39**, 2399-2410.

8. N. Blouin and M. Leclerc, *Acc. Chem. Res.*, 2008, **41**, 1110-1119.

9. E. C. Constable, *Chem. Soc. Rev.*, 2007, **36**, 246-253.

10. S. Encinas, L. Flamigni, F. Barigelletti, E. C. Constable, C. E. Housecroft, E. R. Schofield, E. Figgemeier, D. Fenske, M. Neuburger, J. G. Vos and M. Zehnder, *Chem.-Eur. J.*, 2002, **8**, 137-150.

11. E. Baranoff, J. P. Collin, L. Flamigni and J. P. Sauvage, *Chem. Soc. Rev.*, 2004, **33**, 147-155.

12. E. A. Medlycott and G. S. Hanan, *Chem. Soc. Rev.*, 2005, **34**, 133-142.

13. J. E. Beves, E. C. Constable, C. E. Housecroft, C. J. Kepert and D. J. Price, *CrystEngComm*, 2007, **9**, 456-459.

14. E. C. Constable, *Coord. Chem. Rev.*, 2008, **252**, 842-855.

15. C. Bazzicalupi, A. Bencini, A. Bianchi, A. Danesi, E. Faggi, C. Giorgi, S. Santarelli and B. Valtancoli, *Coord. Chem. Rev.*, 2008, **252**, 1052-1068.

16. S. D. Cummings, *Coord. Chem. Rev.*, 2009, **253**, 449-478.

17. B. Bozic-Weber, E. C. Constable, N. Hostettler, C. E. Housecroft, R. Schmitt and E. Schonhofer, *Chem. Commun.*, 2012, **48**, 5727-5729.

18. A. Wild, A. Winter, F. Schlutter and U. S. Schubert, *Chem. Soc. Rev.*, 2011, **40**, 1459-1511.

1. S. M. Bonesi and R. Erra-Balsells, *J. Lumin.*, 2001, **93**, 51-74.

2. A. R. Katritzky, G. W. Rewcastle and L. M. V. Demiguel, *J. Org. Chem.*, 1988, **53**, 794-799.

3. S. E. Creutz, K. J. Lotito, G. C. Fu and J. C. Peters, *Science*, 2012, **338**, 647-651.

4. J. V. Grazulevicius, P. Strohriegl, J. Pielichowski and K. Pielichowski, *Prog. Polym. Sci.*, 2003, **28**, 1297-1353.

5.  N. Dubey and M. Leclerc, *J. Polym. Sci. Pol. Phys.*, 2011, **49**, 467-475.

6.  S. R. Cowan, N. Banerji, W. L. Leong and A. J. Heeger, *Adv. Funct. Mater.*, 2012, **22**, 1116-1128.

7.  J. L. Li and A. C. Grimsdale, *Chem. Soc. Rev.*, 2010, **39**, 2399-2410.

8.  N. Blouin and M. Leclerc, *Acc. Chem. Res.*, 2008, **41**, 1110-1119.

9.  E. C. Constable, *Chem. Soc. Rev.*, 2007, **36**, 246-253.

10. S. Encinas, L. Flamigni, F. Barigelletti, E. C. Constable, C. E. Housecroft, E. R. Schofield, E. Figgemeier, D. Fenske, M. Neuburger, J. G. Vos and M. Zehnder, *Chem.-Eur. J.*, 2002, **8**, 137-150.

11. E. Baranoff, J. P. Collin, L. Flamigni and J. P. Sauvage, *Chem. Soc. Rev.*, 2004, **33**, 147-155.

12. E. A. Medlycott and G. S. Hanan, *Chem. Soc. Rev.*, 2005, **34**, 133-142.

13. J. E. Beves, E. C. Constable, C. E. Housecroft, C. J. Kepert and D. J. Price, *CrystEngComm*, 2007, **9**, 456-459.

14. E. C. Constable, *Coord. Chem. Rev.*, 2008, **252**, 842-855.

15. C. Bazzicalupi, A. Bencini, A. Bianchi, A. Danesi, E. Faggi, C. Giorgi, S. Santarelli and B. Valtancoli, *Coord. Chem. Rev.*, 2008, **252**, 1052-1068.

16. S. D. Cummings, *Coord. Chem. Rev.*, 2009, **253**, 449-478.

17. B. Bozic-Weber, E. C. Constable, N. Hostettler, C. E. Housecroft, R. Schmitt and E. Schonhofer, *Chem. Commun.*, 2012, **48**, 5727-5729.

18. A. Wild, A. Winter, F. Schlutter and U. S. Schubert, *Chem. Soc. Rev.*, 2011, **40**, 1459-1511.

19. A. Winter, M. D. Hager, G. R. Newkome and U. S. Schubert, *Adv. Mater.*, 2011, **23**, 5728-5748.

20. A. Winter, G. R. Newkome and U. S. Schubert, *ChemCatChem*, 2011, **3**, 1384-1406.

21. L. Flamigni, J. P. Collin and J. P. Sauvage, *Acc. Chem. Res.*, 2008, **41**, 857-871.

22. M. W. Cooke and G. S. Hanan, *Chem. Soc. Rev.*, 2007, **36**, 1466-1476.

23. K. M. C. Wong and V. W. W. Yam, *Coord. Chem. Rev.*, 2007, **251**, 2477-2488.

24. I. Eryazici, C. N. Moorefield and G. R. Newkome, *Chem. Rev.*, 2008, **108**, 1834-1895.

25. G. Accorsi, N. Armaroli, F. Cardinali, D. Wang and Y. X. Zheng, *J. Alloys Compd.*, 2009, **485**, 119-123.

26. X. G. Chen, Q. G. Zhou, Y. X. Cheng, Y. H. Geng, D. G. Ma, Z. Y. Xie and L. X. Wang, *J. Lumin.*, 2007, **126**, 81-90.

27. Z. F. Chen, K. M. C. Wong, E. C. H. Kwok, N. Y. Zhu, Y. B. Zu and V. W. W. Yam, *Inorg. Chem.*, 2011, **50**, 2125-2132.

28. S. H. Hwang, P. S. Wang, C. N. Moorefield, L. A. Godinez, J. Manriquez, E. Bustos and G. R. Newkome, *Chem. Commun.*, 2005, 4672-4674.

29. A. Maier, H. Fakhrnabavi, A. R. Rabindranath and B. Tieke, *J. Mater. Chem.*, 2011, **21**, 5795-5804.

30. E. K. Pefkianakis, N. P. Tzanetos and J. K. Kallitsis, *Chem. Mater.*, 2008, **20**, 6254-6262.

31. A. C. Ribou, T. Wada and H. Sasabe, *Inorg. Chim. Acta*, 1999, **288**, 134-141.

32. W. Y. Tam, C. S. K. Mak, A. M. C. Ng, A. B. Djurisic and W. K. Chan, *Macromol. Rapid Commun.*, 2009, **30**, 622-626.

33. R. Gompper and H. U. Wagner, *Angew. Chem. Int. Ed. Engl.*, 1988, **27**, 1437-1455.

34. M. Kivala and F. Diederich, *Acc. Chem. Res.*, 2009, **42**, 235-248.

35. S. Barlow and S. R. Marder, in *Functional Organic Materials*, eds. T. J. J. Müller and U. H. F. Bunz, Wiley-VCH, Weinheim, 2007, pp. 393-437.

36. C. Aurisicchio, B. Ventura, D. Bonifazi and A. Barbieri, *J. Phys. Chem. C*, 2009, **113**, 17927-17935.

37. Z. R. Grabowski, K. Rotkiewicz and W. Rettig, *Chem. Rev.*, 2003, **103**, 3899-4031.

38. A. Baschieri, L. Sambri, I. Gualandi, D. Tonelli, F. Monti, A. Degli Esposti, N. Armaroli *RSC Advances*, **2013**, in press, DOI: 10.1039/C3RA23380D

39. R. E. Stratmann, G. E. Scuseria and M. J. Frisch, *J. Chem. Phys.*, 1998, **109**, 8218-8224.

40. M. E. Casida, C. Jamorski, K. C. Casida and D. R. Salahub, *J. Chem. Phys.*, 1998, **108**, 4439-4449.

41. R. d. Bauernschmitt and R. Ahlrichs, *Chem. Phys. Lett.*, 1996, **256**, 454-464.

42. J. H. Wang and G. S. Hanan, *Synlett*, 2005, 1251-1254.

43. K. Osowska, T. Lis and S. Szafert, *Eur. J. Org. Chem.*, 2008, 4598-4606.

44. Y. S. Zhang, R. P. Hsung, M. R. Tracey, K. C. M. Kurtz and E. L. Vera, *Org. Lett.*, 2004, **6**, 1151-1154.

45. A. Winter, D. A. M. Egbe and U. S. Schubert, *Org. Lett.*, 2007, **9**, 2345-2348.

46. C. Hamacher, N. Hurkes, A. Kaiser, A. Klein and A. Schuren, *Inorg. Chem.*, 2009, **48**, 9947-9951.

47. C. I. Simionescu and M. Grovu, *Polym. Bull.*, 1981, **6**, 217-223.

48. J. F. Ambrose and R. F. Nelson, *J. Electrochem. Soc.*, 1968, **115**, 1159-1164.

49. S. K. Lee, Y. B. Zu, A. Herrmann, Y. Geerts, K. Mullen and A. J. Bard, *J. Am. Chem. Soc.*, 1999, **121**, 3513-3520.

50. L. R. Faulkner and A. J. Bard, *in Electroanalytical Chemistry*, Bard, A. J., New York, 1977.

51. C. Adamo and V. Barone, *J. Chem. Phys.*, 1999, **110**, 6158-6170.

52. C. Adamo, G. E. Scuseria and V. Barone, *J. Chem. Phys.*, 1999, **111**, 2889-2899.

53. J. P. Foster and F. Weinhold, *J. Am. Chem. Soc.*, 1980, **102**, 7211-7218.

54. A. E. Reed, R. B. Weinstock and F. Weinhold, *J. Chem. Phys.*, 1985, **83**, 735-746.

55. M. D. Hanwell, D. E. Curtis, D. C. Lonie, T. Vandermeersch, E. Zurek and G. R. Hutchison, *J. Cheminformatics*, 2012, **4**, doi:10.1186/1758-2946-4-17.

56. R. Cammi, S. Corni, B. Mennucci and J. Tomasi, *J. Chem. Phys.*, 2005, **122**, 104513.

57. R. Improta, V. Barone, G. Scalmani and M. J. Frisch, *J. Chem. Phys.*, 2006, **125**, 054103-054109.

58. T. Yanai, D. P. Tew and N. C. Handy, *Chem. Phys. Lett.*, 2004, **393**, 51-57.

59. D. Jacquemin, E. A. Perpete, G. E. Scuseria, I. Ciofini and C. Adamo, *J. Chem. Theory Comput.*, 2008, **4**, 123-135.

60. C. A. Guido, D. Jacquemin, C. Adamo and B. Mennucci, *J. Phys. Chem. A*, 2010, **114**, 13402-13410.

61. R. Siebert, A. Winter, U. S. Schubert, B. Dietzek and J. Popp, *J. Phys. Chem. C*, 2010, **114**, 6841-6848.

62. R. Improta, G. Scalmani, M. J. Frisch and V. Barone, *J. Chem. Phys.*, 2007, **127**, 074504.

63. D. J. Tozer, *J. Chem. Phys.*, 2003, **119**, 12697-12699.

64. A. Dreuw and M. Head-Gordon, *J. Am. Chem. Soc.*, 2004, **126**, 4007-4016.

65. V. A. Galievsky, S. I. Druzhinin, A. Demeter, P. Mayer, S. A. Kovalenko, T. A. Senyushkina and K. A. Zachariasse, *J. Phys. Chem. A*, 2010, **114**, 12622-12638.

66. A. P. de Silva, T. S. Moody and G. D. Wright, *Analyst*, 2009, **134**, 2385-2393.

67. M. J. Frisch, G. W. Trucks, H. B. Schlegel, G. E. Scuseria, M. A. Robb, J. R. Cheeseman, G. Scalmani, V. Barone, B. Mennucci, G. A. Petersson, H. Nakatsuji, M. Caricato, X. Li, H. P. Hratchian, A. F. Izmaylov, J. Bloino, G. Zheng, J. L. Sonnenberg, M. Hada, M. Ehara, K. Toyota, R. Fukuda, J. Hasegawa, M. Ishida, T. Nakajima, Y. Honda, O. Kitao, H. Nakai, T. Vreven, J. A. Montgomery Jr., J. E. Peralta, F. Ogliaro, M. Bearpark, J. J. Heyd, E. Brothers, K. N. Kudin, V. N. Staroverov, R. Kobayashi, J. Normand, K. Raghavachari, A. Rendell, J. C. Burant, S. S. Iyengar, J. Tomasi, M. Cossi, N. Rega, J. M. Millam, M. Klene, J. E. Knox, J. B. Cross, V. Bakken, C. Adamo, J. Jaramillo, R. Gomperts, R. E. Stratmann, O. Yazyev, A. J. Austin, R. Cammi, C. Pomelli, J. W. Ochterski, R. L. Martin, K. Morokuma, V. G. Zakrzewski, G. A. Voth, P. Salvador, J. J. Dannenberg, S. Dapprich, A. D. Daniels, O. Farkas, J. B. Foresman, J. V. Ortiz, J. Cioslowski and D. J. Fox, *Gaussian 09, Revision A.02*, (2009) Gaussian, Inc., Wallingford CT.

68. J. Tomasi, B. Mennucci and R. Cammi, *Chem. Rev.*, 2005, **105**, 2999-3093.

69. A. D. Mclean and G. S. Chandler, *J. Chem. Phys.*, 1980, **72**, 5639-5648.

70. R. Krishnan, J. S. Binkley, R. Seeger and J. A. Pople, *J. Chem. Phys.*, 1980, **72**, 650-654.

71. S. Corni, R. Cammi, B. Mennucci and J. Tomasi, *J. Chem. Phys.*, 2005, **123**, 134512.

72. J. N. Demas and G. A. Crosby, *J. Phys. Chem.*, 1971, **75**, 991-1024.

73. S. R. Meech and D. Phillips, *J. Photochem.*, 1983, **23**, 193-217.

# 9) New cyclometallating tetrazole ligands for blue-emitting iridium complexes

In recent years, increasing interest has been devoted to phosphorescent metal complexes and their application as emitters in electroluminescent devices, i.e. organic light-emitting diodes (OLEDs) or light-emitting electrochemical cells (LEECs) for displays and lighting applications.[1] Luminescent complexes are generally based on heavy metals, and compounds based on iridium are the most studied due to their relatively short excited-state lifetime, high emission quantum yield, and facile color tuning.[2] The triplet character of the emission, induced by the strong spin–orbit coupling in these complexes, is of great importance, since it allows for harvesting of both the singlet and the triplet excitons produced when electrons and holes recombine, reaching up to 100% internal efficiency.[3]

In order to develop full-color display and lighting technologies, a key factor is the employment of molecules that can emit the primary colors (red, green, and blue). One of the advantages of cyclometallated Ir(III) complexes is that the emission color can be tuned by an appropriate design of the chemical structure and nature of the cyclometallated ligands.[4,5] Although efficient red- and green-emitting Ir(III) complexes have been described and are now in the commercialization phase due to their excellent stability in devices, finding stable and efficient blue emitters is still an issue.[6]

Among the cyclometallating ligands employed to prepare Ir(III) complexes, the most widely used are those in which a carbon from a phenyl ring acts as a donor and the adjacent fragment involved in formation of the metallocycle is an N-heterocycle ring,[4] and in fact 2-phenylpyridine (ppy) and its derivatives are typical compounds used as C^N ligands. Finally a neutral or anionic appropriate ancillary ligand is exploited to form the final complexes.

Through rational synthetic strategies, the C^N ligands and/or the ancillary ligand can be easily substituted with electron-withdrawing or electron-donating groups, so that these substitutions have an important effect on the HOMO and LUMO energies of the metal complex and consequently on the light emission. In order to obtain blue emitters, several options can be followed.

One approach to obtain blue-emitting complexes is to stabilize the highest occupied molecular orbital (HOMO) on the C^N moieties by introducing electron-withdrawing groups on the aryl group, typically fluoride substituents, when arylpyridines are used as cyclometallating ligands; otherwise, a more effective strategy could be to raise the LUMO of the complex by switching the pyridine moiety to a smaller N-heterocyclic ring having higher reduction potentials than pyridine. In fact, blue shifts of the emission maxima have been obtained using pyrazoles,[7] *N*-heterocyclic

carbenes (NHC),[8] or triazoles.[9] Notably, tetrazole containing cyclometallating ligands have not be so far reported.

In our group, we were able to successfully employ 2-methyl-5-phenyl-2*H*-tetrazole as cyclometallating ligand to modify the emission of the Ir (III) complexes. Herein, preliminary results on the synthesis and the properties of highly blue-emitting charged Iridium(III) complexes containing two identical 2-methyl-5-phenyl-2*H*-tetrazole as cyclometallating ligands and different N^N ancillary ligands or isocyanides are presented, (Figure 1).
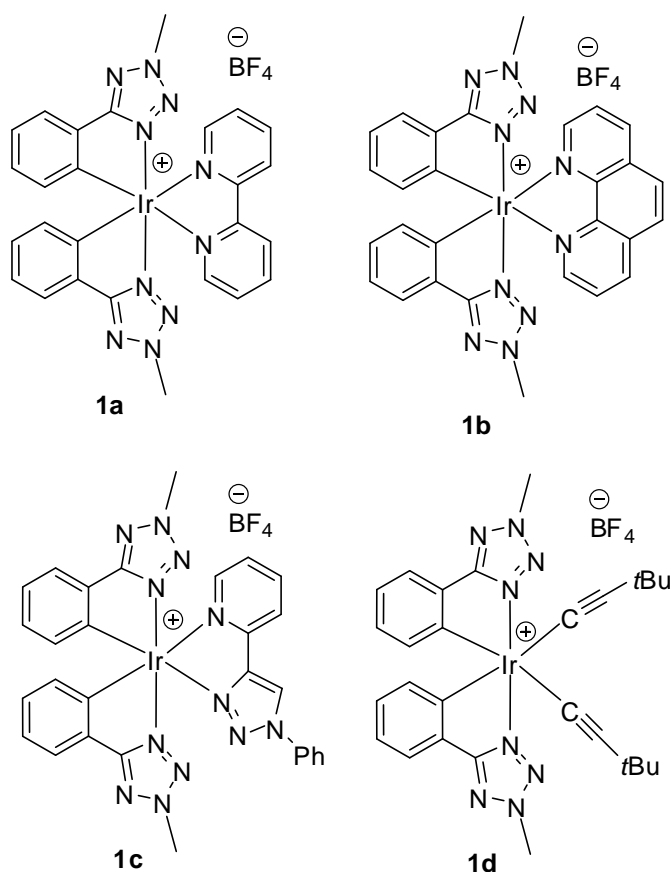


Figure 1: Iridium complexes

## 9.1 - Results and discussion

### 9.1.1 - Synthesis and characterization

The cyclometallating ligand 2-methyl-5-phenyl-2*H*-tetrazole **3** was synthesized by methylation of 5-phenyl-2*H*-tetrazole with methyl iodide under basic conditions in almost 60% yield after careful purification from the undesired isomer 1-methyl-5-phenyl-2*H*-tetrazole.

Any attempt to obtain the classical cyclometallated Ir(III) μ-dichloro bridged dimer [{(C^N)$_2$Ir(μ-Cl)}$_2$], generally used for the subsequent synthesis of Ir(III) complexes containing ancillary ligand,

failed, probably owing to the formation of a $IrCl_3$-tetrazole salt. Therefore, a further step involving a reagent able to promote the removal of chloride ion from $IrCl_3$ proved to be necessary. Essentially, the methyl tetrazole **3** was reacted with $IrCl_3 \cdot nH_2O$ in a 3:1 mixture of 2-ethoxyethanol/$H_2O$ overnight at reflux.[10] The obtained yellow salt was filtered off and refluxed in $CH_2Cl_2$ with $AgBF_4$ in order to satisfactory obtain the solvate-complex $[Ir(C^\wedge N)_2(CH_3CN)_2]^+BF_4^-$ ($C^\wedge N$ = 2-methyl-5-phenyl-2*H*-tetrazole) **4** in 40% yield after purification, (Scheme 1).
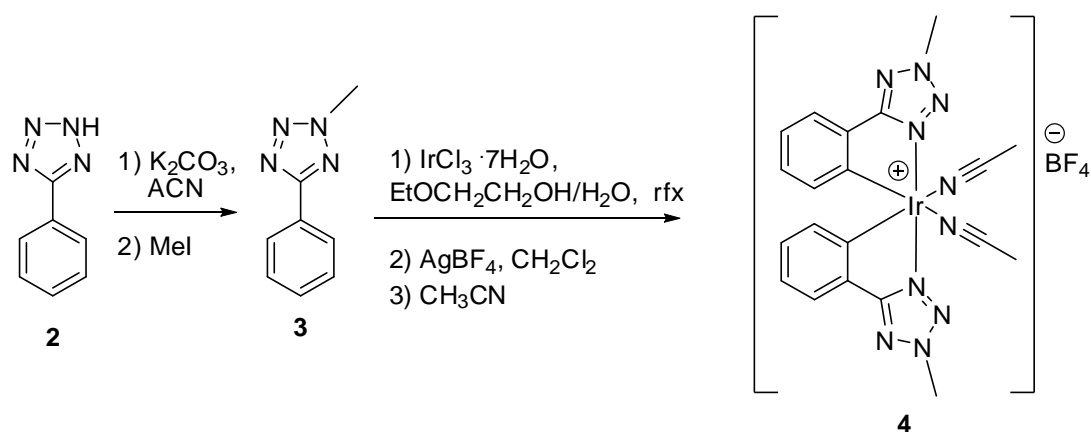


Scheme 1

Crystallization of **4** in $CH_3CN/Et_2O$ gave crystals suitable for X-rays analysis and the X-rays structure is reported in Figure 2.
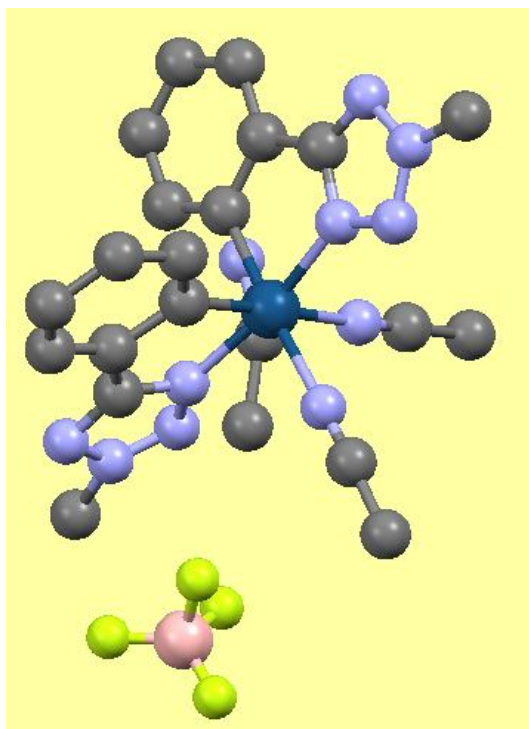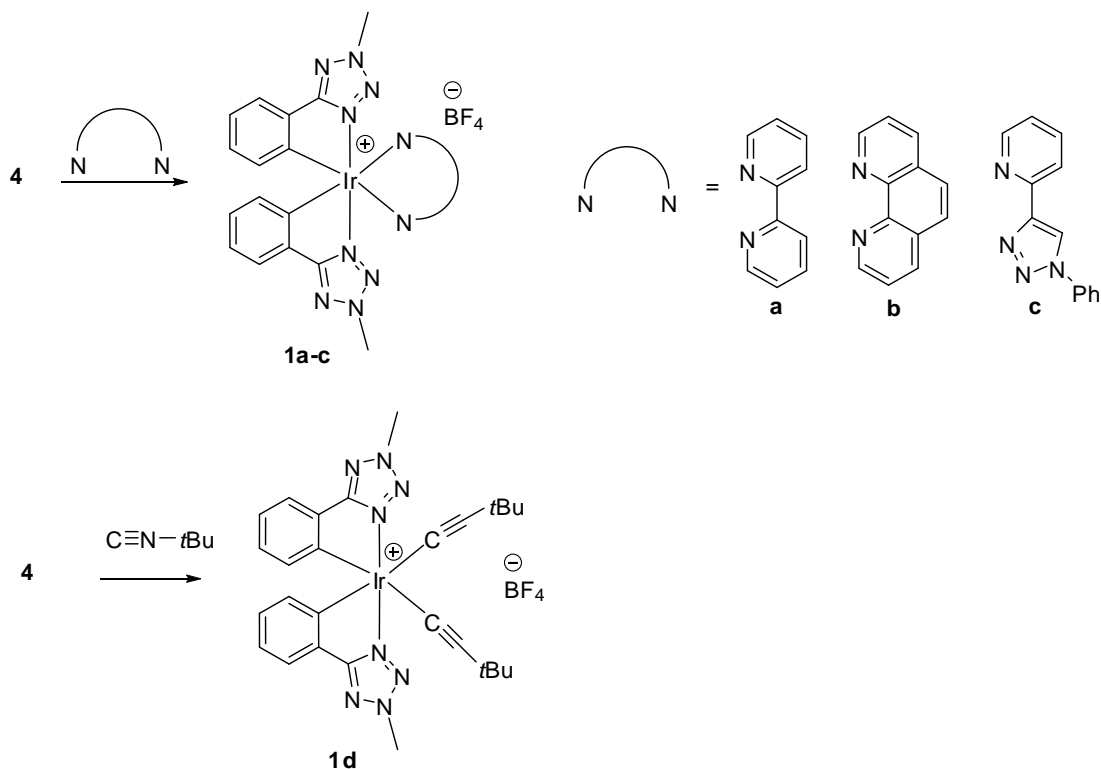


Figure 2. X-rays structure of **4**.

The complexes **1a-d** were obtained reacting the ancillary ligands with the solvato complex **4** in a 3:1 mixture of $CH_2Cl_2$/EtOH (75-80% yield), (Scheme 2).



Scheme 2. Synthesis of complexes **1a-d**.

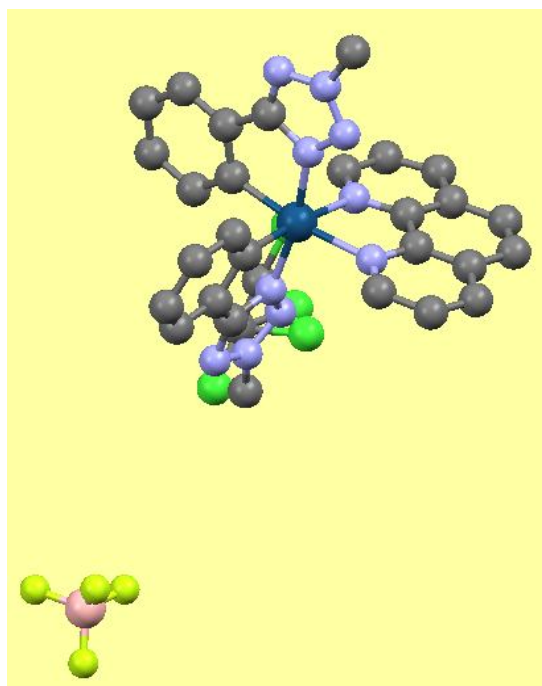The X-ray structure of **4b** is reported in Figure 3.



Figure 3. X-ray structure of **4b**.

## 9.1.2 - Electrochemical properties

The electrochemical behaviour of **1a-d** was investigated by cyclic voltammetry (CV) in deaerated ACN *vs.* SCE (Figure 4).
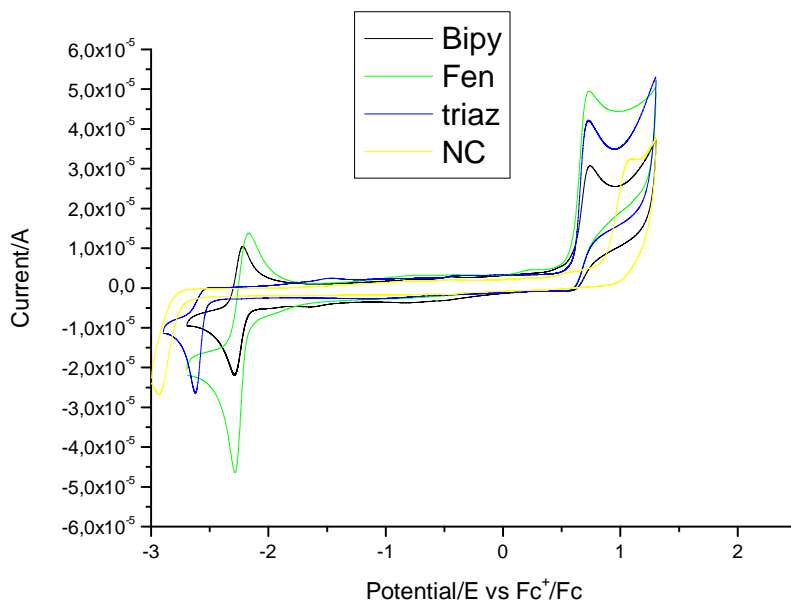


Figure 4: Cyclic voltammograms of **1a** (black), **1b** (green), **1c** (blue) and **1d** (yellow) in ACN solution with 0.1 M NBu$_4$PF$_6$ at 0.1 V s$^{-1}$ (concentration about mM). The working electrode was glass carbon, the reference electrode was Ag/AgNO$_3$ 0.1 M in acetonitrile and the counter electrode was a Pt wire. The potential is referred to the E$^{\circ}_{Fc+/Fc}$ potential

The CVs recorded for all compound show a catodic and a anodic wave. The reduction of Bipy and Fen is a reversible process and the $\Delta E_p$ is respectively equal to 70 and 76 mV suggesting that only electron is involved in the reduction. From these processes the D values for the Bipy and Fen were estimate and they was used to calculate the number of exchanged electrone for the other processes. The other process showed only forward processes in the employed experimental condition. In order to investigate the kinetics of those processes the scan rate was changed in the range 0.01 ÷ 10 V s$^{-1}$. Increasing the scan rate the backward waves of the anodic process of Bipy, Fen and Triaz appeared suggesting the presence of reactions that follow the first oxidation processes. From the analysis of the current recorded at the electrode at different scan rates we can say that the mechanism of the oxidation for these three compounds is ECE (electrochemical reaction, chemical reaction and electrochemical reaction). From the analysis of the CV at high scan rate, when the effect of following reaction is negligible, the number of the exchanged electron and the formal potentials of the first oxidation processes were estimate and these parameter are reported in Table 1. Moreover

141

the reduction processes of Triaz is EC and the number of exchanged electron is one. Finally the all processes concerning the NC are irreversible and involve one electrone. Comparing the formal potential with literature[11] the reduction of Bipy and Fen involve the N-N ligand.

| Complex | First reduction process | | | First oxidation process | | |
|---|---|---|---|---|---|---|
| | Electrode kinetics | $E_{red}°$(V vs Fc$^+$/Fc) | $\Delta E_p$ (V)/$n_{red}$ | Electrode kinetics | $E_{ox}°$(V vs Fc$^+$/Fc) | $n_{ox}$ |
| **1a** - Bipy | Rev | -2.254 | (0.070)/1 | ECE | + 0.687 | 1* |
| **1b** - Fen | Rev | -2.238 | (0.076)/1 | ECE | + 0.710 | 1* |
| **1c** - Triaz | EC | -2.695 | 1** | ECE | + 0.787 | 1** |
| **1d** - NC | Irrev. | -2.973 | 1** | Irrev. | + 1.100 | 1** |

* calculated from the peak current and the diffusion coefficient calculated from the cathodic process reversible ** calculated from the peak current and the diffusion coefficient calculated for the Bipy

Table 1

### 9.1.3 - Photophysical properties

In Figure 5 the RT absorption spectra in dichloromethane of all the synthesized complexes and for comparison, the absorption spectra of archetypal [Ir(ppy)$_2$(bpy)]$^+$ and [Ir(dfppy)$_2$(bpy)]$^+$ are reported. All complexes show bluer absorption onset than the bluest diphenylpyridin cyclometallated Ir(III) complex, [Ir(dfppy)$_2$(bpy)]$^+$.
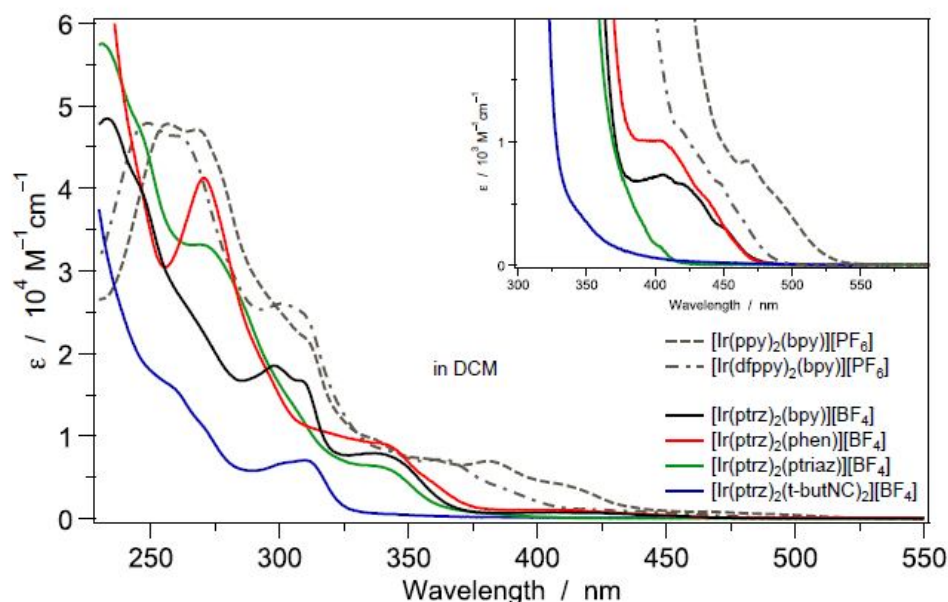


Figure 5. Absorption spectra in DCM of complexes **1a-d** and reference compounds.

In Figure 6 and in Table 2 preliminary photophysical data of the obtained complexes are reported. Emission studies were carried out at room temperature both in dichloromethane and acetonitrile, and at 77K (DCM glass). Basically, **1a** and **1b** are strongly emissive and their emission is extremely

blue, despite the band shape is indicating a pronounced MLCT character. The emission profile of **1a** is almost superimposed on the bis-fluorinated-phenylpyridine bipyridine Ir(III) complex emission band. On the other hand complex **1c** and **1d** are substantially not emissive.



(a) Emission spectra in RT DCM.

(b) Emission spectra in RT ACN.

(c) Emission spectra in DCM at 77 K.

- - - - [Ir(ppy)$_2$(bpy)][PF$_6$]
- · - · [Ir(dfppy)$_2$(bpy)][PF$_6$]

——— [Ir(ptrz)$_2$(bpy)][BF$_4$]
——— [Ir(ptrz)$_2$(phen)][BF$_4$]
——— [Ir(ptrz)$_2$(ptriaz)][BF$_4$]
——— [Ir(ptrz)$_2$(t-butNC)$_2$][BF$_4$]
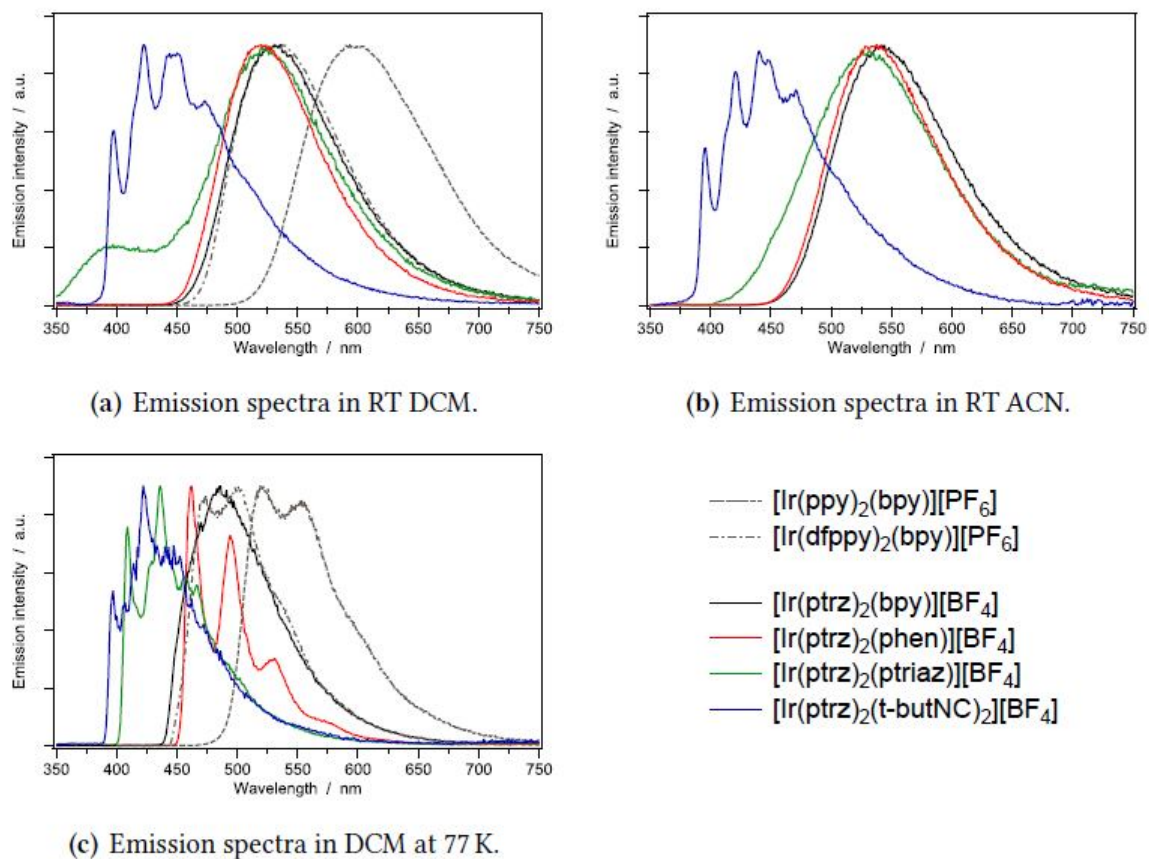
Figure 6: Preliminary emission spectra of the Ir(III) tetrazolate complexes.

| Complex | Medium | $\lambda_{max}$ (nm) | $\phi_{em}$ (%) | $\tau$ ($\mu$s) |
|---------|--------|----------|---------|--------|
| **4a** | CH$_2$Cl$_2$ | 532 | 67,7 | 1,27 |
| | ACN | 544 | 54,0 | 1,27 |
| | 77 K CH$_2$Cl$_2$ | 485 | | 2,82 |
| **4b** | CH$_2$Cl$_2$ | 520 | 71,9 | 1,56 |
| | ACN | 536 | 66,5 | 1,7 |
| | 77 K CH$_2$Cl$_2$ | 462, 495… | | 13,5 |
| **4c** | CH$_2$Cl$_2$ | 517 | 0,2 | X |
| | ACN | 530 | 0,1 | X |
| | 77 K CH$_2$Cl$_2$ | 410, 436… | | X |
| **4d** | CH$_2$Cl$_2$ | 400,425,450 | 0,5 | X |
| | ACN | 440 multi | 0,7 | X |
| | 77 K CH$_2$Cl$_2$ | 396, 422… | | X |

Table 2. Preliminary photophysical properties

## 9.2 - Conclusions

This work is still in progress, and therefore all the reported results are preliminary. However, the synthesis of new iridium complexes containing tetrazolated ciclometalated ligands is reported for the first time.

From the obtained photophysical data, the complexes **1a** and **1b** show very good blue emission and the quantum yields, both in solution and in the solid state, are extremely high (about 70%): these results are really remarkable considering that these complexes are fluoride-free.

## 9.3 - Experimental section

### *Materials and methods*

$^1$H, $^{13}$C, NMR spectra were recorded on a Varian AS 300 or on a Mercury 400 spectrometer. Chemical shifts ($\delta$) are reported in ppm relative to residual solvent signals for $^1$H and $^{13}$C NMR ($^1$H NMR: 7.26 ppm for CDCl$_3$; $^{13}$C NMR: 77.0 ppm for CDCl$_3$). $^{13}$C NMR spectra were acquired with $^1$H broadband decoupled mode. Mass spectra were recorded on a micromass LCT spectrometer using electrospray (ES) ionisation techniques. Analytical grade solvents and commercially available reagents were used as received, unless otherwise stated. Chromatographic purifications were performed using 70-230 mesh silica.

*Synthesis of 2-methyl-5-phenyl-2H-tetrazole 2*:, A solution of 5-phenyl-2*H*-tetrazole (1.0 g, 6.8 mmol) in CH$_3$N (70 mL) was treated with K$_2$CO$_3$ (3.8 g, 27.4 Mmol) followed by addition of methyl iodide (0.86 mL, 13.6 mmol), according to a described procedure (**DOI: 10.1021/jo00058a061**). The reaction was stirred at reflux for 72 h, then it was cooled to room temperature, the residual solid was filtered off and the solution was concentrated in vacuo to give a dark oil. The oil was then purified by column chromatography on silica eluting with CH$_2$Cl$_2$/petroleum ether= 4/6 and then CH$_2$Cl$_2$/EtOAc= 98/2. Fractions homogeneous by TLC were combined and concentrated in vacuo to give **2** (0.67 g, 59.1% yields, less polar spot) as a pale yellow solid [$^1$H NMR (CDCl$_3$) $\delta$: 4.33 (s, 3H), 7.35-7.50 (m, 3H), 8.05-8.15 (m, 2H); $^{13}$C NMR (CDCl$_3$) $\delta$: 39.5 (CH$_3$), 126.8 (CH), 127.3 (C), 128.9 (CH), 130.3 (CH), 165.2 (C)] and 1-methyl-5-phenyl-2*H*-tetrazole (0.26 g, 23.7% yields) as a white solid [$^1$H NMR (CDCl$_3$) $\delta$: 4.18 (s, 3H), 7.55-7.60 (m, 3H), 7.70-7.75 (m, 2H); $^{13}$C NMR (CDCl$_3$) $\delta$: 35.0 (CH$_3$), 123.8 (C), 128.6 (CH), 129.3 (CH), 131.3 (CH), 165.9 (C)]

**Synthesis of Ir(III)-solvato complex 3.** The reactions were performed under $N_2$ and in the absence of light. The solvents were not dried, but they were deoxygenated by bubbling with $N_2$. The ligand **2** (48 mg, 0.3 mmol) was dissolved in a 3:1 mixture of ethoxyethanol: water ( 2ml) and then $IrCl_3 \cdot xH_2O$ (30 mg) was added. The mixture was stirred overnight at 140 °C under $N_2$. After cooling, the obtained yellow solid was filtered, washed with water, dried and dissolved in $CH_2Cl_2$ (8 ml). $AgBF_4$ (40 mg) was added, and the solution was then refluxed for 6 h. After cooling, the solution was filtered through a paper filter to remove AgCl and evaporated to dryness. The resulting crude Ir(III) solvato complex was dissolved in $CH_3CN$ and precipitated with $Et_2O$ to give **3** (25 mg 40% yield). $^1H$ NMR (CDCl$_3$) δ: 4.65 (s, 3H), 6.14 (d, 1H, $J_{HH}$=7.5), 6.80 (dt, 1H, $J_{HH}$=7.5, $J_{HH}$=1.4), 6.92 (dt, 1H, $J_{HH}$=7.5, $J_{HH}$=1.2), 7.64 (d, 1H, $J_{HH}$=7.5, $J_{HH}$=1.4) ; $^{13}C$ NMR (CDCl$_3$) δ: 40.8 (CH$_3$), 122.8 (CH), 123.6 (CH), 129.8 (CH), 130.0 (C), 130.1 (C), 133.6 (CH), 174.3 (C)]

ESI-MS$^+$: 593 (M$^+$+2ACN); 552 (M$^+$+ACN)

**Synthesis of Ir(III) Complexes 4a-c.** The solvato-complex **3** (10 mg, 0.015 mmol) was dissolved in a 3:1 mixture of $CH_2Cl_2$/EtOH (2 ml) and the bidentate ligand (0.027 mmol) was added. The mixture was left to stir overnight at r.t., and then the solvent was evaporated. The solid was dissolved in acetone, precipitated with $Et_2O$ and the obtained solid purified by column chromatography (DCM/MeOH=98/2) to give pure complexes **4a-c.**

**Complexes 4a** (9.1 mg, 80 % yields). $^1H$ NMR (CD$_2$Cl$_2$) δ: 4.27 (s, 6H), 6.24 (d, 2H, $J_{HH}$=8.8), 6.98 (t, 2H, $J_{HH}$=8.8), 7.05 (t, 2H, $J_{HH}$=8.8), 7.36 (t, 2H, $J_{HH}$=7.0), 7.70 (d, 2H, $J_{HH}$=7.0), 8.00-8.10 (m, 4H), 8.51 (d, 2H, $J_{HH}$=7.0); $^{13}C$ NMR (CD$_2$Cl$_2$) δ: 42.1 (CH$_3$), 123.6 (CH), 124.8 (CH), 127.7 (CH), 129.2 (C), 131.5 (CH), 132.6 (CH), 140.2 (2CH), 145.6 (C), 151.7 (CH), 156.7 (C), 174.6 (C)]

**Complexes 4b** (77 % yields). $^1H$ NMR (CD$_2$Cl$_2$) δ: 4.17 (s, 6H), 6.35 (d, 2H, $J_{HH}$=7.6), 7.02 (dt, 2H, $J_{HH}$=7.5, $J_{HH}$=1.6), 7.08 (dt, 2H, $J_{HH}$=8.8, $J_{HH}$=1.9), 7.36 (t, 2H, $J_{HH}$=7.0), 7.70-7.75 (m, 4H), 8.02 (s, 2H), 8.33 (dd, 2H, $J_{HH}$=5.5, $J_{HH}$=1.9), 8.57 (dd, 2H, $J_{HH}$=8.5, $J_{HH}$=1.6); $^{13}C$ NMR (CD$_2$Cl$_2$) δ: 41.5 (CH$_3$), 123.7 (CH), 124.8 (CH), 126.0 (CH), 128.7 (CH), 129.4 (C), 131.1 (C), 131.4 (CH), 132.7 (CH), 138.7 (CH), 144.9 (C), 147.7 (C), 156.7 (C), 152.0 (C), 174.6 (C)]

**Complexes 4c** (75 % yields). $^1H$ NMR (CD$_2$Cl$_2$) δ: 4.29 (s, 3H), 4.30 (s, 3H), 6.27 (d, 2H, $J_{HH}$=7.5), 6.90-7.10 (m, 4H), 7.22 (bt, 1H, $J_{HH}$=6.7), 7.40-7.50 (m, 3H), 7.69 (dd, 2H, $J_{HH}$=7.1, $J_{HH}$=11.3), 7.78 (bd, 1H, $J_{HH}$=7.1), 7.89 (d, 1H, $J_{HH}$=5.2), 8.0 (bs, 1H), 8.5 (bs, 2H), 9.5 (s, 2H); $^{13}C$ NMR (CD$_2$Cl$_2$) δ: 41.6 (CH$_3$), 41.7 (CH$_3$), 120.7 (CH), 123.2 (CH), 123.5 (CH), 123.6 (CH), 124.1

(C), 124.3 (CH), 124.7 (CH), 126.0 (CH), 129.3 (C), 129.35 (C), 130.0 (CH), 130.2 (CH), 130.6 (CH), 131.3 (CH), 132.5 (CH), 133.0 (CH), 136.1 (CH), 140.0 (CH), 151.0 (CH), 141.8 (C), 145.1 (C), 150.2 (C), 150.3 (C), 174.4 (C), 174.8 (C)]

**Synthesis of Ir(III) Complex 4d**. Caution! tert-Butyl isocyanide is a foul-smelling volatile liquid, therefore ensure adequate ventilation. The solvato-complex **3** (10 mg, 0.015 mmol) was dissolved in a 3:1 mixture of $CH_2Cl_2$/EtOH (2 ml) and *t*-butyl isocyanide (0.027 mmol) was added. The mixture was left to stir overnight at 30 °C, and then the solvent was evaporated. The solid was dissolved in acetone and the product was precipitated with $Et_2O$ to give pure complex **4d** (75 % yields). $^1$H NMR (CD$_2$Cl$_2$) δ: 1.44 (s, 18H), 4.70 (s, 6H), 6.15 (d, 2H, $J_{HH}$=7.5), 7.01 (dt, 1H, $J_{HH}$=7.5, $J_{HH}$=1.6), 7.09 (dt, 2H, $J_{HH}$=7.5, $J_{HH}$=1.4), 7.76 (d, 2H, $J_{HH}$=7.5); $^{13}$C NMR (CD$_2$Cl$_2$) δ: 30.0 (CH$_3$), 42.2 (CH$_3$), 65.6 (C), 124.2 (CH), 124.8 (CH), 128.3 (C), 131.2 (CH), 131.3 (CH), 149.1 (C), 157.6 (C), 174.8 (C)]

## 9.4 - Bibliography

1.      H. Yersin, Highly Efficient OLEDs with Phosphorescent Materials; Wiley-VCH: Weinheim, **2008**.

2.      M. E. Thompson, P. E. Djurovich, S. Barlow, S. Marder, *Comprehensive Organometallic Chemistry III*; Elsevier: Oxford, **2007**; *12*, 101−194.

3.      H. Yersin, A. F. Rausch, R. Czerwieniec, T. Hofbeck, T. Fischer, *Coord. Chem. Rev.* **2011**, *255*, 2622−2652.

4.      Y. Chi, P. T. Chou, *Chem. Soc. Rev.* **2010**, *39*, 638−655.

5.      Y.M. You, S. Y. Park, *J. Am. Chem. Soc.* **2005**, *127*, 12438–12439.

6.      R. J. Holmes, S. R. Forrest, T. Sajoto, A. Tamayo, P. I. Djurovich, M. E. Thompson, J. Brooks, Y. J. Tung, B. W. D'Andrade, M. S. Weaver, R. C. Kwong, J. Brown, *J. Appl. Phys. Lett.* **2005**, *87*, 243507.

7.      T. Sajoto, P. I. Djurovich, A. B. Tamayo, J. Oxgaard, W. A. Goddard, M. E. Thompson, *J. Am. Chem. Soc.* **2009**, *131*, 9813− 9822.

8.      T. Sajoto, P. I. Djurovich, A. Tamayo, M. Yousufuddin, R. Bau, M. E. Thompson, R. J. Holmes, S. R. Forrest, *Inorg. Chem.* **2005**, *44*, 7992−8003.

9.      J. M. Fernandez-Hernandez, C.H. Yang, J. I. Beltran, V. Lemaur, F. Polo, R. Frohlich, J. Cornil, L. De Cola, *J. Am. Chem. Soc.* **2011**, *133*, 10543–10558.

10.     M. Nonoyama, *Bull. Chem. Soc. Jpn.* **1974**, *47*, 767–768.

11.     S. Ladouceur, D. Fortin, E. Zysman-Colman, *Inorg. Chem.* **2011**, *50*, 11514–11526.